Keele
UNIVERSITY

This work is protected by copyright and other intellectual property rights and duplication or sale of all or part is not permitted, except that material may be duplicated by you for research, private study, criticism/review or educational purposes. Electronic or print copies are for your own personal, non-commercial use and shall not be passed to any other individual. No quotation may be published without proper acknowledgement. For any other use, or to quote extensively from the work, permission must be obtained from the copyright holder/s.

Cell models to evaluate oligodendrocyte lineage cell growth on biomaterials

Farhana Chowdhury

Doctor of Philosophy in Neuroscience

March 2022

Keele University

Abstract

Oligodendrocyte lineage and neuronal cells are essential neural populations required for axonal remyelination after spinal cord injury (SCI). Injection of an exogenous cell population into the site of neural injury has posed translational barriers, such as greater than 95% cell death without the use of neural cell protective delivery systems. Additionally, there is a lack of biomaterials approved for human implantation which could act as a neural cell delivery system. Furthermore, majority of scaffolds often have an isotropic structure, and may lack the ability to direct and guide axonal growth and remyelination through the damaged regions in SCI.

This thesis demonstrates the growth and maturation of oligodendrocyte lineage cells in the FDA approved, neurosurgical grade, three-dimensional (3D) biomaterial DuraGen Plus™ when co-seeded with astrocytes, which act as a supportive cell population for oligodendrocyte lineage survival. This cellular construct showed potential for use as an implantable scaffold in neural injuries which may result in demyelination. Additionally, encapsulating neuronal enriched cells within DuraGen Plus™ demonstrated that the scaffold enables the maturation of neurons. However, future work is required to improve viability of the cells within the construct. There is scope to produce a pre-differentiated neural circuit in the DuraGen Plus™ matrix that can be integrated into lesioned sites in the CNS to promote regeneration. Moreover, oligodendrocyte lineage cells were seeded onto a poly-L-caprolactone (PCL), 3D aligned Cellevate nanomatrix to demonstrate the cell alignment capabilities of the matrix. The findings show that Cellevate was able to sustain the survival and

maturation of oligodendrocyte precursors (OPCs) and promoted the alignment of OPCs within the scaffold. It thereby mimicked the *in vivo* neuro-cytoarchitecture that would aid in guiding axonal remyelination. Oligodendrocyte cell alignment, however, was not as prominent in the matured constructs and hence, future work could focus on further scaffold modifications which may be required to enhance cellular alignment.

Table of Contents

List of Tables and figures

Acknowledgements

First and foremost, I would like to thank my supervisors Professor Divya Chari and Dr Chris Adams for their continuous support throughout the years, without them I would not have been able to complete my PhD. Professor Chari has taught and aspired me to delve deep into my work and that no road is easy. She has always tried to help in any way she can. I am grateful to have been under her supervision.

I wish to also thank the School of Medicine, the Post Graduate research Committee and Keele Acorn for funding me throughout my PhD.

I would also like to thank my friends and fellow lab members: Dr Aina Mogas Barcons, Dr Emma Green, Dr Yolanda Gomez Galvez, Jessica Wiseman and Catia Nascimento. They were always there to encourage me throughout my PhD and ensured that the office was both a fun and nurturing working environment. Anne Sadler to whom I am indebted to for helping me put my thoughts to paper and for going out of her way to ensure that I presented my best work. I would also like to thank Dr Jacqueline Tickle for her words of encouragement and advice throughout the past 4 years and Dr Stuart Jenkins who was always available to provide his technical expertise for aspects of my work.

A special thanks to my friend, Hanna Zafar who has been my number one cheerleader from the day I started. Thank you for putting up with me and for always putting things into perspective. A special thanks also to my friends: Gulnar Vasta,

Sofia Azam, Laiba Hussain, Tasmin Nahar and Neelam Rai for always encouraging me to do better.

My family, specifically my parents Mobub Hussain Chowdhury and Zakia Khanom who have always pushed me to do better and greater things, you finally got yourselves a Doctor! My sister, Fahmida Chowdhury and my niece, Humayra who always knew the right things to say when the going got tough.

Lastly, I would like to thank my husband, Sayid Molik who has had to deal with me whilst writing this thesis, he is a brave man for sure! Thank you for always supporting me.

Abbreviations

Spinal cord injury	SCI
Chondroitin sulphate proteoglycans	CSPGs
Glial fibrillary acidic protein	GFAP
Immature form of nerve growth factor	ProNGF
P75 neurotrophic receptor	$P75^{(NTR)}$
Myelin associated glycoprotein	MAG
Cerebral spinal fluid	CSF
Central nervous system	CNS
American Spinal Injury Association	AISA
National Acute Spinal Cord Injury Study	NASCIS
Methylprednisolone	MP
Hematopoietic stem cell transplantation	HSCT
Multiple Sclerosis	MS
Extra cellular matrix	ECM
Poly lactic acid	PLA
Poly e caprolactone	PCL
Poly glycolic acid	PGA
Poly ethylene glycol	PEG
Poly vinyl alcohol	PVA
Progenitor motor neurons	PMNs
Chondroitinase ABC	ChABC
Neural stem cells	NSCs
Induced pluripotent stem cells	IPSCs
Myelin basic protein	MBP
Oligodendrocyte precursor cells	OPCs
Guanosine5’-diphosphate	GDP
Neurotrophin-3	NT-3
Food and Drug Administration	FDA
Adipose derived stromal stem cells	ASCs
Basic fibroblast growth factor	bFGF
Polydioxanone	PDO
3-dimensional	3D
Bovine spongiform encephalopathy	BSE
Meniscus fibrochondrocytes	MFC
Mesenchymal fibrochondrocytes	MSFc
Mesenchymal stem cells	MSCs
Autologous Schwann cells	SCs

Normal human astrocyte	NHA
Embryonic stem cells	ESCs
Human ipscs	HiPScs
Blood brain barrier	BBB
Botulinum neurotoxins	BONT
Poly ethyl glycol	PEG
Magnetic nanoparticles	MNPs
Poly-L-Ornathine	POR-N
Anti-β-tubulin	TUJ-1
4',6-diamidino-2-phenylindole	DAPI
Dulbecco's Modified Eagle Medium	DMEM
Poly-D-Lysine	PDL
Platelet-derived growth factor	PDGF-aa
Revolutions per minutes	Rpm
Triiodothyronine	T3
Thyroxine	T4
Fetal bovine serum	FBS
DIV	Days in vitro
Phosphate buffered saline	PBS
Paraformaldehyde	PFA
Vesicular glutamate transporter 1	Vglut-1
Room temperature	RT
Gabaergic neurons	GABA
Progenitor cell marker	NG2
Scanning electron microscopy	SEM
Critical point dried	CPD
2-dimensional	2D
Immunocytochemistry	ICC
Signal to noise ration	SNR
Traumatic brain injury	TBI
Lactate and pyruvate	LPR
Embryonic	E
Post-natal murine retinal cells	RPNCs

Chapter 1

General Introduction

1.1 Spinal cord injuries show limited regenerative capacity

1.1.1 Epidemiology and socioeconomic consequences of SCI

Spinal cord injury (SCI) is an insult to the spinal cord, resulting in a change to motor, sensory or automatic functions of the spinal cord which may be temporary or permanent,with 2.5 million people affected worldwide (Fakhoury, 2015). In the UK, it is estimated that there is an incidence of 12 to 16 cases per million individuals with SCI and from these injuries, there are approximately 40,000 individuals living with long term disabilities (NHS England, 2013; NICE, 2016). Demographically, males are at most risk from 20-29 years and over 70 years whereas females are most at risk from the ages 15 to 19 and over 60years (WHO, 2013).

There are roughly 12,500 new cases yearly and costs equate to $9.7 billion nationally for SCI treatment (NSCISC, 2017; Spinalcord, 2020) Depending on the severity and location of damage inflicted on the spinal cord, disabilities can vary from paraplegia (affecting the lower body) to quadriplegia which affects all four limbs (NSCISC, 2017). This poses major problems to health care systems which must deal with the economic burden. The financial pressures are due to patients presenting with various degrees of cognitive and physical deficits that require palliative care (medical care, respite, long term residential care and nursing home care). This level of provision results in an approximate annual spend of £8 billion and $100 billion for the UK and US, respectively (WHO, 2017).

1.1.2 Clinical features of SCI

SCI can be categorised as either traumatic or non-traumatic. Examples of primary traumatic SCIs include blunt trauma or a penetrating injury. Non-traumatic SCI causes can arise from cases where the cord is compressed due to bone metastasis from cancer, multiple sclerosis or a disc prolapse (Lee and Thumbikat, 2015). Approximately 90% of spinal cord injuries are due to traumatic incidents (WHO, 2013). In the USA, over 30% of traumatic SCIs are caused by motor vehicle accidents with nearly 80% of these cases seen in men. The clinical features of SCI depend on the severity of the injury in addition to the location in the spinal cord. The symptoms of SCI may include partial or complete loss of motor and sensory functions of the arms, legs and/or body. Trauma to the spine can occur anywhere along the length of the spinal cord however, SCI is largely located in the anatomic regions low cervical (C5-C7) and mid thoracic (T9-T9) as seen in Figure 1 (NSCISC, 2020). Furthermore, injuries to the cervical levels often results in some degree of quadriplegia whereas injuries to the thoracic regions typically result in some degree of paraplegia (Siebert *et al.,*2015).

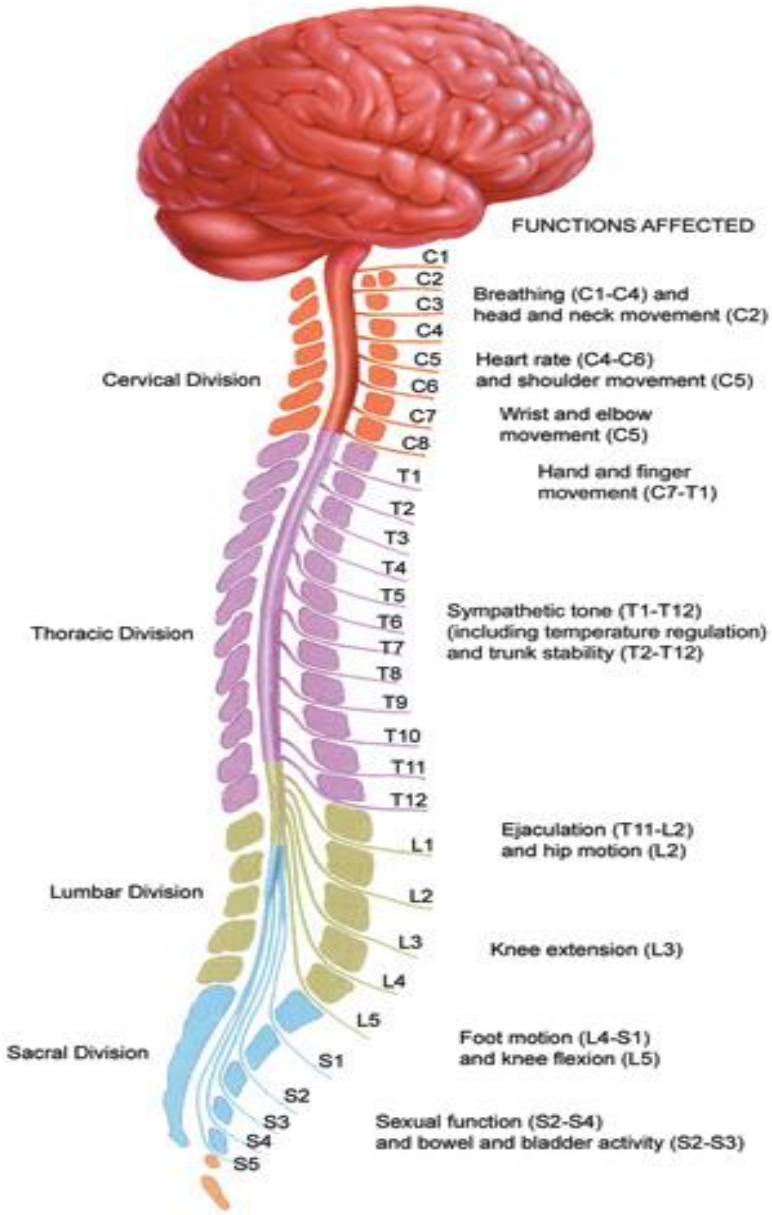

Figure 1.0 Different regions of the spinal column and the areas of the body affected by spinal cord injury (McDonald, 1999).

1.1.3 The pathophysiology of SCI and the barriers to regeneration in SCI

The biological response to SCI is divided into three stages which are acute, (instantly) secondary (minutes to weeks after injury) and chronic (months or years post injury) as seen in figure 1.2. (Oyinbo, 2011).

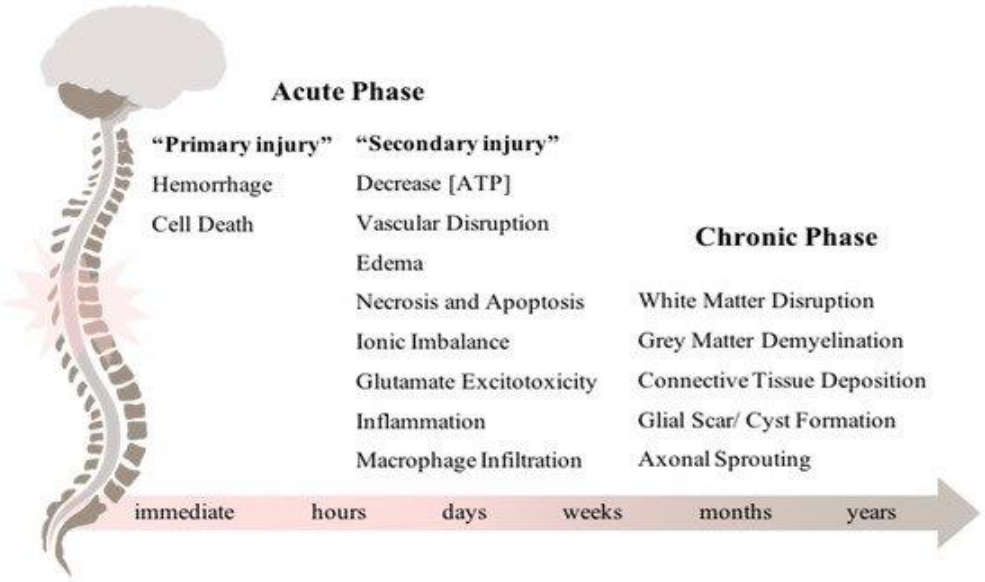

Figure 1.1 Stages of biological events during acute and chronic phases after spinal cord injury. Primary insults lead to a secondary injury which lasts minutes to weeks. The chronic phase occurs months to years after injury (Pereira *et al.*, 2019).

Primary SCI occurs at the acute injury stage where the initial mechanical damage, in cases of contusion or compression of the spinal cord, results in the physical forces being concentrated at the weakest point of the unmyelinated axons, at the nodes of ranvier which causes axonal rupture. As a result, it creates a rapid influx of extracellular Ca^{2+} due to the exposure of the axoplasm to the extracellular environment and activates phospholipase A_2 which in turn, triggers the cut end of the

axon to reseal (Yawo and Kuno, 1985). This Ca^{2+} dependent event also determines if the damaged axonal tip develops into a functional growth cone or an end bulb (Kamber *et al.*, 2009).

The secondary stages of injury involve a biochemical insult where a cascade of inflammatory factors are released. This includes an increased production of pro-inflammatory cytokines and free radicals which help mediate the clearance of cell debris by recruiting microglia and macrophages (Lucas *et al.*, 2006; Shoichet *et al*, 2008). However, these factors also promote neuronal and oligodendrocyte apoptosis and the formation of a cystic cavity containing cerebral spinal fluid (CSF) in the damaged region. The axons and dendrites that have lost communication with the original neural pathway due to the insult, degenerate at the epicentre of the cystic cavity with retraction and dieback of the axons resulting in their demyelination (Katoh *et al.*2019).

Furthermore, the inflammatory components trigger the migration of astrocytes for the formation of a reactive glial scar, to isolate the lesion from healthy tissue. This is achieved by astrocytes becoming hypertrophic and upregulating glial fibrillary acidic protein (GFAP) expression, thereby leading to widespread proliferation to form a dense astrocytic boarder surrounding the lesion site (Sofroniew and Vinters, 2010). Additionally, the astrocytes express the extracellular matrix protein chondroitin sulphate proteoglycans (CSPGs) which inhibit axonal growth. CSPGs, alongside the other inflammatory factors also inhibit axonal regeneration (Lucas *et al.*, 2006; Rauvala *et al.*, 2017). This disruption to the neural circuit due to cell loss is a critical cause of functional impairment (Katoh *et al.*2019).

Oligodendrocytes are responsible for myelin ensheathment of axons, and are susceptible to the toxicity of the acute lesion site after SCI. There are reports of oligodendrocyte loss detected as early as 15 minutes post injury with continuous loss occurring for 4 hours in rat SCI models (Almad *et al.*, 2011).The secondary loss of oligodendrocytes is due to glutamate release induced by SCI which reaches concentrations that are toxic to oligodendrocytes (550mM) (Xu *et al.*, 2004). Additional factors that cause oligodendrocyte apoptosis is the formation of free radicals within the lesioned site in addition to the trauma to the spinal cord (Almad *et al.*, 2011; Hall, 2011).The latter results in the increased synthesis of the immature form of nerve growth factor (proNGF) by astrocytes and activated microglia, which interact with the upregulated p75 neurotrophic receptor p75$^{(NTR)}$ on the surface of oligodendrocytes to induce pathologic apoptosis (Beattie *et al.*, 2002; Meeker and Williams, 2015).

Oligodendrocyte cell loss results in demyelination of axons, and the excess breakdown of myelin products within the lesion, with the debris containing the myelin proteins myelin associated glycoprotein (MAG), myelin oligodendrocyte glycoprotein (MOG). Nogo-66 and Nogo-A which are all reported to be highly inhibitory for neuronal regeneration, as they cause retraction of the axonal growth cone (Maier *et al.*, 2009; Harlowa and Macklin, 2014). The death of oligodendrocytes triggers the recruitment and migration of quiescent populations of oligodendrocyte precursor cell (OPCs) that are distributed throughout the grey and white matter of the central nervous system (CNS) (constitutes to 3-8% of CNS cells), to mature into oligodendrocytes, in order to contact denuded axons for remyelination (Sasaki *et al.*, 2007). The myelin sheath that is formed during remyelination is thinner and shorter than expected for the axon, in comparison to an unaffected myelinated axon

(Franklin and Ffrench-Constant, 2008; Duncan *et al.*, 2017). However, during the chronic stages of SCI, remyelination failure occurs, possibly due to repeated episodes of demyelination at the lesion site, causing depletion of the endogenous OPC population (Blakemore and Irvine, 2008; Franklin and Goldman, 2015).

1.1.4 Current clinically approved treatments for SCI are ineffective for promoting regeneration

Given the complexity of the biological response to SCI by glial and neuronal cells, treatments for SCI are limited. Current therapies offer functional recovery but do not have the capacity to regenerate a damaged spinal cord. For acute SCI patients, the offered treatment include surgical decompression; physical therapy and pharmacological drugs to stabilise the spine and prevent additional neurological injury (Cristante *et al.*, 2012). A study by Fehlings *et al.*,(2012) indicated that surgical decompression of patient spinal cords within 24 hours of injury, improved neurologic outcome and improvement of at least 2 grades in the American Spinal Injury Association (AISA) impairment scale (Fehlings *et al.*, 2012). However, if a patient has cervical and thoracic SCI, only 1% to 1.8% of patients have been shown to walk 6 months after surgical decompression (Cristante *et al.*, 2012).

A clinical trial conducted by the National Acute Spinal Cord Injury Study (NASCIS) II, involved investigating treatments of high doses of the synthetic anti-inflammatory corticosteroid methylprednisolone (MP) used to reduce oedema in SCI, by dampening the inflammatory response and decreasing the extravasation of microglia, thereby reducing the cytotoxic effects of tumour necrosis factor alpha and nitic oxide (Sloka and Stefanelli, 2005). MP was administered to patients within 24 hours post

injury, with data showing to improve motor function, between 6 weeks and 6 months post injury (Bracken *et al.*, 1997). However, there are side effects of this treatment with Khan *et al.*,(2013) and Wang *et al.,*(2013) highlighting that high dose of MP treatment, used for SCI causes problems such as gastrointestinal haemorrhaging, higher incidence of wound infection and 3 times higher risk of pulmonary embolus (Stuijver *et al.*, 2013). Additionally, recent studies have shown that high doses of MP does not contribute to better neurological recover and thus, this treatment is no longer recommended after early SCI (Liu *et al,*2019).

These treatments however do not yet address the underlying biological mechanisms that prevent SCI repair, meaning there is a need for further development of clinical treatments that would aim to promote regeneration in SCI.

1.2 Cell therapies offer a platform to achieve combinatorial therapy in neurological injury

Due to the complex nature of spinal cord injuries, one single pharmaceutical drug cannot address the multiple symptoms. Additionally, monotherapies cannot repair the damage caused in the degenerated regions. It would therefore be beneficial to use a combinatorial approach, where multiple therapeutic interventions could be used for the treatment of SCI. Currently there are a number of therapeutic approaches that are being developed to target multiple issues that prevent functional SCI recovery. Of particular interest are combining exogenous cells such as oligodendrocyte

precursors, neuronal cells or stem cells, and encapsulating them into biomaterials, for delivery into the SCI site, in order to promote regeneration by the remyelination of axons (Siebert *et al.,* 2015).

Strategies that have been trialled extensively to replace, repair, and create a more conducive environment for regeneration have been cell-based therapies. Cell therapies may have the potential to alter the biochemical processes at the hostile lesioned areas that limit axonal regeneration (Katoh *et al.*2019). This could be achieved by introducing a healthy population of cells with the aim of integrating them into the impaired region to replace the damaged neural cells, by secreting their own molecules which could aid in repair, making the area more favourable for regeneration (Katoh *et al.*2019).

CNS stem cell therapies have been investigated by researchers such as Nash *et al.*, (2017). They explored a phase 2 trial using high dose immunosuppressive therapy with autologous hematopoietic stem cell transplantation (HSCT), in patients with the demyelinating disease multiple sclerosis (MS), who do not respond to disease modifying drugs. This was an intense chemotherapy treatment used for individuals who had highly active relapsing MS which caused inflammation, during the early stages of the disease. The rationale for using HSCT was to replace what are believed to be highly active immune cells attacking the CNS in MS patients, which in turn, could reduce relapses and stabilise symptoms. The study involved 24 individuals between the ages 18 - 60 years. Stem cells were encouraged to migrate out of the bone marrow into peripheral circulation with bone marrow stimulation medication and the cells were then collected approximately 10 days later, stored, ready to be used for the procedure. After the immune system was reset with

chemotherapeutic drugs, the HSCTs were reintroduced, with the aim being to rebuild the immune system and stop any further attacks. Over the time-course of the 5-year study, three participants died due to progression of the disease. The cause of death for all cases was reported as cardiac arrest and not attributed to the HSCT therapy. Overall, 19 out of the 24 participants were shown to be in remission with no relapses, and no evidence of disease progression due to the HSCT treatment. However, this is an aggressive treatment and complications can include risk of infections as recovery time is between 3 to 6 months. Nevertheless, HSCT appears to offer the potential as a promising therapy for treating relapsing MS that fails to respond to first line treatment (Nash *et al.*, 2017; MS, 2020).

1.3 Translational challenges associated with the transplantation of neural cells into hostile lesion areas

Although cell-based therapies offer the potential to be clinically translatable for neurological conditions, there are translational challenges associated with the transplantation of neural cells into the host. Transplanted cells directly delivered to the site of SCI using a fine bore needle or glass capillaries via intrathecal injection, result in poor survival rate of the cell population, with studies showing less than 5% of injected cells remaining in the site post transplantation (Pease *et al.*, 2007). Additionally, delivery of a large dose of cells requires either a single large injection or multiple injections which then carry the risk of injection-related injury. This application may create cell shearing stresses on the membrane of the transplant cells during delivery, resulting in cell clumping and death. A combination of these factors in the

already hostile lesion area, activates a greater immune response (Hill *et al.*, 2007; Pease *et al.*, 2007). Research relating to the use of injections for SCI cell delivery has shown a quantified survival rate as low as 1% (Amer *et al.*,2015). Other factors that contribute to the low survival rate include the inflammatory microenvironment of the host and failure for the cells to be equally distributed in the target lesion area (Guest *et al.*, 2011).

Stem cells used for transplantation of neural cells can be extracted from multiple sources, but they must meet a set of criteria if they are to be used for CNS clinical applications. This selection process means that the cells must be able to differentiate and replace the required type of neural cell. e.g. striatal neurons for Huntington's disease or dopamine cells in Parkinson's disease (Silvestro *et al.*, 2020). Additionally, the stem cells must demonstrate their robustness and reproducibility in a laboratory in both 2D and 3D cultures. They should also exhibit this rigour and replicability in animal models of disease during the preclinical stages, prior to reaching clinical trials. It should also be established whether the cells can survive long term in these cultures and animal models, and if they exhibit any functional benefits in the animal models (Siddiqi and Wolfe, 2016). Lastly, there should be no evidence of malignant cell growth in the transplant cell population (Silvestro *et al.*, 2020).

Due to the reasons cited above, **there is a need to find an alternative method to safely and effectively deliver a transplant population of cells into the damaged areas in the SCI. One potential way this could be achieved is by encapsulating cells into hydrogels to act as a scaffold.**

1. 4 Using biomaterials as a cell carrier to support cell delivery and regeneration in SCI

Biomaterials are scaffolds that offer the potential to be used for SCI repair, to bridge the physical gap between the SCI cavity and healthy tissue, in order to allow for neuronal outgrowth and remyelination for axonal tract reformation by providing guidance cues, in addition to stabilising the injury and reducing the glial scar to promote regeneration (Hlavac *et al.*, 2020). The ideal properties of a biomaterial to promote SCI repair include that the material must be biocompatible with the host tissue to decrease graft rejection and ideally, biodegradable to rates that are comparable to native extracellular matrix deposition, after allowing the transplant cells to integrate into the lesion site without the risk of delayed immune rejection and chronic nerve compression (Kubinová and Sikova, 2012; Hlavac *et al.*, 2020).The material should also be minimally immunogenic so not to cause further inflammation to the SCI lesion site. Structurally, the scaffold should have mechanical strength to allow for implantation into the spinal cord, but the scaffold should also be able to conform and integrate into the injury site (Serrano-aroca, 2018). The biomaterial should allow for cell adhesion or encapsulation to the scaffold and support cell survival, proliferation, differentiation, and maturation. Additionally, the scaffold should be able to remain in the typically irregularly shaped lesion sites. Furthermore to support cell survival, the scaffold should have a microporous structure that facilitates good oxygen permeability and allows nutrients and waste products to move freely throughout the scaffold (Montoro *et al.*,2014). It would also be beneficial if the scaffold allowed for angiogenesis as this would allow for the mimicking of *in vivo* nutrient delivery and the removal of toxic products (Giraudo *et al.*, 2020).

Biomaterials have been tested in the pre-clinical and clinical stages for this purpose as a supportive matrix for cell encapsulation and delivery (Li *et al.*, 2016). In clinical research, biomaterials consist of natural, synthetic or hybrid polymers. Natural hydrogels include polymers such as gelatin, collagen, elastin, and fibronectin, which are found in the native host, and they are typically biocompatible and biodegradable. Natural polymers contribute to the *in vivo* neuro-cytoarchitecture and are found in many biological systems such as the extra cellular matrix (ECM), cartilage, keratin of hair and skin and the cytoskeleton. The application of natural polymers has been found for uses such as surgical sutures in medicine (Maitz, 2015; Vasile *et al.*, 2020). Synthetic polymers are now used extensively in research due to manufacturers' ability to change the physical, chemical, and mechanical characteristics as required and in addition, they have an extended shelf life in comparison to natural hydrogels.

In the biomedical field, the most common synthetic polymers include poly lactic acid (PLA), poly e caprolactone (PCL), poly glycolic acid (PGA), poly ethylene glycol (PEG) and poly vinyl alcohol (PVA) to produce a biodegradable hydrogel (Vasile *et al.*,2020). These polymers can also be used to produce aligned nanofiber matrices utilised as guidance cues, in order mimic *in vivo* neuro-cytoarchitecture, by aligning neural cells, in order to guide cell growth along the fibre orientation, to promote cell migration, differentiation, neurite outgrowth and axonal extension in the spinal cord lesion site (Hoffman-kim *et al*,2010; Kubinová and Sikova, 2012; Hlavac *et al.*, 2020). However, many synthetic polymers lack bioactive properties, meaning that they do not interact and integrate with the host tissue. Therefore, by combining the bioactive properties of natural polymers with the mechanical properties of synthetic polymers, forming a hybrid hydrogel can bypass this issue and produce a scaffold that is both robust and biocompatible (Maitz, 2015; Vasile *et al.,*2020).

1.5 Biomaterial cell encapsulation studies for the treatment of SCI

Many pre-clinical studies have tried to demonstrate the utility of biomaterials for cell encapsulation in the treatment of SCI.

In their pre-clinical study, Caron *et al.*,(2016) discussed the use of a hydrogel containing the polymers; agarose, carbomer and PEG. They encapsulated human mesenchymal stem cells into the hydrogel and implanted the construct into a rat *in vivo* spinal cord injury model. There was evidence that the scaffold was able to immunomodulate the pro-inflammatory environment at the site of injury, by increasing the population of M2 macrophages. M2 secrete anti-inflammatory cytokines to reduce inflammation thereby creating a pro-regenerative environment, which is the desired outcome for treating SCI. Wilems *et al.*,(2015) encapsulated embryonic stem cell derived progenitor motor neurons (pMNs) into a fibrin scaffold for the treatment of SCI. The scaffold was modified to provide the delivery of anti-inhibitory molecules NEP1-40 and chondroitinase ABC (ChABC) and neurotropic growth factors heparin and ATIII peptide in a rat sub-acute SCI model. Interestingly, the results showed that the scaffolds that contained pMNs with growth factors had lower levels of CSPG, compared to scaffolds containing anti-inhibitory molecules with pMNs. Additionally, all combination treatments showed pMNs viability for 2 weeks. However, this was decreased in the scaffolds containing only anti-inhibitory molecules and pMNs cells, possibly due to an increased infiltration of macrophages in the rat SCI lesion site.

Overall, the viable cells that remained after 2 weeks, in all conditions, showed pMNs neural differentiation and the extension of axons.

Alginate encapsulated neural stem cells (NSCs) in a rat *in vivo* model of SCI were investigated to determine the effects of the hydrogel on cell viability and functional recovery (Hosseini *et al.*, 2016). This research showed that anti-inflammatory markers and caspase-3 levels which are indicative of cell death were lower for the encapsulated NSCs at the lesion site, in comparison to cells that were not encapsulated. Additionally, there was improved neurological outcome after 12 weeks with hindlimb locomotion being scored at 15, in comparison to 8 for rats with induced spinal cord injury, but with no cell transplantation in the Basso, Beattie and Bresnahan (BBB) scoring system (21 indicates no impairment as observed in un-injured rats) (Hosseini *et al.*, 2016).

1.6 Encapsulating exogenous Oligodendrocyte precursor populations into biomaterials for the promotion of remyelination

Similarly, Nazari *et al.*,(2019) also utilised a fibrin hydrogel but with the aim of encapsulating and promoting the differentiation of induced pluripotent stem cells (iPSCs) into immature oligodendrocyte lineage cells. The fibrin hydrogel improved cell viability in comparison to 2D cultures, and promoted the differentiation of the iPSCs into pre-oligodendrocytes, with the confirmation of the expression of oligodendrocyte markers such as Olig2 and O4, MBP, Sox10 and PDGFRα. The

study concluded that the hydrogel could provide a metabolically active microenvironment for induced oligodendrocyte lineage cells and that there is potential for it to be used for tissue engineering in SCI. Egawa *et al.*,(2017) conducted a functionality study to develop a 3D culture platform of oligodendrocyte precursor cells (OPCs) in a 3D hydrogel, to observe how OPCs responded to their microenvironment in terms of proliferation and differentiation *in vitro*, for use as a platform for examining mechanisms for OPC functionality. For this study, rat derived primary OPCs were encapsulated into a collagen/hyaluronan hydrogel which contained Gelin-S (thiol- modified collagen), Gycosil (thiol-modified hyaluronan) and Extralink (thiol reactive PEGDA). This particular hydrogel as chosen due to Egawa *et al's.*,(2017) prior work showing that CD44, which is a receptor for hyaluronan is required for the migration of transplanted OPCs in a rat SCI model (Piao *et al.*, 2013). The study demonstrated that the hydrogel could support the survival, proliferation, and maturation of OPCs. However, Egawa *et al.*,(2017) stated that further work is needed to investigate the effects of varying concentrations of the hydrogel and altered seeding densities on OPC functionality. Moreover, it would be worthwhile to co-culture the OPCs with neurons to observe if the matured OPCs could myelinate the axons in the 3D scaffold.

A rapidly gelling, purine cross linked injectable chitosan sponge described by Mekhail *et al.,* (2014) has also proved to be useful for the encapsulation of OPCs and promoting their differentiation into mature oligodendrocytes. The results showed that the hydrogel which contained guanosine5'-diphosphate (GDP) and neurotrophin-3 (NT-3), encouraged the survival, attachment and differentiation of rat OPCs in the scaffold. Additionally, NT- 3 is believed to also enhance remyelination post SCI due to the hydrogels' ability to slowly release the growth factor over 30 days. Mekhail *et*

al,(2014) observed that OPCs can be encapsulated when there was a high entrapment efficiency of bioactive molecules in the sponge. In addition, encapsulated cells with pro-regenerative molecules in the hydrogel could be delivered direct to the target site. However, whilst studying the paper, it was observed that there was evidence of cell clumping within the sponge, which may affect the distribution of cells within the scaffold. Moreover, if the cell encapsulated hydrogel were to be implanted into a SCI site, the gel may swell excessively and increase interspinal pressure, which could contribute to the expansion of the spinal cord injury lesion (Khaing *et al.*, 2015; Marquardt and Heilshorn, 2016).

1.7 FDA approved surgical grade biomaterials as an avenue for cell encapsulation

As the literature suggests, there are multiple hydrogels at the pre-clinical stages that have the potential to support neural cell populations and particularly OPCs for their encapsulation and implantation into the site of injury. The majority of biomaterials that are studied however, are formulated in laboratories and have not been tested for human use. They are also not approved for CNS clinical use by regulatory approval bodies such as the Food and Drug Administration (FDA) who dictate appliances that can be utilised for clinical purposes. It is estimated that it takes approximately seven years to approve a biomaterial from the pre-clinical to clinical stages (Van and Gail,2016 a; Van and Gail, 2016 b). Due to this prolonged time interval, approval for use of new biomaterials for cell encapsulation does not meet current need in CNS therapies. One alternative route for addressing this challenge is to *repurpose surgical*

grade biomaterials that have already gained regulatory approval, and utilise them for cell encapsulation.

Biomaterials are subject to rigorous safety testing periods which include preliminary bench testing and then animal testing and during this stage, the biomaterial enters further evaluation and redesigning, costing between $10 to $20 million, a process which takes approximately 2 to 3 years. This period is followed by a further 3 to 4 years in the clinical trials phase, prior to receiving FDA approval for medical use. Therefore, using FDA approved scaffolds would be beneficial as the safety requirements have already been met, thus removing the need to spend time and money on developing a scaffold (Van and Gail,2016 a; Van and Gail, 2016 b).There are multiple surgical grade materials that are FDA approved for specific usage however, there is precedent for repurposing these materials to potentially be utilised for CNS cell encapsulation. These include sealants such as Duraseal™, Tisseel™, ARTISS, Floseal ™, Bioglue, Evicel (Johnsons& Johnsons) Adherus Dural Sealant and biomaterial hydrogels such as Cerafix Dura and DuraGen plus ™.

1.7.1 Fibrin Sealants

Fibrin sealants are surgical adhesives that are used to aid homeostasis for controlling bleeding during surgical procedures and they also act as a sealant as an alternative to sutures. There are multiple fibrin glues approved by the FDA that have been used for clinical purposes which can contain natural or synthetic polymers as seen in table 1. Fibrin surgical sealants consist of two components; fibrinogen and thrombin, which when combined, simultaneously mimic a fibrin mesh. The concentration of thrombin

relative to fibrinogen dictates whether the fibrin sealant will have thinner fibrils and smaller pores (Caliari and Burdick, 2016).

Table 1.0 FDA Approved Clinical Grade Surgical Sealants Adapted From Ge and Chen,(2020)

Categories	**Commercial product**	**Manufacturer**	**Constituents**
Natural or biological adhesives	Crosseal	Omrix	Human fibrinogen, human thrombin, human fibronectin, human factor XIII, calcium chloride
	TachoSil	Pharmaceuticals International GmbH	Equine collagen patch, human fibrinogen, human thrombin
	Vitagel	Stryker	Bovine collagen, bovine thrombin, patients own plasma
	ProGel	NeoMend	Human Serum Albumin, PEG di NHS
	Tisseel™	Baxter	Human fibrinogen, human fibronectin, human thrombin, human Factor XIII, bovine aprotinin, calcium chloride
	Artiss™	Baxter	Human pooled plasma
	Floseal™	Baxter	Bovine derived gelatine matrix, calcium chloride and plasma derived human thrombin
	Evicel™	Ethicon	Human fibrinogen, human thrombin, human factor XIII, calcium chloride
	CryoSeal	Thermogen	Human fibrinogen, human thrombin, human fibronectin, human Factor XIII, human Factor VIII, human vWF, human thrombin from individual units of plasma

	Bioglue™	Cryolife	Bovine serum albumin (BSA) and glutaraldehyde
Synthetic polymer-based tissue adhesive	Surgiseal	Adhezion Biomedical	2-Octyl-2-cyanoacrylate
	Octylseal	Medline Industries	2-Octyl-2-cyanoacrylate
	Omnex	Ethicon	n-Octyl-2-cyanoacrylate/butyl lactoyl-2-cyano acrylate
	DuraSeal™	Integra Life Sciences	Tetra-NHS-derivatized PEG and trilysin
	Adherus	Hyperbranch	Activated PEG and branched poly(ethylene imine)
	FocalSeal-L	Focal Inc.	Photopolymerizable PEG-co-poly(lactic
	CoSeal	Cohesion Technologies	Tetra-NHS-derivatized PEG and tetra-thiol-derivatized PEG

There is evidence of using fibrin glues for cell encapsulation with Hopfner *et al.*, (2018) showing how adipose derived stromal stem cells (ASCs) were encapsulated within Tisseel™ in a mouse diabetic wound model. It was found that Tisseel™ seeded with cells, enhanced wound healing in comparison to cells seeded alone (16 days compared to 18 days). The fibrin glue also prolonged ASC cell survival *in vivo* and there was an increase in the expression of pro regenerative cytokine such as basic fibroblast growth factor (bFGF) from the encapsulated ASCs in the wound, which promoted healing, in comparison to cells seeded alone.

A comparison between the surgical sealants Tisseel™, Adherus™ and Bioglue™ was made by Kalsi *et al.,*(2017) regarding the reimplantation of peripheral nerves in an *in vivo* rat brachial plexus repair model, to observe the histological and inflammatory aspects of these glues. This study involved creating a posterior midline

cervical incision in the rats, with the dura opened and the dorsal root at T1 transacted. The surgical sealants were then applied, and observations were made up until day 28 in euthanised rats. Results suggest that Tisseel™ created mild focal inflammation to the spinal cord which decreased by day 28 in comparison to Bioglue™ and Adherus™. Furthermore, there were no complications with the use of Tisseel™ in terms of spinal cord compression. There was however, evidence of spinal cord compression from the mass of the glue with the two latter surgical sealants, as one of the rats in the Bioglue™ group suffered from hind limb paralysis with one rat from the Adherus™ group developing partial paralysis on one side of the body. These observations suggest that both Bioglue™ and Adherus™ may be used as a dural sealant. However, due to the nature of the sealant and the way it expands within a cavity, it should be used with caution in potential CNS cell encapsulation therapies which include the intradural space and areas near the spinal cord (Kalsi *et al.*, 2017).

The Vivostat system is another fibrin glue that utilises autologous thrombin and fibrinogen, harvested from a patient's own blood, to produce the fibrin sealant. This fibrin glue has been examined in a pre-clinical study to encapsulate autologous porcine keratinocytes for the treatment of acute wounds in burns patients. It was chosen due to Vivostats' ability to promote haemostasis and also because of its autologous nature which is beneficial as a non-immunogenic therapy (Grant *et al.*, 2002). A porcine wound model was used where a wound bed was created by excising the tissue to the muscle fascia prior to spraying the Vivostat sealant with keratinocytes on the site. It was reported that large convoluted surfaces of the wound could be covered by the sprayable hydrogel with the cells, and that these cells were able to expand within the sealant in 1 to 3 days and populate the wound as the fibrin glue degraded (Grant *et al.*, 2002).

Floseal™ is another homeostatic sealant that was used to encapsulate human MSCs which were implanted into a rat myectomy model which mimics muscle injury, to observe muscle regeneration over 35 days. It was concluded that at day 35, in all treatment groups (Floseal™ encapsulated with cells vs. no Floseal™), the dorsiofloxer muscle functionality was similar in value to that of intact muscles prior to injury. The Floseal™ sealant was able to maintain cell survival, however it was reported to create a greater inflammatory response in comparison to the control group, where no Floseal ™ was used (Pereira *et al.*, 2014).

1.7.2 DuraSeal™ has shown to cause post-operative spinal cord compression

DuraSeal™ is a surgical sealant but with synthetic origins. It is produced by Integra Life Sciences consisting of a PEG and amine-based solution. The purpose of the sealant is to seal the dura after a duraplasty, as a replacement for using sutures to provide a watertight closure and prevent CSF leakage. The product has been reported as being resorbed *in vivo* in a 9 to 12 weeks' timeframe which is believed to be a sufficient interval for normal wound healing (Integra Life, 2014, 2018).
In a clinical study by Cosgrove *et al.*, (2007), DuraSeal™ had been used in 111 patients with no reported spontaneous CSF leakage immediately following duraplasty, with only 2 patients reported with a CSF leak at the 3-month post-operative stage (Integra Life, 2014). Although there is no evidence of cell encapsulation with DuraSeal™. Lin *et al.*, (2010) demonstrated its use for peripheral nerve repair. It was reported that when DuraSeal™ was used in a rat nerve gap model where the sciatic nerve was excised, leaving a 5mm gap, DuraSeal™ showed

evidence of promoting peripheral nerve repair which was defined as nerve continuity and remyelination. DuraSeal™ was reported to also restore motor and electrophysiological functions in comparison to tissue glue and nerve regeneration was achieved without causing neurotoxicity. However, in some cases DuraSeal™ has been shown to cause post-operative spinal cord compression or cauda equina syndrome upon expansion in the cavity (Lee *et al.*, 2013; Han *et al.*, 2020). Although this material may be biocompatible for CNS cell encapsulation, expansion of the gel and compression of the spinal cord must be considered if designing a therapy with this hydrogel.

1.7.3 Cerafix Dura

Cerafix dura is another FDA approved dural substitute that is used during duraplasty, with manufacturers claiming the material to be minimally immunogenic and preventative in the leakage of CSF. It is a fully synthetic, porous nanofabricated biomaterial, consisting of polyglactin (PGLA) and polydioxanone (PDO) polymers which are commonly found in re-absorbable sutures (Bennett, 2018; Macewan *et al.*, 2018 a; Schmalz *et al.*, 2018). Cerafix dura has been used in a canine duraplasty model by MacEwan *et al*, (2018a) where the material was implanted to repair small and large dural defects to observe any possible CSF leakage and neurological abnormalities. The grafts were explanted at 4 or 13 weeks after surgery and histopathology confirmed that the graft was gradually reabsorbed with an increase in the infiltration of the native dura cells. Additionally, all dural defects were observed to be repaired by week 13.

In a further study, Macewan *et al.*, (2018b) compared the performance of the semi synthetic bovine collagen dural graft, DuraMatrix™ (Stryker) with Cerafix in a rabbit duraplasty model. The comparison involved repairing an induced bilateral dural defect with either material and securing the material in place with on-tension sutures and monitoring the animals for post-operative CSF leakage and inflammation. It was reported that both dural grafts were effective in preventing CSF leakage and repairing the dura. However, it was found that there was an increased, induced inflammatory response with DuraMatrix™, with a greater infiltration of immune cells within the graft, in comparison to Cerafix. The outcome of the study suggests that Cerafix is a suitable non-biological, fully synthetic graft that can be used in a dural repair. It therefore has potential to be utilised for CNS cell encapsulation therapies.

1.7.4 DuraGen Plus™ has shown evidence clinically, and in research for successfully supporting encapsulated cell populations for transplantation purposes

DuraGen Plus ™ matrix is an FDA approved, 3-dimensional (3D) biomaterial that has been used by neurosurgeons in over 750,000 patients during duraplasty. It is beneficial for use in a dural repair as it creates a rapid mechanical barrier for preventing CSF leakage, by allowing fibrin clot formation within the matrix. This clot formation is achieved by the infiltration and distribution of fibroblasts, which utilise the pores of the matrix to establish a new collagen layer. During this process, the DuraGen Plus ™ matrix is reabsorbed and replaced with the new dura. Additional benefits claimed by Integra Life Sciences include allowing the repair of the dura without the formation of scar tissue or encapsulation (Integra, 2010, 2018). DuraGen Plus™ matrix is composed of semi-synthetic, 95% ultra-pure type 1

collagen. This is derived from bovine deep flexor tendons and has been described as ‘minimally immunogenic’, due to its purification process. This procedure reduces the risk of transmission of bovine spongiform encephalopathy (BSE), by deactivating and destroying the abnormal prion proteins present, which in turn, reduces the potential of an inflammatory response to the material (Integra, 2010, 2018).

Several studies have investigated utilising the DuraGen Plus™ matrix for cell encapsulation and transplantation purposes and these include **orthopaedic research, nephrology and neurology**. In orthopaedic research, DuraGen™ plus has been used for regenerating meniscus fibrochondrocytes (MFC), a cell type that is located in knee joints and displays a poor regenerative capacity after injury. MFC cells generate meniscal cartilage which is responsible for aiding and providing joint stability, protection and absorption of shock to the joints. Adesida *et al's.*,(2012) rationale for using DuraGen plus ™ was to determine whether this particular matrix can support the survival of MFCs, in addition to maintaining their phenotypical characteristics. MFC cells were derived from human menisci, which had been isolated from patients that underwent total knee replacement surgery. The cells were cultured for 4 weeks until a confluent culture was achieved. $1x10^6$ of the cultured MFC cells in a 10µL volume, were then seeded onto 6mm pieces of DuraGen Plus™ matrix which was at a total thickness of 3.6mm. Histological analysis showed that there was migration of the menisci cells in the pores of the DuraGen Plus™ matrix and that the cells resembled a chondrocyte-like morphology.

In another orthopaedic study, Kallai *et al.*,(2010) genetically engineered mesenchymal fibrochondrocytes (MSFCs) which were used to promote bone growth induction in mice non-union fractures The MSFCs were genetically engineered to over express a bone morphogenetic protein gene which accelerates

bone regeneration in segmental fractures. DuraGen Plus™ was used to seed 2x 10^6 engineered MSFCs onto a standard 1mm by 3mm DuraGen Plus™ slice. The matrix with the engineered cells was then inserted into a 2.5mm radius in the middle of a damaged right forelimb. Bone formation in the non-union fracture was then evaluated with micro-CT scans, 10 and 35 weeks after implantation. The results showed that bone formation in the non-union fracture site at 35 weeks was similar to that on untreated bone (Kallai *et al.*, 2010). For renal research, Geng *et al.*, (2017) utilised DuraGen Plus™ matrix to encapsulate mesenchymal stem cells (MSCs) for the potential treatment of acute kidney injury, onset by rhabdomyolysis, a condition that involves a major breakdown of skeletal muscles, with myoglobin being released into the bloodstream. This in turn causes myoglobin-induced renal toxicity due to the increased inflammation, oxidative stress, vasoconstriction, and apoptosis. DuraGen Plus™ was used for this study due to its biological membrane characteristics. For instance, the pores in the matrix have been shown to allow fibroblast growth, thus having the capability to maintain cell encapsulation. In addition, it has the ability to be reabsorbed 6 to 8 weeks *in vivo*. The study found that MSCs encapsulated into DuraGen Plus™, which were then packed into injured renal tissue, preserved renal function, reduced renal tubular lesions and apoptosis in mice. This therefore demonstrated that DuraGen Plus™ graft can support MSCs cell delivery, growth, and renal function.

1.7.5 DuraGen Plus™ used for neural cell encapsulation

Additional studies particular to CNS regeneration, have utilised the DuraGen Plus™ matrix to treat traumatic brain injury in rats. Shin *et al.*,(2015) used 87 Sprague-Dawley male rats and categorised them into four groups which were traumatic brain injury (TBI) rats with a DuraGen Plus™ graft (IC), sham rats with a DuraGen Plus™

graft (SC), TBI rats with no graft (IN) and sham rats with no graft (SN). For controlled cortical impact (CCI), a parasagittal craniectomy which was 8mm in diameter was performed and a TBI was simulated with a 6mm in diameter bevelled impactor tip, with the depth of the injury being 2.6mm. A piece of 0.3mm thick DuraGen plus™ matrix graft was then situated over the 8mm craniotomy site, which included the TBI injury in the IC and SC rat groups, and the area was sutured whilst ensuring the DuraGen Plus™ plus was situated at the site of injury. It was found that using the DuraGen Plus™ graft for repairing cortical injuries in rats resulted in an improvement in spatial memory acquisition, which was demonstrated by the rats' response to the beam balance test. Furthermore, histological sections retrieved from the sacrificed rats showed that there was a significant reduction in lesion volume in the IC group with the DuraGen Plus™ graft, in comparison to the IN group where no graft was implanted. There was also a significant decrease in neuronal cell loss in the IC group, when compared to the IN group. Shin *et al.*,(2015) therefore, demonstrated that DuraGen Plus™ may have neuroprotective effects when used for TBI.

The recent study by Finch *et al.*,(2020) utilised the DuraGen Plus™ scaffold to encapsulate murine NSCs to demonstrate whether the biomaterial could support the survival, proliferation and differentiation of the cells within the matrix as a potential cell transplantation treatment for spinal cord injury. The study found that DuraGen Plus™ could support the survival of 95% of the cell population. Additionally, there was also evidence that DuraGen Plus™ could maintain stem cell phenotypes and promote NSC differentiation into neurons, astrocytes, and oligodendrocytes within the scaffold. Furthermore, genetically engineered NSCs were also shown to be supported by the biomaterial, demonstrating its use as a potential combinatorial

approach for cell replacement and functional protein delivery into a spinal cord lesion site, in order to promote axonal regeneration and remyelination (Finch et al, 2020).

1.7.6 DuraGen Plus™ used for cell encapsulation in human clinical trials for peripheral nerve repair promoted regeneration

Gersey *et al.*,(2017) has also trialled DuraGen Plus™ matrix and investigated its use for peripheral nerve repair in human clinical trials. The trials were conducted on a patient with a boat propeller injury (patient 1) and another with a gunshot wound (patient 2). Patient 1 sustained complete transection of the sciatic nerve to their left upper thigh and had complete sensory loss. Patient 2 sustained a 5cm gunshot wound posterior to their right thigh, with fragments of the bullet lodged in the sciatic nerve which were later removed but left partial sensory loss to the damaged regions. For patient 1, three days post-injury, autologous Schwann cells (SCs) were harvested from a 0.5cm piece of traumatised sciatic nerve and a 5cm piece of sural nerve which was ipsilateral to the injury. For patient 2, the SCs were derived from the sural nerve, 9 days after trauma. In both cases, the SCs were then cultured for seven days until they reached 80% confluency with 28.8 million and 110 million SCs seeded onto the DuraGen Plus™ graft for patient 1 and 2 respectively, which was then implanted into the site of injury - 30 days post injury for patient 1 and 41 days after initial injury for patient 2. The results showed that both patients displayed improvement in motor and sensory functions and there was a reduction in pain at the site of injury. In addition, the safety profile of the SCs encapsulated DuraGen Plus™ graft was also monitored 12- and 36- months post-implantation and showed that neither patient demonstrated evidence of tumour formation, a potential concern with cellular autologous transplantation.

1.7.7 There is potential for utilising DuraGen Plus™ for oligodendrocyte lineage cell encapsulation

As shown, DuraGen Plus™ has demonstrated *in vivo*, its applicability as a clinical biomaterial with the capability to encapsulate and support a cellular population for potential use in cell transplantation therapy, with a recent study emphasising that it can support an NSC population *in vitro* and support differentiation into the progeny cell types. There is however no evidence of research thus far, that has utilised DuraGen Plus™ in oligodendrocyte lineage encapsulation. Oligodendrocyte cell loss results in demyelination of axons, and axonal regeneration cannot be achieved without myelin ensheathment by oligodendrocytes. Therefore, it would beneficial to investigate the applicability of DuraGen Plus™ for supporting a myelinogenic cell population, as a potential therapeutic application, to aid in repairing demyelination caused by SCI.

1.8 Multiple neural models are used for biomaterial cell encapsulation testing

Testing new biomaterial encapsulation strategies uses a wide variety of cell sources. Due to this, studies often generate contradictory results when translated *in vivo,* and this could partially be due to the different neural cell models that are used. Key biological differences in these systems often includes cellular composition, the maturation time of the cultures and culture medium composition (Baldassarro *et al.*,

2016). It is therefore beneficial to understand the advantages and disadvantages of the variety of neural cell sources used in biomaterial cell encapsulation testing.

1.8.1 Cell lines

Glial cell lines have extensively been used as a tool to study glial cell biology in addition to their application in regenerative medicine therapies. The advantage of using immortalised cells lines in comparison to primary cultures is that there are an unlimited number of cells that are available to be utilised for studies in addition to not having to sacrifice animals for generating cultures (De Vries and Boullerne, 2010). Furthermore, utilising cell lines can generate cellular populations that are purified with a single glial cell type. There are many established glial cell lines (Table 2) with their origins being derived from either human, rat, or mouse.

Table 1.1 Established glial cell lines.
(Adapted from (De Vries and Boullerne, 2010)

Cell line name	Cell type	Methods used to derive cells
G4 (CG-4)	Oligodendrocyte	Spontaneous immortalization of OPC from mixed glial culture of neonatal cortex (Sprague–Dawley rat)
OLN-93	Oligodendrocyte	Spontaneous immortalization of OPC from mixed glial culture of neonatal brain (Wistar rat)
Oli-neu	Oligodendrocyte	Transfection with a *t-neu* oncogene of primary culture enriched in oligodendrocytes from day 15 embryos (NMRI mouse)
N19 N20.1	Oligodendrocyte	Transfection with temperature-sensitive *SV40 large T antigen* of primary culture enriched in oligodendrocytes from neonatal brain (BALB/cByJ mouse)
G26-20 G26-24	Oligodendrocyte	Clones derived from the glioma G26 induced by methylcholanthrene treatment (C57BL/6 mouse)
HOG	Oligodendrocyte	Clone derived from a surgically removed oligodendroglioma (human)

MO3.13 (M03.13)	Oligodendrocyte	Fusion of a human tumor rhabdomyosarcoma RD cell line with a human primary culture of oligodendrocytes from surgery (human)
C6	Astrocyte	Clone derived from a brain tumor induced by N-nitrosomethylurea treatment of adult animals (outbred Wistar rat)
DI TNC1	Astrocyte	Transfection with *SV40 large T antigen* under the control of GFAP promoter of type 1 astrocytes in primary culture isolated from the diencephalon of neonatal brain (Sprague–Dawley rat)
BALB SFME	Astrocyte	Clone derived from spontaneous immortalization of day 16 embryonic brains cultured in medium deprived of serum (BALB/c mouse)
A172 (A-172)	Astrocyte	Clone derived from a surgically removed solid glioblastoma (human)
U-87MG (U87-MG)	Astrocyte	Clone derived from a surgically removed malignant astrocytoma grade III (human)

For example, the cell line ‘normal human astrocyte, (NHA) which has the ability to differentiate into neural cells, was used to test the applicability of the hydrogel PuraMatrix^{TM} to understand the genetic responses of astrocytes and neurons within the biomaterial and demonstrate whether it can support the cells (Knight and Serrano, 2017). The study showed that the cells within the hydrogel allowed the formation of a neuronal and glial coculture, with the neurons forming clusters that were surrounded by glial cells. In addition, it was found that there was upregulation of multiple gene biomarkers that influenced neuronal differentiation in the encapsulated cells. Other studies have used the human oligodendrocyte lineage cell lines HOG and MO3.13 which have been used for *in vitro* functional studies of oligodendrocytes lineage differentiation and dysfunction of the cells. Additionally, these cell lines have been used to investigate immune-mediated injury, the effects of viral infection and

also CNS diseases such as MS and Schizophrenia (Schoenfeld *et al.*, 2010; Dasgupta and Ray, 2017; De Kleijn *et al.*, 2019).

1.8.2 Disadvantages of cell lines

Although there are advantages for the use of cell lines, the disadvantages may outweigh this. Cell lines are not an ideal model to mimic physiological conditions and to predict the behaviour of primary cells. They are also homogeneous cultures that have been expanded from a relatively small original cell source, through multiple passages which can result in the loss of key functions and traits of the cell source they are meant to represent , due to genetic drift and selective pressure (Jenkins *et al.*, 2016). Additionally, cell lines can mask cytotoxicity by resisting cell death and behave in a homogenous manner unlike cells *in vivo*. Resistance to apoptosis could hinder analysis of cell viability within hydrogels as the biomaterial may not be suitable to support a primary cell population thus, conducting a study with cell lines may produce inaccurate data which may not be physiologically relevant and become more costly when cellular toxicity is evident at later stages of biomaterial testing (Hughes *et al.*, 2007; Jenkins *et al.*, 2016). An example of how cell lines and primary cells behave differently was reported by Pinkernelle *et al.*,(2012). They compared green fluorescent tagged magnetic nanoparticle uptake between PC12 cells, which are a rat pheochromocytoma cell line that are used as a neuronal cell model against primary rat neuronal cells. The results demonstrated that particle uptake was significantly higher in the PC12 cells in comparison to primary neurons, therefore suggesting that cell lines do not reflect or predict *in vivo* endocytic abilities like primary cells.

1.8.3 Induced Pluripotent cells used for biomaterial cell encapsulation

Induced pluripotent stem cells (iPSCs) are derived from autologous and allogeneic cell sources that have been utilised for biomaterial cell encapsulation. These are differentiated adult somatic cells that can be derived from patients' skin fibroblasts, fat cells or peripheral mononuclear cells from blood, and be programmed to return back to their embryonic stages (Tam *et al.*, 2014). Takahashi and Yamanaka,(2006) reported how introducing the transcription factors SOX2, OCT4, c-Myc and KLf-4, which play a pivotal role in maintaining pluripotency of embryonic stem cells (ESCs) could reverse somatic cells back to their ESC state. The added advantage of iPSCs is that there is the avoidance of immune rejection since the cells are derived from the patient. Furthermore, the iPSCs are not derived from embryos hence, there are reduced ethical issues surrounding this in comparison to using ESCs (Gorecka *et al.*, 2019).

Human iPSCs (hiPSCs) can be used to derive the glial cell types astrocytes, oligodendrocyte, and microglia. For instance, astrocytes can be derived in three stages. The hiPSCs are first differentiated into neuroepithelial cells which takes between 0-21 days. These then transition to astroglial progenitors with the addition of EGF and FGF in growth medium from 21-90 days. The last stage is when the progenitors mature into immature astrocytes which occurs after day 90 at which point, they start to express CD44-FGFAP post differentiation (Zheng *et al.*, 2018). The cells were reported to display distinct functional features which includes having glutamate receptors and transporters, promoting synaptogenesis and aiding in the formation of the blood brain barrier (BBB) (Krenick *et al.*, 2011). This process of

differentiating astrocytes from iPSCs has been shorted by 35 to 80 days by modifying the optimisation process (Zheng *et al.*, 2018).

hiPSCs have also shown to differentiate to produce oligodendrocyte lineage cells. Douvaras and Fossati (2015) found iPSCs differentiated into NSCs within 8 days, which then gave rise to oligodendrocyte lineage transcription factor 2- positive (OLIG2(+) cells at day 12. The cells then began to express NKX2.2 transcription factor at approximately day 18 and SOX10 at day 40. OPC positive cells were identified by day 50 by the O4 antibody. After 75 days, at this stage, 43% of the cell population can be utilised for OPC studies or they can be matured to produce myelinating oligodendrocytes. Pantoja *et al.*,(2020) used peripheral blood mononuclear cells from stable and progressive MS patients, to generate autologous iPSCs in order to produce oligodendrocytes. Healthy control donors were also used to generate iPSCs for comparison and it was found that in all cases, the iPSCs could differentiate into mature oligodendrocyte lineage cells.

Wang *et al.*, (2014) showed how iPSCs used to derive OPCs, could remyelinate the brains of myelin-deficient shiverer mice and it was evident that there was no tumour formation 9 months post transplantation. The results suggest that OPCs produced in this manner have potential to be utilised for demyelinating conditions. hiPSC derived NSCs have also been encapsulated in a poly ethyl glycol (PEG) hydrogel to develop a cell-based neurotoxicity screening model (Pellett *et al.*, 2015). To determine the sensitivity of the model, botulinum neurotoxins (BoNT) were used. BoNTs are potent human neurotoxins that exert toxicity by entering the peripheral nervous system, and attacking neuronal cells which in turn, blocks the release of neurotransmitters at muscular junctions. It was found that firstly, induced NSCs could differentiate and

mature in the hydrogel and that BoNT sensitivity was detected 2 weeks earlier in NSCs in the PEG hydrogel, in comparison to cells that were seeded onto tissue culture polystyrene surfaces. Additionally, it was found that the results from this study were comparable to data reported for other cell-based assays and *in vivo* models (Pellett *et al.*, 2015).

However, iPSCs are not without limitations. To generate these cells requires the use of lentiviruses and retroviruses. However, these can cause insertional mutagenesis to the cells resulting in tumour formation, and the use of the Myc gene for reprogramming may cause the iPSCs to become oncogenic (Gorecka *et al.*, 2019). This is highly unfavourable for use in cell transplantation, particularly if they are being used for gene therapies (Takahashi and Yamanaka, 2006; Tam *et al.*, 2014). In addition, Yamanaka (2012) reported that the transfection efficiency of producing IPSCs is less than 1% so a large yield of somatic cells would have to be retrieved from the donor to get a sufficient amount for transplantation (Bhartiya *et al.*, 2013).

1.8.4 NSCs for biomaterial cell encapsulation

Other biological models that have been trialled include using NSCs (Trounson, 2011). NSCs are a class of multipotent cells derived from the nervous system and are a reliable source in terms of creating glial cell types, as they can differentiate into neurons, oligodendrocytes, and astrocytes. Also, they can be retrieved from the sub ventricular zone in the lateral walls of the ventricles and the sub granular zone in the hippocampus in foetuses, neonates and adult brains (Trounson, 2011; Tam *et al.*, 2014; Trounson and McDonald, 2015; Boese *et al.*, 2018).

A chitosan-based hydrogel was used to encapsulate rat adult NSCs to determine whether this hydrogel was able to promote differentiation into neurons and whether it could support cell survival (Farrag and Leipzig, 2018). The cell encapsulated constructs were then implanted in the subcutaneous space in the cervical, thoracic, and lumbar regions of rats. After 4 to 8 weeks, the scaffolds were removed and it was found that the scaffold supported cell survival and cellular differentiation into Beta-tubulin positive neurons (Farrag and Leipzig, 2018). Adams *et al.*,(2016) used a combinatorial approach and transfected NSCs with magnetic nanoparticles (MNPs) and encapsulated the cells as 3D spheroids, into a hydrogel consisting of the extra-cellular matrix (ECM) protein, collagen. The rationale for using collagen was because it has greater translational and physiological relevance, as it mimics better the mechano- elastic properties of a brain and spinal cord microenvironment, in comparison to NSCs grown on non neuromimetic substrates (Adams *et al.*, 2016). Additionally, utilising MNPs may be beneficial for mediating the delivery of genes, drug delivery, or for use as a non-invasive method for cell tracking for CNS therapies (Tickle and Chari, 2019). Results demonstrated that the construct supported over 90% of cells within the biomaterial. MNP transfected NSCs could retain their stem cell phenotype and when promoted to differentiate, were able to transform into astrocytes, neurons, and oligodendrocytes within the hydrogel (80%, 16% and 4% respectively). These results were comparable to cells grown on 2D surfaces.

However, there are disadvantages in using NSCs, as a proportion of daughter cells derived from the stem cells cannot produce a purified culture of neurons or a glial cell type. Multiple studies involve investigating the cellular response of a purified, single cell population for biomaterial testing, nanoparticle, and pharmacology studies.

Utilising NSCs for this purpose may be disadvantageous as it is difficult to produce a purified population of a single glial lineage cell type, due to the heterogenous nature of NSCs which form a tripotent population of neurons, astrocytes and oligodendrocytes at a reported proportion of 20%, 75% and 5% respectively (Fernandes and Chari, 2016; Li *et al.*, 2019).

1.9 Utilising a cortical mixed glial model for CNS research

A possible solution to overcome the issues mentioned above, is to utilise a model that allows for the generation of glial lineage cells which can be used as co-cultures, to control the ratio of cells, or used as isolated cell populations. These cultures can be achieved by using a primary mixed glial model which has been reported in more than 2,500 research papers for pharmacological, molecular and biochemical studies (Vellis and Cole, 2011). Using this model with a chemically defined medium can promote the generation of three major glial cells: microglia, OPCs and astrocytes, derived from post-natal cortical tissue; typically from rats between postnatal day 0 to 3.The benefits of this model are that the cells can be isolated by sequential rotary shaking. This method aims to generate glial cell sub-populations with a high degree of purity (i.e. greater than 95%) and high cell viability, which can be used extensively for CNS therapeutic studies, and more specifically for investigating the cellular response for biomaterial testing (Chen *et al.*, 2007; Jenkins *et al.*, 2016).

An example of the versatility of the rat mixed glial model has been demonstrated in two studies investigating the uptake of PEG coated, stealth nanoparticles for therapeutic CNS screening applications. In the first study Jenkins *et al.*, (2015), a

mixed glial model was used to generate a 50:50 co-culture of glial cells to observe competitive nanoparticle uptake between microglia and OPCs versus microglia and astrocytes. In the second study, purified monoculture populations of microglia, OPCs and astrocytes were generated to investigate uptake (Jenkins *et al.*, 2016). High cell purity and viability of glial co- and mono-cultures was seen in both studies, evidenced by healthy rounded nuclei and the expression of cell-specific markers; thus demonstrating the reproducibility of the model.

The majority of studies that use a mixed glial culture derive tissue from post-natal rat cortices. Therefore, there is infrequent reference in literature to the use of mice for producing these cultures. Although rat, rather than mice, cortices have conventionally been favoured, due to their larger size which yields greater cell numbers, mice mixed glial cultures may offer distinct advantages over rats. Rats are expensive to breed and maintain in comparison to mice, costing approximately £150 compared with £30. There is also the added advantage of having availability of a large number of transgenic mouse populations to mimic a range of neurological disease states (Ellenbroek and Youn, 2016). Although the reproductive lifespan of both mice and rats is similar (12-16 months), mice reach sexual maturity 1 week earlier than rats- 6 to 8 weeks compared with 7 to 8 weeks (Sengupta, 2013). Gestation length is similar for both (18-22 for mice; 23 for rats) (Murray *et al.*, 2010). Moreover, housing costs are less for mice in terms of feeding requirements. Thus, in comparison to rats, mice are a more readily available, cost-effective resource (UBC, 2018). Furthermore, mice require less food and water, with only 3 grams of food and 3mL of water needed per day while rats need 15 to 30 grams of food and 15 to 60mL of water. These figures further emphasise that it is financially more attractive to use mice for research purposes over rats (UBC, 2018).

1.10 Using post-natal cortical tissue for establishing an *in vitro* neuronal model for biomaterial testing

As one of the consequences of SCI results in neuronal cell loss and damage, investigating the neuronal response in a biomaterial is also essential for developing neuronal replacement therapies and to investigate if a scaffold can promote axonal and neurite outgrowth, to bridge the gap between healthy spinal cord tissue and the lesion site (Azari and Reynolds, 2016).The applicability of post-natal cortical tissue derived from mice can also be used for establishing neuronal cultures. *In vitro* neuronal models typically utilise embryonic cortical tissue due to the axons and dendrites not yet developing, which makes the neurons less vulnerable to damage during the dissociation process of the tissue (Sciarretta and Minichiell, 2010). Typically, the age of the tissue used for these cultures is between E11 and E17, as this is the time frame where the majority of the cerebral cortical neurons are generated (Goldman and Kuypers, 2015). Additionally, the population of the culture is primarily neuron-rich, with the population of oligodendrocytes and astrocytes, by comparison, quite poor due to genesis of these cells occurring after E12 and E18, respectively. A further advantage of embryonic culture usage is that the meninges and the connective tissue sheath can be easily removed due to the stage of development of the cortices, therefore producing a cleaner culture (Sciarretta and Minichiell, 2010; Barateiro and Fernandes, 2014; Goldman and Kuypers, 2015; Reemst *et al.*, 2016). These cultures can be grown and maintained easily at low or high densities for biochemical studies and gene manipulation and expression studies.

However, in comparison to embryonic neuronal models, there are several advantages to developing a *post-natal* neuronal enriched model. A post-natal model reduces the necessity of killing several animals. i.e., only a few pups from a litter are required to be euthanised, avoiding the need to terminate the life of the mother to extract the embryos, thus making the process technically less challenging and leaving the mother to be used for further breeding purposes (Sciarretta and Minichiell, 2010). This model also makes it possible to study neurons from genetically engineered mice at the early post-natal stages through gene 'knock in' or 'knock out' processes. This, in turn, facilitates investigation of neuronal structure and function for biochemical analysis, imaging analysis, electrophysiology, or utilisation of the cells in the testing of biomaterial neuronal cell encapsulation (Sciarretta and Minichiell, 2010; Beaudoin *et al.*, 2012),

In consideration of the above arguments, a niche was established to develop and utilise a post-natal, cortical, mixed glial model, derived from mice to complement the existing rat mixed glial model, and to establish a post-natal, cortical neuronal, enriched model for cell encapsulation in biomaterial testing and therapeutic applications, for SCI regeneration.

This literature review supports the above summary and has highlighted the following knowledge gaps and areas for further development:

1. A glial cell model of murine origin is desirable as an inexpensive and reliable model for trialling regenerative medicine therapies. Currently (2020) there are few such simplified primary biological models available to generate glial

lineage cells. Generally, utilisation of rat brains is chosen over mice due to their larger cortical size.

2. There is a need to test and identify clinically approved biomaterial scaffolds which support the survival and maturation of oligodendrocyte lineage cells. This is because there is currently a limited number of scaffolds that are FDA approved for these purposes.

3. There is a need to increase the use of neuronal enriched models generated using post-natal pups as this method would be technically less challenging in comparison to establishing an embryonic neuronal model. It would also ensure the sustainability of the breeding stock to produce more litters. At present, the majority of studies use neurons derived from embryonic mice for biomaterial and CNS therapeutic testing.

1.11 Thesis Aims

- To develop a simplified primary mouse mixed glial model using existing mixed glial culture derivation protocols to create a culture system that is cheaper to use. Furthermore, to demonstrate that the model can be as robust and reproducible when compared to the frequently used rat mixed glial model.

- To develop a murine, post-natal neuronal enriched model that aims to be technically less challenging to establish in comparison to embryonic neuronal

models. Additionally, to demonstrate the robustness and reproducibility of the model.

- To test DuraGen plus™, which is FDA approved for neurosurgical procedures, as a potential biomaterial for the seeding and maturation of oligodendrocyte lineage cells, derived from the mouse mixed glial model, in order to determine whether these cells can survive within the construct.

- To assess whether DuraGen plus™ material can successfully support the survival and maturation of neurons.

- To determine whether oligodendrocyte lineage cells be aligned to the scaffold Cellevate, to mimic cellular alignment found in the native neuro-cytoarchitecture.

Chapter 2

Materials and Methods

2.1 Materials and Coatings of Materials

Tissue culture-grade plastics were purchased from Greiner Bio One Ltd (Stonehouse, UK). Media, media supplements (including foetal bovine serum [FBS-Ref. 11573397]) and reagents for cell cultures, except where stated, were from Fisher Scientific (Loughborough, UK), Sigma- Aldrich (Dorset, UK) and Peprotech (London, UK).

For immunohistochemistry, the primary antibodies used were Glial Fibrillary Acidic Protein (GFAP), DakoCytomation (Ely, UK), NG2, Millipore (USA), the glycoprotein Tomato Lectin (Sigma), IBA-1 from Alpha Laboratories (UK). Myelin Basic Protein (MBP) (Bio-Rad, UK) and anti-β-tubulin (TUJ-1) from BioLegend, UK. The secondary antibodies fluorescein (FITC) and Cy3-conjugated were purchased from Jackson Immunoresearch Laboratories Ltd (Westgrove, PA, USA). Normal donkey serum (NDS), used as a blocker was from Stratech Scientific (Suffolk, UK) and Vectashield shield mounting medium containing DAPI (4',6-diamidino-2-phenylindole) was from Vector Laboratories (Peterborough, UK). Reagents for cell viability assays were calcein -AM from VWR (Lutterworth, UK), ethidium homodimer and the nuclear stain hoechst, Fisher Scientific (Loughborough, UK). The use of animals to produce cell cultures was in accordance with the Animal Scientific Procedures Act, 1986 (UK).

2.1.1 DuraGen Plus™ cutting

The DuraGen Plus™ matrix was donated by Integra Neurosciences, United Kingdom (UK) and was provided as a dry 5cm x 5cm square collagen matrix, in sterile packaging. Uncut DuraGen Plus™ was stored in the double sealed plastic, original packaging. A section of DuraGen Plus™ was removed with a scalpel for processing and each plastic layer of the packaging was sealed with tape to ensure that the material remained sterile.

2.1.1.0 Optimisation of DuraGen Plus™ thickness for the seeding of oligodendrocyte lineage and neuronal enriched cells

The material was cut into a 5mm by 5mm width piece, using a sterile scalpel in a laminar flow hood within a square petri dish. Next, to cut the DuraGen Plus™ into the desired thickness, a Mcllwain tissue chopper was used, which is typically employed in the laboratory for producing organotypic brain and spinal cord slices (Weightman *et* al, 2017). Slicing of the DuraGen Plus™ was initially trialled using this dry 5mm by 5mm piece at an initial thickness of 500µm. However, cutting with dried DuraGen Plus ™ was difficult as the DuraGen Plus ™ piece was unstable on the chopping disc. It continually moved when sliced, which led to inconsistent thicknesses of the DuraGen Plus ™ slices. Additionally, as the DuraGen Plus ™ was very lightweight, it was suctioned into the vents of the laminar flow hood. Therefore, this method was discontinued.

Subsequently, we trialled securing the dried DuraGen Plus ™ with sterile tape onto the chopping board. This took place prior to slicing DuraGen Plus ™ but as the slices were adhered to the tape, this led to the tearing of the DuraGen Plus ™, when trying to collect the slices with forceps. Therefore, an alternative technique was trialled. Finally, we tested adding a few drops of Dulbecco's Modified Eagle Medium (DMEM) to another 5mm by 5mm DuraGen Plus ™ piece, after placing it on the chopping disc. Once the medium was absorbed by the material, this piece of DuraGen Plus ™ remained in place and allowed the cutting of consistent slices of our desired thickness. These DuraGen Plus ™ slices were then washed off the board with DMEM and collected into a petri dish. They were then viewed under a dissection microscope to ensure that they were all separated and undamaged, prior to being stored at 4ºC, ready for use. See figure 2.0 for the DuraGen Plus ™ chopping process.

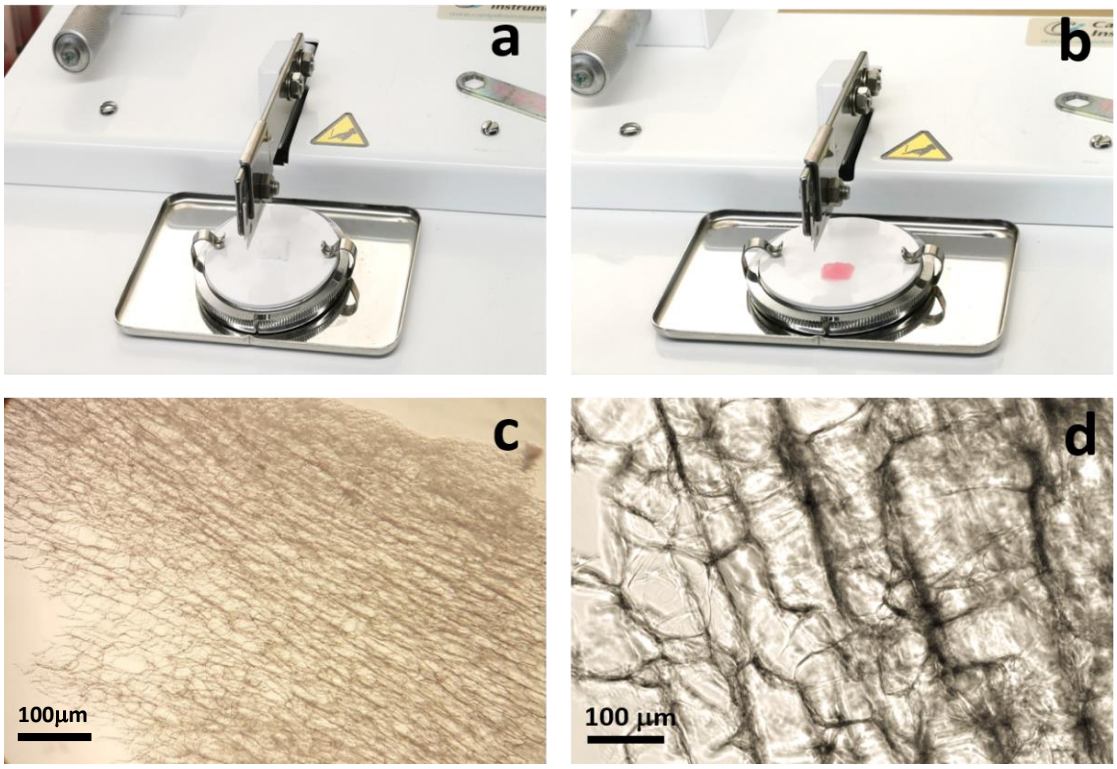

Figure 2.0 Cutting DuraGen PlusTM into the desired thickness using a McIlwain tissue chopper. The diagram depicts **a)** A dry piece of 5mm by 5mm DuraGen Plus™ placed on the tissue chopper plate and aligned with the metal blade; **b)** A few drops of DMEM was added to the DuraGen Plus™ so that it remained in place whilst chopping and it was then cut into its desired thickness; **c & d)** Slides show collected pieces of DuraGen Plus™ viewed at x10 and x20 magnification under phase-contrast microscopy.

For pilot experiments for the seeding of oligodendrocyte lineage cells and neuronal enriched cells respectively, the thicknesses that were trialled were 250µm and 500µm. However, 250µm was taken forward for all subsequent experiments as it was observed to be better for optimal imaging purposes and data analysis (Chapter 4 sections 4.2.2 and 4.2.3).

2.1.2 DuraGen Plus™ optimisation

2.1.2.0 Coating DuraGen Plus™ with poly-L-ornithine and laminin to improve cellular attachment and viability of oligodendrocyte lineage and neuronal enriched cells

To determine whether coating DuraGen Plus™ had any effect in improving day 14 oligodendrocyte lineage cell viability (Chapter 4, 4.2.2) and neuronal enriched cell survival and attachment (Chapter 4.2.3), DuraGen Plus™ was coated with poly-L-ornithine (POR-N) and laminin (Sigma-Aldrich). The rationale for doing so is because literature has suggested that coating 2D or 3D substrates can enhance cellular attachment and survival of cells. Poly-L-ornithine is a synthetic polymer that creates positively charged sites for cellular binding and is commonly used for primary cultures of neurons and glial cells for their attachment to a substrate surface (Ge *et al.*, 2015). Laminin, which is a crucial constituent in forming the basement membrane of the extracellular matrix of most tissues, is essential for cellular proliferation, survival, adhesion, migration and differentiation *in vivo*, and has been used in multiple studies for 2D cultures, and for the coating of 3D scaffolds to test its regenerative potentials for peripheral and CNS nerve repair amongst other cell types (Talovic. *et al.*, 2017).

Pre-cut DuraGen Plus™ slices were incubated with 300 µL of (0.1 mg/mL) of POR-N for 1 hour at 37ºC and then washed once with sterile distilled water. Next, 300 µL of (1 mg/mL) laminin was added to the wells of a 24 well plate, incubated at 37ºC (5%

CO_2 and 95% humidified air) for an hour, and then aspirated. The DuraGen Plus™ was then washed 3 times with sterile distilled water. Prior to the addition of cells, the water was replaced with culture medium and kept at 37°C. The medium was also aspirated before the cells were added. Coating of the material however did not improve attachment of cells to the biomaterial or cell viability therefore, uncoated DuraGen Plus™ scaffolds were used for all subsequent experiments as seen in chapter 4 section 4.2.2. and 4.2.3 for oligodendrocyte lineage cells and neuronal cells respectively.

2.1.3 Propagation of oligodendrocyte lineage cells on Cellevate Fibres

Non-aligned and aligned Cellevate scaffolds were provide by Cellevate (Sweden).

2.1.3.0 Coating of fibres with poly-L- ornithine and laminin for the attachment of cells

Non-aligned and aligned fibres were coated with 0.1mg/ mL POR-N solution for 1 hour at 37°C and subsequently washed with autoclaved water 3 times. Next, the fibres were coated with 1mg /mL laminin for 1 hour and again, incubated at 37°C prior to being washed 3 times with water.

2.2 Cell culture protocols glass, DuraGen Plus™ and Cellevate

2.2.1 Establishment of a mouse mixed glial culture the isolation of glial cells

Disaggregated cortices of CD1 mice litters between postnatal days 1 to 3 were used for the generation of these cultures. Mixed glial cultures for the generation of microglia, oligodendrocyte precursor cells (OPCs) and astrocytes were derived from disaggregated cortices of CD1 mice litters between postnatal day 1-3. The dissection procedure to extract cortices was followed as described by McCarthy and de Vellis (1980) and Chen et al (2007). This procedure involved mincing the cortices into 2-3 mm pieces with a sterile scalpel, which were then transferred with D10 medium into a universal tube. The tissue was then carefully triturated 40 times with a sterile paster pipette, followed by further trituration and mechanical dissociation with a 21 gauge and 23 gauge hypodermic needle 3 times each. The cells were then centrifuged at 1000rpm (78 x g) for 4 minutes, followed by being resuspended in D10, with the suspension then filtered through a 70 μm and 40 μm cell strainers. Cell viability was then assessed before plating by performing a cell count using trypan blue, a dye that selectively stains dead cells dark blue and live cells appear bright and round.
Next, cells were cultured in D10 medium (Dulbecco's modified Eagle's medium) which had the addition of 1mM sodium pyruvate, 2mM glutaMAX, 10% fetal bovine serum (FBS), 50 U/mL penicillin and 50 U/mL streptomycin, and were seeded into 10μg/mL poly-D-lysine (PDL) coated T175 flasks. Flasks were coated in PDL for 20 minutes, followed by 3 consecutive washes in sterile dH20 at 5-minute intervals. Mixed glial cultures were maintained with D10 medium and a 50% change of medium was conducted every 2-3 days. Cultures were kept in a humidified incubator at 37 ^{o}C

in an atmosphere of 5% CO_2 and 95% humidified air. The mixed glial cultures were initially cultured for 10 days to form a stratified cell layer of basal astrocytes, an intermediate later of OPCs and lastly, top dweller microglia.

2.2.2 Isolation of Microglia, OPCs and Astrocytes from a Mouse Mixed Glial Culture

Sequentially shaking culture flasks after 10 days, allowed for the isolation of purified microglia, OPC's and astrocytes for monolayer cultures. Microglia and astrocytes were maintained in D10 medium, whereas OPCs were supplemented by a chemically defined medium to limit differentiation. This medium consisted of DMEM, 2mM glutaMAX, 1mM sodium pyruvate, 50 U/mL penicillin, 50 U/mL streptomycin, 0.1% bovine serum, 5µg/mL insulin, 50µg/mL transferrin, 10nM biotin, 30nM sodium selenite, 10ng/mL of basic fibroblast growth factor (FGF2) and 10ng/mL platelet-derived growth factor (PDGF-aa) (Peprotech, USA).

2.2.2.1 Microglia- Shake 1

Mechanical shaking of the mixed glial culture flasks for 2 hours on the orbital shaker at 220 rpm, detached the loosely adherent, surface microglia. Cells were collected and centrifuged at 1000 rpm (78 x g) for 4 minutes prior to being resuspended in D10 medium. A cell count was performed by mixing 10µL of cell suspension with 40 µL of 0.4% trypan blue (a dye that selectively stains dead cells) and then adding 10µL of the mixture into a hemocytometer chamber. Viable cells appeared bright and round, whereas dead cells were dark blue. These cells were seeded at a density of 6 $x10^5$ live cells/mL in D10 on PDL coated coverslips, in a 24 well plate (0.3 mL/well).

2.2.2.2 OPCs- Shake 2

Prior to shaking off OPCs, the culture flasks were incubated at 37° C (5% CO_2/95% humidified air) for a minimum 2-3 hours to re-gas, to restore the physiological pH. Following this, flasks were sealed with a double layer of parafilm to prevent gas escape and were placed on the orbital shaker overnight at 220 rpm for 16-18 hours, to allow enough time for the OPCs to detach from the astrocyte bed layer. OPCs were then pooled and centrifuged at 1500 rpm (176 x g) for 6 minutes and were resuspended in OPC maintenance medium, to maintain the cells in their OPC state. The medium consisted of DMEM, 2mM glutaMAX, 1mM sodium pyruvate, 50 U/mL penicillin and 50 U/mL streptomycin, 0.1% bovine serum, 5µg/mL insulin, 50µg/mL transferrin, 10nM biotin, 30nM sodium selenite, 10ng/mL of basic fibroblast growth factor (FGF2) and 10ng/mL platelet-derived growth factor (PDGF-aa) (Peprotech, USA). The latter two reagents stimulate OPC proliferation and suppress differentiation.

A cell count was then conducted using 0.4% trypan blue exclusion and OPCs were then seeded at a density of 2 $x10^5$ cells/mL in OPC medium, on PDL coated coverslips in a 24 well plate (0.3 mL/well), with cultures incubated at 37 ^oC in 5% CO_2 and 95% humidified air. 50% medium was changed every 2-3 days.

2.2.2.3 Differentiation into Oligodendrocytes

Differentiation of OPCs into oligodendrocytes was initiated by the removal of FGF2 and PDGF-AA from growth medium after maintenance for 2-3 days as OPCs and involved using a chemically defined medium consisting of DMEM, 2mM glutaMAX, 1mM sodium pyruvate, 50 U/mL penicillin and 50 U/mL streptomycin, 1x N2 supplement (insulin, human transferrin, progesterone, putrescin, selenite), 30nM

triiodothyronine (T3) and 30 nM thyroxine (T4). Cells were cultured in this medium for various times, indicated in the results section.

2.2.2.4 Astrocytes

To remove residual OPCs from the now predominantly astrocytic flask, it was shaken for a further 16-18 hours after being re-gassed for 2 hours. Residual OPCs were removed and culture flasks were then washed with phosphate buffered saline (PBS) to remove traces of medium as it contains FBS which inhibits trypsin. Next, TrypLE^{TM} (a cell dissociation enzyme milder than trypsin), 15mL/T175 flask was added to the cell culture flasks and then placed on the orbital shaker for 15 minutes at 200 rpm and at this point, cells were visibly detached from the surface. TrypLE^{TM} was inactivated by the addition of D10 and the resulting solution was then collected and centrifuged at 1000 rpm (78 x g) for 4 minutes.

A cell count was performed using trypan blue. Astrocytes were then seeded at a density of 2.4 x10^5 cells/mL in D10, on PDL coated coverslips in a 24 well plate (0.3 mL/well). For sub-culturing of purified astrocytes, the remaining cells were seeded into a PDL coated T175 flask and once the culture became sub-confluent with approximately 70% coverage of the base of the flask (2-3 days post plating), the cells were passaged again, either to expand the culture or for monolayer plating. Astrocytes from up to 3 passages per culture were used for experiments.

2.2.3 Derivation of rat oligodendrocyte lineage cells from a primary rat mixed glial culture

Rat oligodendrocyte lineage cells were derived and cultured with the protocols described above in section 2.2.1 and 2.2.2.

2.2.4 Establishment and optimisation of a cortical neuronal culture

2.2.4.1 Mechanical dissociation of cortex to derive neuronal cells

A post-natal neuronal culture was generated using disaggregated cortices of CD1 litters between post-natal days 0 to 3. The culture was established using McCarthy and Devilli's 1980 protocol. The dissociation protocol is described as mentioned same as above. Cultures were maintained with neuronal culture medium which contained 96% neurobasal A, 2mM Glutamax-1, 2% B27 and 0.5 U/mL penicillin/streptomycin.

2.2.4.2 Problems encountered with the use of mechanically dissociating cortex to produce neuronal enriched cultures

This mechanical dissociation protocol however, produced excess cellular debris (section 1a, results) which could not be removed with consecutive medium changes and PBS washes for the duration of the culturing period. Therefore, an alternative protocol involving enzymatic dissociation was trialled.

2.2.4.3 Establishment of a Cortical Neuronal Culture Using Enzymatic Dissociation

Disaggregated cortices of CD1 mice litters between postnatal days 0 to 3 were used. The dissection procedure for producing this culture involved extracting the cortices and removing the olfactory bulb, hindbrain and most importantly, the meninges under a dissection microscope. The meninges are more adherent in the brains of postnatal

animals and thus, can result in cultures having a lower yield of healthy cells and also non-neuronal cells (Beaudoin *el al*, 2012). Next, the cortices were pooled and minced with a scalpel and transferred with dissection medium (DMEM: F12) into a 15mL tube which was then centrifuged at 1200 rpm (113 x g) for 3 minutes. The supernatant of the cell suspension was discarded and the pellet was dislodged from the bottom of the tube, prior to the addition of 0.1% Trypsin: 0.05%DNAse I .The mixture was then incubated at 37 ^{o}C for 20 to 25 minutes in 5% CO_2 and 95% humidified air, and the cell suspension was gently shaken every 5 minutes during this period. 0.05% DNAse I was then added to the suspension to wash the cells and to prevent cell clumping before the addition of FBS to stop the trypsinization reaction. The cells were then resuspended with 5mL of Neurobasal A basic medium, prior to being centrifuged at 1200 rpm (113 x g) for 3 minutes. Next, the supernatant was discarded, and the pellet was dislodged and resuspended with 2mL of neuronal culture medium. The cell suspension was then filtered through a 70µm and then a 40µm strainer to reduce large clumps that remained after the enzymatic digest process. A cell count was performed using 0.4% trypan blue on dissociated cells to calculate the proportion of live cells. Description of cell seeding is in the subsequent sections.

2.2.4.4 Determining the optimal seeding density for cortical neuronal enriched culture

To determine the optimal seeding density for growing a neuronal enriched culture, three different densities were trialled. These were $1x10^5$, $2.5x10^5$ and $4x10^5$ cells/mL. Cells were enriched in neuronal culture medium containing 96% neurobasal A, 2mM Glutamax-1, 2% B27 and 0.5 U/mL penicillin/streptomycin. The timepoints chosen to

observe cellular viability and development of the cultures at these seeding densities were 3,6 and 9 DIV

The optimal seeding density taken forward for subsequent experiments was $4x10^5$ cells/mL as this yielded a larger density of cell bodies (Chapter 3, section 3.2.6, Figure 3.11).

2.2.4.5 The use of coverslips for the plating of neuronal enriched cultures

300 µL/well of cell suspension was seeded at the required density on 10µg/mL poly-D-lysine (PDL) and 1 mg/mL laminin coated coverslips in 24-well plates and incubated at 37 ºC in 5% CO_2 and 95% humidified air. Within an hour, cellular attachment to the surface of the coverslip was visualised under a phase-contrast microscope and the medium was then aspirated to remove debris and replaced with 600µL neuronal culture medium. 50% medium was then changed every 2-3 days. The chosen time points for cell viability assays were 3,6 and 9 DIV, with 12 DIV chosen for immunohistochemistry.

2.2.5 Optimisation of cell seeding technique for DuraGen Plus™

2.2.5.1 flooding of wells with oligodendrocyte lineage cells or neuronal enriched cells on DuraGen Plus™

Prior to the seeding of cells, individual slices of pre-cut DuraGen Plus™ were placed with forceps at the bottom of a well in a 24 well plate. To ensure that the DuraGen Plus™ slices were not folded within the wells, 200µL of culture medium was added and the slices were flattened with forceps. The medium was then aspirated prior to the seeding of cells.

Next, a 300µL cell suspension of OPCs at a density of $2x10^5$ cells/mL were added to the wells and then viewed using phase-contrast microscopy to observe whether the cells had adhered to the surface of DuraGen Plus™ slice. The same procedure was carried out for neuronal enriched cells which were seeded at the densities $1x10^5$, $2.5x10^5$ and $4x10^5$ cells/mL onto the biomaterial.

The flooding of wells, with the cells seeding technique resulted in not all of oligodendrocyte lineage cells and neuronal enriched cells adhering to the material, with evidence of some cells floating in the surrounding medium as figure 2.1 schematically illustrates. (Chapter 4, section 4.2.3). Additionally, 14DIV oligodendrocyte lineage cells showed reduced viability on DuraGen Plus™. Therefore, an alternative 'focal seeding' approach was decided upon, as used by Adesida *et al* (2012) in order to observe whether this method would resolve these issues.

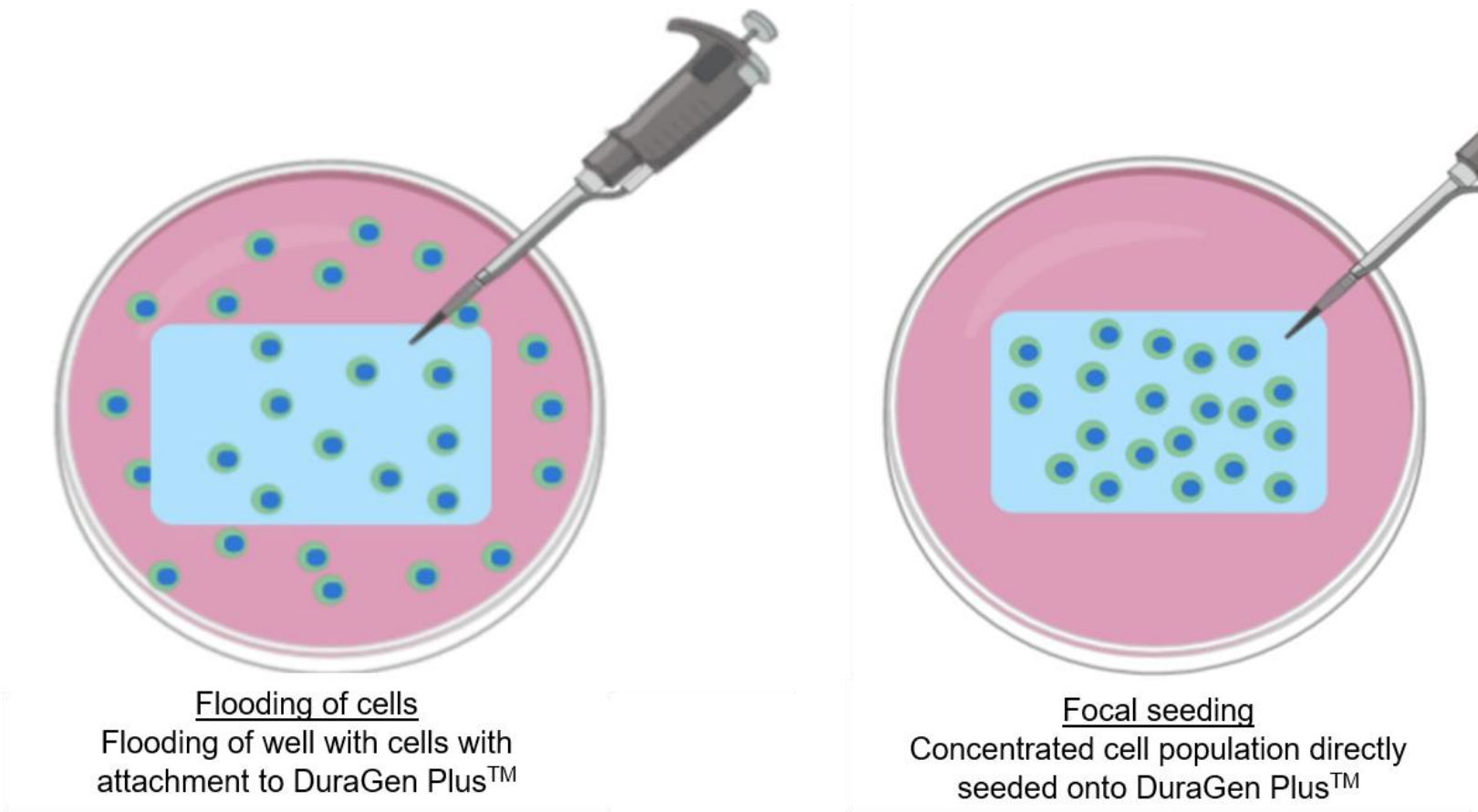

Figure 2.1 Illustration of flooding of cells in comparison to focal seeding in DuraGen Plus™. Flooding of cells involved adding a 300 µL cell suspension to the well in comparison to focal seeding, where a concentrated cell suspension of 10 µL was directly seeded onto te scaffold, followed by gradual addition of medium to the well.

Focal seeding involves directly loading a concentrated population of cells onto DuraGen plus™. The advantage of this technique is that it will allow a greater population of cells to adhere to the biomaterial, which in comparison to flooding of wells with cells, where the total volume of cells added to the well may not have adhered to the DuraGen plus™ scaffold.

2.2.5.2 Focal seeding of Oligodendrocyte lineage and Neuronal enriched cells in DuraGen Plus™

Pre-cut DuraGen Plus™ slices were added to individual wells in a 24 well plate with the addition of 200µL of culture medium. These pieces were then flattened with forceps, which was followed by the aspiration of the medium. Cells grown on glass were used as the control to ensure that the populations of cells used for these experiments were healthy and that initial cell viability, when seeding them on DuraGen Plus™ was not an issue. The seeding density on DuraGen Plus™ was greater than that on glass (i.e.2 x10^5 cells/10 µL and 4 x10^5 cells/10 µL per DuraGen Plus™ slice for oligodendrocyte lineage and neuronal enriched cells respectively) in comparison to 6 x10^4 cells (oligodendrocyte lineage), or 1.2 x10^5 (neuronal enriched cells) per 300µL, per well, on glass.

The rationale for using a higher seeding density on DuraGen Plus™ was due to this being a 3D matrix. In a 2D matrix, cells are only able to attach to the surface of the coverslip so, if the 3D seeding density (e.g. 2 x10^5 cells/10 µL for oligodendrocyte lineage cells) was used for a 2D coverslip, there would have been insufficient space

for the cells to grow and thus cell death would occur. However, in a 3D matrix, like DuraGen Plus™, the cells (Oligodendrocyte lineage cells enriched in OPC medium, or neuronal cells in neuronal culture medium) can be impregnated throughout all the material and can therefore support a higher cell seeding density. As described by Adesida *et al* (2012) 10µL volume of concentrated cells was seeded onto DuraGen Plus™ and incubated at 37°C for 15 minutes to allow for initial cell attachment to the biomaterial. 100µL medium (OPC maintenance medium or neuronal culture medium) was then gently added to the individual wells of a 24 well plate and after a further 30 minutes of incubation at 37°C, 500µL of medium was added to the well to gradually increase the final volume of medium to 600µL. The DuraGen Plus™, which seeded with either oligodendrocyte lineage or neuronal enriched cells was then viewed using phase-contrast microscopy, to observe whether the cells had attached to the material. The focal seeding technique increased the overall density of cells on the scaffold and thus, this method was taken forward for all future DuraGen Plus™ experiments.

The timepoints used to assess cellular viability and cellular morphology for oligodendrocyte lineage cells in the scaffold were 3DIV for OPCs and 7 and 14DIV for mature oligodendrocytes. For neuronal cells within the construct, the chosen timepoints to assess viability were 3,6 and 9 DIV with immunocytochemistry conducted at 12DIV.

2.2.5.3 Co-culturing oligodendrocyte lineage cells with astrocytes to improve overall cell viability within the construct with focal seeding technique

To improve the viability of oligodendrocyte lineage cells on DuraGen Plus^{TM}, they were co-cultured with astrocytes as studies have suggested that astrocytes secrete growth factors that help support glial cells and also provide structural support (Court and Alvarez, 2016).

The focal seeding method on DuraGen Plus^{TM} was taken forward for co-culturing oligodendrocyte lineage cells and astrocytes with the thickness of 250μM Initially, a 10 μL volume of concentrated oligodendrocyte lineage cells, derived from a mixed glial culture (2x10^5 cells/ DuraGen Plus^{TM} piece) was seeded on to a DuraGen Plus^{TM} scaffold and incubated at 37°C for 15 minutes to allow for initial cell attachment on the material. Next, a 10 μL concentrated seeding density of astrocytes which were trypsined to detach from the base of the flask, shortly after the OPCs were collected from the mixed glial cultures (2.4 x10^5 cells/DuraGen Plus^{TM}) was added to the biomaterial and again, incubated at 37°C for 15 minutes to allow for initial cell attachment to the DuraGen Plus^{TM}. 100μL OPC maintenance medium was then gently added to the individual wells of a 24 well plate and after a further 30 minutes of incubation at 37°C, 500μL of this medium was added to the well to gradually increase the final volume of medium to 600μL. The DuraGen Plus^{TM}, co-cultured with precursor oligodendrocyte lineage cells and astrocytes, was then

viewed using phase-contrast microscopy, to observe the attachment of the cells to the biomaterial.

The OPCs, co-cultured with astrocytes were maintained as precursors for 3 days, before they were triggered to mature into mature oligodendrocyte lineage cells using differentiation medium. Figure 2.2 below demonstrates the process of how co-constructs of oligodendrocyte lineage cells and astrocytes were developed.
The same timepoints as mentioned above in section 2.2.5.2 for cell viability and assessing cellular morphology were used for the co-culture constructs.

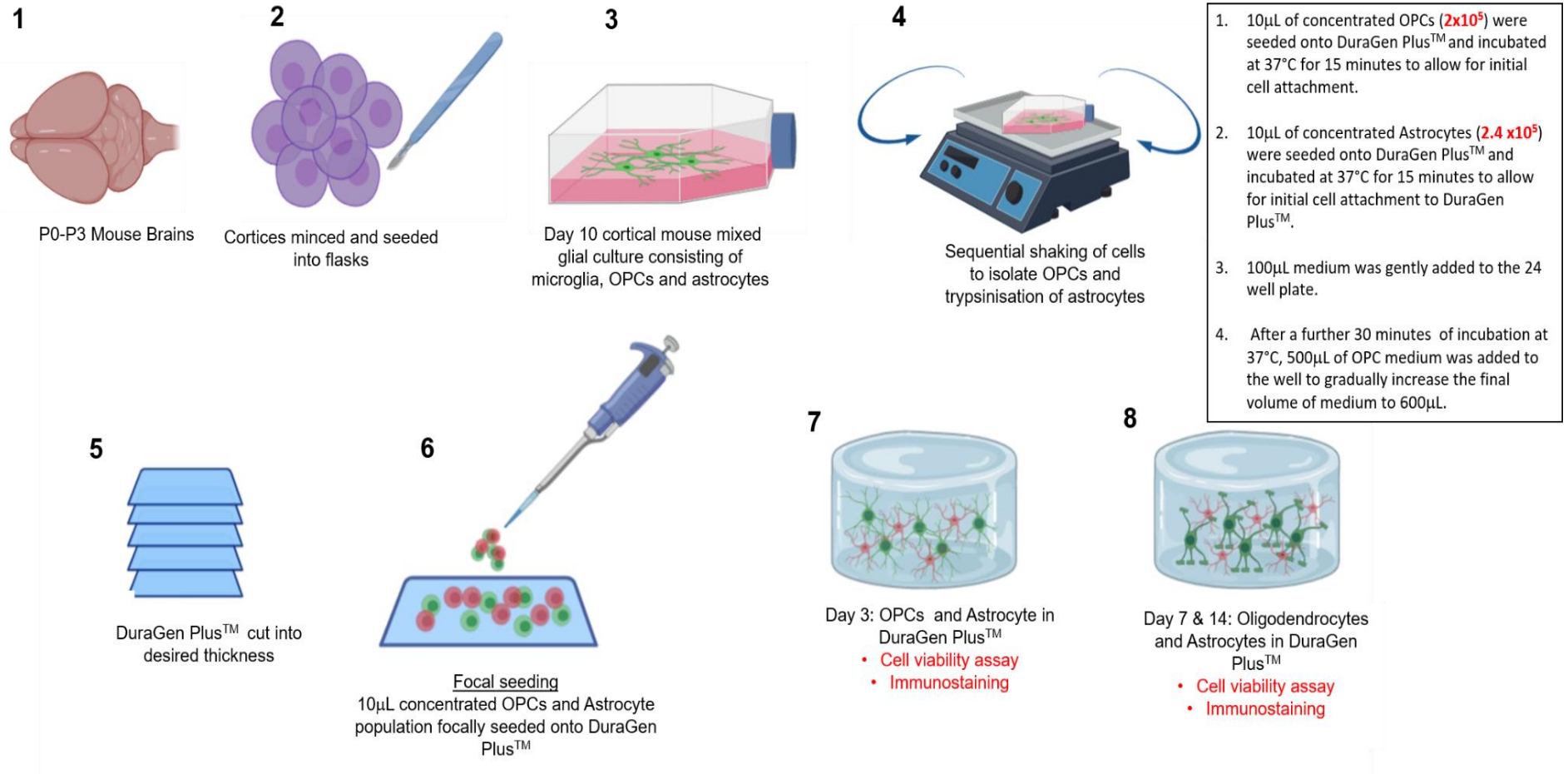

Figure 2.2 Development of oligodendrocyte lineage and astrocyte co-cultures on DuraGen Plus™ constructs using a focal seeding technique.

2.2.6 Generation, seeding and maturation of oligodendrocyte lineage cells on Cellevate scaffolds

Oligodendrocyte lineage cells were isolated and seeded separately from primary rat and mouse mixed glial cultures, via a sequential shaking process on an orbital shaker at 220rpm (4 x g) for 16-18 hours. The cells were then pooled and centrifuged at 1500 rpm (176 x g) for 6 minutes and were resuspended in OPC maintenance medium (see section 2.2.2.2 for components). Next, the oligodendrocyte lineage cells were seeded onto the Cellevate scaffolds which were inserted into a 24 well plate, at a density of 2.5 $x10^5$ cells/mL in 300µL of OPC maintenance medium, per well and left at 37ºC (5% CO_2 and 95% humidified air) for 1 hour to allow for initial cell attachment. An additional 300µL of OPC medium was then added to make a total of 600µL per well. A 50% medium change was conducted every 2-3 days. Figure 2.3 shows a schematic of the random and aligned fibres that cells were seeded on.

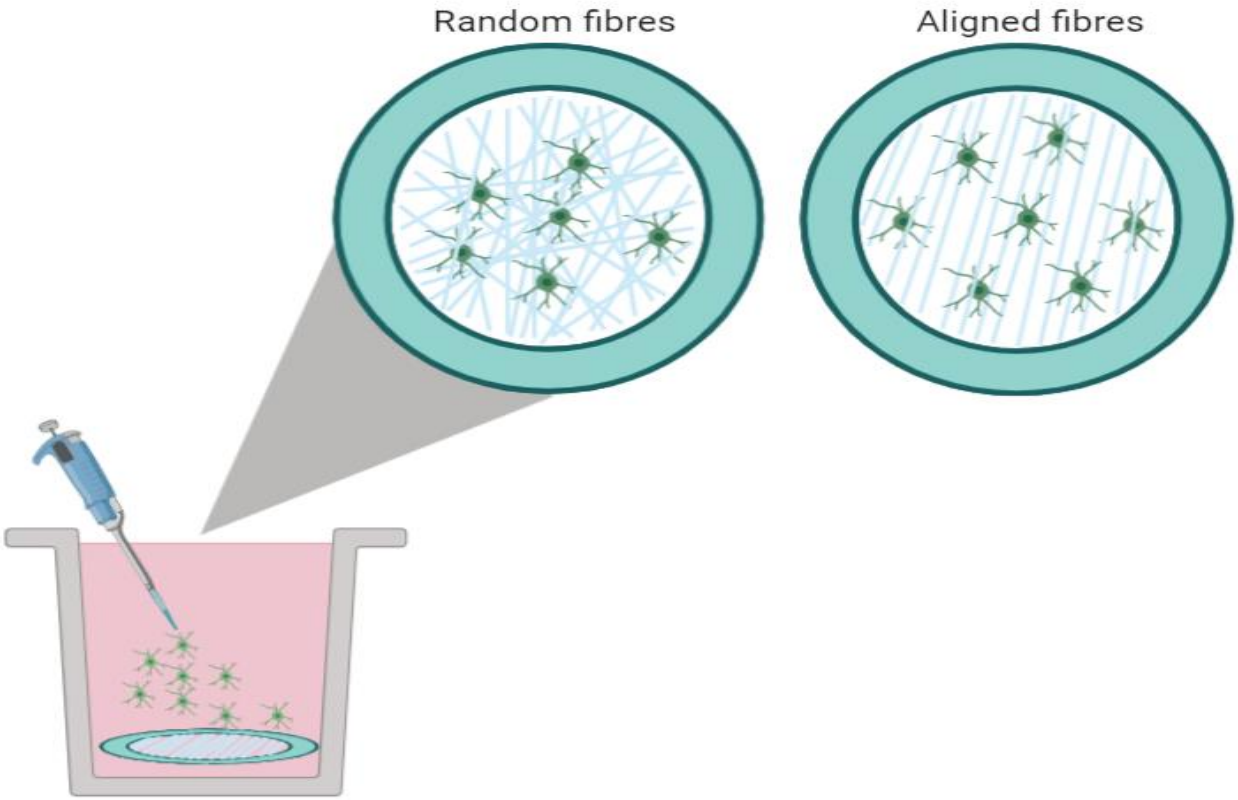

Figure 2.3. Schematic representation of the seeding of oligodendrocyte lineage cells on non-aligned and aligned Cellevate fibres.

After 3 days *in vitro*, the precursor oligodendrocyte lineage cells were induced to mature into oligodendrocytes by using chemically defined medium (see section 2.2.2.3 for components) for a total period of 7 days.

The timepoints chosen to monitor cell viability and assess the morphology of the cells within the scaffolds was 3DIV for the precursors and 7DIV for the mature oligodendrocyte lineage cells.

2.3 Cell Viability Assays

2.3.1 Cell viability assay for Oligodendrocyte lineage cells and neuronal enriched cultures on glass coverslips

For monolayer cells, cell viability was determined by conducting a live/dead assay at desired time points. Prior to the addition of the live/dead components, selected wells were washed 3 times with PBS to remove any cellular debris before and after incubation for 15 minutes (37° C, 5% CO_2/95% humidified air) in 0.3mL/well culture medium. This medium contained calcein-AM which stains viable cells green (4 µM/mL), ethidium homodimer which stains the DNA of dead cells red as it can pass through their membrane (5µM/mL) and the nuclear stain hoechst (1µg/mL), before live imaging of cells.

2.3.2 Optimisation of the cell viability assay for DuraGen Plus™

Selected wells containing cells within DuraGen Plus™, were washed, once with PBS, after the removal of cell culture medium and then they were incubated in a mixed solution of calcein (4 μM/mL), ethidium homodimer (5μM/mL) and Hoechst (1μg/mL), in a final volume of 0.3 mL OPC medium per well. Initially, a 15-minute incubation period at 37°C (5% CO_2/95% humidified air), only resulted in a faint fluorescent signal in trial experiments, therefore the incubation time was increased to 1 hour and wells were washed 3 times with PBS to remove residual live/dead solution. Furthermore, it was found that unfixed DuraGen Plus™ slices that were used to assess cell viability, showed increased cell death with increasing imaging time (indicated by excessive red ethidium homodimer staining), seen in figure 2.4.

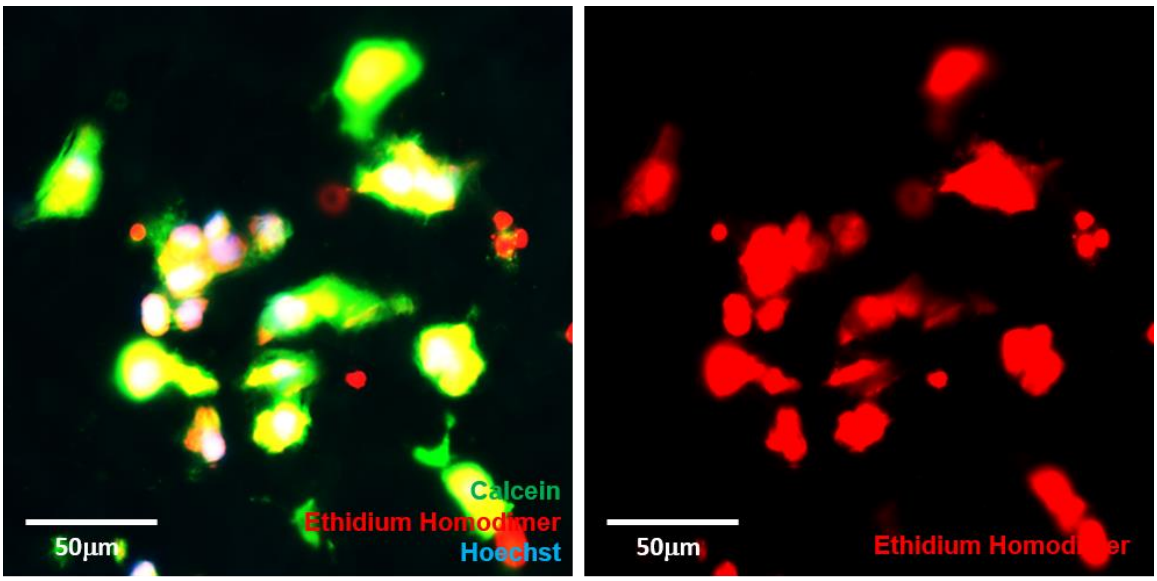

Figure 2.4. Technical difficulties with cell viability assay. Increased cell death with increasing imaging time of cells encapsulated I unfixed DuraGen Plus ™ constructs, resulted in bleed though of ethidium homodimer.

It was therefore decided to fix DuraGen Plus™ slices with paraformaldehyde (PFA) prior to imaging to provide a more accurate representation of cell viability at the experimental timepoints. Therefore, selected DuraGen Plus™ slices were initially incubated with calcein, ethidium homodimer and heoscht, before being fixed for 20 minutes with 4% PFA. The PFA was then removed and the slices were washed 3 times with PBS (5 minutes/wash). This method was taken forward for all subsequent DuraGen Plus™ cell viability assays. In DuraGen Plus™ slices, to identify viable cells, nuclei were counterstained with ethidium homodimer which indicated the dead cells as seen in Figure 2.5 (red arrow). Live cells were distinguished by their calcein stained green cell bodies (Figure 2.5 white arrow) and debris (yellow arrow) was identified by the absence of the co-localisation of the nuclei with ethidium homodimer.

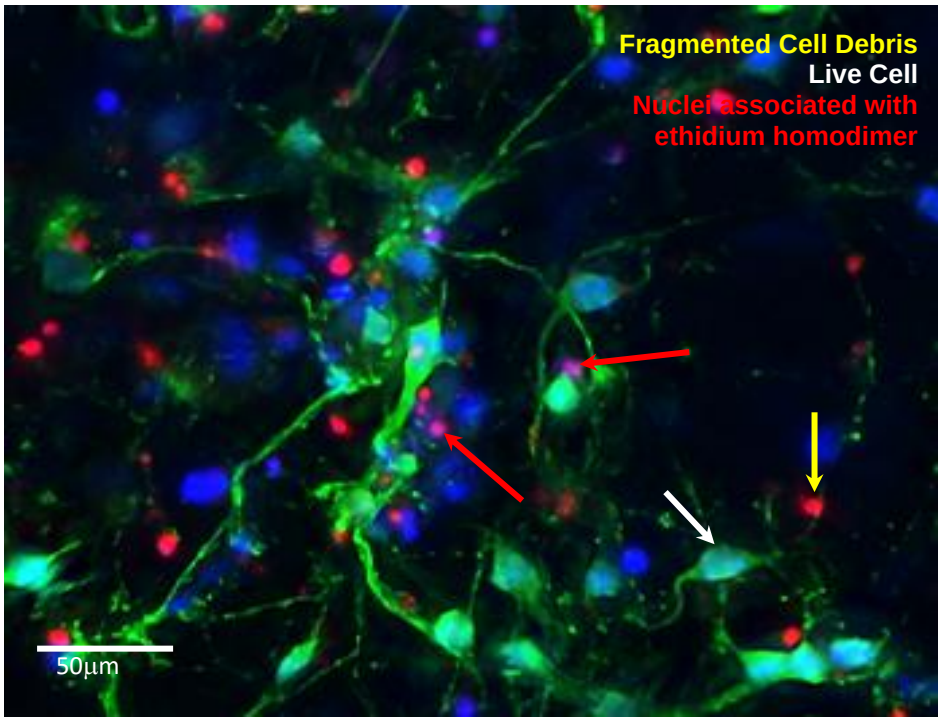

Figure 2.5. Example image demonstrating the classification of live and dead cells. White arrow indicates Calcein stained viable cell. Red arrow indicates a dead cell, with ethidium homodimer colocalised with the nuclei. Yellow arrow demonstrates fragments of cell debris.

2.3.3 Cell viability of oligodendrocyte lineage cells on Cellevate scaffolds

Selected wells were washed once with PBS, prior to the addition of calcein-AM (4 μM/mL), ethidium homodimer (5μM/mL) and hoechst (1mg/mL) in 0.3 mL of culture medium/well and incubated for 30 minutes at 37ºC, 5% CO_2 and 95% humidified air. The wells were then washed 3 times with PBS before being imaged. It was found however that with increased imaging time with unfixed scaffolds, there was increased cell death (indicated by red ethidium homodimer staining). Therefore, the wells were fixed for 20 minutes with 4% PFA and the scaffolds were then washed 3 times with PBS (5 minutes/wash) before being imaged for analysis.

2.4 Immunocytochemistry

2.4.1 Immunocytochemistry on glass coverslips and list of antibodies used for experiments

Cells were rinsed twice with PBS and then fixed with 4% paraformaldehyde (PFA) diluted in PBS (0.3mL/well) for 20 minutes at room temperature (RT), and wells were then washed 3 times with PBS in 5-minute intervals. PFA fixed cells were then incubated with 0.2mL/well blocking solution (5% normal donkey serum in PBS, with 0.3% Triton X-100) for 30 minutes at RT, followed by the addition of primary antibodies, diluted in blocker (0.2mL/well) and incubated at 4°C overnight . For the selective labelling of microglia, the glycoprotein Tomato Lectin was used (Sigma). The primary antibodies used were IBA-1 for microglia (1:200 and 1:2000 respectively), polyclonal anti- glial fibrillary acidic protein (GFAP) (1:500) for astrocytes, NG2 (1:150) for OPCs, Myelin Basic Protein (MBP) (1:200) for

oligodendrocytes, neuron-specific Beta tubulin (Tuj-1) (1:1000) , which is a neuronal cytoskeletal marker, vesicular glutamate transporter 1 (VGlut-1) (1:150) for glutamatergic neurons and GABA (1:500) for GABAergic neurons. Following overnight incubation, cells were washed 3 times with PBS (5 minutes/wash) and then incubated at RT with blocker (0.2mL/well) for 30 minutes. Next, 0.2mL/well of FITC and/or Cy3 conjugated secondary antibody diluted in blocker (1:200), was added to the wells and the cells were incubated at RT for 2 hours, ensuring that they were protected from light to prevent bleaching of slides. Cells were then washed 3 times with PBS (5 minutes /wash) and mounted with mounting medium containing 4',6-diamidino-2-phenylindole (DAPI). Finally, coverslips were sealed with nail varnish prior to imaging.

2.4.2 Immunocytochemistry optimisation for cells encapsulated in DuraGen Plus™

Cell fixation and immunocytochemistry protocols for cells in DuraGen Plus™, including the dilutions of primary and secondary antibodies were the same as those used for staining monolayer cells on coverslips (as seen in section 2.4.1) with minor adjustments to the protocol to achieve optimal staining. Specifically, it was found that using mounting medium which contained DAPI, stained the DuraGen Plus™ collagen fibres blue which thus created background fluorescence when imaging the cells. Therefore, Hoechst (1μg/mL) was used instead as a nuclear stain to circumvent this issue. Hoechst was added to PBS and 0.2mL of solution was added per well and incubated in the dark at RT for 30 minutes. The wells were then washed 3 times with PBS (5 minutes /wash) and mounted with Vectashield fluorescence mounting medium and sealed with nail varnish prior to being imaged.

2.4.3 Immunocytochemistry of oligodendrocyte lineage cells on Cellevate scaffolds

Cellevate scaffolds seeded with cells were subjected to the same cell fixation and immunocytochemistry protocols used for staining cells in DuraGen Plus™ (as seen in section 2.4.2) The primary antibodies used were NG2 (1:150) for OPCs and MBP (1:200) for oligodendrocytes. Hoechst (1μg/mL) was used as an alternative to the nuclear stain DAPI to prevent the Cellevate fibres staining blue.

Prior to imaging the cells within the scaffolds, the scaffolds had to be removed from their brackets for imaging purposes. The manufacturer protocol advised that the scaffolds should be cut out of their lock ring. This is a circular bracket that the scaffold insert sits between to prevent it from collapsing in on itself as figure 2.6 shows.

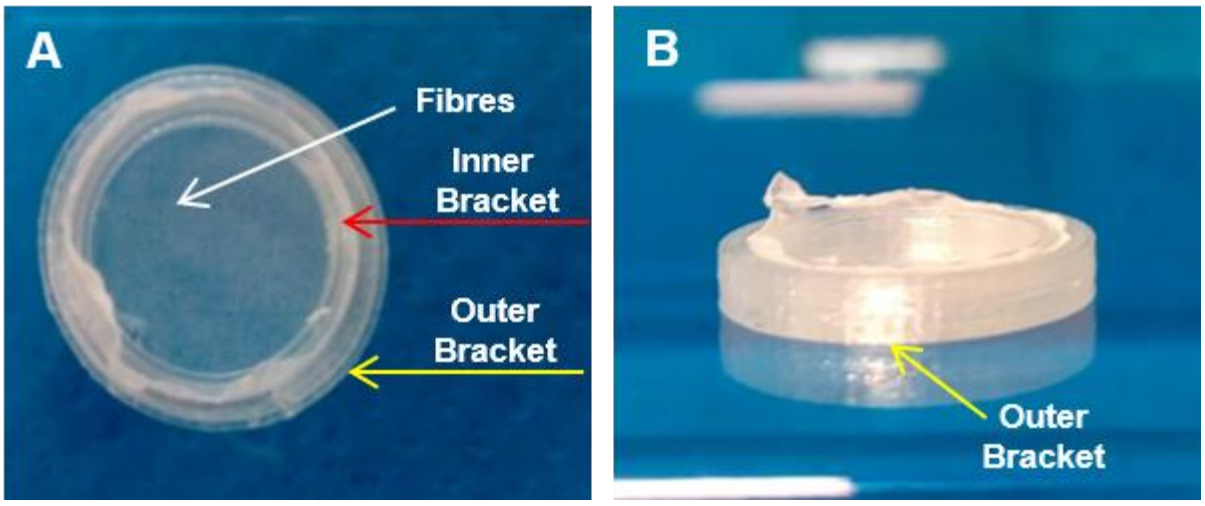

Figure 2.6. Cellevate scaffold annotated demonstrating the fibres (white arrow), inner (red arrow) and outer brackets (yellow arrow).

Cutting out the cell-seeded scaffold proved to be challenging and consequently, cells were damaged during this process. Therefore, a different approach was trialled. This involved separating the brackets so that the scaffold insert could then gently be

peeled away with tweezers and then mounted onto a glass slide with Vectashield florescence mounting medium, before being sealed with nail varnish, and imaged for analysis. Figure 2.7 below illustrates how this was achieved.

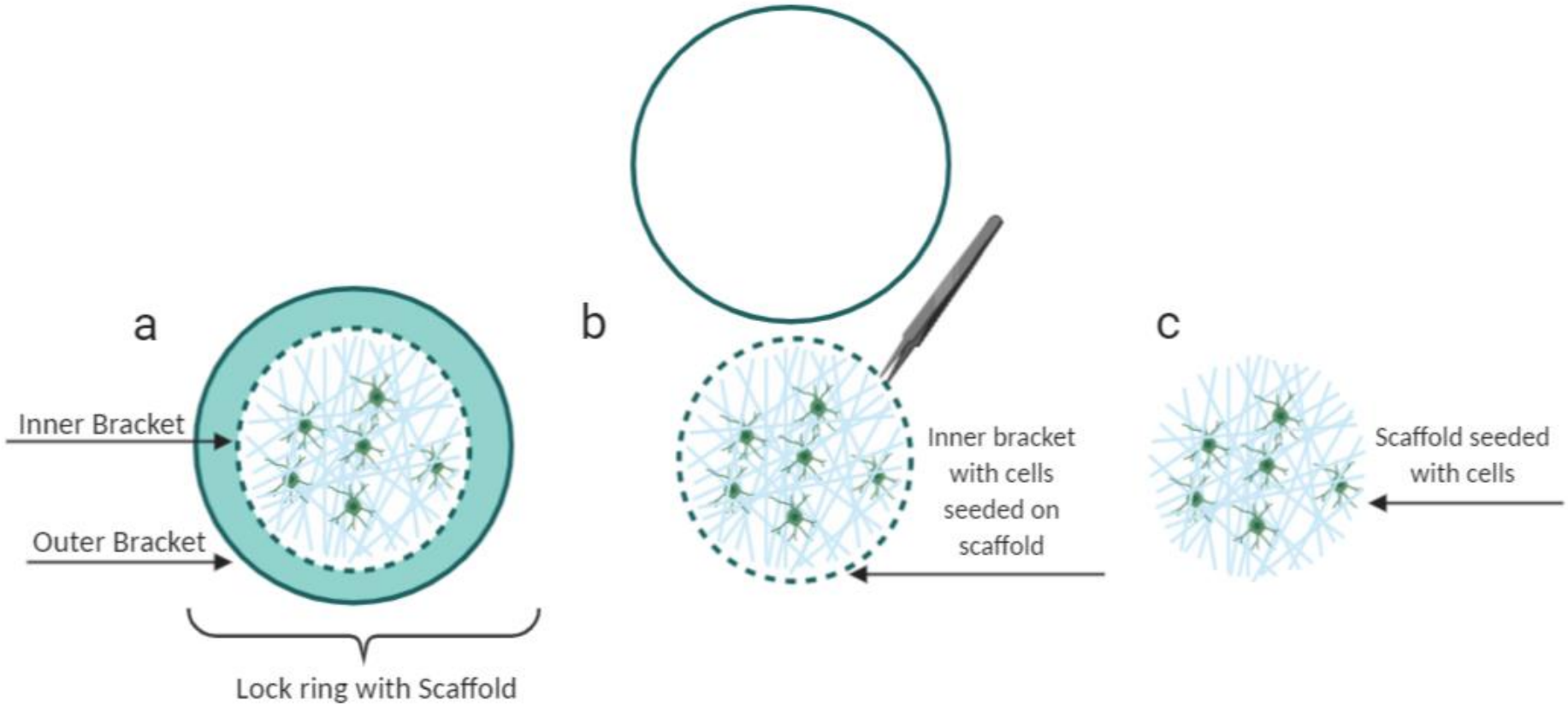

Figure 2.7. Deconstruction of cell seeded Cellevate scaffolds for mounting onto glass slide. **a)** shows the cell-seeded scaffold with the lock ring. **b)** The brackets were separated, and the scaffold was peeled away from the inner bracket with tweezers. **c)** Cell-seeded scaffold was then mounted onto a glass slide.

2.4.4 SEM of rat oligodendrocyte lineage cells seeded on Cellevate scaffolds

For Scanning electron microscopy (SEM), the aligned and non-aligned Cellevate scaffolds seeded with primary rat oligodendrocyte lineage cells, the cells were fixed with 2.5% glutaraldehyde in 0.1M sodium cacodylate (pH 7.4) containing 2mM calcium chloride for 2 hours. The fixative was then washed off with sodium cacodylate 3 times in 5-minute intervals for a total of 15 minutes. The samples were then placed in 1% osmium tetroxide, diluted in distilled water for 1 hour, followed by 6 washes in distilled water in 5-minute intervals. Next, saturated aqueous thiocarbohydrazide, diluted in distilled water was added for 20 minutes to the samples, and samples were then washed a further 6 times in distilled water in 5-minute intervals. 1% osmium tetroxide was added again to the samples for 2 hours and then washed 6 times in distilled water in 5-minute intervals. The samples were further placed again in saturated aqueous thiocarbohydrazide solution for 20 minutes with the same wash steps as before. The last stage of this process was to again immerse the samples in 1% osmium tetroxide for 2 hours with the same washing process.

Next, the samples were either immersed in 70% ethanol at 4^{o}C overnight, ready to be processed further for the following day, or the wells were dehydrated with a series of ethanol. This involved dehydrating the samples with 80%, 90% and 100% ethanol respectively, for 30 minutes for each ethanol percentage. Following this, the samples were further dehydrates with 100% dry ethanol for 30 minutes (ethanol was dried using a molecular sieve).

The samples were then critical point dried (CPD) from dry ethanol using liquid carbon dioxide as the exchange fluid, to be compatible with the vacuum in the SEM microscope. This is because water would disrupt the vacuum and image, ultimately causing deformation or collapse of the structure of the sample. Six changes of liquid carbon dioxide over a period of 1.5 hours was conducted.

The purpose of CPD was to preserve the micro and nano surface structure of the sample which would otherwise be damaged due to the surface tension when liquids change to a gaseous state (Leica, 2020). Lastly, the samples were then attached to scanning stubs using silver DAG electroconductive paint/ The samples were then analysed using a Hitachi S-4500 filed emission electron microscope operated at 2-3 kV.

2.5 Image /processing, deconvolution of images

2.5.1 Optimisation of imaging on DuraGen Plus™ compressed vs uncompressed

3D imaging of unmounted DuraGen Plus™ slices proved difficult as cellular morphology within the construct could not be observed due to increased diffraction of light throughout the construct. The generated images provided little information about cellular morphology and quantification was also problematic. Therefore, we next trialled compressing the DuraGen Plus™ slices between two glass coverslips with Vectashield mounting medium, to attempt to bring all the DuraGen Plus™ fibres into one plane. As a result, the quality of the 3D images generated for the DuraGen

Plus™ construct improved as both the cells within the construct and the fibres were easier to visualise because of the decreased diffraction of light.

2.5.2 Phase and Fluorescence microscopy: 2D and 3D imaging of Cells on Glass, DuraGen Plus™ and Cellevate for cellular morphology

For 2-dimensional (2D) quantification, immuno-stained-glass slides were imaged using fluorescence and phase-contrast microscopy on a Zeiss, Axioscope A1 microscope with an AxioCam ICc1 digital camera processed with Axiovision software (Carl Zeiss Microimaging GmbH, Goettingen, Germany). Quantitative imaging of DuraGen Plus™ and Cellevate scaffolds was performed using an Axio Observer.Z1 equipped with an AxioCam MRm powered by Zen 2 (blue edition) software (Carl Zeiss MicroImaging GmbH, Goettingen, Germany) for 3D imaging.

For each DuraGen Plus™ and Cellevate construct, five fields were chosen for imaging (200X magnification) and for each field, a stack of images were taken, with parameters set as the first fibre seen at the bottom of the DuraGen Plus™/ Cellevate slice, and the last fibre at the top to produce a Z stack of set intervals of 5µm for cell viability assays and 2µm for ICC constructs. These Z stacks could then be processed as single images or used as videos to show the distribution of cells throughout the construct. Figure 2.8 below illustrates how 3D z-stack images were taken on a piece of DuraGen Plus™/ Cellevate.

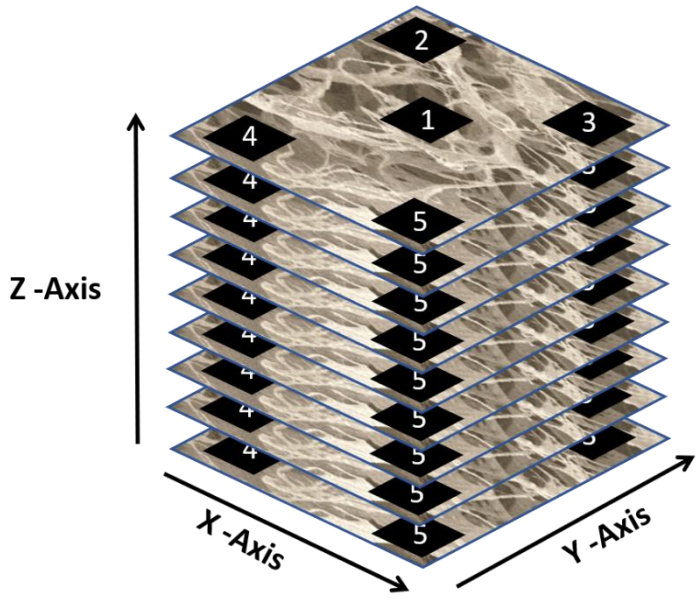

Figure 2.8. 3D Z stack imaging for the quantification of cells. Five separate fields as shown in the diagram (1-5) were imaged for cell quantification.

2.5.3 Directionality analysis of oligodendrocyte lineage cells on non-aligned and aligned Cellevate scaffolds

Analysis for the alignment of the Cellevate fibres was conducted using a directionality plug-in for ImageJ Fiji. The plugin was used to deduce the preferred orientation of the Cellevate fibres. The plug-in computed a histogram to indicate the amount of fibres what were oriented in a particular direction and this was expressed as an angle (°). Fibres that were isotropic, i.e. show no directionality were expected to produce a flat histogram whereas fibres with a preferred orientation were expected to produce a histogram with a peak at that orientation.

The brightfield Cellevate fibres and their counterpart florescent cell images were analysed separately with the directionality plug-in using, low magnification images. A four courier components method was used to calculate the orientation of the Cellevate fibres and the florescent stained cells using , a 90° to -90 ° angles and a results table and orientation map was generated to indicate the amount of fibres and cells at a specific direction.

To confirm that cells on the Cellevate fibres were either aligned or non-aligned, the exact orientation peak i.e. the angle in which most cells are orientated at was calculated using the formula:

$$IF(AND(A2 > A1, A2 > A3),\text{"PEAK","0"})$$

The data used in the formula was then rotated so that the peak corresponded with 0°, in order to normalise the data so that comparisons for directionality could be made between biological repeats for both the aligned and non-aligned constructs.
The data was plotted as an XY scatter graph with the angle (0°) on the X axis and the amount of alignment (calculated by the histogram) on the Y axis. The number of cells with the particular alignment was calculated by the histogram.

2.5.4 Deconvolution of Z stack images

For the purpose of visualisation of cells in DuraGen Plus™ and Cellevate scaffolds, Z stack imaging was required. This method was chosen as it was expected to provide a number of images from different planes in the Z-axis (see figure 2.8 for z-stack diagram). However, the images were unclear due to the thickness and opaque nature of the biomaterial, which made it difficult to visualise the cell body and cellular processes in the same Z stack plane.

To circumvent this issue, all Z-stack CZI images were deconvolved with Huygens Professional version 19.04 (Scientific Volume Imaging, The Netherlands, http://svi.nl), using the CMLE algorithm, with signal to noise ratio (SNR):40 and maximum 50 iterations.

When an image is originally produced, it is a convoluted microscopic image which creates some blurring. Convolution (blurring) of an image uses the mathematical equation, g= h x f where the image, g is produced for the convolution of the real light sources, f (the object) and the point spread function (PSF) h. Blurring of a 3D image is called the point spread function (PSF) and this plays an essential function for the formation of fluorescent images. A wider PSF leads to a greater blurred 3D image (Huygens, 2020).

Deconvoluting an image involves enhancing the signal to noise ratio (SNR) and the resolution. This is executed by reassigning light that is out of focus due to the original convolution process, that creates blurring, and noise created by photons. Deconvolution works by putting light back to its original location which creates a better representation of the real object which is visually clear. The Classic Maximum Likelihood Estimation (CMLE) algorithm used in the Huygens software, for the deconvolution process, allows for the fine tuning of the SNR. In addition, it improves the brightness and contrast of the 3D image, thus producing a clearer image. The 3D, deconvoluted image was then viewed in the 2D ortho slicer and exported as a JPEG image (Huygens, 2020). A comparison of images before and after the deconvolution process is illustrated in figure 2.9 below. These images were solely used for display purposes. All analysis was conducted using the original, uncompressed z stack images.

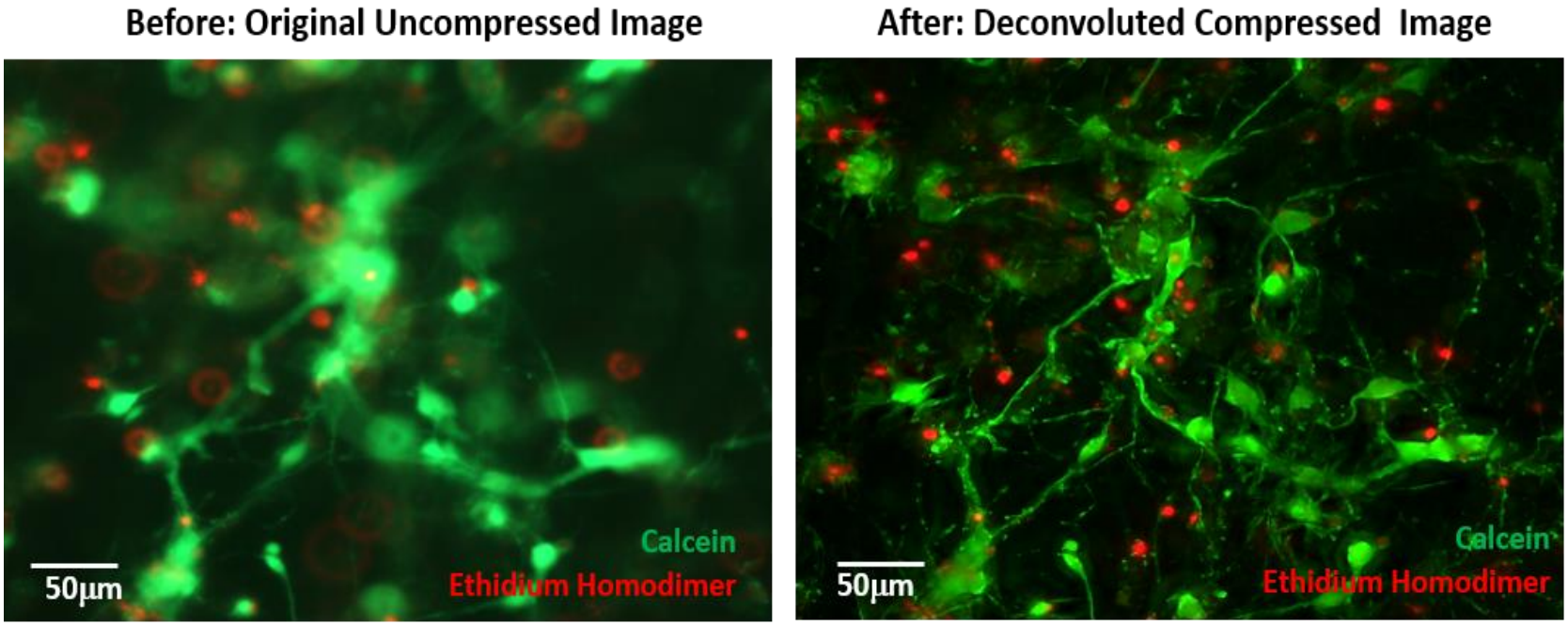

Figure 2.9. Illustrating the difference in visual clarity of the Z stack images before and after deconvolution with Huygens software.

2.5.6 Image analysis and cell quantification

To quantify cellular viability of cells within the DuraGen Plus™ and Cellevate scaffolds, 3D compressed z-stack images, that were not deconvoluted, were used. Live cells, which stained green, were identified with Calcein staining. Dead cells, which stained red, were identified using ethidium homodimer. A total cell count including live and dead cells was quantified from 5 fields and a percentage viability was calculated. Results were tabulated as a bar chart using Graphpad Prism software for a minimum of n=3/4 (see section 2.3).

For identification of specific cell types on glass coverslips and within DuraGen Plus™ and Cellevate scaffolds, histological markers were used to either identify, neurons, astrocytes and oligodendrocyte lineage cells. A total cell count from 5 fields per construct, of immune stained cells was taken along within non-stained cell bodies that had nuclei, to calculate an overall percentage purity of the cells. Results were tabulated as a bar chart using Graphpad Prism software for a minimum of n=3/4.(see section 2.4).

2.6 Statistics

2.6.1 Statistical analysis for oligodendrocyte lineage cells seeded independently and as co-constructs with astrocytes; cortical neuronal enriched cells on DuraGen Plus™

For each experimental timepoint for oligodendrocyte lineage cells seeded alone, or as co-constructs with astrocytes, results were recorded as the mean and the standard deviation of the mean. For cell viability on DuraGen Plus™, statistical analyses were conducted using Graphpad Prism software (CA, USA). with a one-way ANOVA and Bonferroni's MCT were used to determine whether there was a significant difference in viability between 3,7 & 14 DIV viability in the scaffold. To compare the percentage of NG2 and MBP positive cells on the scaffold at 3,7 & 14 DIV, a one-way ANOVA and Bonferroni's MCT was applied using Graphpad Prism software (CA, USA).

For cortical neuronal cells within the scaffold, results were recorded as the mean and the standard deviation or the standard error of the mean. A one-way ANOVA and Bonferroni's MCT was produced using Graphpad Prism software (CA, USA) and were used to determine whether there was a significant difference in cell viability between 3,6 & 9 DIV neuronal enriched cells in the scaffold.

2.6.2 Statistical analysis for rat and mouse Oligodendrocyte lineage cells seeded onto Cellevate scaffolds

For statistical analysis of primary rat and mouse oligodendrocyte lineage cells seeded onto aligned and non-aligned Cellevate scaffolds, results were recorded as

the mean and the standard deviation of the mean. Data for cell viability was analysed using Graphpad Prism software (Ca, USA) using an unpaired t-test with Welch's correlation to determine whether there was a difference in viability between the 3 and 7 DIV data for cells on non-aligned and aligned scaffolds.

Additionally, a one-way ANOVA and Bonferroni's MCT using Graphpad Prism software (CA, USA) was used to compare the expression of NG2 and MBP on non-aligned and aligned scaffolds at 3 & 7 DIV respectively.

Chapter 3

Development of new culture systems utilising post-natal murine brains to isolate major neural cell populations

3.1 Introduction

3.1.1 The need for in vitro primary cortical neural culture models

The development and the improvement in techniques to generate cortical cultures *in vitro* has resulted in a greater understanding of the structure, and biochemical functions of the brain (Mecha *et al.*, 2011). In particular, the development of the mixed glial model originally created by (McCarthy and De Vellis, 1980) has allowed neuroscientists to use it as an investigative tool at a cellular and molecular level, to observe the functions and properties of glial cell types within the CNS, and particularly, how they respond to insult, and their response towards a therapeutic biomaterial (Mecha *et al.*, 2011).

The mixed glial culture system is both robust and reproducible in terms of generating cortical derived glial cells (McCarthy and De Vellis, 1980). The model commonly uses rat cortices to generate a mixed glial culture, consisting of a bed layer of astrocytes, an intermediate layer of oligodendrocyte precursor cells (OPCs) and loosely attached top dweller microglia. The glial cells can be derived via a sequential shaking process for isolated enriched populations of microglia, OPCs and mild trypsinisation for astrocytes (McCarthy and De Vellis, 1980; Chen *et al.*, 2007). Isolated populations of the glial cell types from the mixed glial model are achievable due to the manner in which the culture stratifies and the differential adherent properties of the glia cells (Chen et al., 2007). The microglia are loosely adhered to the basal layer of astrocytes in comparison to the OPCs. Therefore, microglia detach

between 60 to 120 minutes on the orbital shaker in comparison to 16 to 18 hours for OPCs. Astrocytes require mild trypsinisation as they are strongly adhered to the surface of the flask which is achieved by the cleavage of the peptide bonds of lysine and arginine at the c-terminal of the astrocytes.

This mixed glial model has broad applicability in the regenerative neurology field. Examples include using glial derivatives of the mixed glial model for studying the pharmacological effects of drugs, such as microglial response to pro-inflammatory cytokines (Obuchowicz *et al.*, 2006).

The primary rat mixed glial model has also been used by Giorgi-Coll *et al.*, (2017) to understand the pathophysiology of acute traumatic brain injury (TBI) and SCI post injury, specifically to investigate metabolic performance of mixed glial cells with mitochondrial dysfunction which contributes to pathological changes following traumatic CNS injury. Giorgi-Coll *et al.*, (2017) pursued this by developing a reductionist in vitro model of mitochondrial dysfunction by exposing mixed glial cells to mitochondrial complex I inhibitor rotenone. Analysis involved measuring extracellular metabolites such as glucose, lactate, and pyruvate (LPR), which are clinical biomarkers used to determine the outcome of TBI. The evidence suggested that rotenone created metabolic deficits by the elevation of LPR which is indicative of increased glycolytic activity and reduction of mitochondrial function, which is associated with poor clinical outcome. The supplementation of succinate, which plays a key role in metabolism for glial cells, improved the metabolic deficits created by rotenone, by directly interacting with the mitochondrial electron transport chain within the cells. This in turn allows a faster route to ATP production through oxidative metabolism and has been considered as a possible treatment for TBI. This study

confirmed how a mixed glial cellular model can be applied for developing treatment methods for TBI.

The model has also been used for nanomaterial bio-screening testing which involved observing the effects of magnetic nanoparticle uptake in microglia, OPCs and astrocytes independently or as co-cultures to investigate their endocytotic potentials of particle uptake by the cells which is essential, as the glial cell response is a key predictor for how successful a therapy may be (Jenkins *et al.,* 2015).

As the mixed glial model consists of multiple glial types, the model can also be used for developing 3D in vitro models for either studying glial cell morphology and interaction in a 3D environment, or for studying neuroinflammation, to investigate the effects of gliosis, cytotoxicity and glial scar formation, which is necessary, as inflammation is a major component in both acute and chronic CNS conditions (Koss *et al.*, 2017; Watson *et al.*, 2017).

3.1.2 The utilisation of primary rat mixed glial cultures for biomaterial encapsulation

Tsui *et al.*, (2020) for example used a primary rat mixed glial culture, derived from post-natal day 1 rat cortices, to investigate the impact of mechanical forces associated with mild traumatic brain injury, created by rapid head rotation, and they specifically observed the inflammatory response by microglia. For their study, primary rat glial cells and a volume of 20 x 10^6 cells/mL were encapsulated into a 3D HAMA hydrogel, consisting of 1% v/w methacrylated hyaluronic acid and basal lamina protein mixture, which allowed for the intake of nutrients and removal of waste,

originally created by Jeffery *et al.*,(2014). Their aim was to mimic rapid head rotational forces with an apparatus capable of delivering 45 radians per second (rad/s), which is angular velocity that in literature, is associated with mild TBI. These forces were applied to the 3D scaffolds *in vitro* to investigate whether this motion could activate microglia, and transform the cells from their resting state, where they have multiple projections which protrude from the cell body, into their amoeboid form morphology. The latter morphology has less projections that are characteristically associated with the activation of microglia in response to injury in an affected region. The results from the 24 and 48 hour time points however, showed no measurable microglia cell reactivity detected, which was measured by nitric oxide secretion and pro-inflammatory release of tumour necrosis factor and interleukin 1-beta, in addition to the proportion of amoeboid microglia. Thus suggesting that rapid rotational forces alone do not activate microglia. Tsui *et al.*, (2020) suggested that microglial activation may not have been observed due to the presence of oligodendrocytes and astrocytes within the construct, which may have elicited dampening the activation of microglia. This study however did demonstrate how a rat mixed glial culture could be used as a 3D *in vitro* model to reduce the costs associated with *in vivo* studies, thereby minimising animal usage.

Jeffery *et al.*, (2014) utilised the HAMA hydrogel to encapsulate primary rat microglia and astrocytes, derived from a mixed glial culture, to produce a robust and reproducible *in vitro* model of glial scarring. Specifically, they investigated the foreign body response of microelectrodes, which are used for therapies such as deep brain stimulation in the treatment of patients with advanced Parkinson's disease, to improve symptoms such as tremors and dyskinesis (Themistocleous *et al.*, 2017). 1×10^7 cells/mL were encapsulated into the matrix which included the insertion of a

microelectrode. Viability and the inflammatory response were assessed over a 2-week period for the glial cells. An initial increase of microglia at the electrode site was reported, evident by increased cell density at the site and amoeboid morphology of microglia which indicates their activated stage. This was followed by astrocytes later reacting to the electrode, being observed in a linear pattern, becoming hypertrophic and forming a dense glial scar around the electrode.

Again, the benefits of using a primary mixed glial culture have been demonstrated in the establishment of a potential 3D *in vitro* model for assessing glial scarring when microglia and astrocytes are introduced to foreign objects.

The primary rat mixed glial culture has also been used by Koss *et al.*,(2017) to produce a hydrogel incorporated with hyaluronic acid and basal lamina proteins, to generate a 3D model encapsulated with microglia, oligodendrocytes and astrocytes, as a model to study glial cell interactions that result in glial scar formation. For this,$1x10^7$ mixed glial cells, derived from 14 DIV cultures were encapsulated into individual hydrogels, with results highlighting that the glial cells within the 3D platform were morphologically distinct from 2D cultures. Oligodendrocytes within the construct appeared to have round processes protruding radially from their cell body, and seemed to extend their processes along the established, interconnected network of astrocyte processes that were branched throughout the scaffold. Microglia were observed to have fine processes protruding from the cell body which is consistent with *in vivo* morphology, and were dispersed throughout the scaffold (Koss *et al.*, 2017). The authors here, had demonstrated the robustness and significance of a primary rat mixed glial culture for designing a 3D model to investigate glial bioreactivity which includes cytotoxicity and neuroinflammation that collectively impairs the regeneration of damaged CNS tissue.

Isolated cell populations of mixed glial derived cells have also been encapsulated in biomaterials to investigate the cellular response to the material, in the hope of usage as a potential avenue for cellular therapies.

Moshayedi *et al.*,(2014) utilised primary rat astrocytes and microglia, derived from a P2-P3 rat mixed glial culture, and seeded the cells within a polyacrylamide substrate of varying mechanical stiffnesses of 100Pa which mimics brain tissue elasticity and on stiffer substrates of 30kPa and 10kPa, in order to investigate the foreign body reaction to hydrogels, by observing glial cell activation and their inflammatory response. 50,000 and 100,000 astrocytes and microglia respectively were co-seeded onto individual gels of the stiffnesses referred to above, with results showing that cell morphology was dependent on substrate stiffness. The 100Pa substrate contained cells with spherical morphologies, with some astrocytes demonstrating star-like morphologies as seen *in vivo.* Glial cells on the stiffer substrates were dispersed throughout the construct and produced significantly more astrocytes with extended processes, which is a phenotype of activated cells, than those on the softer 100Pa substrate. Western blot analysis showed that there was also an upregulation of inflammatory genes and proteins pro-interleukin 1 beta and pro-caspase 1, from the glial cells in the stiffer hydrogels which may contribute to an inflammatory response to biomaterials *in vivo*. The benefits of using a primary mixed glial culture here are evident as Moshayedi *et al.*,(2014) had demonstrated how the culture has been valuable to provide possible indications of glial inflammatory responses that may be dependent on the stiffness of a substrate.

Balasubramanian *et al.*, (2016) utilised astrocytes derived from P1 to P3 cortical mice mixed glial cultures to explore their heterogenous response to regulating metabolic homeostasis, synaptogenesis, and neurotransmission in a 3D

environment. Disruptions to astrocyte maturation *in vivo* can result in neurodevelopmental and neurodegenerative problems and also unfavourable responses to SCI and TBI. However, the mechanisms that direct these functions have not been thoroughly investigated to determine what occurs to the heterogeneity of the cells within a biomaterial. For this study, $7.5x10^{5}$ cells/mL were seeded into 3D collagen hydrogels to examine astrocyte morphologies within the scaffold and these were compared against astrocytes grown on a 2D collagen coated coverslip, at a density of $7.5x10^{3}$. Additionally, the cells were seeded onto their respective substrates in serum free and serum containing medium, as the authors stated that the presence of serum may influence astrocyte morphology and in turn, their function. Viability was first measured at 4 DIV for the cells on the 2D and 3D substrates with 90% and 84% respectively reported. Next, GFAP expressing astrocytes within the 3D and 2D environments were classified into four morphological groups *in vitro* which were round, bipolar, stellate and putative perivascular-like astrocytes. Immunocytochemistry for cells in serum and serum free medium, determined that at 4DIV, astrocytes grown in a 3D environment were predominantly round with a few bipolar cells. By 10 DIV, the cells had transformed into mature round, stellate and putative perivascular cells, with the latter situated near blood vessels *in vivo* as illustrated in Table 3. Astrocytes on the 2D substrate however shifted predominantly from round and bipolar morphologies to stellate, with no evidence of perivascular morphologies Balasubramanian *et al.*, (2016).

Table 3.0. Astrocyte profile morphologies at 4 and 10 DIV in serum or serum free medium in a 3D collagen hydrogel (Balasubramanian et al., 2016)					
	Astrocyte Morphologies (%)				
		Round	**Stellate**	**Bipolar**	**Perivascular**
4 DIV	**Serum containing media**	83%	6%	13%	0%
	Serum free media	91%	4%	5%	0%
10 DIV	**Serum containing media**	71%	10%	8%	11%
	Serum free media 3D	73%	9%	5%	13%

By utilising a mouse mixed glial culture, Balasubramanian *et al.*, (2016) have been able to isolate a population of astrocytes, in order to create quantitative data, demonstrating the importance of utilising 3D cultures for supporting the heterogeneity of astrocytes *in vitro*. This is to develop a better representation of the heterogenous profiles of the cells *in vivo,* as they are required to investigate the response of astrocytes in traumatic SCI for regenerative neurology research, and additionally to explore their potential for therapeutic interventions.

Less commonly used primary mixed glial models that have been investigated involve using rabbit cortices in order to derive microglia, for the purpose of developing an *in*

vitro cell model to study HIV-I infection in the CNS (Hassan *et al.*, 1991) . HIV-I infects glial cells and specifically microglia as HIV-I infection is characterised as the aggregation of microglial nodules and multinucleated giant cells, where multiple microglia combine. To study the immunopathogenesis of HIV-I infection and the possible roles of microglia in this infection, the characterisation of the cells *in vitro* was essential. Hassan *et al.*,(1991) therefore modified McCarthy and De Vellis's, (1980) protocol by enzymatically dissociating postnatal day 1 rabbit cortices to generate a mixed glial culture, rather than using mechanical dissociation. Microglia were then isolated 3 weeks after initial cell seeding as a mixed glial culture. The cells were seeded at a density of $2x10^5$ cells/coverslip and maintained *in vitro* for a further 3 weeks. The microglia were analysed for the presence of mononuclear cells and also stained positive for the expression of the enzymes nonspecific esterase and acid phosphatase. These enzymes were stated as being shared characteristics of microglia, derived from both human-fetal and mice cortices.

Additionally, Hassan *et al.*,(1991) tested for the presence of CD4 receptors on the cell surface which are involved in the binding and entry of HIV-I into the cell. The authors however reported that there were no CD4 receptors on the rabbit microglia and stated that HIV-I infections in rabbits may occur via a separate mechanism that may not involve CD4 receptors. Hassan *et al.*,(1991) supported this statement with reference to an account of HIV-I entry into human cells which lack CD4 receptors. Overall, the authors believed that there was scope to develop an *in vitro* microglia model, derived from rabbit mixed glial cultures to study HIV-I in the CNS and thus, this demonstrates the benefits of utilising a mixed glial culture for diseases affecting the CNS.

Alnasser *et al.*,(2018) also used the same rabbit mixed glial culture to observe the response of microglia within the mixed glial model, against polyamidoamine (PAMAM) dendrimers which are nanoparticles with potential for use as a drug delivery vehicle and also as a diagnostic tool. The rationale was to gain further insight into the mechanisms that allow the uptake of dendrimers within resting and activated microglia as the activated glial cells which mediate CNS neuroinflammation, have shown to accumulate dendrimers. Alnasser *et al.*,(2018) accomplished this by determining and quantifying dendrimer uptake, using confocal microscopy and flow cytometry of the fluorescently tagged dendrimers. Their analysis showed that 1-hour post incubation, the dendrimers entered microglial cells predominantly using the endocytotic pathway and that the activated microglia (LPS-treated) engulfed more dendrimers than the resting microglia (38% vs. 28% respectively). However, by 24 hours, the extent of uptake was similar for both resting and activated microglia. This study provided insight into mechanisms that are involved in glial cell uptake of dendrimers, with the possibility of the rabbit mixed glial model being used to further optimise dendrimer based drug delivery for targeting glial cells in the CNS, in order to treat CNS conditions.

3.1.3 The use of murine mouse cortices as an alternative for rat mixed glial cultures

The literature described thus far has shown the multiple benefits of employing a primary, cortical mixed glial culture for investigating pathologies associated with CNS disorders and how the mixed glial model can be used for testing therapies to repair the damaged regions of the CNS.

As referred to in the general introduction and evident in references within this chapter, studies using a mixed glial culture typically use rat cortices due to their larger cortice size which yields greater cell numbers. There are however multiple advantages to employing a mixed glial culture, derived from mouse cortices. These include financial benefits as mice are cheaper to maintain than rats. In addition, mice can also be genetically modified to mimic a range of neurological diseases (Ellenbroek and Young, 2016).

Mice are of great use for techniques such as optogenetics which involve genetically modifying specific sets of neurons for either inhibition or stimulation of certain neuronal pathways. Additionally, although mice are 8 to 10 times smaller than rats, this is an advantage for drug development studies (Ellenbroek and Youn, 2016). Therefore, these studies would be more cost effective to carry out on mice than using rats as dose dependency of a drug is based on body weight (Ellenbroek and Youn, 2016).

Furthermore, there are similarities in cortical developmental timelines for neurogenesis of both rat and mouse brains , as seen in Table 3.1 and thus, it is predicted that using a mouse mixed glial culture may generate comparable results to that of the rat mixed glial model (Liggett, 2004; Pressler and Auvin, 2013). Therefore, using a mouse mixed glial model would complement the existing rat model without compromising the robustness and reproducibility of the model (Liggett, 2004; Pressler and Auvin, 2013).

Table 3.1. Comparison of the development of the cortex between rats and mice (Pressler and Auvin, 2013)		
Parameters	**Rats**	**Mouse**
Neurogenesis: Birth	E12-E15	E11-E13
Neurogenesis: Waiting	E16-E17	E14-P0
Neurogenesis: Death (0-80% cells)	E20-P30	E18-P21
Neuronal migration	Mainly observed between E19 and E21	The preplate (PP) appears at E12. At E14, the intermediate zone is traversed by migrating neurons enroute to the cortical plate (CP). At E16, the normal CP increases in thickness following the arrival of young neurons
Synaptogenesis: Duration of synaptogenesis	Synaptogenesis continues for the first 3 weeks postnatally, peaking in the first 2 weeks	

3.1.4 Comparison of glial cell developmental timelines in rat and mice cortices

When comparing the developmental timeline of OPCs in rats and mice, Bergles and Richardson,(2016) stated that in the forebrain, the first wave of OPCs appears at the telencephalon at embryonic day (E) E12.5 in mice and E14 in rats. This is situated in the medial ganglionic eminence (MGE) under the transcriptional control of NKx2.1 which is expressed by the sonic hedgehog (SHH) gene. These OPCs then migrate laterally and dorsally to colonise the entire forebrain. Next, at E15.5 and E16 for mice and rats respectively, the second wave of OPCs emerge from the developing

forebrain from the lateral ganglionic eminence and this migration is driven by the transcriptional control of Gsh2 (GSx2) (Bergles and Richardson, 2016; Spitzer *et al.*, 2018).These OPCs then move dorsally to the cortex and throughout the rest of the forebrain. Lastly, the third wave of OPCs emerge and occur at P0 in both mice and rats. Infiltration of these OPCs occurs radially from the dorsal subventricular zone (SVZ) and the outer SVZ which is directly below the developing corpus colossum. These OPCs then merge with the OPCs from the ganglionic eminence (Barateiro and Fernandes, 2014; Goldman and Kuypers, 2015).

At the postnatal stages, oligodendrocytes' maturation can be divided into four different stages which are oligodendrocyte precursor cells (OPCs), preoligodendrocytes (late OPCs), immature oligodendrocytes (pre-myelinating) and mature oligodendrocytes (myelinating). By postnatal day 2 (P2) in rats and mice, a majority of the oligodendrocyte lineage cells display characteristics of pre-oligodendrocytes, with a small population demonstrating immature oligodendrocyte characteristics in the cerebral white matter (Barateiro and Fernandes, 2014). By P7, there are approximately 80% of immature oligodendrocytes present that initiate myelination. Histological markers that are indicative of mature oligodendrocytes such as MBP are initially seen at P7, with an increase in expression of this marker by P14 (Barateiro and Fernandes, 2014).

During astrocytogenesis which is the generation of astrocytes within embryonic mice and rat brains, this process is first observed in the ventricular zone at E12 at low levels (Farhy-Tselnicker and Allen, 2018). By E15 however, the expression of GFAP increases in the periventricular regions of the cerebrum and the hippocampus in radial glia, the precursors of astrocytes. At E18 to P0, there is a further increase in the expression of GFAP with the radial glia maturing into astrocytes (Farhy-

Tselnicker and Allen, 2018; Akdemir *et al.*, 2020). From P0 to P22, the astrocyte population divides, expands, and migrates, first tangentially along the white matter tracts and then moves radially in the gray matter to their final positions in the cortex. The astrocytes then begin terminal differentiation to mature and induce synapse maturation, via the contact of the fine astrocytic processes coming into contact with neuronal synapses (Stolp *et al.*, 2012; Farhy-Tselnicker and Allen, 2018; Akdemir *et al,*, 2020).

Microglia, unlike OPCs and astrocytes are derived from the mesoderm which is situated in the embryonic yolk sac. In mice and rats, the cells, of myeloid origins migrate from the mesoderm, into the brain at approximately E10.5, through the ventricles and meninges during the beginning of neurogenesis and synaptogenesis in both rats and mice. The microglia progressively colonise the brain parenchyma when neural circuits start to assemble. Once the blood brain barrier (BBB) closes at E13.5 – E14.5, microglia proliferate within the region *in situ,* and the cells proliferate to populate the entire CNS (Ginhoux *et al.*, 2013; Kaur *et al.*, 2017; Tay *et al.*, 2017). Once colonisation of the CNS has occurred, microglial proliferation continues until it reaches its peak at P14. After this peak period, microglial numbers decrease from P0 to P28 until a stable population of the cells is achieved (Lenz and Nelson, 2018).

The literature suggests that there are similarities in glial cell developmental timelines in both rat and mouse cortices and therefore, in further relation to the justification of using a murine mixed glial model, there is scope to characterise a murine based mixed glial model for applicability in regenerative neurology for therapeutic testing, specifically using this model for glial cell encapsulation within biomaterials.

3.1.5 *In vitro neuronal models and their use in CNS research*

The generation of *in vitro* neuronal culture models from either using primary cultures or immortalised cell lines, is fundamental for understanding the mechanisms involved with neuronal development, synaptic function, morphology, metabolism and cellular interaction with other cells (Gordon, *et al*., 2013; Azari and Reynolds, 2016; Sahu *et al.*, 2019).

Additionally, as CNS diseases and disorders result in neuronal cell loss and damage, exploring the underlying mechanisms of the causes is beneficial for developing therapies for neuronal cell treatment and replacement (Azari and Reynolds, 2016). Banker and Cowan,(1977) initially developed a primary *in vitro model* for studying hippocampal neuronal cultures from E18 rats with minimal non-neuronal cells present within the culture (2% at 24h). The intention was to investigate neuronal cell development, neurite process formation and to also study cell surface markers. The hippocampus from embryonic E19 foetuses was excised and dissociated with trypsin and the cells were then seeded onto poly lysine coated coverslips. The isolated neurons within the culture could only survive for 3 DIV until cell viability declined to 1%, whereas when they were co-cultured with hippocampal explants, the neuronal cultures could be maintained for up to 2 weeks (Banker and Cowan, 1977). Since the development of this *in vitro* model, there have been advances in improving neuronal cell survival in addition to promoting neurite elongation by utilising supplements such as, basic fibroblast growth factor (bFGF) and B27 in neurobasal medium which

protects neurons from cell death in hypoxic conditions (Ray *et al.*, 1993; Sünwoldt *et al.*, 2017).

There are advantages to using immortalised neuronal cell lines derived from neuronal tumours instead of primary cells. Immortalised cells have the advantage of producing an unlimited population of cells in addition to minimising the variability between the cultures (Gordon, *et al.*, 2013). For example, PC12 cells derived from rat adrenal gland tumours are used to investigate aspects such as the differentiation process of neurons during development, neurotoxicity, neuroinflammation, neuroprotection and synaptogenesis due to the ease of culturing these cells, in addition to having knowledge of their proliferation and differentiation capabilities (Wiatrak *et al.*, 2020). As PC12 cells display features similar to mature dopaminergic neurons that store dopamine, they are used extensively as a model for the purposes of characterising the secretion of dopamine and norepinephrine in addition to ion channels and neurotransmitter receptors. Moreover, the cells when cultured with nerve growth factor, can differentiate into sympathetic ganglion neurons both functionally and phenotypically (Wiatrak *et al.*, 2020). PC12 cells have also been used to create complex neurobiological models in studies investigating neuroinflammation involving microglia. Udomruk *et al.*,(2018) studied the neuroprotective effects of sesamin, a lignans in sesame seeds and oil, and its effects on toll-like receptor 4 (TLR4), expressed on BV2 microglia (cell line), which is involved in microglial activation and neuroinflammation and how the lignans effects neuron-like PC12 cells. The study showed how sesamin pre-treatment of microglia at 24 and 48h hrs, significantly reduced TLR4 expression in comparison to the control which as a result, reduced nitric oxide production and pro-inflammatory cytokines, produced by the microglia, thereby reducing microglia-induced PC12 cell death.

Udomruk *et al.*,(2018), with the co-culture of PC12 cells and microglia, have shown how sesamin may be utilised as a potential therapy to be used to prevent the progression of neuroinflammation in neurodegenerative diseases.

As mentioned previously, cell lines have the benefit of being easy to culture, do not require harvesting live animals and provide an unlimited population of cells for studies. The disadvantages, however, are that neuronal cell lines do not mimic the physiological differences of neurons found *in vivo* (Gordon *et al.*,2013; Carter and Shieh, 2015). The cell lines undergo multiple passages which may result in the expression of genes that are not seen in the native CNS. Moreover, after several passages, cellular characteristics using neuronal cell lines may change which, therefore, do not mimic what is seen *in vivo*. Hence, it is advantageous to use primary cultured cells as these issues can be bypassed, and the results may be more representative of what is observed *in vivo* (Gordon *et al,* 2013; Carter and Shieh, 2015).

3.1.6 Rationale for developing an in vitro *post-natal neuronal enriched model*

In vitro neuronal culture models typically utilise embryonic cortical tissue because the prenatal stages of the neuronal cells have not yet developed extensive axonal and dendritic branches, which makes the neurons less vulnerable to damage during the dissociation process of the tissue (Sciarretta and Minichiell, 2010).

Typically, the age of the tissue from murine and rat cortices used for these cultures is between E11 and E17, as this is the time frame when a majority of the cerebral cortical neurons are generated (Sciarretta and Minichiell, 2010; Pacifici and Peruzzi,

2012). Additionally, the population of the culture is primarily enriched with neurons as the population of oligodendrocytes and astrocytes is insignificant, due to the genesis of these cells occurring after E12 and E18 respectively (Goldman and Kuypers, 2015; Akdemir *et al*., 2020). Another advantage is that the meninges and the connective tissue sheath can easily be removed due to the stage of development of the cortices, therefore producing a cleaner culture (Sciarretta and Minichiell, 2010; Goldman and Kuypers, 2015; Reemst *et al.*, 2016). These cultures can be grown and maintained easily at low and high densities for biochemical studies, gene manipulation and expression studies (Roppongi, Champagne-jorgensen and Siddiqui, 2017). The embryonic neuronal culture has been used for instance by Kaneko and Sankai,(2014) to encapsulate primary rat E18-E19 hippocampal neurons into a PuraMatrix^{TM} nanofiber hydrogel with the aim of investigating the viability and morphology of the cells within the 3D construct. Analysis showed that the hydrogel promoted neuronal survival and the extension of neurites, in addition to suppressing cellular aggregation, therefore was able to provide a model that mimics *in vivo* like culture conditions (Kaneko and Sankai, 2014).

As described in the literature above, there are benefits of utilising embryonic cortical tissue for the establishment of neuronal cultures. However, there are also several advantages in developing a post-natal neuronal enriched culture in comparison to embryonic derived neurons. A post-natal model reduces the necessity of killing several animals. i.e. only a few animals from a litter are required to be euthanised, avoiding the need to kill the mother as no embryos are extracted and thus making the process technically less challenging and leaving the mother to be used for further breeding purposes (Beaudoin *et al.*, 2012).

Numerous post-natal neuronal culture protocols have been established for the generation of murine primary neuronal cultures from authors such as Ahlemeyer and Baumgart-vogt,(2005), Beaudoin *et al.*, (2012) and Kaar, Morley and Rae, (2017). Postnatally derived neuronal cultures have also been used by Lautenschläger *et al.*, (2018) for the study of Parkinson's disease which is involved in the degeneration of dopaminergic neurons (Weihe *et al.*, 2006; Mamelak, 2018). The neuronal model contained P0-P2 rat-derived mesencephalic neurons from the substantia nigra and the ventral tegmental area and incorporated a glia feeder layer. The authors stated that the post-natal neuronal model had a greater percentage of tyrosine hydroxylase positive cells, a marker for dopamine, in comparison to embryonic neuronal cultures (Weihe *et al.*, 2006). The protocol that Lautenschläger *et al.*, (2018) used to establish the culture however takes 5 hours to complete which may hinder neuronal survival. However, there are optimised protocols that have been employed by Moutin *et al.*,(2020) but specifically for the isolation of P0 to P3 mouse hippocampal neurons for genetic manipulation and transfection of neurons, where cellular dissociation and plating had been achieved in less than 2 hours, thus improving neuronal survival. Post-natal neuronal models also make it possible to study neurons from genetically engineered mice at the early post-natal stages by gene knock in or knock out, for the purposes of investigating neuronal structure and function for biochemical analysis, imaging analysis, electrophysiology, or utilising the cells for the testing of biomaterial neuronal cell encapsulation (Beaudoin *et al.*, 2012).

In summary the literature has justified that there is scope for establishing a postnatal neuronal model, derived from murine cortices but specifically for regenerative neurology purposes and therapeutic biomaterial testing. Additionally, as stated

previously, there is also potential to characterise a murine based mixed glial model for biomaterial cellular encapsulation.

Hence, the aims of this chapter are to:

1. Develop a mouse mixed glial culture model using the protocol established by McCarthy and deVillis in 1980, to generate purified populations of glial cells (microglia, oligodendrocyte lineage cells and astrocytes).

2. Establish a neuronal culture model using post-natal mouse cortices

3. Characterise the biological models and determine the purity of the cell populations

3.2 Results

3.2.1 The mouse mixed glial model matured and stratified to give rise to microglia, OPCs and astrocytes

The mechanical dissociation process established by McCarthy and deVillis (1980) was replicated using murine cortices and the process for isolating neural glial cells as pictorially demonstrated in figure 3, with figure 3.1 showing the developmental stages of the culture. Microscopic observations were also made for the developmental stages throughout the 10 DIV of the culture which is seen in Table 3.2. In all cultures, it was also observed that populations of microglia, OPCs and astrocytes could reproducible be produced.

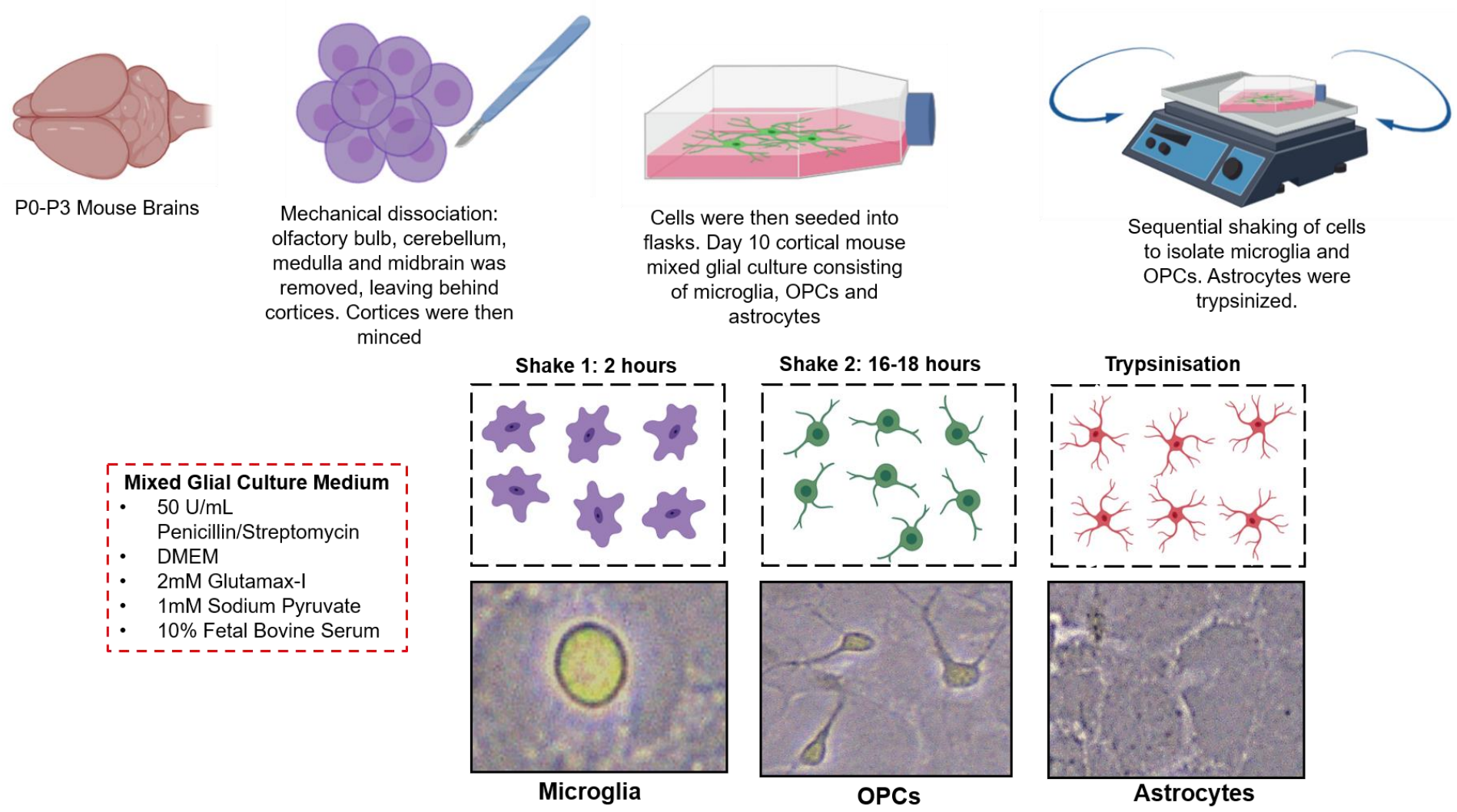

Figure 3.0. Illustrating the procedure for the development of a mouse mixed glial culture and isolated glial cultures. Images are not to scale and zoomed to highlight morphology.

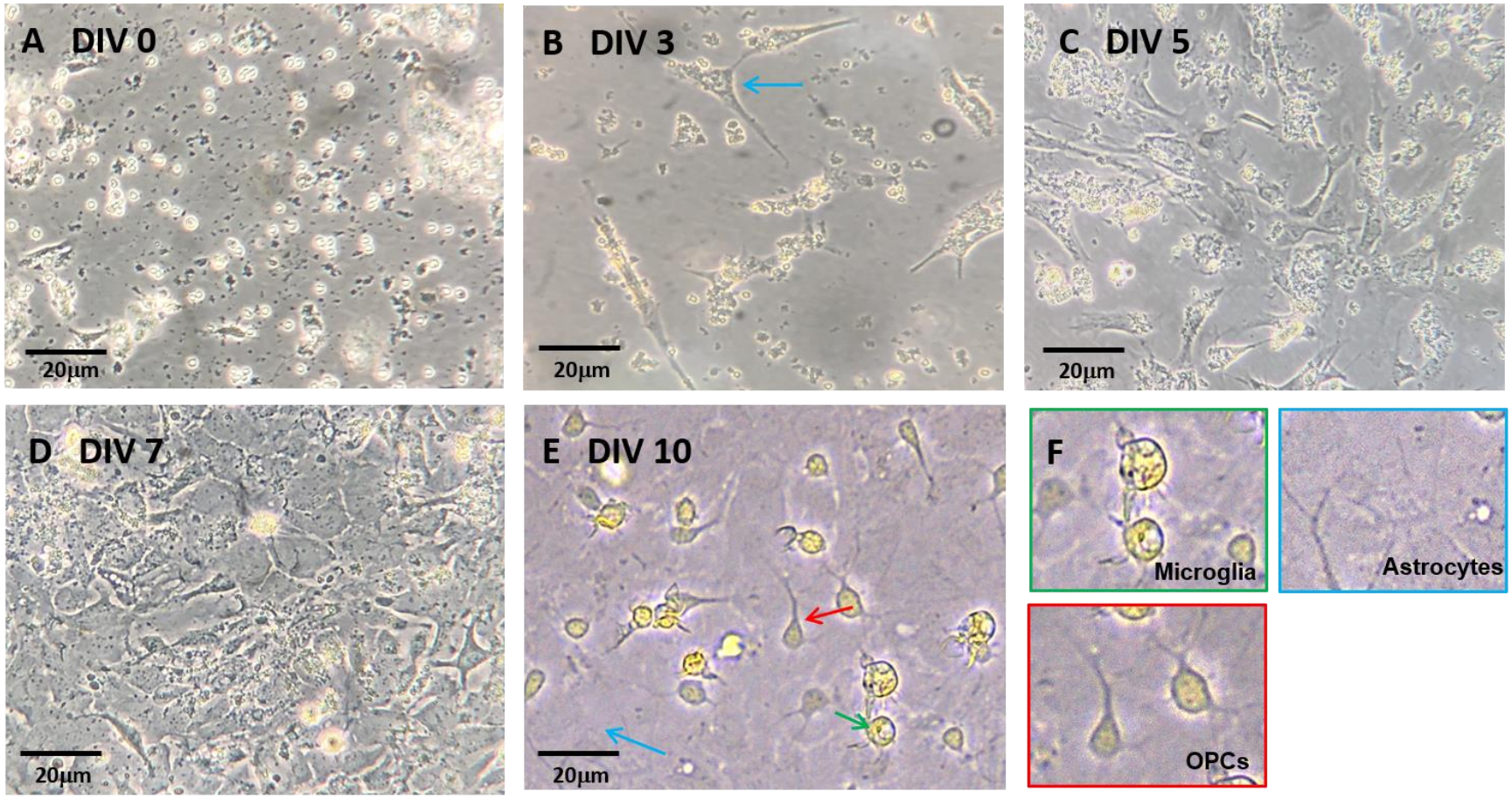

Figure 3.1. Developmental stages of the mouse mixed glial culture from day 0 to day 10. Blue arrows and boxes indicate astrocytes. Green arrow and boxes indicate microglia and the red arrow and box indicate to OPCs. n=3 **Images are not to scale and zoomed to highlight morphology.**

Table 3.2. Observations for the development and stratification of a mouse mixed glial model over 10 DIV

DIV	Observation
0	There was a significant amount of cellular debris present in the culture, due to the mechanical dissociation process. At this stage, the individual cell types could not be distinguished.
3	Cells had attached to the base of the flask and appeared to have stellate morphology which is typically seen for astrocytes grown on a 2D surface. Cellular debris started to become reduced in the culture through consecutive medium changes and microglia engulfment of debris.
5	The culture was becoming more confluent, with an evident basal layer of astrocytes, identified by their relatively large phase-grey cell bodies, with no visible extension of cellular processes. Microglia were distinguished by their circular phase-bright morphology. At this stage, OPCs could not visually be distinguished as the culture was not yet mature.
7	The majority of the cellular debris had been phagocytosed by microglia, thus resulting in a cleaner culture and the astrocytes had established a full basal layer of the flask, thus slowly forcing the OPCs and microglia to be positioned above the astrocytes.
10	The culture was fully confluent and there was visually only a minute amount of debris present. The OPCs were distinguished from the other glial types by their small cell body and fine bipolar cellular processes. The OPCs appeared phase-dark in contrast to the phase-grey astrocytes. Hence, by 10 DIV, there was a basal layer of astrocytes, an intermediate layer of OPCs and top dweller microglia.

3.2.2 Purified populations of murine glial cells can be produced using the mixed glial culture protocol

Once mixed glial cultures were ready i.e. the three glial cell types were present within the culture with minimal cellular debris, isolated cultures were derived. All isolated cultures displayed a viable population of cells (figure 3.2). Microscopic observations indicated that there were high proportions of cells staining positive for the live cell marker, Calcein (figure 3.2. A, B,C) after quantification. There was shown to be over 90% viability for all isolated neuroglial cultures (figure 3.2. D) n=3.

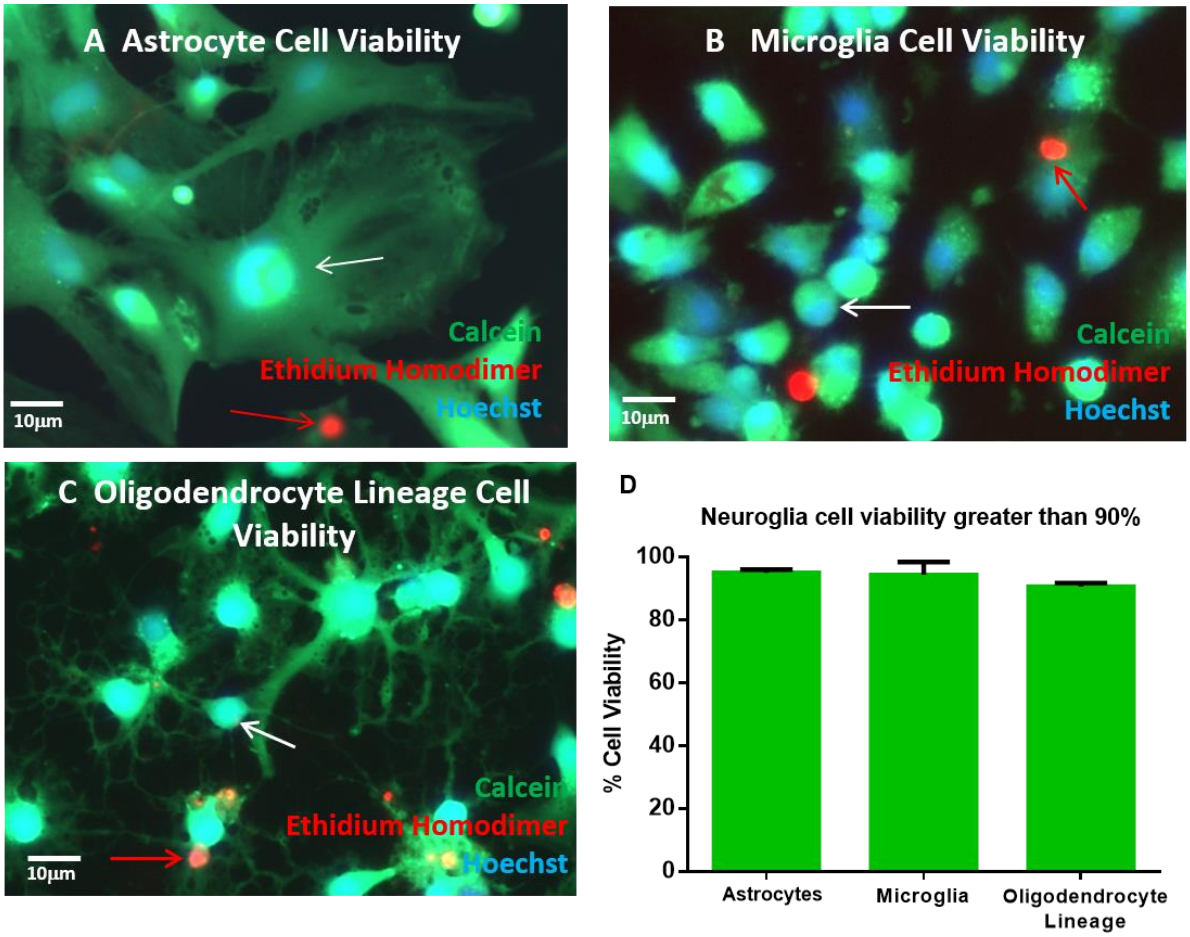

Figure 3.2. Neuroglia percentage cell viability. A, B and C are representative cell viability images. White arrows indicate viable cells and red arrows illustrate dead cells. Images depict A) astrocytes, B) microglia and C) OPCs respectively, with D) demonstrating the percentage viability of the glial cell types. n=3. Total astrocytes counted was 1180 of which 1127 were viable. Total microglia counted was 1010 cells of which 970 were viable. Finally, total OPCs counted were 2141 of which 1949 were viable.

Histological markers were used to validate the phenotypic and cellular composition of the glial types. As monocultures, the histological markers GFAP and NG2 for astrocytes and OPCs respectively, and IBA-1 for microglia were used (Figure 3.3). There were two distinct types of astrocyte morphologies seen in the monocultures (Figure 3.3, A) which were type 1 astrocytes which have a flattened morphology and type 2 astrocytes that are branched. Microglia (Figure 3.3, B) showed ameboid morphologies, suggesting that they are in their reactive state and OPCs (Figure 3.3, C) can be seen to be bipolar and multipolar in morphology which are typically seen in the pre-oligodendrocyte linage states. After quantification of the histological markers in the isolated neuroglial cultures (Figure 3.3,D), all cultures displayed >93% purity with residual-cross-cell contamination reported at no greater than 7%, thus demonstrating the robustness and reproducibility for generating isolated murine neuroglia populations.

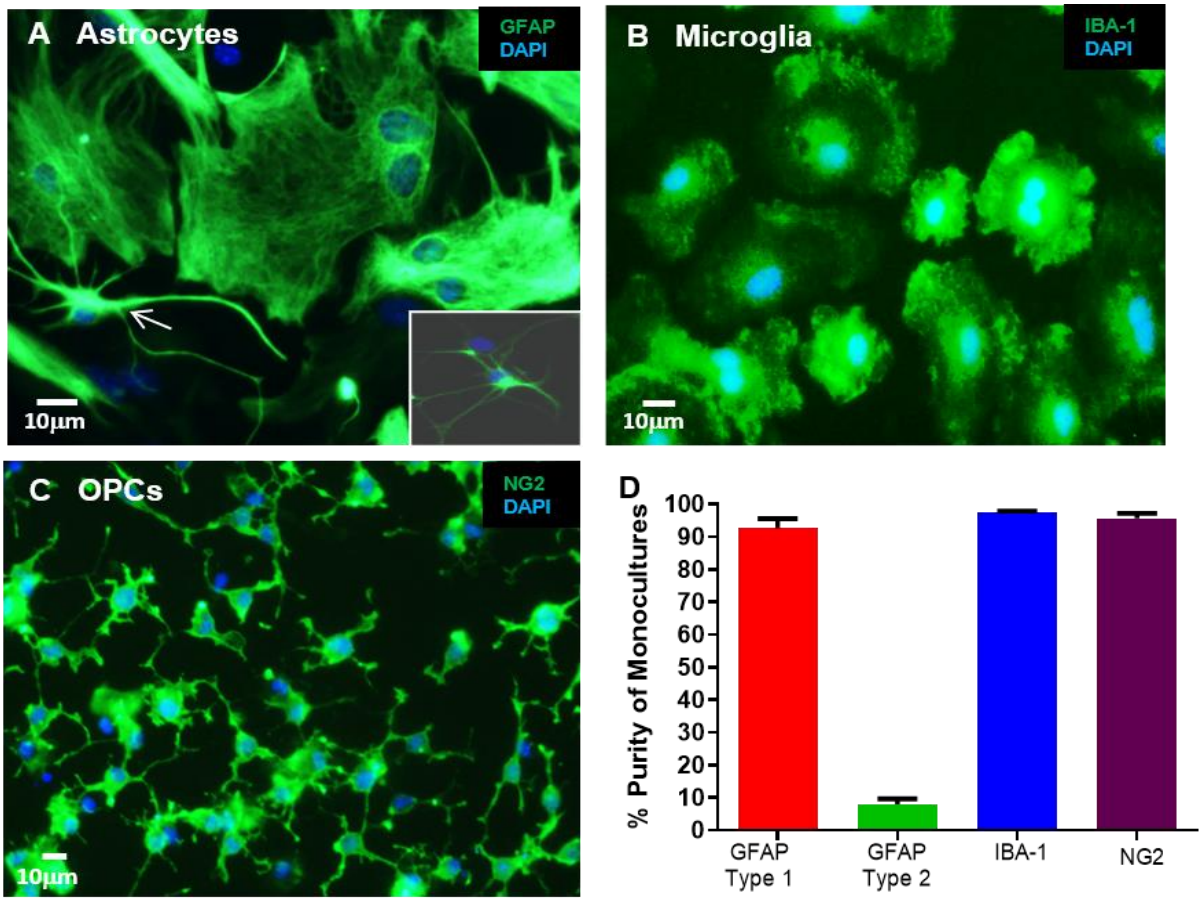

Figure 3.3. Histological validation and quantification of percentage purity of monolayer cells derived from mouse mixed glial cultures. Representative fluorescent images of glial cells stained for (**A**) astrocyte marker, GFAP with main image showing type 1 astrocytes and inset and arrow showing type 2 astrocytes. Please note, astrocytes display two distinct morphologies in culture namely type 1 (flattened) and type 2 (branched) astrocytes (**B**) microglial marker, IBA-1 and (**C**) oligodendrocyte precursor marker, NG2, (**D**). Bar chart displaying the numbers of each cell type in the derived monocultures. Note that type I and II astrocytes are found in the same culture. Percentage purity of each monoculture was found to be > 93%. n=3. Total type 1 astrocytes counted was 1182 of which 992 cells were GFAP positive and 8 cells were type 2 astrocytes. The total number of microglia counted was 2350 cells of which 302 were lectin positive and 1560 cells were IBA-1 psotive respectively. Lastly, the total OPCs counted was 1785 of which 1392 were NG2 positive.

3.2.3 Generation of a neuronal enriched culture using post-natal murine cortices

For the establishment of the neuronal enriched culture, pilot studies were conducted with two different protocols; mechanical dissociation and enzymatic dissociation, with Figure 3.4 illustrating the variables that were trialled and the protocol that was taken forward.

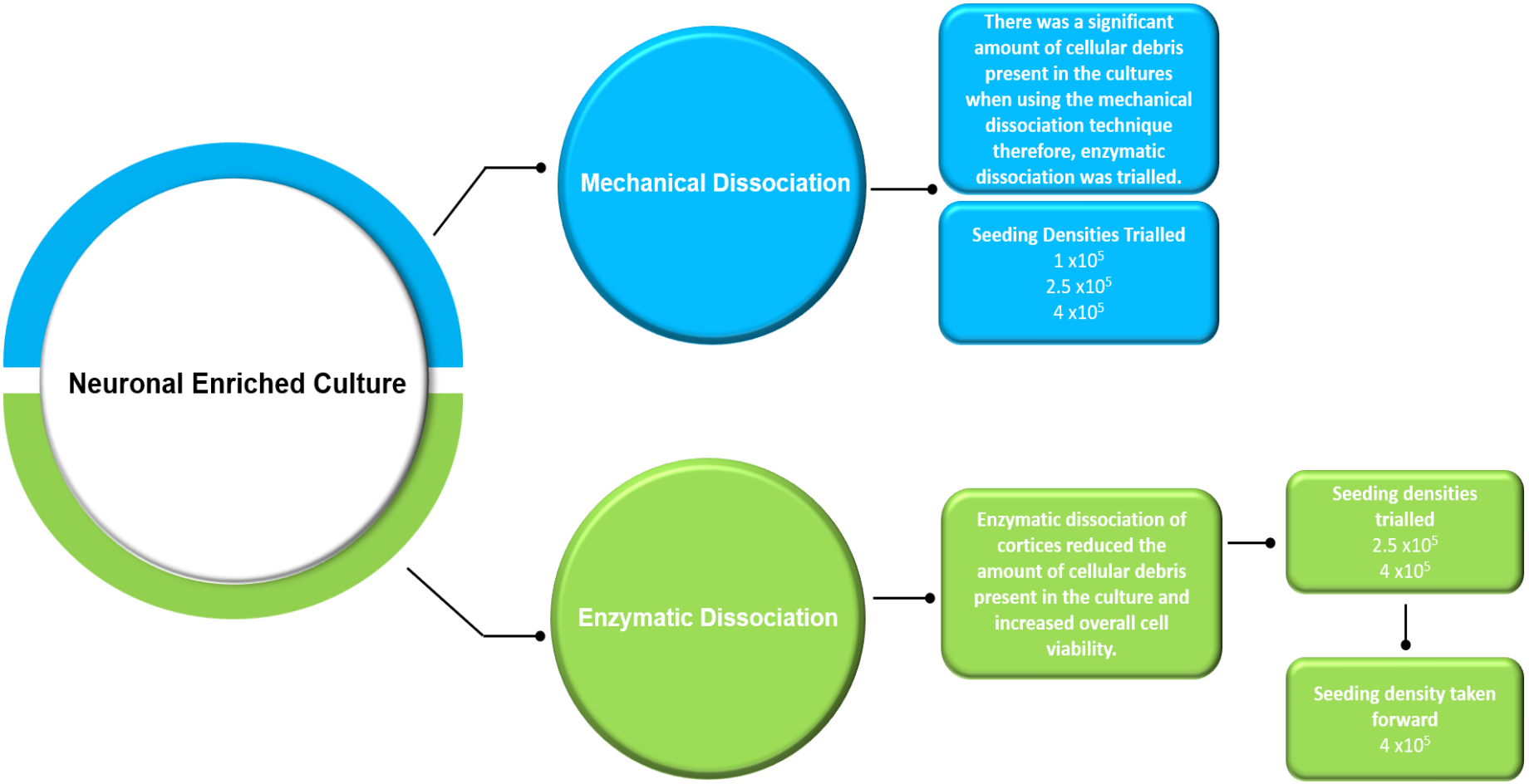

Figure 3.4. A schematic illustration of the methods trialled for the generation of a neuronal enriched culture. Initially a mechanical dissociation protocol was trialled for the generation of the neuronal culture. However, as this generated considerable amounts of cellular debris, enzymically dissociating the cortices was then trialled. The latter protocol was taken forward alongside the seeding density $4x10^5$ cells/mL .

3.2.4 Pilot study: Mechanical dissociation of cortices for the generation of a post-natal neuronal enriched culture

Similar to the generation of the mouse mixed glial culture in chapter 3.1, the concept of mechanically dissociating the cortices was applied for the generation of a post-natal neuronal enriched culture. The only difference here was that neuronal culture medium was used to give rise to the neuronal enriched culture. Figure 3.5 illustrates the stages of mechanical dissociation for generating the post-natal neuronal enriched culture.

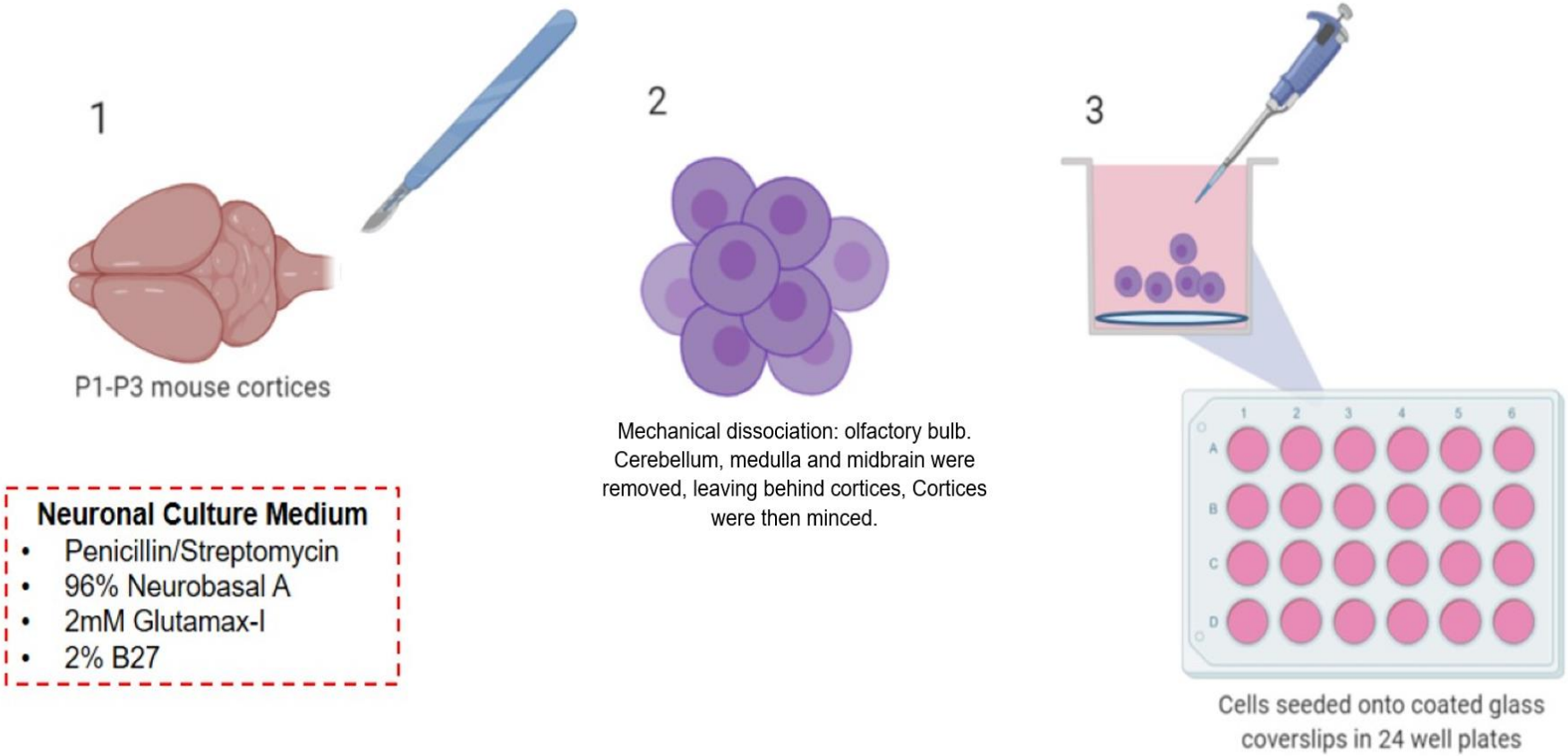

Figure 3.5. Mechanical dissociation of the cortices for the generation of post-natal neuronal enriched cultures.

Initially, the seeding densities $1x10^5$, $2.5\ x10^5$ and $4x10^5$ cells/mL were trialled to determine which density was optimum for the establishment of the culture. Cell viability for these pilot studies at 9 DIV was analysed (Figure 3.6) showing that although there were viable cells at each seeding density, there were remnants of cellular debris within the cultures, indicated by the red ethidium homodimer stain. The greatest percentage of viable cells was 30%. This was observed at the density $4x10^5$ cells/mL in table 3.3.

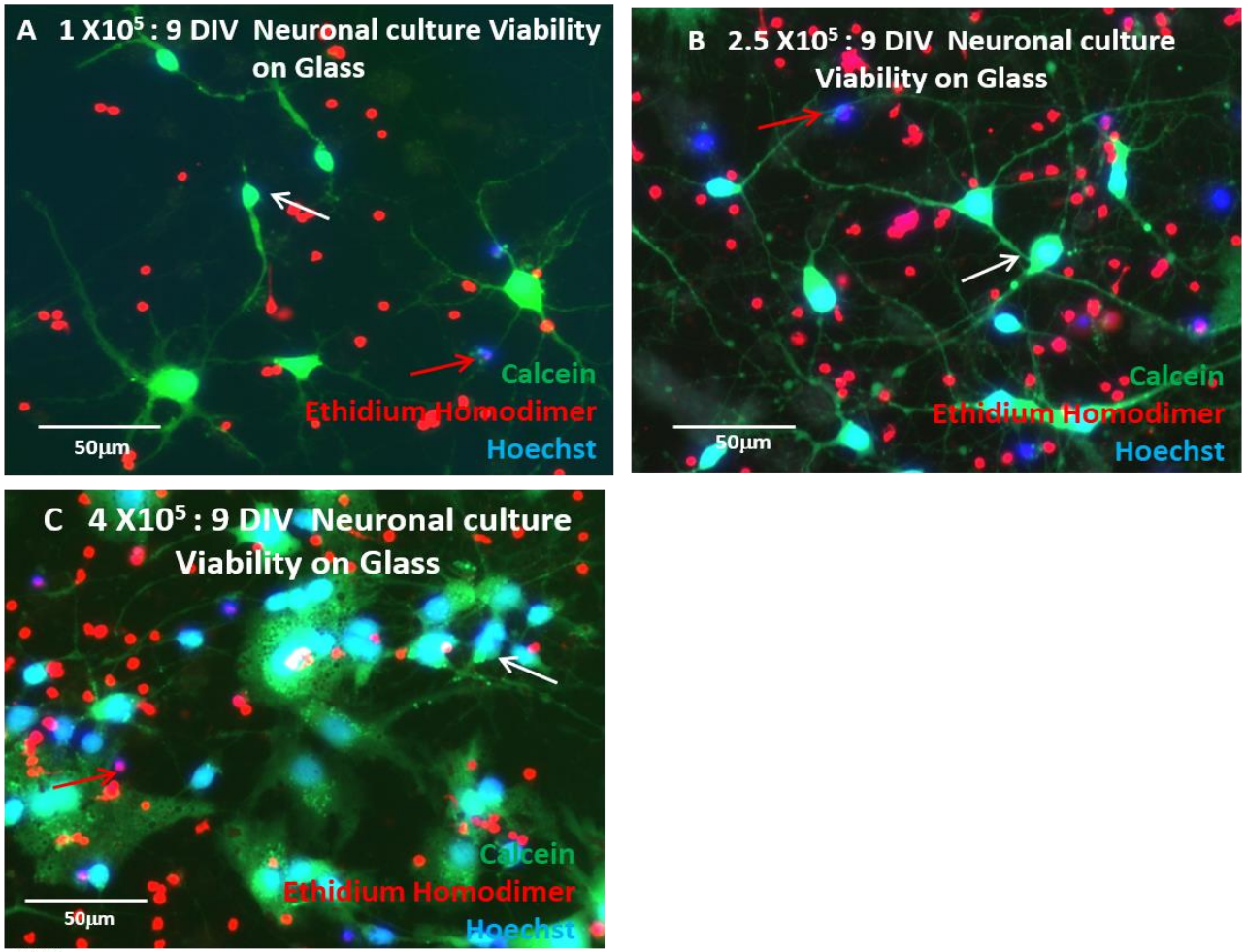

Figure 3.6. Pilot study for 9 DIV cellular viability of mechanically dissociated neuronal enriched cultures at three different seeding densities. White arrows indicate live cells with red arrows highlighting dead cells. Representative images demonstrate cell viability at the seeding densities **A)** 1 X10^5 **B)** 2.5 X10^5 **C)** 4 X10^5 cells/mL. n=1.

Table 3.3. Pilot Study: 9 DIV cell viability of neuronal enriched culture using mechanical dissociation (n=1)

Seeding Density (cells/mL)	% Cell Viability
1×10^5	14
2.5×10^5	15
4×10^5	30

Next, to determine the percentage of neurons within these cultures, histological validation was conducted at 12 DIV with cell specific markers (Figure 3.7). Pilot data illustrates that at all densities, there were Tuj-1 positive neurons and GFAP positive astrocytes in the cultures, and there was also non-specific staining of debris which may have been remnants of mechanically dissociating the cells (white arrows in Figure 3.8). Phenotypically, the neurons appeared to have a small soma and multipolar morphology, with the astrocytes appearing to have a flattened morphology. Quantification of this pilot data seen in table 3.4. showed that the cultures at all densities contained greater than 70% population of Tuj-1 positive neurons.

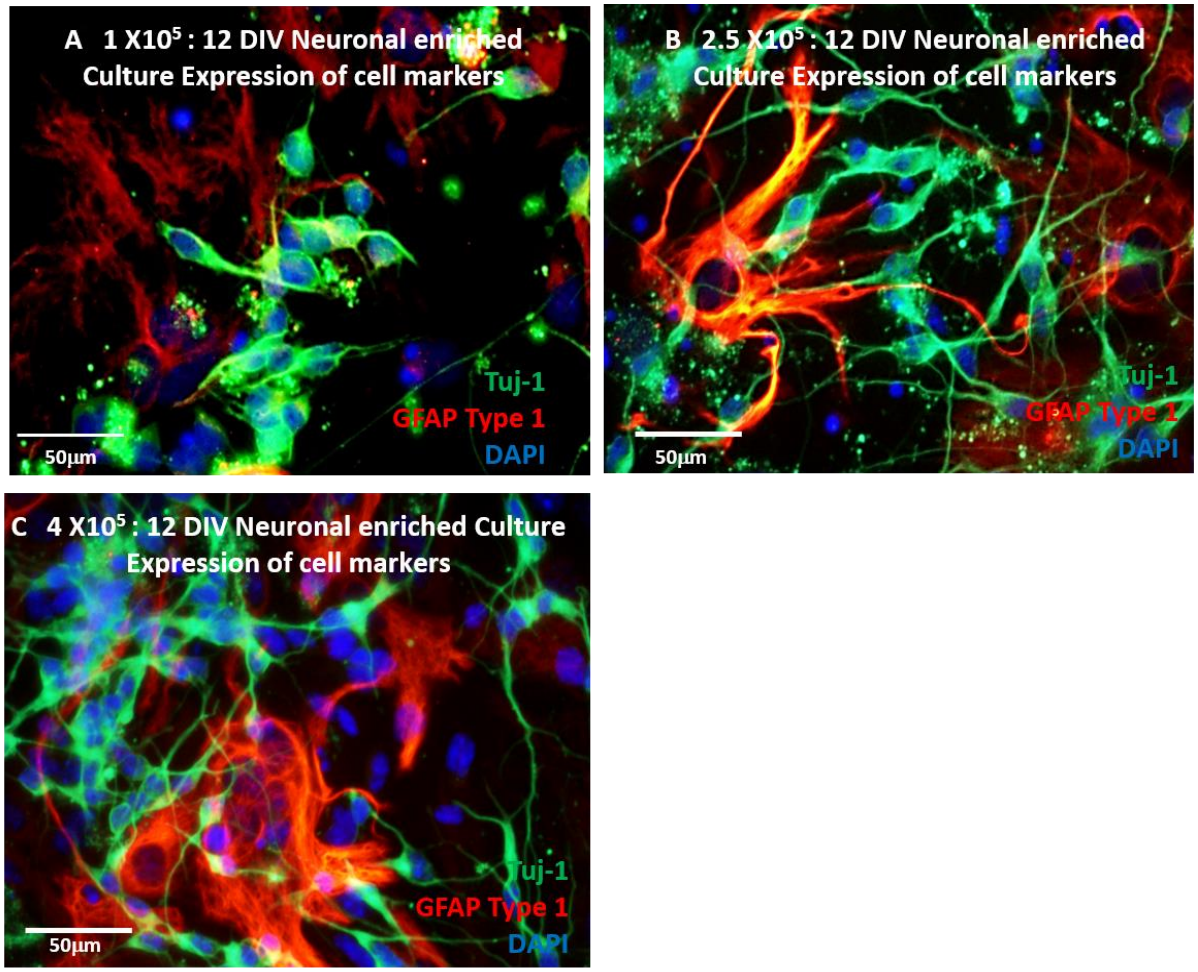

Figure 3.7. Pilot study for 12 DIV neuronal enriched culture histological staining at three seeding densities. A, B and C are representative images of neuronal enriched cultures stained with Tuj-1, a neuron-specific marker (green) and GFAP, an astrocyte marker (red). Images **A**, **B** and **C** also demonstrate neuronal enriched cultures at the densities 1 X10^5 **,** 2.5 X10^5 and 4 X10^5 cells/mL respectively, with the white arrows indicating regions of cellular debris produced from mechanically dissociating the cells. n=1.

Table 3.4. Pilot Study: 12 DIV Neuronal enriched culture expression of cell markers for mechanically dissociated cells (n=1)

Seeding Density (cells/mL)	Tuj-1 Positive (%)	GFAP Positive (%)
1 x 10^5	73	27
2.5 x 10^5	79	21
4 x 10^5	69	31

The pilot data demonstrated that a neuronal enriched culture can be achieved using a chemically defined medium and the mechanical dissociation process. However, there is evidence of low viability at the chosen timepoints and cellular debris in both the cell viability assay and immunocytochemistry. Therefore, we next trialled enzymatically dissociating the mouse cortical tissue to determine whether this could reduce the amount of debris present in the cultures.

3.2.5 Pilot study: Enzymatically dissociating post-natal murine cortices for generating a neuronal enriched culture with reduced cellular debris and improved viability

The rationale for enzymatically dissociating post-natal cortical tissue, to produce a single cell suspension of cortical neuronal cells is that it removes the need of using mechanical dissociation, which may generate excessive cellular debris and yield low cell viability as evident in the pilot data above. Enzymatically dissociating the cortices required a series of steps which are schematically seen in Figure 3.8. The protocol involved the removal of the meninges which can contribute to cellular debris prior to enzymatically dissociating with Trypsin and DNase, plus the additional stage of filtering the cell suspension prior to seeding onto coverslips in a 24 well plate. The seeding density $1x10^5$ cells/mL was discontinued and taken forward were the densities of $2.5\ x10^5$ and $4x10^5$ cells/mL,as they provided a denser culture of cells and high density neuronal cultures are reported to having sustainable cell survival rates and functional activity (Aebersold *et al.*, 2018).

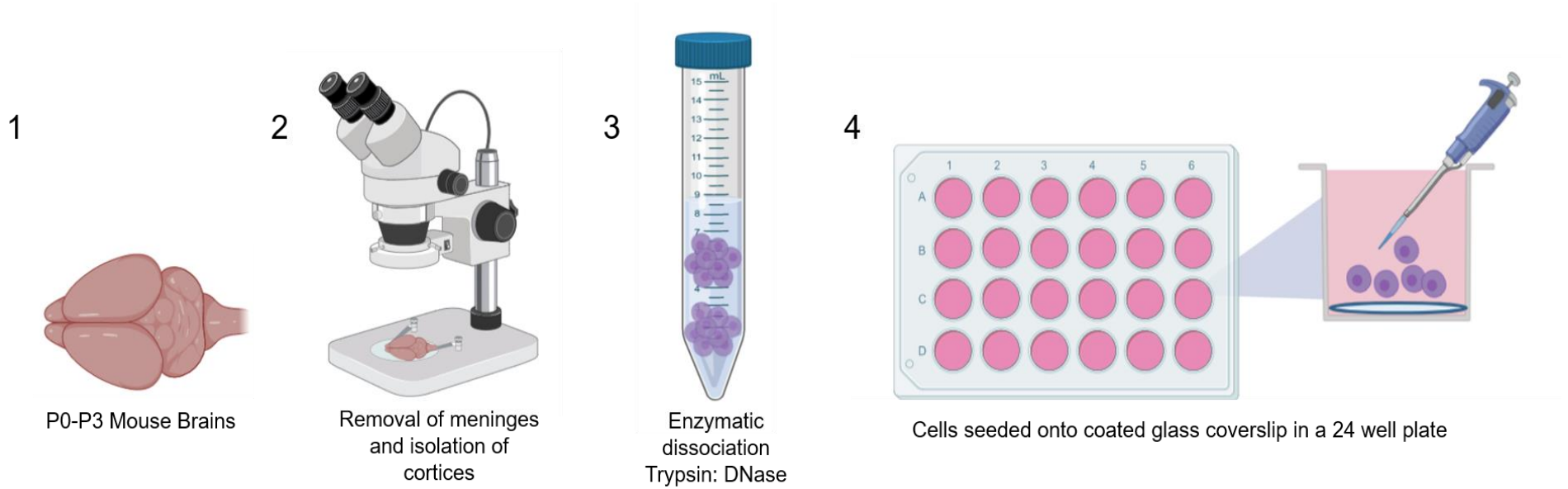

Figure 3.8. Enzymatic dissociation of post-natal mouse cortices for the generation of a neuronal enriched culture.

The pilot data showed that at 9 DIV, cell viability at both densities was greater than 90% with minimal cellular debris, as seen in the 9 DIV representative images (Figure 3.9, A and B and Table 3.5). Furthermore, additional time points were tested to investigate viability earlier to 9DIV. These were 3 and 6 DIV which also showed viability greater than 70% at both densities and time points.

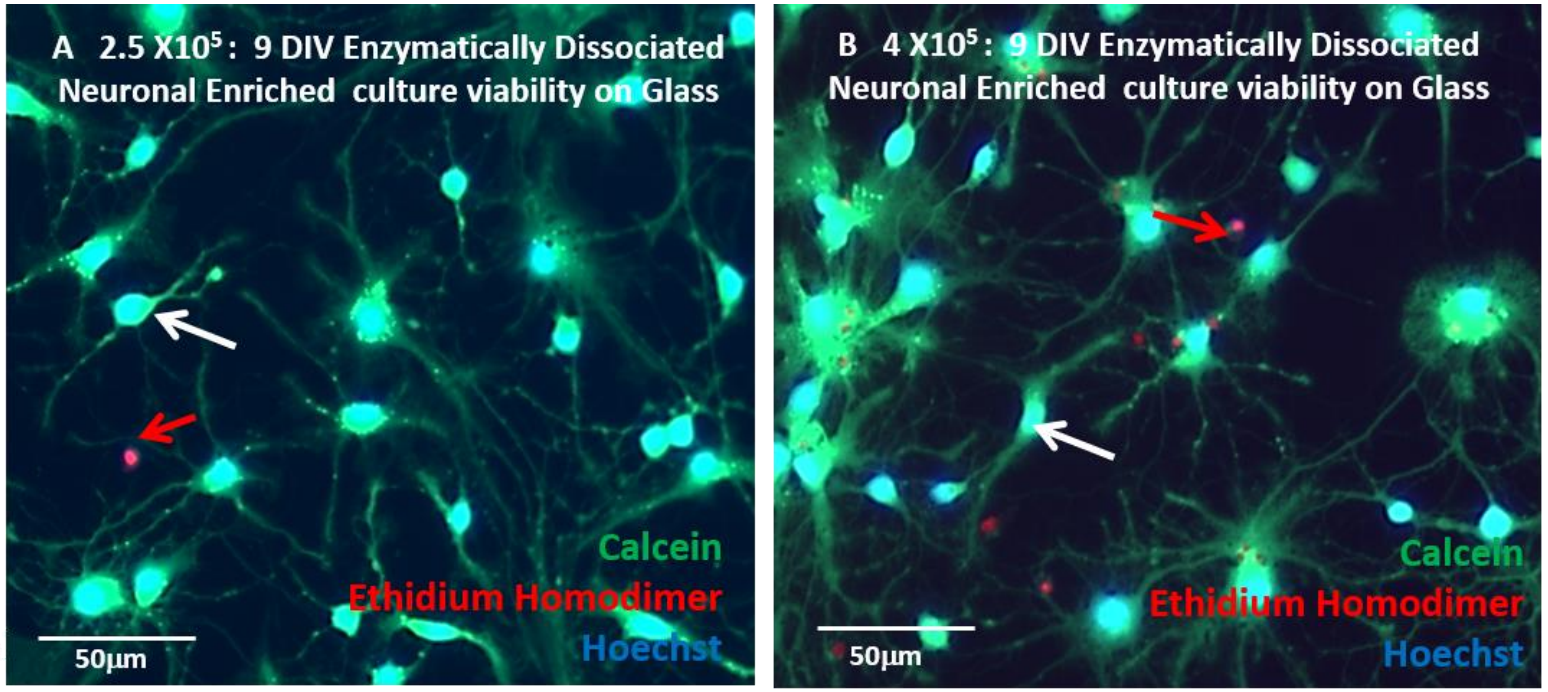

Figure 3.9. A and B are representative images of 9 DIV cell viability of enzymatically dissociated neuronal culture at 2.5 x 10^5 and 4 x 10^5 cells/mL densities. White arrows indicate live cells stained with calcein with red arrows showing dead cells stained with ethidium homodimer. n=1.

Table 3.5. Pilot study: Cell viability of neuronal enriched culture using enzymatic dissociation (n=1)

Seeding Density (cells/mL)	Cell Viability (%)		
	Day 3	Day 6	Day 9
2.5 x 10^5	83	76	93
4 x 10^5	86	89	91

Utilising enzymatic dissociation of cortices to generate a single cell suspension helped to reduce the amount of cellular debris in the cultures. Therefore, it was decided that enzymatic dissociation would be utilised to generate a neuronal enriched culture. Additionally, as both densities showed similar percentages of viable cells, the seeding density taken forward was 4 x10^5 cells/mL in order to try and generate a higher absolute number of neurons in the culture.

3.2.6 Enzymatically dissociated neuronal enriched model yielded high cell viability

To determine how robust and reproducible this culture system is, cell viability assays were conducted at 3, 6 and 9 DIV and the model was characterised with cell-specific markers at 12 DIV which were believed to be sufficient time for the formation of a neuronal network within 2D *in vitro* cultures (Beaudoin *et al.*, 2012; Kuijlaars *et al.*, 2016). In addition, the developmental timeline of the culture from 3 to 9 DIV was also

observed. The viability of the enzymatically dissociated cells at the 4 x10^5 cells/mL seeding density at 3, 6 and 9 DIV (Figure 3.10, A,B,C) demonstrated the presence of viable cells (calcein, green) with small proportions of dead cells (ethidium homodimer, red). Microscopic observations also indicted that cell viability was >80% across all time points (Figure 3,10, D) (n=3).

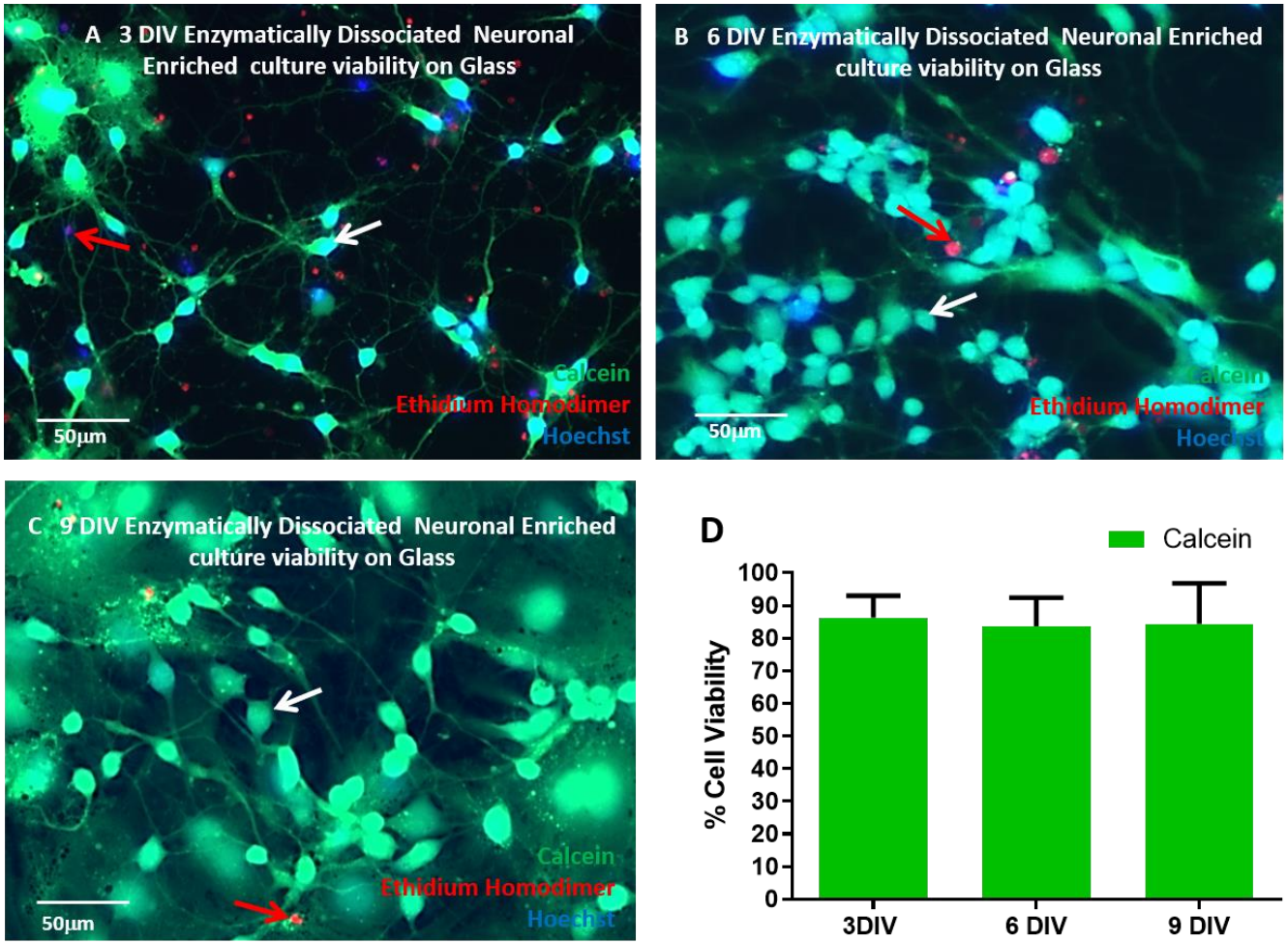

Figure 3.10 Viability of enzymatically dissociated neuronal culture on glass at the seeding density 4 x 10^5 cells/mL. White arrows indicate live cells with red arrows highlighting dead cells. **A**, **B** and **C** show neuronal culture viability at 3,6 and 9 DIV respectively, with **D** showing the percentage of viable cells at these time points. n=3. Figure 3.10 continued below.

Figure 3.10 continued. Total cells counted for 3 DIV was 1091 of which 946 were viable. The total cells counted at 6 DIV was 1160 of which 1005 were viable. Lastly, the total cells counted at 9 DIV was 1567 of which 1397 were viable.

Observations for the development of the neuronal enriched culture were derived from the cell viability assay images at 3, 6 and 9 DIV, and can be seen in Table 3.6.

Table 3.6. Observations for the development of a neuronal lineage enriched post-natal cortical culture

DIV	Observation
3	There was the presence of multipolar cells which had neuron-like phenotypic characteristics, a small soma and axons. There was also evidence of cellular debris (red) in the cultures.
6	By 6 DIV, the development of a basal layer of astrocytes beneath the neurons which were recognised by their stellate morphology was evident. Additionally, the amount of cellular debris in the culture seemed reduced in comparison to 3 DIV.
9	There was a confluent basal layer of astrocytes with top dweller cells resembling neurons which appeared to form a neuronal network.

For cellular characterisation, cells were stained with neuronal markers Tuj-1 which stain neuron cell bodies in addition to a GABA antibody which specifically stains GABAergic nuclei of neurons and the antibody VGLUT which stains for glutamaterigic neurons. Additionally, the glial cell markers GFAP, MBP and IBA-1 were also used to stain for type 1 and type 2 astrocytes, oligodendrocytes, and microglia respectively. Morphological staining (Figure 3.11) illustrated that the

neuronal enriched cultures contained Tuj-1 and Gaba positive neurons which were evidenced by the staining of multiple extended processes (neurites) projecting from the axon and co-localisation of nuclei staining for GABA (Figure 3.11, A).

There was also evidence of oligodendrocytes and astrocytes within the cultures (Figure 3.11,B, C and D respectively) with the latter glial type showing flattened stellate morphology, indicative of type 1 astrocytes on 2D surfaces and type 2 astrocytes which phenotypically appear to have finer branched projections from their cell body. No staining was evident with VGLUT-1 and IBA-1, suggesting that these specific cell types were absent from the neuronal enriched culture.

The individual cell types were then quantified to determine the proportion of each cell type with Figure 3.11, E graphically showing that there were approximately 45-50% Tuj-1 positive neurons in addition to approximately 50% GFAP positive astrocytes and less than 10% oligodendrocytes. Furthermore, the percentage of GABAergic positive neurons was also quantified from the Tuj-1 positive cell population, which was found to be approximately 60% ±10%, and the remainder of the population being a GABA-negative neuronal cell type.

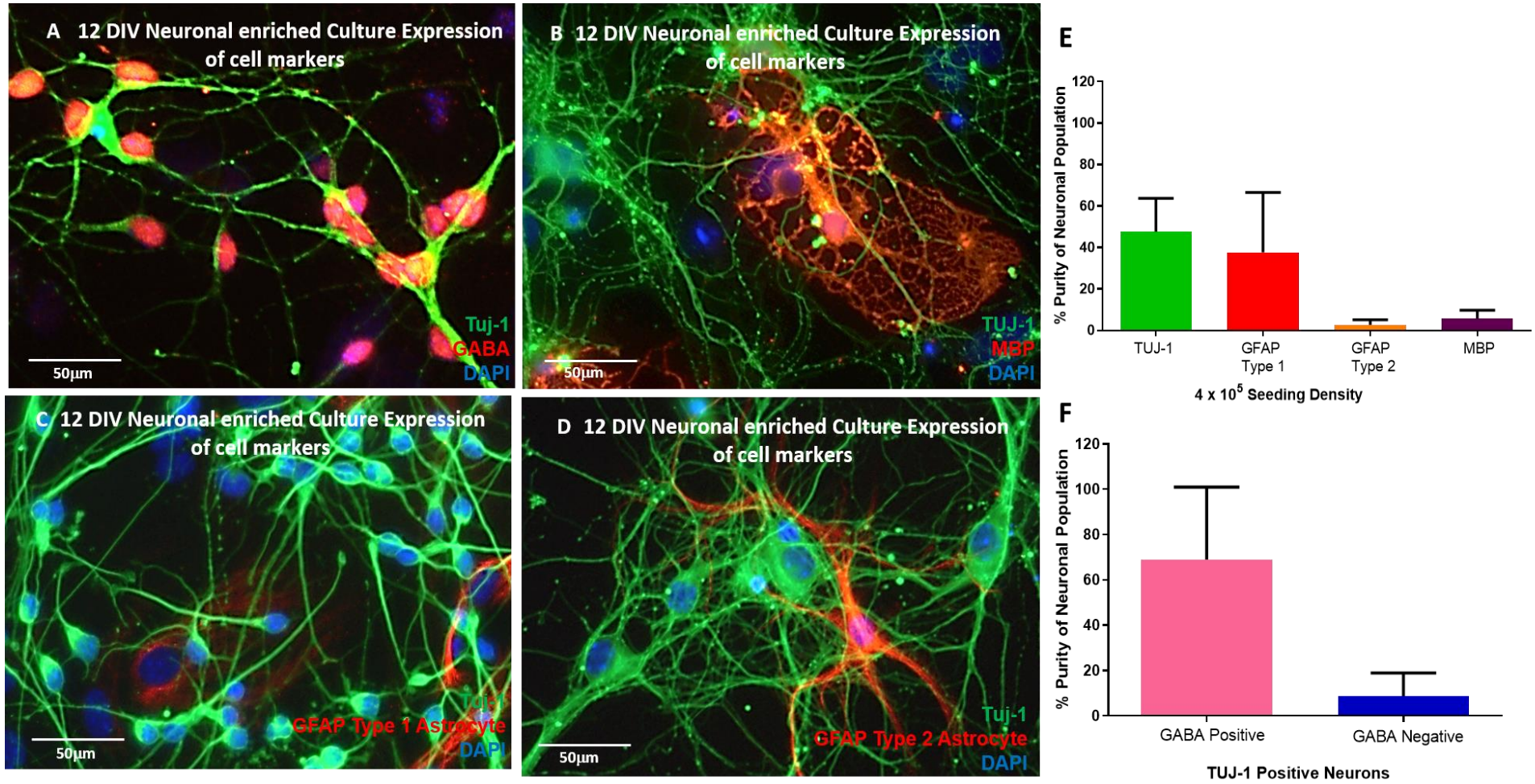

Figure 3.11. 12 DIV neuronal enriched culture histological staining. Representative fluorescent images of neuronal enriched cultures that was enzymatically dissociated and stained for (**A)** Tuj-1, a neuron-specific marker (green) and GABA, a Gabaergic neuronal marker (red). **Figure 3.11 continues below**.

Figure 3.11 continued **(B)** showing cells positive for MBP , an oligodendrocyte marker and TUj-1 (green) **(C)** showing GFAP positive type 1 astrocytes (red) with Tuj-1 positive neurons (green) and **(D)** type 2 GFAP astrocytes (red) with TUJ-1 neurons (green). Note that type I and II astrocytes are found in the same culture **(E)**. Bar chart displaying the percentage of each cell type found within the neuronal enriched culture and **(F)** illustrates the percentage of GABA positive neurons, from the total population of Tuj-1 positive cells. n=3. Total cells counted for graph **E** was 1366 cells of which there was 774 TUJ-1 positive neurons, with there also being 501 GFAP positive type I astrocytes, 30 type II astrocytes and 61 MBP positive oligodendrocytes. Total cells counted for graph **F** was 2034 with there being 836 cells that were GABA positive neurons and 161 cells that are GABA negative neurons and lastly, 796 cells being non-neuronal cells (the latter data was not included in the graph).

3.3 Discussion

Our laboratory has extensively used the rat derived mixed glial model for nanomedicine applications. However using a mouse derived mixed glial model as an alternative could offer several advantages which include having a cheaper source to generate the litter, glial cell developmental timeline similarities, thus cells can be isolated in a comparable timeframe to that of rats. Using mice also promotes the option of using genetically modified mice (Beaudoin *et al.*, 2012; Ginhoux *et al.*, 2013; Bergles and Richardson, 2016; Farhy-Tselnicker and Allen, 2018).

To first determine the robustness and reproducibility of the murine derived model, it was characterised prior to utilising the isolated neuroglia for biomaterial testing in chapters 4 and 5.

The developmental time frame analysis of the murine mixed glial culture revealed that over 10 DIV, the model was able to mature and stratify to give rise to microglia, OPCs and astrocytes, with minimal cellular debris seen by 10 DIV. When compared to the rat mixed glial model, similar observations were made in terms of cellular development and morphology (Mccarthy, Ken D., DeVellis, 1980).The duration for the culture to stratify is in line with the development of the rat mixed glial cultures which ranges from 7 to 10DIV (McCarthy and De Vellis, 1980; Vellis and Cole, 2011). Further comparisons showed that microglia within the murine mixed glial model were evident from 5 DIV, appearing circular and phase bright, whereas in the rat mixed glial model, Vellis and Cole,(2011) reported that microglia were observed from 6 to 7DIV. In addition, the rat mixed glial model, stratified initially with an astroglia cell layer and oligodendrocyte lineage cells, which appeared phase dark with fine cellular processes, growing on top of the astrocytic layer, and rapidly developed within the

first few days of the culture(McCarthy and De Vellis, 1980). Though astrocytes were observed by 3DIV in the mouse mixed glial model, oligodendrocyte lineage cells also appeared phase dark, similar to the rat-derived cells, however they could not be visually distinguished until 7DIV.

Another observation from Mccarthy and DeVellis', (1980) study was that there was no evidence of neurons present within the post-natal rat cultures which were similar to the mouse derived mixed glial model. The reasons for this may be the age of the post-natal pups as it has been reported that neurons derived from pups older than P2 show limited survival (Lautenschläger *et al.*, 2018). Additionally, neurons may not have survived in the rat and murine mixed glial cultures as the growth mediums (Eagles medium and D10 medium respectively) which play a critical role for cellular differentiation, also contain FBS, a significant source for glutamate, that supports astrocytes, microglia and OPCs growth but may hinder neuronal viability, hence they were absent from the culture (Ye and Sontheimer, 1998).

Furthermore neuroglial viability of the isolated populations derived from the murine mixed glial model demonstrated >90% viability (n=3), which was comparable to the rat glial model-derived cells (>90%) (Jenkins *et al.*, 2013). Thus, this shows that murine-derived neuroglia can be isolated and produced repetitively with high viability, similar to the rat mixed glial cells. When exploring the purity of the isolated neuroglial fractions, >93% of the monolayer cultures expressed their cell-specific markers and when compared to the rat mixed glial cells, similar data was obtained (Microglia (97%), OPCs (95%) and astrocytes (99%) (Pickard and Chari, 2010; Jenkins *et al.*, 2013; Tickle *et al.*, 2016).

Morphologically, the cells from the murine and rat mixed glial models also had phenotypical similarities, with microglia showing heterogeneous morphologies with ramified and amoeboid cells, type 1 astrocytes appearing flat and membranous and type 2 branched astrocytes (Tickle *et al.*, 2016; Lin *et al.*, 2017). Lastly, OPCs appeared bipolar and multipolar with limited branching (Pickard and Chari, 2010).

The data derived from the murine mixed glial model demonstrates the robustness and reproducibility that this model can offer for regenerative medicine applications and specifically for therapeutic biomaterial testing. As discussed in the introduction, a mixed glial model has been applied to encapsulate both a mixed and isolated glial cell population into biomaterials, for investigating and understanding how the glial cells may react *in vivo* within a scaffold (Mecha *et al.*, 2011).

Studies that could be conducted with the murine neuroglial model include; investigating within a 3D environment, the glial cell reactions that contribute to an inflammatory response, glial scar formation, and how cells such as microglia and astrocytes may react when introduced to a foreign environment such as a biomaterial (Koss *et al.*, 2017). Additionally, the model could also be used to isolate oligodendrocyte lineage cells for hydrogel encapsulation, to promote the cells to proliferate and mature, in order to examine the mechanisms involved in their cellular functions in a 3D *in vitro* environment (Egawa *et al.*, 2017). The murine model may also be beneficial for trying to understand the metabolic performance of glial cells once encapsulated in a 3D environment, in addition to investigating how the cells respond to mechanical cues such as stiffness of a biomaterial ,cytotoxicity, glial cell morphology and their interactions within a biomaterial (Moshayedi *et al.*, 2014; Watson *et al.*, 2017).

It has also been successfully demonstrated that a neuronal enriched culture can be established using post-natal murine cortices. Initially, to generate the neuronal culture, the cortices were mechanically dissociated and cultured with serum-free Neurobasal A medium, supplemented with the growth factor B27, a component which protects neurons from cell death under hypoxic conditions and supports neuronal growth. The rationale for mechanically dissociating the tissue was due to the protocol being not as technically challenging in comparison to generating an embryonic cortical neuronal culture, which requires euthanising the mother (thereby removing the breeding stock) and extracting the embryos (Pacifici and Peruzzi, 2012). The mechanical dissociation protocol followed similar steps utilised by McCarthy and DeVillis (1980) to generate a rat mixed glial model and this protocol was also used to generate the murine mixed glial model.

The pilot data demonstrated that although a neuronal enriched culture can be established at three different seeding densities ($1x10^5$, $2,5\ x10^5$ and $4x10^5$), there was evidence of cellular debris in both the cell viability analysis (<30% viability, n=1) in addition to non-specific staining of debris seen in the histological staining.

The presence of excessive debris could be due to the preparation procedure of the culture as this was seen in McCarthy and devillis' (1980) protocol. During cortical tissue processing, the meninges and blood vessels were not finely removed, rather, after finely mincing the cortices with a scalpel, the cells were forced through hypodermic needles to further dissociate them, and were then filtered through 70 and 40mm cell sieves, in order to remove the debris. The meninges in post-natal cultures are more adherent to the tissue and therefore, post-natal cultures tend to be less robust and have a lower yield of viable cells in comparison to embryonic neuronal cultures (Beaudoin *et al.*, 2012). This factor may have also contributed to the lower

yield of viable cells within the mechanically dissociated neuronal culture (Weinert *et al.*, 2015).The mechanical dissociation protocol and filtering the cells through cell sieves method worked for removing large chunks of debris, but was unsuccessful for remnants smaller than 40mm. Additionally, there was minimal microglia present in the culture (confirmed by immunohistochemistry), which are a phagocytic glial population that clears cellular debris. Consequently, it may have also contributed to the excessive debris (Herzog *et al.*, 2019).

The purpose of using enzymatic dissociation for the generation of the post-natal neuronal enriched culture, was to determine whether this could reduce the amount of debris and improve cell viability. Trypsin is a proteolytic enzyme used to cut the amino acids, lysine and arginine on the c-terminal (Miersch *et al.*, 2018). This in turn, breaks down the cell adhesion molecule, cadherin in order to dissociate the bond between cells, thereby producing a single cell population (Miersch *et al.*, 2018). Next, to prevent the cells from clumping together, DNAse I was used to digest and minimise the effects of free floating cellular fragments attaching to viable cells and to improve viability (Jager *et al.*, 2016; Miersch, *et al*, 2018). Using this enzymatic dissociation protocol was beneficial as cell viability analysis showed reduced cellular debris in the neuronal culture, with >80% viability across all time points (n=3). Furthermore, when viability of the culture was compared against a postnatal hippocampal neuronal model, developed by Kaar *et al.,(*2017), viability was approximately >60% at 2DIV, this however decreased to 20-40% by 11 DIV. The reduction in viability though may be due to the age of the tissue as Kaar *et al.,(*2017), who used a similar cellular dissociation protocol, used P5 mouse pups which as mentioned previously, may not be beneficial to use as tissue from P0-P2 brains for establishing a neuronal culture, have been described showing greater neuronal

survival *in vitro* in comparison to older pups (Lautenschläger *et al.*, 2018). Characterising the post-natal cortical neuronal culture showed that >45% of the cellular population was Tuj-1 positive neurons and could be derived using cortical tissue from P0 to P2 mice. Comparison for the percentage of neurons present within the culture with Kaar *et al's.,(*2017) study, showed that there were approximately 25% neuron and 75% GFAP positive astrocytes, thereby suggesting that our study generated a greater percentage of neurons. The reason for the decreased neuronal population in Kaar *et al's.,(*2017) research may have been the age of the pups (P5) that were used (Lautenschläger *et al.*, 2018).

The results were also compared with an embryonic rat cortical neuronal culture and showed that there was >80% of neurons present within the culture from 7 to 14DIV (Sahu *et al.*, 2019). However, due to there being minimal glial cells unlike our study, where there were approximately 50% astrocytes, the neurons failed to produce efficient synapses and therefore, it is beneficial to have glial cells, specifically astrocytes within the culture, as they are known to provide homeostatic support for neurons by regulating synaptic activity and synapse formation (Chung *et al.*, 2015; Mederos *et al.,* 2018)

Of the Tuj-1 positive neurons within our neuronal culture, 70% were GABA antibody positive, with the remainder of the population of neurons possibly being glutamatergic. The antibody used to detect the expression of glutamate by the neurons however could not be detected in the cultures. GABAergic neurons are inhibitory neurons that constitute to 20% of cortical neurons, and function to control the flow of information throughout the cortex. They generate the neurotransmitter GABA, to help reduce excitation of glutamatergic neurons in the CNS. They do so by regulating the amount of glutamate released by pyramidal neurons, the projection

neurons in the cortex and also through spiny stellate cells in the fourth cortical layer (Lehmann *et al.*, 2012; Caputi *et al.*, 2013).

The reason for the increased percentage of GABA neurons in the culture may be due to the high percentage of astrocytes being present, as Westergaard *et al.*,(1992) reported, co-culturing neurons with astrocytes for 7DIV, increased the expression of the GABA neurotransmitter in neurons. The authors also reported that astrocytes take up a significant amount of GABA released by the neurons.

3.31 Future Studies

This post-natal murine, cortical neuronal model has been shown to be robust, reproducible and demonstrates high cell viability and comparable in neuronal purity when compared to existing neuronal models. Additional factors that could be trialled for the neuronal culture include increasing the culturing time to a maximum of 28DIV, similar to (Beaudoin *et al.*, 2012) for longer investigations. Further studies that could be conducted to characterise the model involve calcium imaging, to measure the functional properties and electrical activity of the neurons, to assess the neuronal sensitivity and responsiveness of the cells. Calcium ions generate adaptable intracellular signals which control the key functions of neurons such as neurotransmitter release from synaptic vesicles (Grienberger and Konnerth, 2012).

The *in vitro* murine mixed glial and cortical neuronal models described in this chapter could be readily available for the testing of the cellular responses to therapeutic biomaterials. By exploiting these post-natal *in vitro* models, it reduces the reliance on using animals for early pre-clinical studies which typically requires large numbers, in

addition to surgical expertise, time, increased financial cost. Perhaps most importantly, such an approach would circumvent the ethical implications associated with using live animals.

Chapter 4

Utilisation of DuraGen Plus™ as 3-Dimensional matrix for oligodendrocyte lineage cell and cortical neuronal cell encapsulation

4.1 Introduction

One of the factors involved in achieving cell based therapy success is reliance on the efficacy and consistent delivery of the viable cells to the target site, where the cells can generate the required therapeutic effects. However, the efficacy of exogenous cellular transplantation can be hindered by extensive cell loss due to the *in vivo* delivery method (Amer*et al*, 2015).In order to promote remyelination in demyelinated SCI regions, introducing an exogenous population of oligodendrocyte lineage cells could assist in remyelination and functional recovery (Li and Leung, 2015).

As previously mentioned in the main introduction, directly delivering a transplant cell population via injections to the target site, without encapsulating the cells in a protective matrix, is not an optimal therapeutic strategy, as this can result in poor cell survival (Li and Leung, 2015). This may be because of the trauma to the cells being forced through a fine-bore needle, leading to cell shearing, clumping and ultimately cell death (Li *et al.*, 2013). Cell death, associated with direct cellular injections was evident in Czepiel *et als' ,*(2011) study, for example, which assessed the *in vivo* myelinating capacity of iPSCs-derived OPCs, in the demyelinated corpus collosum of cuprizone-fed mice. The OPCs were directly injected into the target region of the mouse model, however it was evident that 80% of the injected cells did not survive the process, while the cells that did survive, developed into mature oligodendrocytes (Nam *et al.*, 2015).

A similar cell survival rate was observed with direct injections of NSCs into chronic mice spinal cord injury models, 3 months post injury by Kumamaru *et al.*, (2013). Although the NSCs had differentiated into neurons and oligodendrocytes, only 16.9% of the engrafted cells survived 42 days post-transplantation. Additionally, it was observed that the transplanted cells had migrated 4mm away from the graft

site. Takahashi *et al.*, (2011) also reported a reduction in viability of directly injected NSCs in the subarachnoid space in a mouse spinal cord injury contusion model, with viability decreasing to 5%, 7 days post-injection and 0.3% after 6 weeks.

The matter of safely delivering an exogenous transplant population of OPCs or neuronal cells into damaged sites of the CNS, can be addressed by exploiting biomaterials, which have the potential to support cells, by providing a matrix allowing for the exchange of nutrients, oxygen and cell metabolites, in addition to enabling cell-to-cell contact and angiogenesis (Li *et al.*, 2013). More specifically, using an FDA approved neurosurgical biomaterial for cell encapsulation may be beneficial, as these materials are produced at a large scale by pharmaceutical companies and have passed the relevant safety requirements for implantation. Therefore, there is precedent for repurposing surgical biomaterials for exogenous cell transplantation (Van and Gail, 2016)

As mentioned in the main introduction (Chapter 1, section 1.7.4-1.7.7), DuraGen Plus™ is an FDA approved, surgical biomaterial that has been trialled in regenerative applications in other systems and shown to support and encapsulate a wide population of cells required for orthopaedic, nephrology and neuroscience research. The most recent study by Finch *et al.*, (2020) has shown the capability of DuraGen Plus™ in supporting an encapsulated population of murine derived NSCs (showing >94% viability) and their differentiated progeny of neurons, astrocytes, and oligodendrocytes. Thus, supporting the notion that DuraGen Plus™ may be a promising biomaterial to use for protected delivery of NSC populations to sites of neurological injury. NSCs however only generate a small percentage of oligodendrocyte lineage cells (5%) in comparison to astrocytes (80-85%) and neurons (10-15%), and this ratio is approximately seen *in vivo* (Fernandes and Chari,

2014). Finch *et als',*(2020) study also confirmed this ratio. The NSC encapsulated DuraGen Plus™ constructs only showed that 2.12% of the differentiated progeny were mature oligodendrocytes, with 18.61% Tuj-1 neurons and 79.58% GFAP astrocytes.

As endogenous OPC populations are depleted during remyelination after chronic SCI injury, introducing an enriched exogenous population of OPCs is reported by Blakemore and Irvine,(2008) to repopulate regions 5 to 10 times faster than endogenous OPCs and therefore, are capable of extensive remyelination (Almad *et al,* 2011). Additionally, as the axons and dendrites of neurons degenerate due to SCI injury causing further demyelination of axons, using an enriched population of exogenous neuronal cells to replace the impaired neurons, could possibly restore the neural circuit and may improve functionality within the site (Katoh *et al.*, 2019). Finch *et al.*, (2020) have shown DuraGen Plus™ supports neuronal cells however, less than 20% of the differentiated progeny were neurons. Therefore, using an enriched population of neurons to compensate extensive neuronal cell loss, may be beneficial for axonal regeneration and neural circuit reconstruction (Cangellaris and Gillette, 2018).

This therefore leaves scope to investigate whether DuraGen Plus™ can sustain the survival of a highly enriched population of OPCs and their mature progeny and additionally, whether this biomaterial could sustain an enriched population of neuronal cells.

Aims

The aims of this chapter therefore were to assess the feasibility:

1. Of oligodendrocyte lineage enriched DuraGen Plus^{TM} constructs derived from the mouse mixed glial culture model

2. Generation of neuron enriched DuraGen Plus^{TM} constructs derived from a postnatal neuronal model

- Determine if DuraGen Plus^{TM} can support the growth and maturation of oligodendrocyte lineage cells and neuronal cells respectively
- Conduct pilot studies to determine the optimum parameters for cell growth and establish that safety parameters which include cell viability, differentiation and maturation are not affected by the biomaterial

4.2 Results

4.2.1 Pilot study: Optimisation of parameters for oligodendrocyte lineage growth and survival in DuraGen Plus™

As the seeding of oligodendrocyte lineage cells had not previously been established on DuraGen Plus™, multiple parameters were trialled to determine the optimum conditions for oligodendrocyte linage growth and survival on the biomaterial. The schematic below (Figure 4.0) demonstrates the initial stages of optimisation that were required for producing an oligodendrocyte lineage DuraGen Plus™ construct.

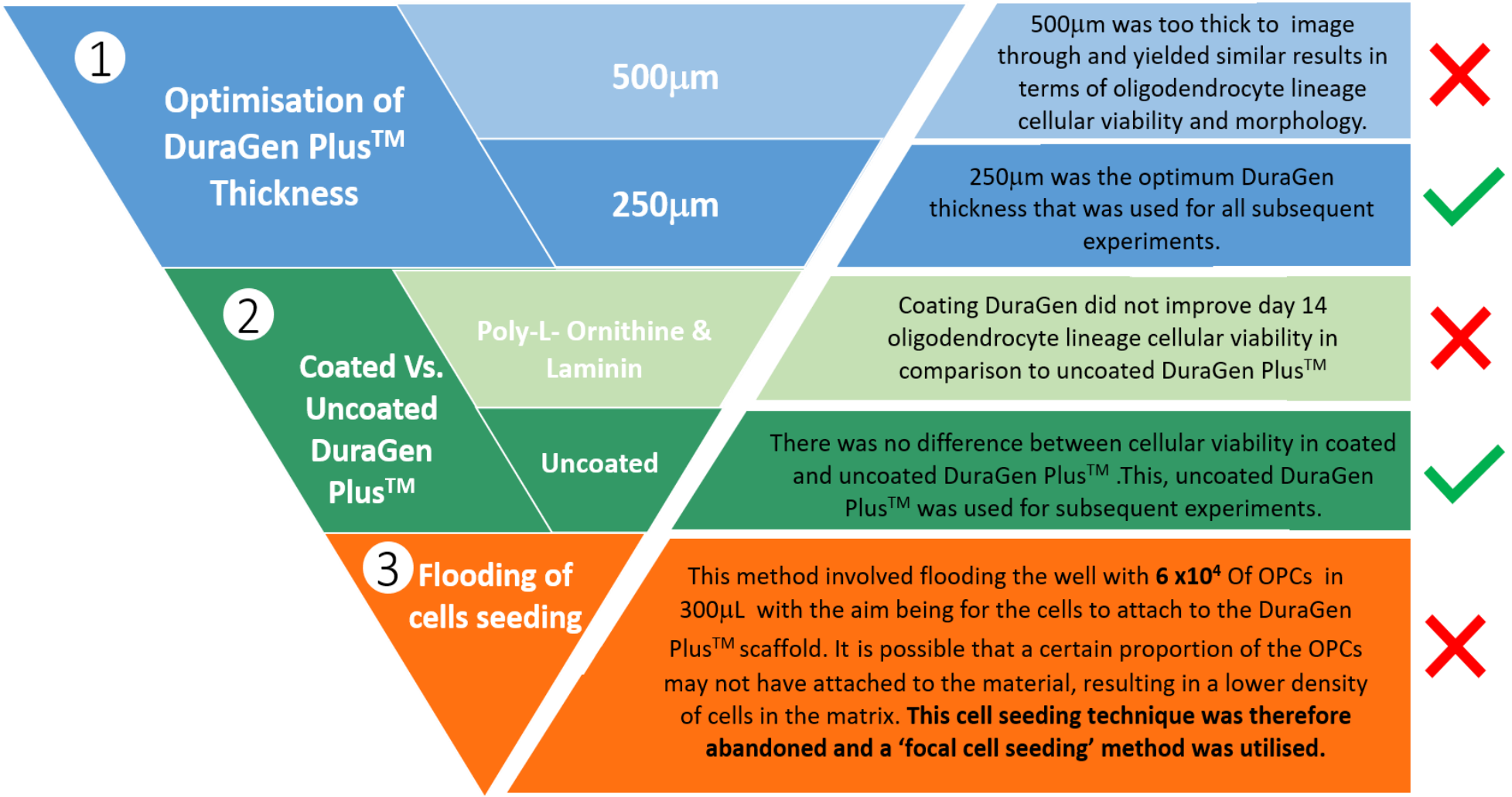

Figure 4.0. Pilot study summary for seeding optimisation stages of oligodendrocyte lineage cells in DuraGen Plus™.

4.2.2. Pilot study: Optimisation of parameters for oligodendrocyte lineage growth and survival in DuraGen Plus™ showed that thickness and coating yielded comparable results

To determine the optimum thickness for the survival and maturation of oligodendrocyte lineage cells on DuraGen Plus™, the thicknesses 250μm and 500μm were trialled. Additionally, a comparison of data between uncoated and poly-L-ornithine and laminin coated constructs was also made to investigate if coating the material would enhance cellular attachment and survival of cells (Ge *et al.*, 2015). The preliminary data to assess viability (Table 4.0 and Figure 4.1) and morphology (Table 4.1 Figure 4.2) of the cells was collected at 3 DIV for OPC lineage cells and 14 DIV for matured oligodendrocyte lineage cells. Classification of live and dead cells within the DuraGen Plus™ construct has been demonstrated in section 2.3.2 in the methods chapter.

The preliminary data indicated a similar percentage of viable cells (Calcein stained, green) and dead cells (ethidium homodimer stained, red) were observed within the construct for both thicknesses and coated and uncoated conditions, with >60% viability at 3DIV (Table 4.0, Figure 4.1 A, B, C, D). At 14DIV however, viability within the differentiated oligodendrocyte lineage constructs had decreased to below 41% (Table 4.0, Figure 4.1 E, F, G, H), with evidence of increased cellular debris and dead cells.

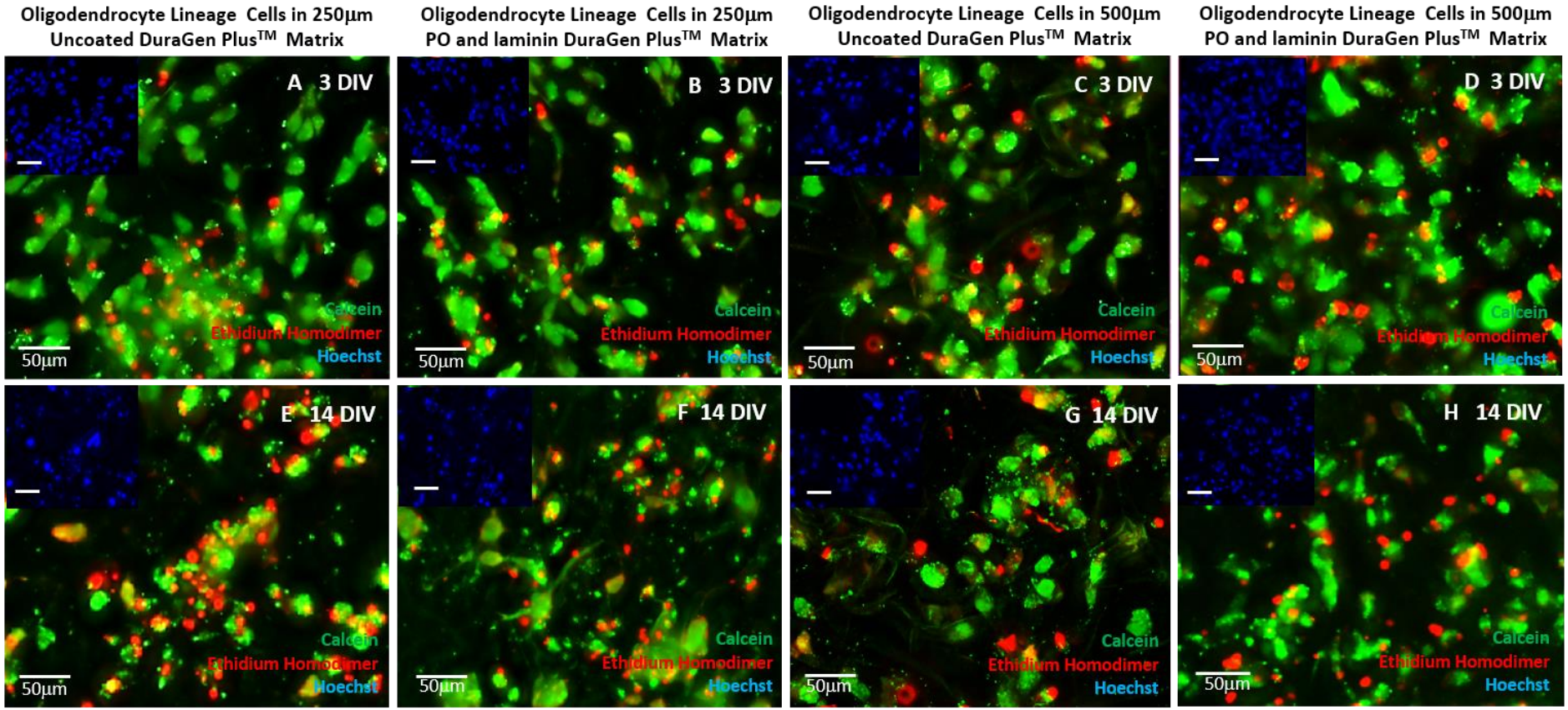

Figure 4.1 Pilot data of 3 & 14DIV oligodendrocyte lineage cell viability seeded in 250µm & 500µm uncoated and PO & laminin coated DuraGen Plus™ constructs, showed no difference in viability at their respective time points. Live cells were stained green with calcein, dead cells in red with ethidium homodimer and cell nuclei were stained blue with hoechst. **A & B)** show 3DIV oligodendrocyte lineage cells in 250mm uncoated and PO & laminin coated DuraGen Plus™ respectively. **C & D)** 3DIV oligodendrocyte lineage cells in 500µm and PO & laminin coated DuraGen Plus™ respectively. **Figure 4.1 continues below.**

Figure 4.1 continued. **E & F)** shows 14DIV matured oligodendrocyte lineage cells in 250 μm uncoated and PO & laminin coated DuraGen Plus™. **G & H)** illustrate 14DIV matured oligodendrocyte lineage cells in 500μm uncoated and PO & laminin coated DuraGen™ plus. n=1. All Z-stack CZI images were deconvolved with Huygens Professional version 19.04 (Scientific Volume Imaging, The Netherlands, http://svi.nl), using the CMLE algorithm, with signal to noise ratio (SNR):40 and maximum 50 iterations.

Table 4.0: Pilot Study: 3DIV 3 & 14DIV Oligodendrocyte lineage cells in Uncoated and POR-N & Laminin Coated DuraGen Plus™ Matrix (n=1)

	Live (%)	Dead (%)
DIV 3: 250μm Uncoated	65	35
DIV 3: 500μm Uncoated	68	32
DIV 14 250μm Uncoated	36	64
DIV 14: 500μm Uncoated	41	59
DIV 3: 250μm POR-N & Laminin	69	31
DIV 3: 500μm POR-N & Laminin	71	29
DIV 14 250μm POR-N & Laminin	40	60
DIV 14: 500μm POR-N & Laminin	22	75

Morphological features of the oligodendrocyte lineage cells within the constructs were also analysed to determine whether the parameters of thickness or coating affected cell morphology. Histological staining at 3DIV emphasised that the myelinogenic cells retained their phenotypic markers, with pilot data quantification showing that all constructs had >50% NG2 positive cells (Table 4.1, Figure 4.2 A, B, C, D), with the remainder of the population possibly being myelinating oligodendrocyte lineage cells. It is important to state here however that visualisation of the morphological features of the cells within the 500μm thickness constructs, was not as clearly distinguishable using microscopy when compared to the 250μm scaffold.

The cells within the 3DIV constructs appeared rounded in morphology, with indication of some processes extending from their cell body, but no obvious pattern or direction in growth. This therefore suggests that the DuraGen Plus™ scaffold can maintain the cells in their pre-oligodendrocyte state with no alteration of their phenotypic characteristics, and that 250μm and 500μm thicknesses, or coating of the biomaterial, generate similar outcomes. The 14DIV constructs were also stained to visualise the presence of matured oligodendrocytes, specifically with MBP, to determine whether DuraGen Plus™ can allow oligodendrocyte lineage cells to mature within the scaffold. Quantification of the pilot data (Table 4.1) shows >50% of the cells at 14DIV were positive for MBP, with the remainder possibly being NG2 positive cells. Additionally, the oligodendrocytes within the constructs appeared highly branched (Figure 4.2 E, F, G, H). The pilot data thus suggested that the thickness of the biomaterial or coating did not increase the percentage of matured oligodendrocytes.

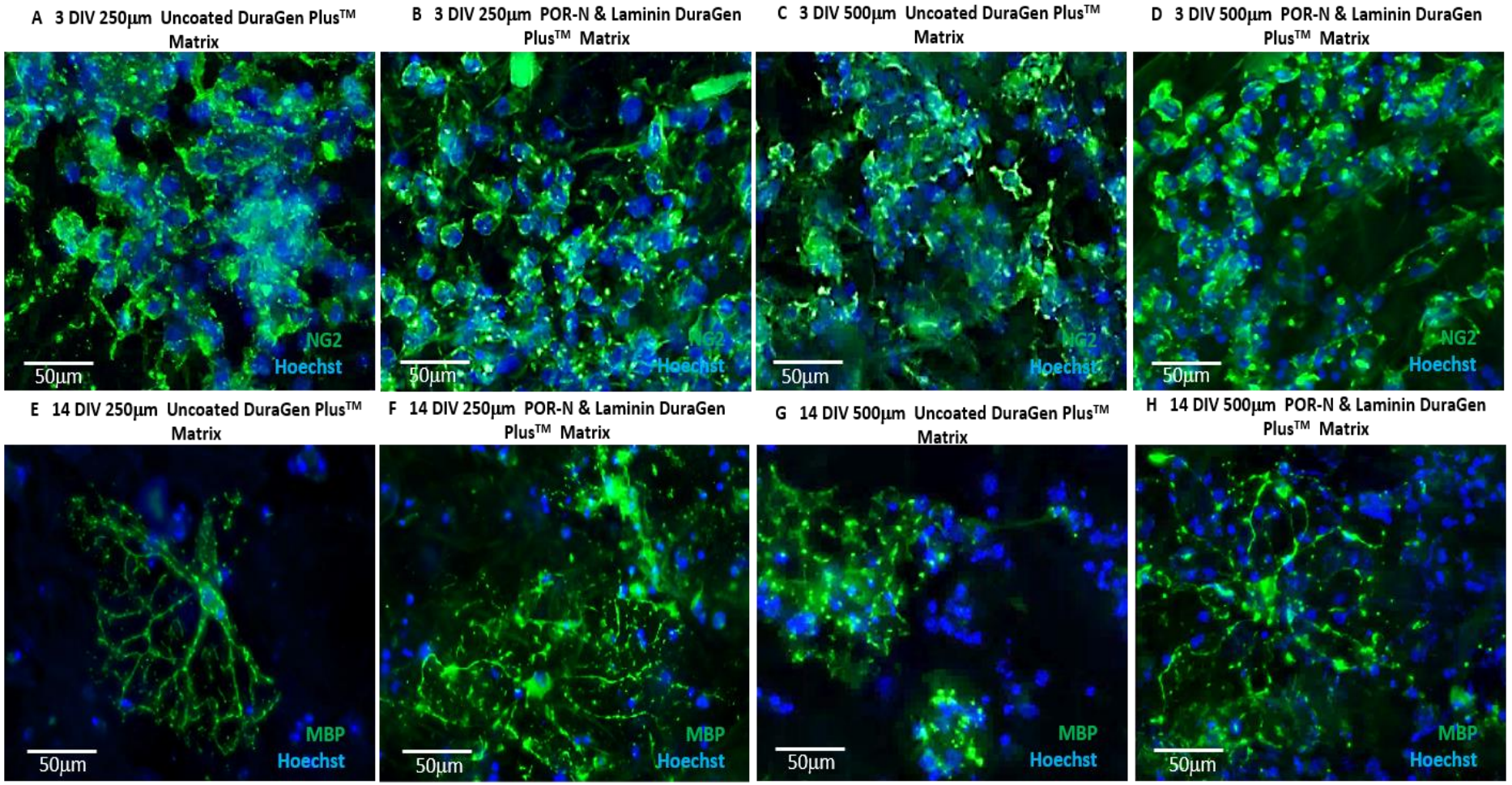

Figure 4.2 Oligodendrocyte lineage cells on coated and uncoated DuraGen Plus™. **A** & **B** show NG2 stained 3DIV OPCs in 250µm and 500µm thickness uncoated DuraGen™ respectively. **C** & **D** show NG2 stained 3DIV OPCs in 250µm and 500µm thickness PO & laminin coated DuraGen™ respectively. Image **E** & **F** is of MBP stained 14DIV matured oligodendrocytes in 250µm and 500µm thickness uncoated DuraGen™ . **Figure 4.2 continues below.**

Figure 4.2 continued. Image **G** & **H** show MBP stained 14DIV matured oligodendrocytes in 250μm and 500μm thickness PO & laminin coated DuraGen™. n=1. All Z-stack CZI images were deconvolved with Huygens Professional version 19.04 (Scientific Volume Imaging, The Netherlands, http://svi.nl), using the CMLE algorithm, with signal to noise ratio (SNR):40 and maximum 50 iterations.

Table 4.1 Pilot Study: 3DIV & 14DIV Oligodendrocyte Lineage Cell Morphology in DuraGen Plus™ Matrix (n=1)

3DIV	NG2 Positive (%)
250μm Uncoated	86
250μm POR-N & Laminin	80
500μm Uncoated	81
500μm POR-N & Laminin	80
14DIV (Differentiated)	**MBP Positive (%)**
250μm Uncoated	34
250μm POR-N & Laminin	29
500μm Uncoated	23
500μm POR-N & Laminin	25

4.2.2 Parameters chosen to take forward for developing oligodendrocyte lineage DuraGen Plus™ constructs

As the pilot data indicated that there was no difference in cell viability and morphological features, when comparing the day 3 and day 14 data for cells grown in 250μm and 500μm DuraGen Plus™, and their respective coated and uncoated counterparts for each respective timepoint, some parameters were discontinued. The discontinued parameters included the 500μm thickness slices of DuraGen Plus™. This was because although oligodendrocyte lineage cells could be visualised within the construct to an extent, visualisation of the cells when imaging, was not as clearly distinguishable when compared to using 250μm slices. Therefore, for all future experiments, 250μm was the chosen thickness as it was observed to be better for optimal imaging purposes and data analysis. POR-N and laminin coating of the construct was also discontinued as there was no increase in cell viability when compared to the uncoated scaffolds. Overall, the pilot data suggests that OPCs and oligodendrocyte lineage cells can be cultured within the DuraGen Plus™ scaffold, however, at 14DIV the overall viability of the construct is low within the construct.

4.2.3 Trialling focal seeding of myelinogenic cells at a high seeding density on DuraGen Plus™ to improve 14DIV cell survival within the construct was ineffective

Next, to help improve the viability of the 14DIV constructs, an alternative 'focal cell seeding' technique was trialled. Pilot experiments thus far used the 'flooding of cell seeding' method (Figure 4.3). The flooding of cells approach involved placing a pre-cut piece of DuraGen at the bottom of a 24 well plate, and then flooding the well with 300μL cell suspension which contained 6 $x10^4$ OPCs (Figure 4.3) The rationale for this approach was that the cells would gradually adhere and distribute in the DuraGen Plus™ matrix however, it is possible that a certain proportion of the OPCs may not have attached to the material and in turn, there may be less than 6 $x10^4$ OPCs in the construct.

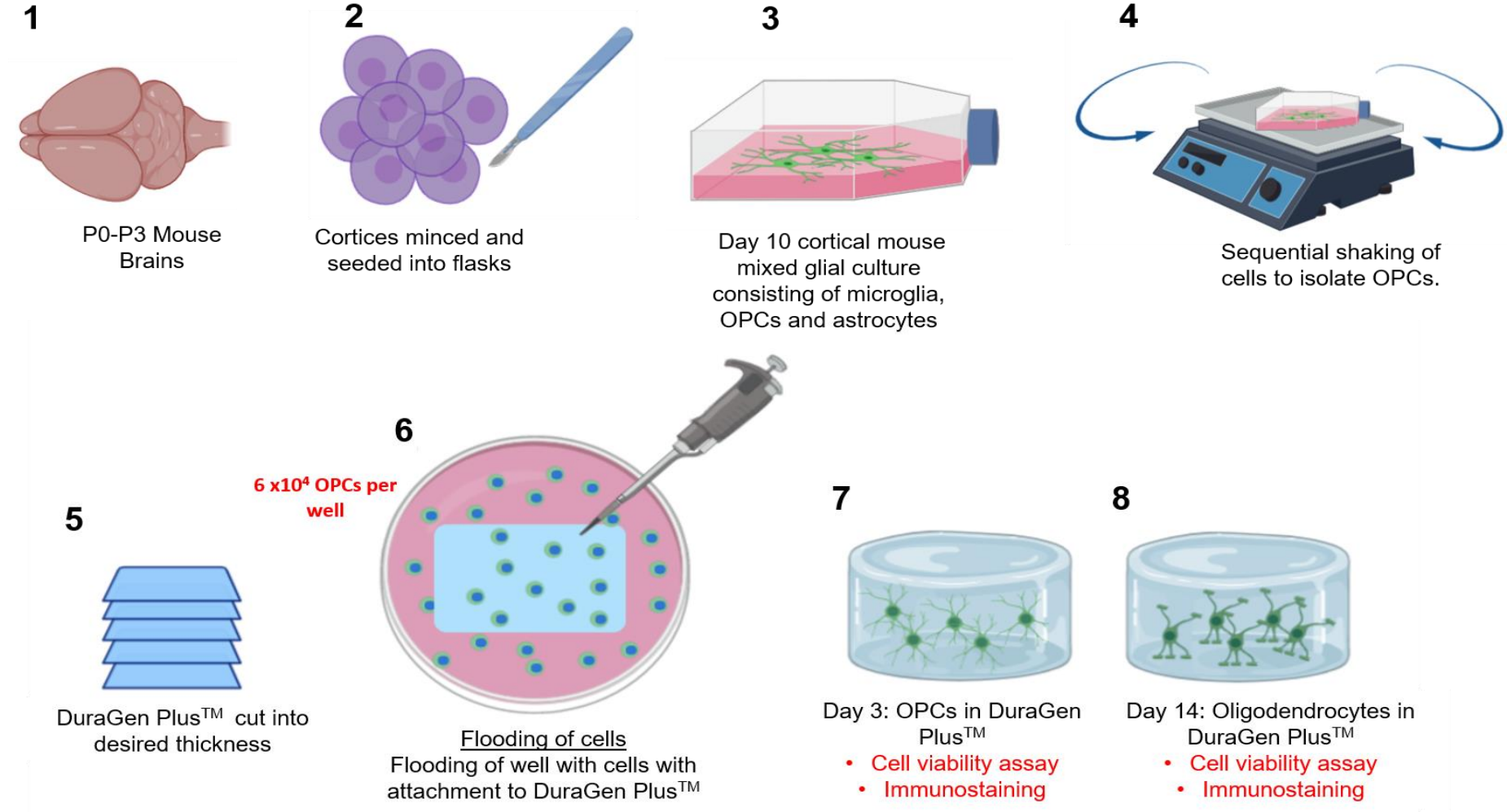

Figure 4.3. Schematic illustration of the flooding of cell seeding method of oligodendrocyte lineage cells in DuraGen Plus™. Steps 1 to 4 illustrate the mechanical dissociation of cortical tissue and the isolation of OPCs via a sequential shaking process. **Figure 4.3 continues below.**

Figure 4.3 continued. Step 5 shows DuraGen^{TM} cut into the desired thickness, for this study, this was 250μm and 500μm .**Step 6** shows the addition of 6x10^4 OPCs in 300μL of OPC maintenance medium that was added into a well, of a 24 well plate for the attachment of the cells to DuraGen^{TM} matrix**. Step 7:** At 3DIV, a cell viability assay and immunostaining were conducted on the constructs, with the medium for some wells being switched for OPC maturation into oligodendrocytes. **Step 8**: At 14DIV post maturation, cell viability assays and immunoassaying were conducted on the cell-seeded constructs.

As oligodendrocytes are highly dependent for cell to cell contact for growth and survival, to improve 14 DIV oligodendrocyte lineage survival, a focal seeding approach was trialled where a concentrated population of OPCs, was directly seeded onto DuraGen Plus^{TM}, rather than flooding the well, and at a higher density, specifically 2 x10^5 OPCs in a 10μL cell suspension per construct (see section 2.2.5.2 in the chapter 2 methods section for protocol). The cells were maintained as OPCs for 3 days in the constructs and were then differentiated into oligodendrocytes for a further 14 days as Figure 4.4 illustrates.

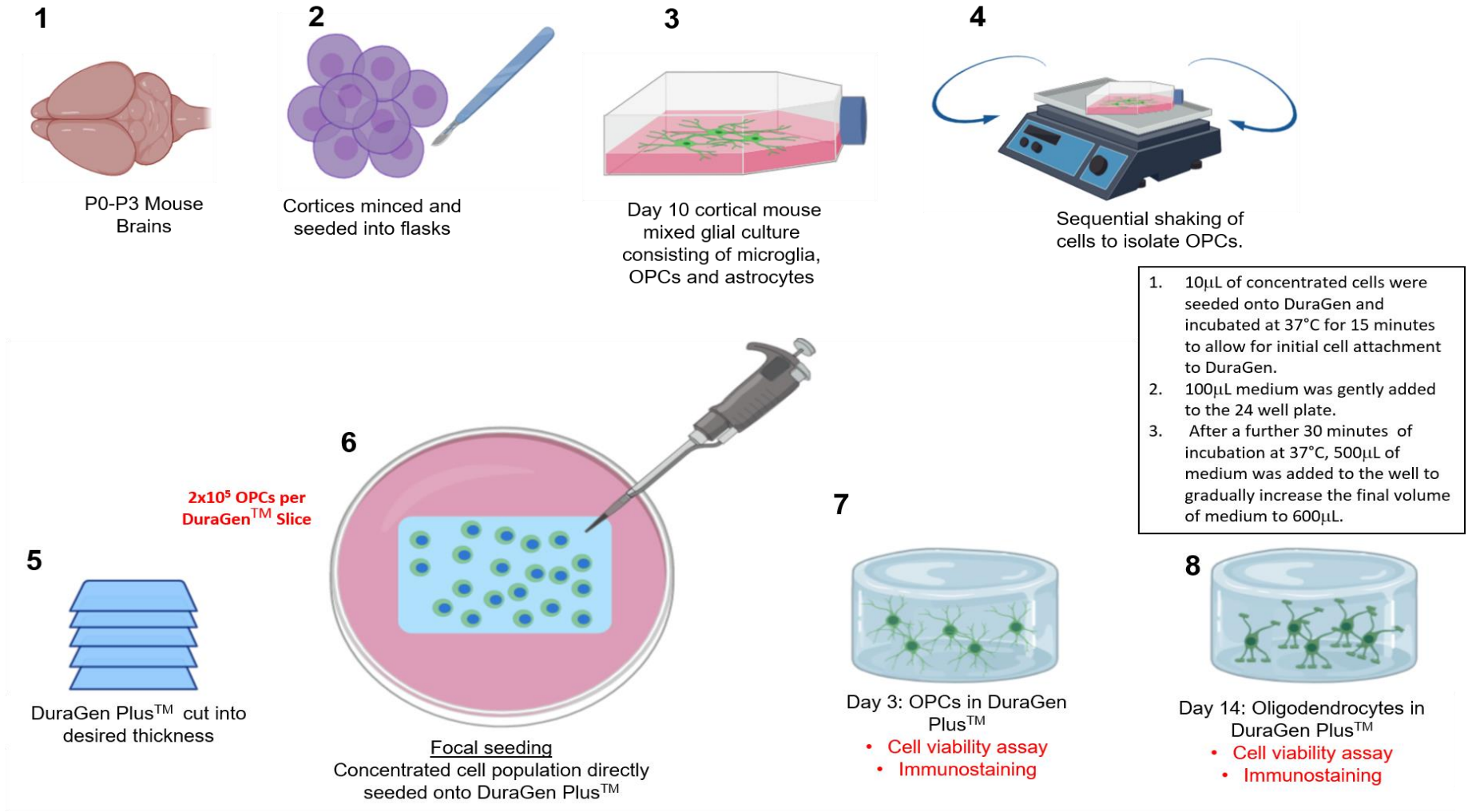

Figure 4.4. Schematic illustration of the focal seeding method of oligodendrocyte lineage cells in DuraGen Plus™.

Steps 1 to 4 illustrate the mechanical dissociation of cortical tissue and the isolation of OPCs via a sequential shaking process.

Figure 4.4 continues below.

Figure 4.4 continued. Step 5 shows DuraGen Plus™ cut into the desired thickness, for this study, this was 250μm and 500μm. **Step 6:** shows the addition of $2x10^5$ OPCs in 10μL of OPC maintenance medium that was directly seeded onto the DuraGen™ construct, in a 24 well plate. The constructs were incubated at 37°C for 15 minutes to allow for initial cell attachment. This was followed by gradual medium addition of 100μL and 500μL per well for each construct. **Step 7:** At 3DIV, cell viability assays and immunostaining were conducted on the constructs. At this stage, with the medium for some wells was switched for OPC maturation into oligodendrocytes. **Step 8**: At 14DIV post maturation, cell viability assays and immunoassaying were conducted on the cell-seeded constructs.

Utilising the focal cell seeding approach on 250μm uncoated constructs showed evidence of >60% viable cells at 3DIV (n=4) (Figure 4.5 A &E), (3DIV oligodendrocyte lineage control cells grown on glass, approximately 90% viability), Figure 4.5 C & E), which is comparable to preliminary data for 3DIV DuraGen Plus™ constructs generated using the flooding of cells seeding method. This viability also suggests that whilst the cells were maintained as OPCs, the increased density of cells in the matrix did not hinder survival. However, by 14DIV, when the DuraGen Plus™ matrix contained mature oligodendrocyte lineage cells, viability decreased to 29% (n=4) in the construct (Figure 4.5 B&F), whereas viability on glass for the cells was >80% (Figure 4.5 D& E). The decreased viability in the DuraGen Plus™ constructs using focal seeding, was similar to the preliminary data generated for 14DIV oligodendrocyte lineage constructs generated by flooding well with cells.

Histological staining of the constructs confirmed that at 3DIV, 70% of the cells retained their NG2 marker (n=4), (Figure 4.6 A & G) in comparison to approximately 95% which was seen in the control (Figure 4.6 D &G). Additionally, phenotypically the cells appeared rounded in morphology, but cellular processes could not be distinctly visualised within the construct.

Immunostaining the 14DIV constructs with NG2 and MBP markers also showed that from the proportion of viable cells, there was the presence of OPCs and mature oligodendrocytes (Figure 4.6 B, C &H). The percentage of mature oligodendrocytes (MBP stained) within the DuraGen Plus™ construct was approximately 15% in comparison to 23% in the controls. Additionally, the oligodendrocytes within the construct also did not appear highly branched when compared to the control (Figure 4.6 E&F). Furthermore, there was a greater percentage of OPCs quantified in the constructs (>50%, NG2 positive, Figure 4.6 B&H), which was comparable to the 14DIVcontrol (Figure E&H). The OPCs within the 14DIV construct also appeared to clump within the construct and there was evidence of some processes extending from the cell body towards neighbouring cells.

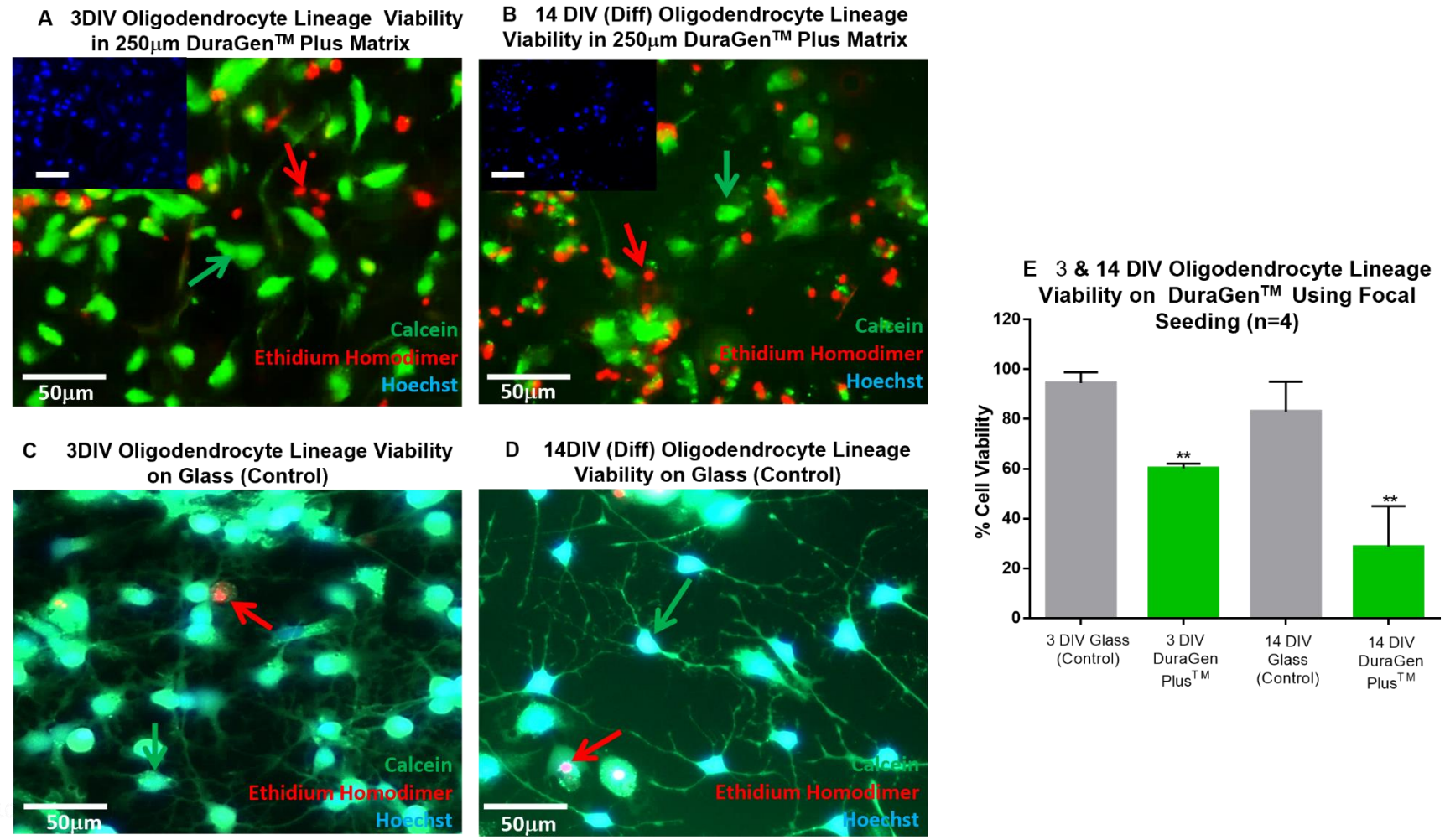

Figure 4.5 Viability of focally seeded 3 & 14 DIV oligodendrocyte lineage cells on 250μm uncoated DuraGen Plus™.

A & B) 3 & 14 DIV oligodendrocyte lineage cell viability in 250μm DuraGen Plus™ respectively, with live cells stained green (calcein) and dead cells stained red (ethidium homodimer). Hoechst was used as a nuclear stain (blue). **Figure 4.5 continues below.**

Figure 4.5 continued. **C & D)** Illustrating the 3 & 14DIV viability of oligodendrocyte lineage cells grown on glass (control). **E)** Graph illustrating 3 & 14 DIV oligodendrocyte lineage cells viability of live and dead cells in the DuraGen Plus™ construct in comparison to the controls (glass). The total cells counted for 3 DIV (glass) was 2986 of which 2834 cells were viable. In comparison, total cells counted for 14 DIV oligodendrocyte lineage cells on glass was 1046 of which 890 were viable. The total cells counted for 3 DIV DuraGen Plus™ was 3822 of which 2249 cells were viable. Lastly, the total cells counted for 14 DIV DuraGen Plus™ was 2308 of which 824 cells were viable. Statistical analysis with a one-way ANOVA and Bonferroni's MCT showed that there was a significant difference between viability of focally seeded cells at 3 & 14 DIV on DuraGen Plus™ constructs (** $P<0.01$). n=4. Additionally, there was also was no significant difference in live cell viability between 3DIV and 14DIV cells grown on glass (control) ($P>0.05$). n=4. All Z-stack CZI images were deconvolved with Huygens Professional version 19.04 (Scientific Volume Imaging, The Netherlands, http://svi.nl), using the CMLE algorithm, with signal to noise ratio (SNR):40 and maximum 50 iterations.

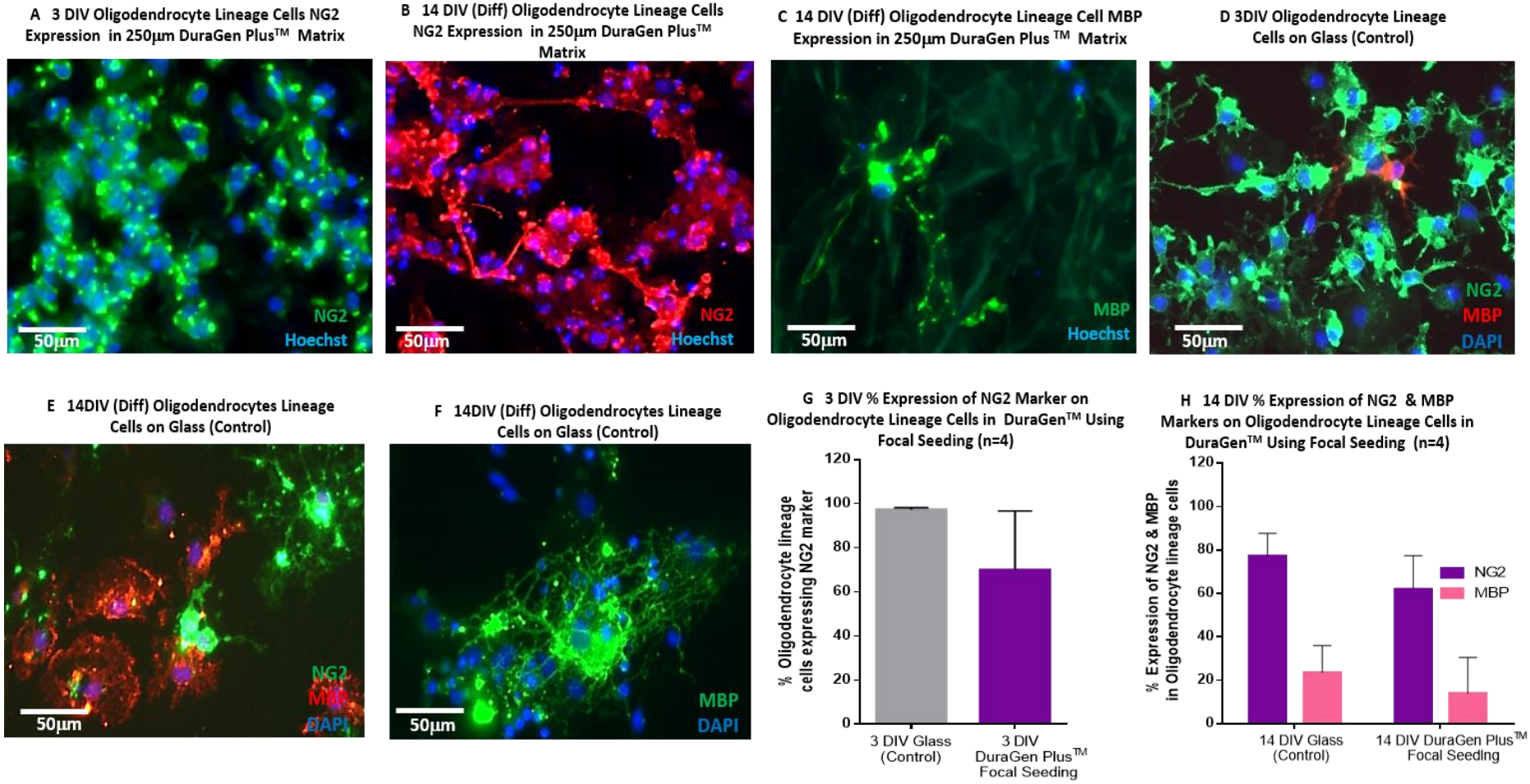

Figure 4.6 Purity of focally seeded 3 & 14 DIV oligodendrocyte lineage cells on 250µm uncoated DuraGen Plus™. A & B) Images illustrating the presence of NG2 positive cells at 3 & 14 DIV respectively in DuraGen Plus™ constructs. **C)** Histological staining with MBP at 14DIV confirming the presence of mature oligodendrocytes within the DuraGen Plus™ construct. **Figure 4.4 continues below.**

Figure 4.6 continued. **D &E)** 3 & 14 DIV oligodendrocyte lineage cells co-stained with NG2 (green), and MBP (red) on glass respectively. **F)** 14DIV mature oligodendrocytes stained with MBP on glass. **G)** Graph showing the quantification of NG2 positive cells at 3DIV in the DuraGen Plus™ construct in comparison to the control (glass) with **H)** showing the percentage of NG2 and MBP positive cells at 14 DIV in the constructs and the control (glass). n=4. The total cells counted for 3DIV glass (control) was 2406 cells of which 2349 were NG2 positive. In comparison, there as a total of 7350 cells counted for 3 DIV DuraGen Plus™ focal seeding, with 5324 of the cells being NG2 positive. For 14 DIV, glass (control) was 1325 with 995 cells being NG 2 positive and 330 cells MPB Positive. A total of 2586 cells were counted for 14 DIV DuraGen Plus™ focal seeding with 2184 cells being NG2 positive and 402 cells being MBP positive. All Z-stack CZI images were deconvolved with Huygens Professional version 19.04 (Scientific Volume Imaging, The Netherlands, http://svi.nl), using the CMLE algorithm, with signal to noise ratio (SNR):40 and maximum 50 iterations.

4.2.4. Establishing the potential supportive role of astrocytes to improve oligodendrocyte lineage cell survival in DuraGen Plus™ constructs

Astrocytes are involved in regulating oligodendrocyte lineage cell development and myelination (Tognatta *et al.*, 2020). Disruption between the gap junction contacts of astrocytes and mature oligodendrocytes, can result in thinner myelin formation and also oligodendrocyte cell loss (Tognatta *et al.*, 2020). The gap junctions between astrocytes are made up of connexin (Cx) 30 and 43 that form heterotypic channels which couples to adjacent oligodendrocytes that express CX32 and Cx47. The

physical contact between the gap junction is also necessary for oligodendrocyte maturation (Nutma *et al.*, 2020). Additionally, astrocytes secrete neurotrophic and growth factors, plus cytokines such as CNTF, LIF, FGF-2 and IL-6 which affect survival, proliferation and maturation of oligodendrocytes (Kıray *et al.*, 2016a). The rationale, therefore, for utilising astrocytes and co-seeding with oligodendrocyte lineage cells, was to determine whether astrocytes could potentially improve mature oligodendrocyte cell survival within the DuraGen Plus™ matrix.

4.2.4.1 Co-culturing of OPCs with astrocytes to improve oligodendrocyte lineage survival in DuraGen Plus™

The focal cell seeding method was taken forward for the co-culturing of cells to ensure adequate and sole coverage onto the DuraGen Plus™ matrix. For the ratio of myelinogenic cells to astrocytes, it was decided to use 2 $x10^5$ / 10mL for OPCs and 2.4 $x10^5$/10mL for astrocytes. Besides the 3DIV and 14DIV timepoints, an additional timepoint of 7DIV was added to investigate viability for matured oligodendrocyte lineage cells at an earlier stage. For the seeding of OPCs and astrocytes onto DuraGen Plus™, a schematic has been provided below (Figure 4.7) which illustrates the steps for generating these constructs.

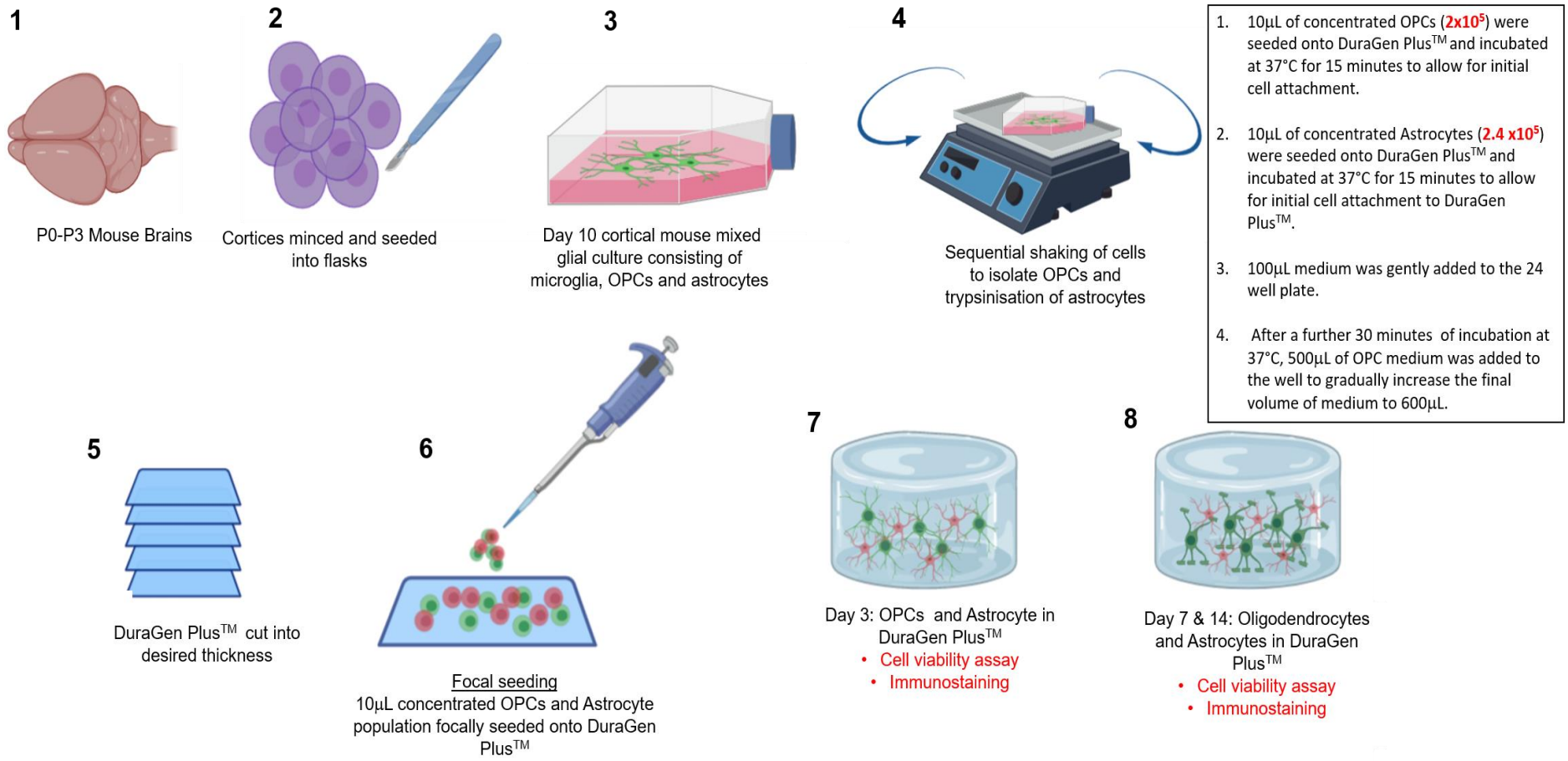

Figure 4.7. Schematic illustration of the focal seeding method of oligodendrocyte lineage cells and astrocytes in DuraGen Plus™ for the generation of a co-construct. Steps 1 to 4 illustrate the mechanical dissociation of cortical tissue and the isolation of OPCs via a sequential shaking process and trypsinisation of astrocytes. **Step 5** shows DuraGen™ cut into the thickness of 250µm. **Figure 4.7 continues below.**

Figure 4.7 continued. Step 6: shows the addition of $2x10^5$ OPCs in 10μL of OPC maintenance medium that was directly seeded onto the DuraGen™ construct, in a 24 well plate. The constructs were incubated at 37°C for 15 minutes to allow for initial cell attachment. Next, 2.4 $x10^5$ astrocytes in 10μL of OPC maintenance was seeded onto the construct. This was followed by gradual medium addition of 100μL and 500μL per well for each construct. **Step 7:** At 3DIV, cell viability assays and immunostaining were conducted. At this stage, the medium for some wells was switched for OPC maturation into oligodendrocytes. **Step 8**: At 14DIV post maturation, cell viability assays and immunostaining were conducted on the cell-seeded constructs.

4.1.4.2 Co -seeding oligodendrocyte lineage cells with astrocytes improved overall viability in DuraGen Plus™ constructs

The 3DIV oligodendrocyte lineage and astrocyte co-constructs demonstrated >80% viability (n=4) (Figure 4.8 A &D), which is approximately a 20% increase in viability when compared to the focally seeded 3DIV oligodendrocyte lineage cells, seeded as a monoculture. Similarly, viability in the 7 DIV matured co-constructs was also approximately 80% however by 14 DIV, this decreased to 66% (Figure 4.8 B, C& D). However, when comparing viability of focally seeded, 14DIV mature oligodendrocyte lineage cells seeded as a monoculture on DuraGen Plus™ to the co-cultured constructs, there was also approximately a 27% increase in viability on the co-constructs. Therefore, suggesting that the addition of astrocytes may have improved overall health of the cells within the construct, however, viability by 14DIV had decreased. Moreover, it is unknown whether the increase in viability at 3, 7 and 14DIV is that of the astrocytes or oligodendrocyte lineage cells solely.

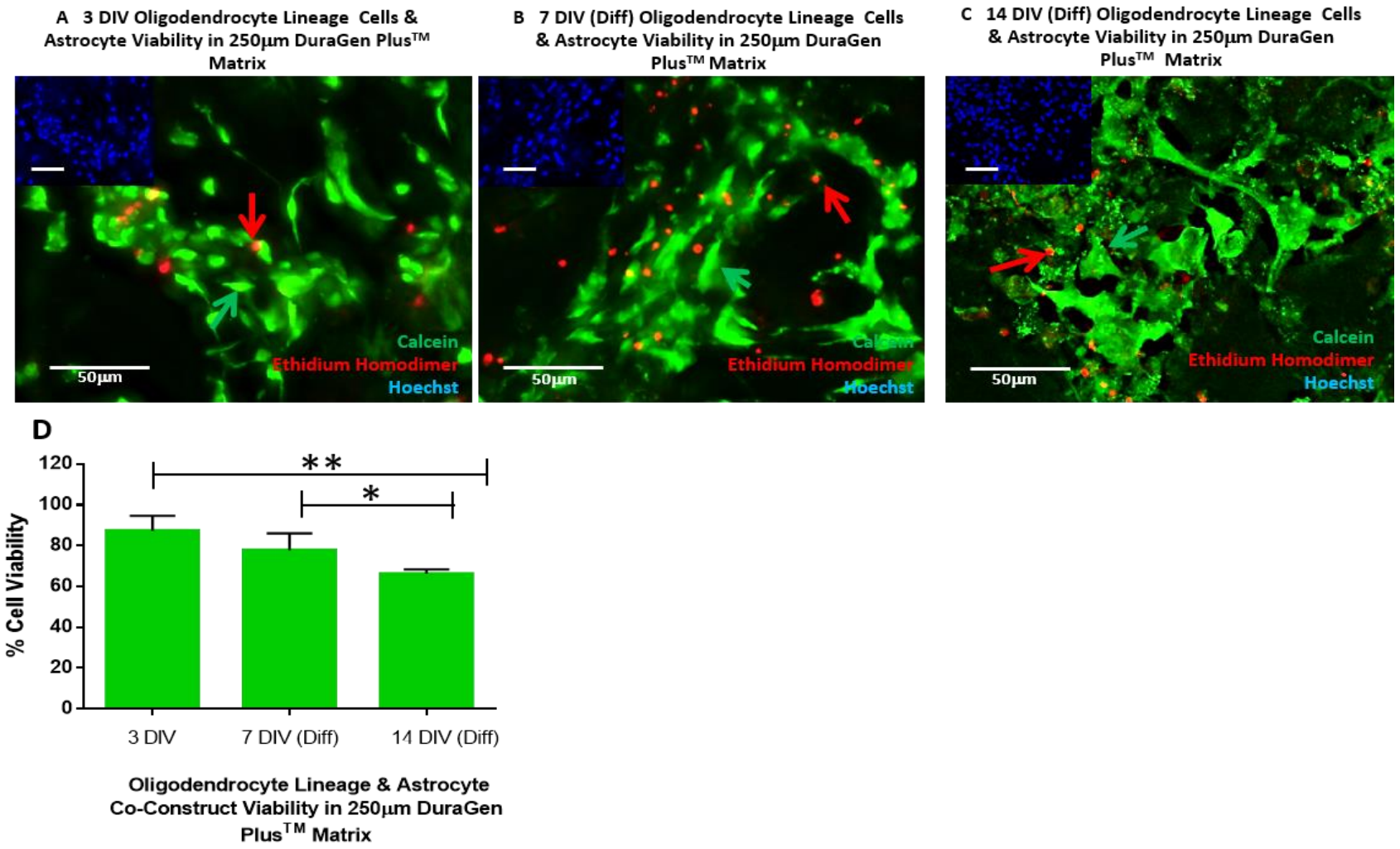

Figure 4.8. Viability of oligodendrocyte lineage cells co-cultured with astrocytes in DuraGen Plus ™ matrix. A, B & C respectively demonstrating 3DIV, 7DIV and 14DIV cell viability in the DuraGen™ constructs. Green arrows indicate the presence of viable cells whereas the red arrows indicate dead cells. **Figure 4.8 continues below.**

Figure 4.8 continued. Graph **D** represents 3DIV and 7DIV viability indicating that cell viability in the constructs is >75% at the timepoints and decreased to 66% at 14DIV. n=4. The total cells counted for 3 DIV was 4334 with 2701 cells being viable, in comparison the total cells counted for 7 DIV was 2876 with 2274 cells being calcein positive, indicating they were viable. Lastly, at 14 DIV, of the 2236 total cells counted, 2000 of the cells were viable.Data was analysed by one-way ANOVA with Bonferroni's MCT and is expressed as mean ± SD. There was no significant difference in viability ($P > 0.05$) when comparing 3DIV and 7DIV timepoints however, there was a significant difference in viability between 3 & 14DIV **($P < 0.01$) and between the 7 and 14DIV timepoints *($P < 0.05$). n=4. Scale bar represents 50μm. All Z-stack CZI images were deconvolved with Huygens Professional version 19.04 (Scientific Volume Imaging, The Netherlands, http://svi.nl), using the CMLE algorithm, with signal to noise ratio (SNR):40 and maximum 50 iterations.

4.2.4.3 There was the presence of highly branched myelinogenic cells in the mature co-seeded DuraGen Plus™ constructs

Greater than 70% of the cells in the co-construct were NG2 positive at 3DIV, indicating that there was a high proportion of OPCs present, with <30% astrocytes (GFAP positive) in the DuraGen Plus™ matrix (Figure 4.9 D, n=3). Phenotypically the OPCs had a rounded cell body and the extension of bipolar processes, with OPCs also occasionally appearing to be situated on top of an astrocyte (Figure 4.9 A). The astrocytes in comparison appeared to have an elongated cell body with a small soma and occasionally, clustered together within the construct. At 7DIV post maturation, there were approximately 40-50% MBP stained, myelinating oligodendrocytes in the co-constructs with processes extending through multiple planes in the matrix and 40 to 60% GFAP positive astrocytes (Figure 4.9 B &E). Lastly, at 14DIV post maturation, there as the presence of approximately 20% highly branched oligodendrocytes with 80% astrocytes (Figure 4.9 C& F).

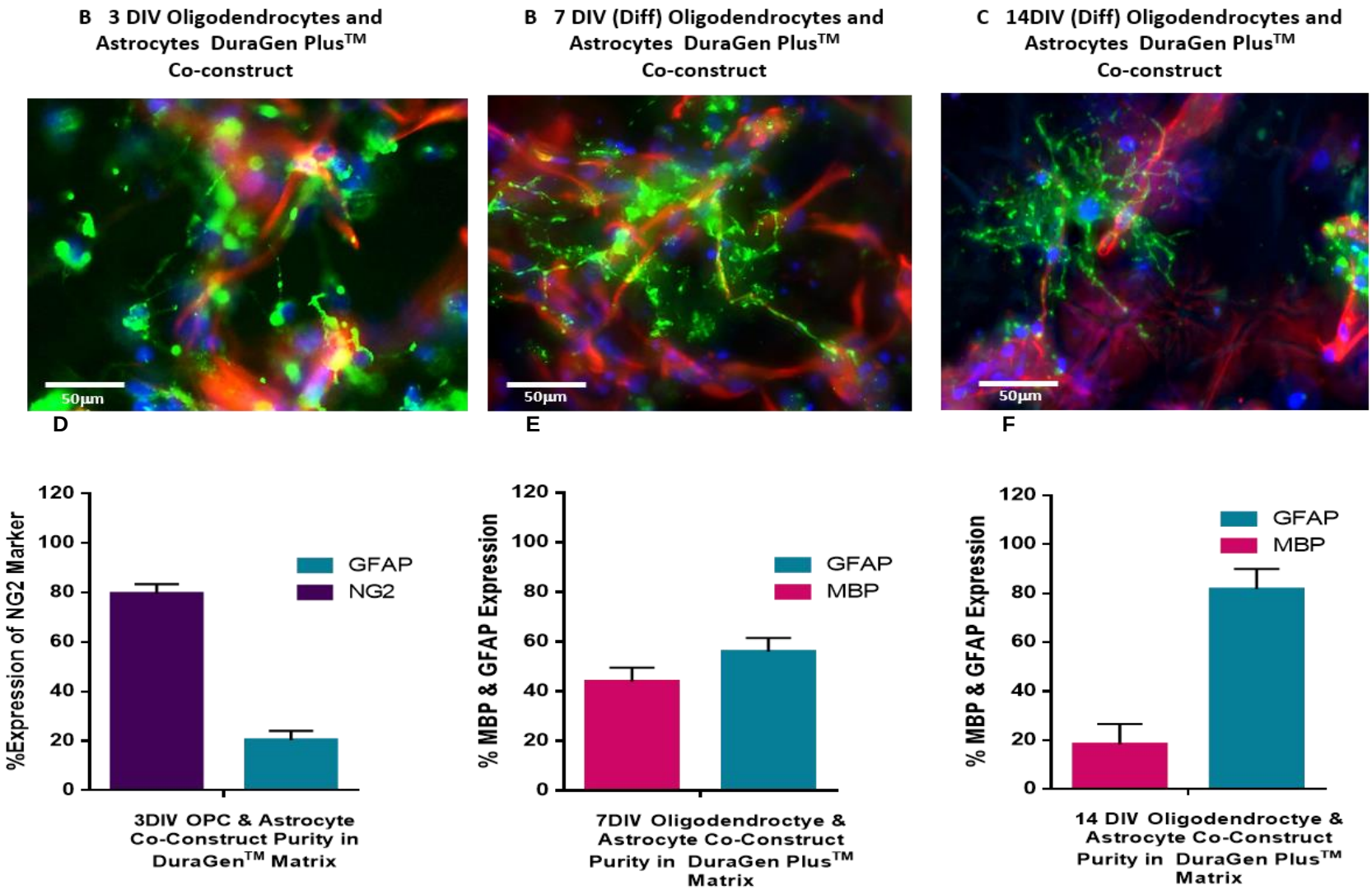

Figure 4.9. Oligodendrocyte lineage cells co-seeded with astrocytes in DuraGen Plus™ demonstrates the presence of branched myelinogenic cells by 7 & 14DIV. A) Illustrates 3DIV OPC (NG2, green) and astrocyte (GFAP, red) morphology in the co-construct with **D)** showing the 3DIV percentage of OPCs and astrocytes in the construct. **Figure 4.9 continues below.**

Figure 4.9 continued. B) confirms the presence of MBP positive (green) mature oligodendrocytes at 7DIV co-seeded with astrocytes (red) with **E)** showing the 7DIV percentage of both MBP & GFAP positive cells within DuraGen Plus^{TM} matrix. Lastly, **C**) represents the presence of highly branched, mature oligodendrocytes (MBP, green) with astrocytes (GFAP, red) at 14DIV in the construct with **F**) showing the 14DIV complimentary data for the percentage of these cells types in the DuraGen Plus^{TM} matrix. n=4. The total cells counted for the 3 DIV constructs was 2375 with 1908 of the cells staining positive for NG2 and 467 cells were GFAP positive. At 7 DIV, of the 1893 cells counted, 855 cells were MBP positive with 1038 cells being GFAP positive. Finally in the 14 DIV constructs, of the 957 cells counted, 195 cells were MBP positive and 762 were GFAP positive. Statistical analysis for the comparison between the percentage of MBP positive oligodendrocytes at 7 and 14DIV, was carried out using a paired, non-parametric T-test with Wilcoxn matched pairs signed rank test, which confirmed that at 7DIV and 14DIV, there was no significant difference for the percentage of MBP positive oligodendrocytes in the DuraGen Plus^{TM} constructs. Data was also analysed to determine the statistical significance in the increase of GFAP positive astrocytes from 3 to 7DIV and 7 to 14 DIV respectively. A one-way ANOVA with Bonferroni's MCT, expressed as mean ± SD, confirmed that there was a significant difference seen in the increase in GFAP positive astrocytes from 3 to 7DIV and 7 to 14DIV respectively **($P<0.01$). All Z-stack CZI images were deconvolved with Huygens Professional version 19.04 (Scientific

Volume Imaging, The Netherlands, http://svi.nl), using the CMLE algorithm, with signal to noise ratio (SNR):40 and maximum 50 iterations.

4.3 Results: Seeding of neuronal enriched cells on DuraGen Plus™ scaffold

`4.3.1 Pilot study: Seeding of mechanically dissociated post-natal cortical neuronal cultures on DuraGen Plus™ generated cellular debris within the construct

As the seeding of cortical neuronal cultures had previously not been established on DuraGen Plus™, the densities 1x10^5, 2.5 x10^5 and 4x10^5 cells/mL were trialled for mechanical dissociation. The thicknesses 250μm DuraGen Plus™ was also used for encapsulation of the cells in the scaffold. The viability of the cells at 9 DIV (Figure 4.10 A,B&C and Table 4.2) showed that there were <20% viable cells at all densities in the matrix, with evidence of extensive cellular debris, indicated by the red ethidium homodimer stain. Classification of live and dead cells within the DuraGen Plus™ construct has been described in section 2.3.2 in the methods chapter. Furthermore, there was also evidence of cellular debris in the immunostained cells (TUJ-1 & GFAP), with evidence of cellular clumping.

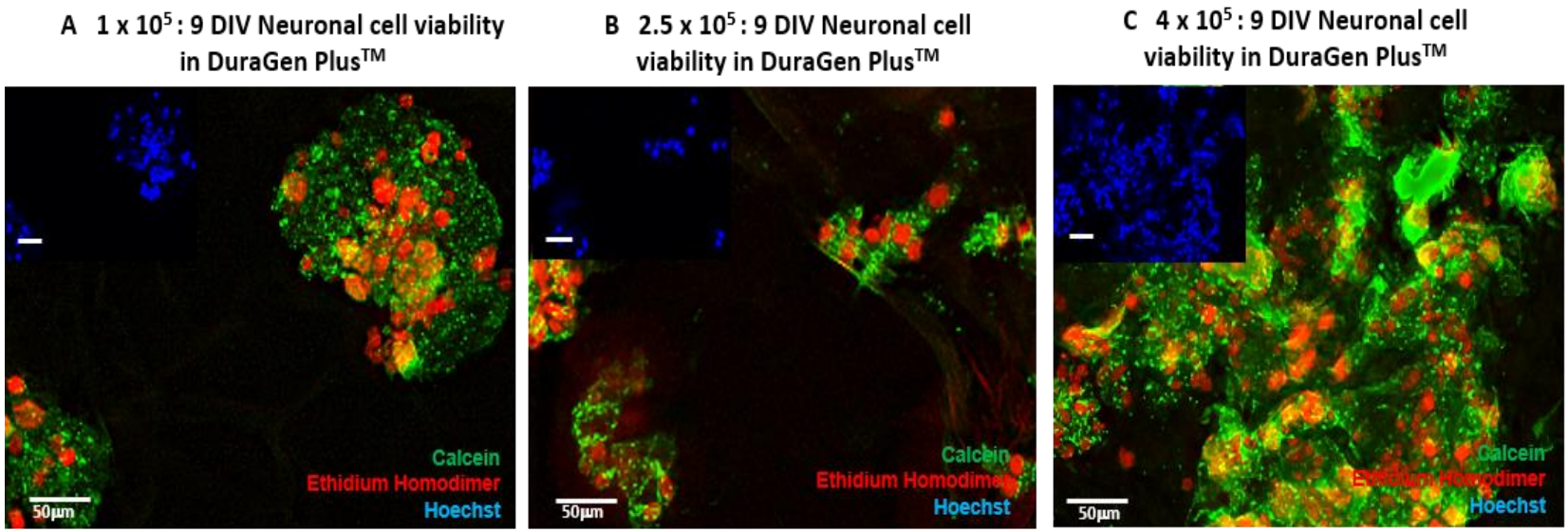

Figure 4.10 Pilot study: 9 DIV cell viability of mechanically dissociated cortical neuronal cultures on 250µm uncoated DuraGen Plus™ matrix showing low viability. Live cells were stained with calcein (green) with dead cells stained with ethidium homodimer (red). Representative images demonstrate cell viability at the seeding densities A) 1 X10^5 B) 2.5 X10^5 C) 4 X10^5 cells/mL respectively. n=1. All Z-stack CZI images were deconvolved with Huygens Professional version 19.04 (Scientific Volume Imaging, The Netherlands, http://svi.nl), using the CMLE algorithm, with signal to noise ratio (SNR):40 and maximum 50 iterations.

Table 4.2. Pilot Study: Cell viability of neuronal culture using mechanical dissociation demonstrated low viability on DuraGen Plus™ (n=1)	
Cell Viability (%)	
Seeding Density (cells/mL)	**Day 9**
1 x10^5	14
2.5 x10^5	16
4 x10^5	20

.

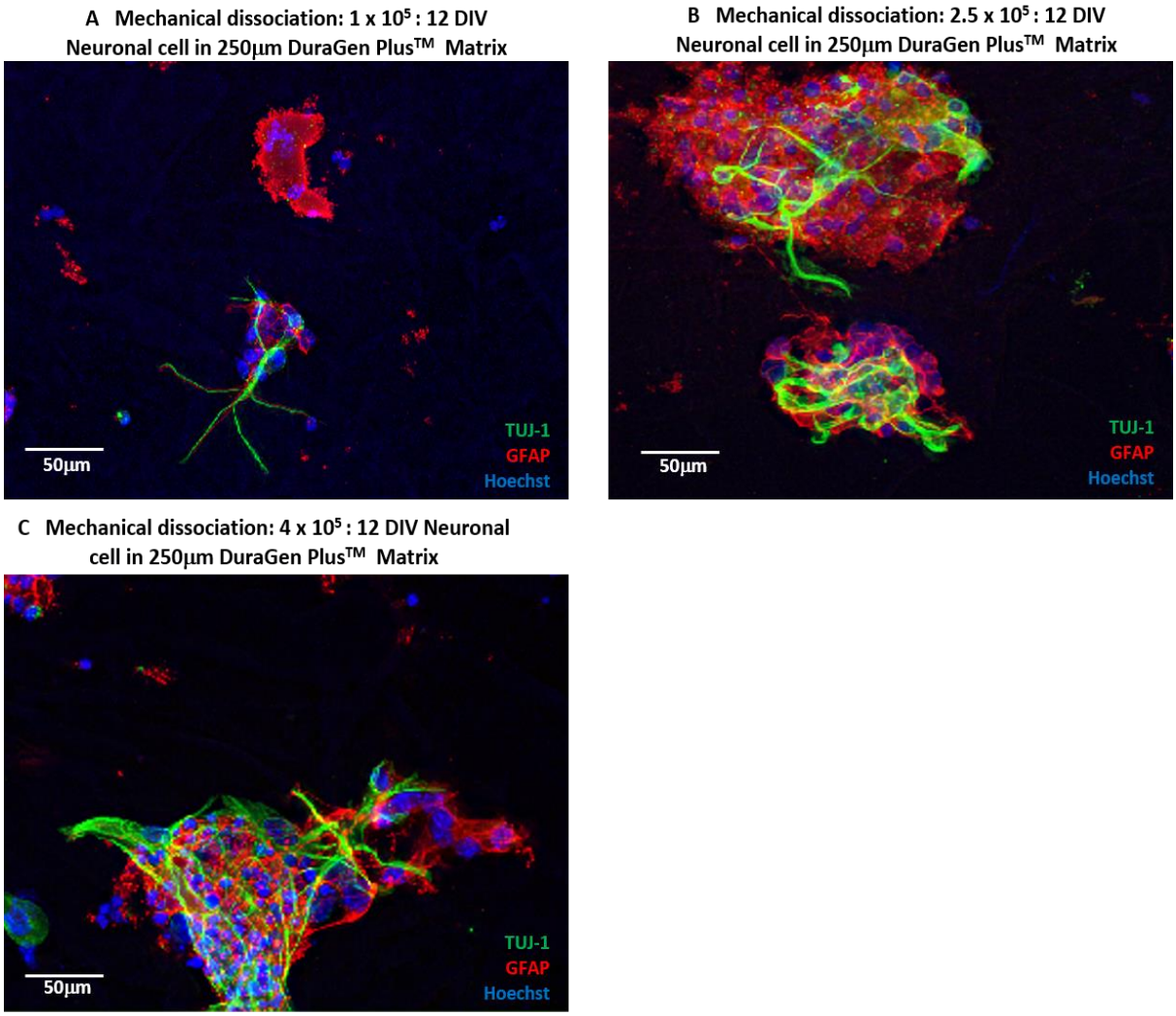

Figure 4.11. Pilot study for 12 DIV histological staining of mechanically dissociated cortical neuronal enriched cells on 250µm uncoated DuraGen™ Plus matrix at three different seeding densities. Representative images demonstrate cells encapsulated in the matrix and the densities **A)** 1 X10^5 **B)** 2.5 X10^5 **C)** 4 X10^5 cells/mL . Cultures were stained with cultures stained with Tuj-1, a neuron-specific marker (green) and GFAP, an astrocyte marker (red). n=1. All Z-stack CZI images were deconvolved with Huygens Professional version 19.04 (Scientific Volume Imaging, The Netherlands, http://svi.nl), using the CMLE algorithm, with signal to noise ratio (SNR):40 and maximum 50 iterations.

4.3.2 Pilot study: Enzymatic dissociation of neuronal cells seeded onto DuraGen Plus ™ improved viability and reduced cellular debris

To reduce cellular debris within the constructs and improve viability, the cortical-neuronal enriched cells were derived using enzymatic dissociation. Going forward, the seeding densities 2.5 and 4 x10^5 were used as they provided a denser culture of cells. Additionally, the time points 3 and 6 DIV were investigated to determine viability earlier than 9 DIV in the constructs, and 12 DIV which were believed to be sufficient time for the formation of a neuronal network within 2D *in vitro* cultures was used as a time point for immunostaining (Beaudoin *et al.*, 2012; Kuijlaars *et al.*, 2016). Utilising the enzymatic dissociation protocol had reduced debris within the constructs, with viability being reported as being >56% across all time points (Figure 4.12, Table 4.3). Although this was an improvement in comparison to the viability of mechanically dissociated cells, there was still a high percentage of dead cells within the construct and viability was below 60%.

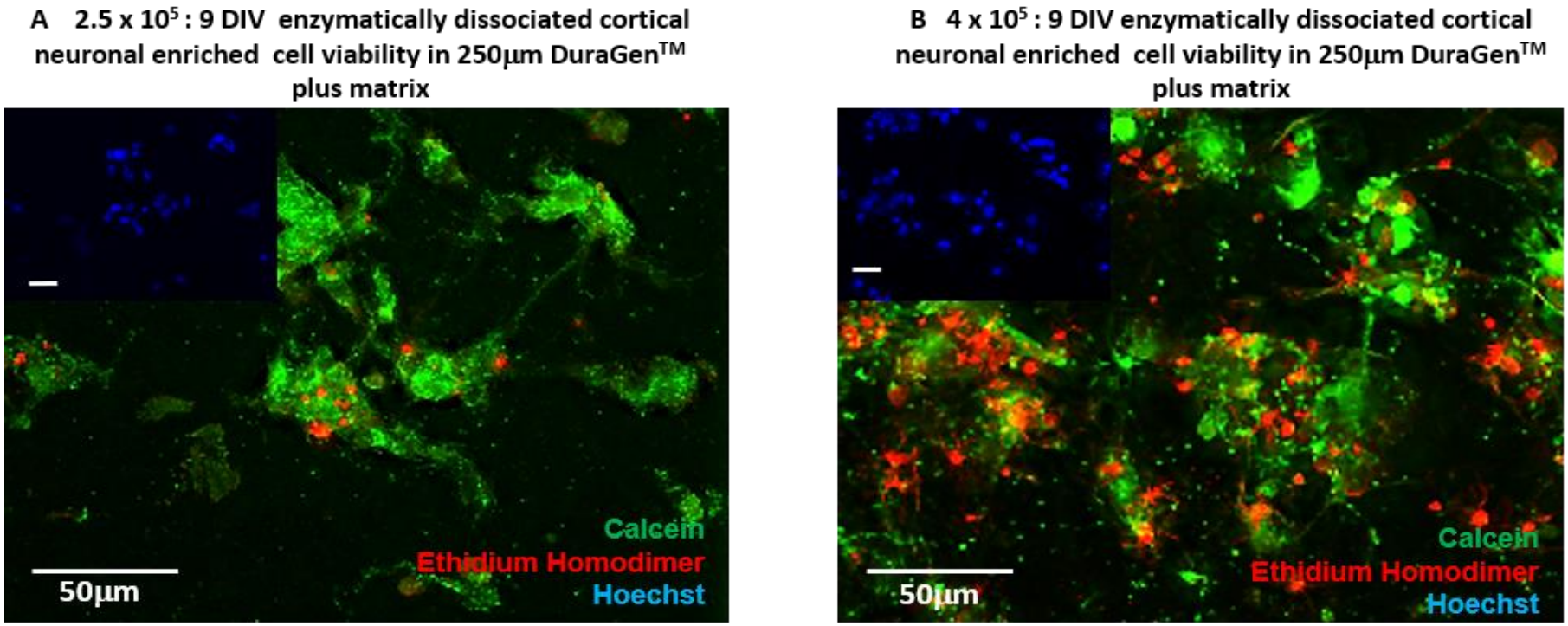

Figure 4.12. Pilot study for 9DIV cell viability of enzymatically dissociated cortical neuronal enriched cells on 250µm uncoated DuraGen Plus™ matrix at two seeding densities. Live cells are stained with Calcein (green) with dead cells stained with ethidium homodimer (red). Representative images demonstrate cell viability at the seeding densities A) 2.5 X10^5 & B) 4 X10^5 cells/mL. n=1. All Z-stack CZI images were deconvolved with Huygens Professional version 19.04 (Scientific Volume Imaging, The Netherlands, http://svi.nl), using the CMLE algorithm, with signal to noise ratio (SNR):40 and maximum 50 iterations.

Table 4.3 Pilot Cell viability of neuronal culture using enzymatic dissociation: 250um uncoated DuraGen Plus™ (n=1)			
Cell Viability (%)			
Seeding Density (cells/mL)	**Day 3**	**Day 6**	**Day 9**
2.5 x10^5	**56**	**59**	**57**
4 x10^5	**60**	**59**	**59**

Staining of the constructs with the cell-specific markers, Tuj-1 and GFAP at 12 DIV (Figure 4.13) , confirmed the presence of both neurons and astrocytes at 2.5 x10^5 and 4 x10^5 cells/mL seeding densities and in addition, showed that there was minimal cellular debris within the constructs. However, it was also observed that the cells were clustered within regions of the scaffold.

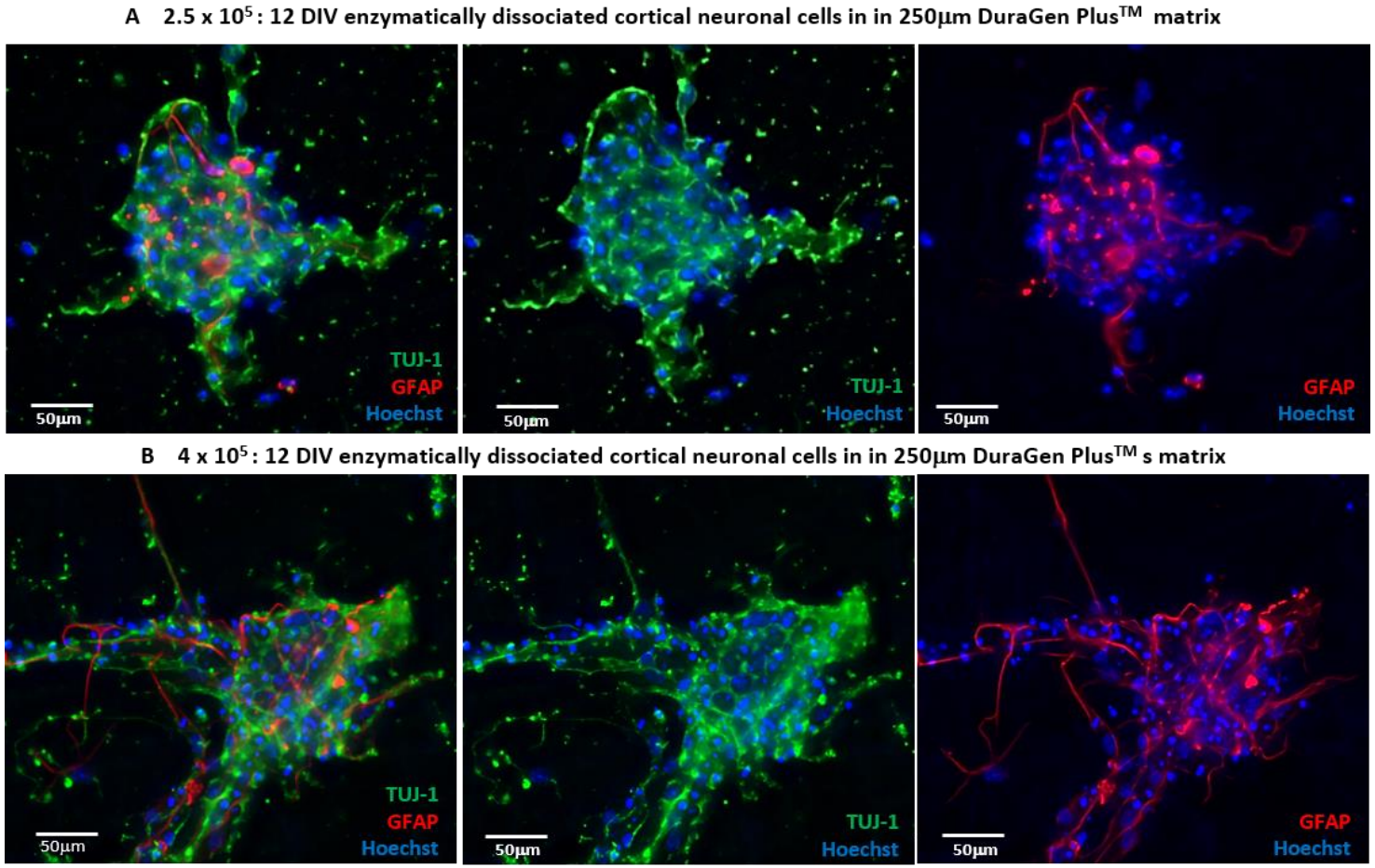

Figure 4.13 Pilot study for 12 DIV histological staining of enzymatically dissociated cortical, neuronal enriched cells on 250µm uncoated DuraGen Plus™ matrix at two seeding densities. Representative images demonstrate cells encapsulated in the matrix at the densities **A)** 1 X10^5 B**)** 2.5 X10^5 cells/mL **C)** 4 X10^5 with Tuj-1 neurons stained green and GFAP positive astrocytes stained red. n=1. **Figure 4.13 continues below.**

Figure 4.13 continued. All Z-stack CZI images were deconvolved with Huygens Professional version 19.04 (Scientific Volume Imaging, The Netherlands, http://svi.nl), using the CMLE algorithm, with signal to noise ratio (SNR):40 and maximum 50 iterations.

4.2.3 Pilot study: Optimisation of parameters to increase the total amount of cells adhered to the DuraGen Plus™ scaffold

We next investigated whether the total amount of cells that adhered to the scaffold could be increased as previously the flooding of cells method was used, where the cells would gradually adhere to the matrix. However, it is possible that a certain proportion of cells delivered this was may have not adhered and therefore, there may be less than the desired seeding density in the construct. So next, a focal seeding approach was trialled which involved seeding a concentrated population of cells directly onto the DuraGen Plus™ matrix. Additionally, to determine the optimum thickness of the matrix for cortical neuronal enriched cells, the thicknesses 250μm and 500μm were trialled. Furthermore, a comparison of data between uncoated and poly-L-ornithine and laminin coated constructs was also made to investigate if coating the material would enhance cellular adherence and survival of cells on the matrix (Ge *et al.*, 2015). As the previous results showed that viability was similar for 2.5 x10^5 and 4 x10^5 cells/mL seeding densities, the latter was taken forward for subsequent experiments. In addition using a high density of neuronal cultures are reported to having sustainable cell survival rates and functional activity (Aebersold *et al.*, 2018).

The preliminary data for cell viability using focal seeding of cells, demonstrated similar viabilities in the 250μm and 500μm uncoated constructs, with >60% (n=1) viability reported in the 3,6 and 9 DIV timepoints (Figure 4.14 A,B,C, D,E & F and Table 4.4). When compared to the POR-N and laminin coated constructs, viability at 3 DIV was <50% (n=1) at both thicknesses, which was observed to be lower than the uncoated constructs. However, at 6 and 9 DIV for the 250μm POR-N and laminin coated constructs, this increased to 60% and 64% respectively. The viability for the 500μm coated constructs though remained at 56% at 6 and 9DIV, therefore suggesting that coating the 500μm construct is not beneficial for sustaining a viable cell population.

.

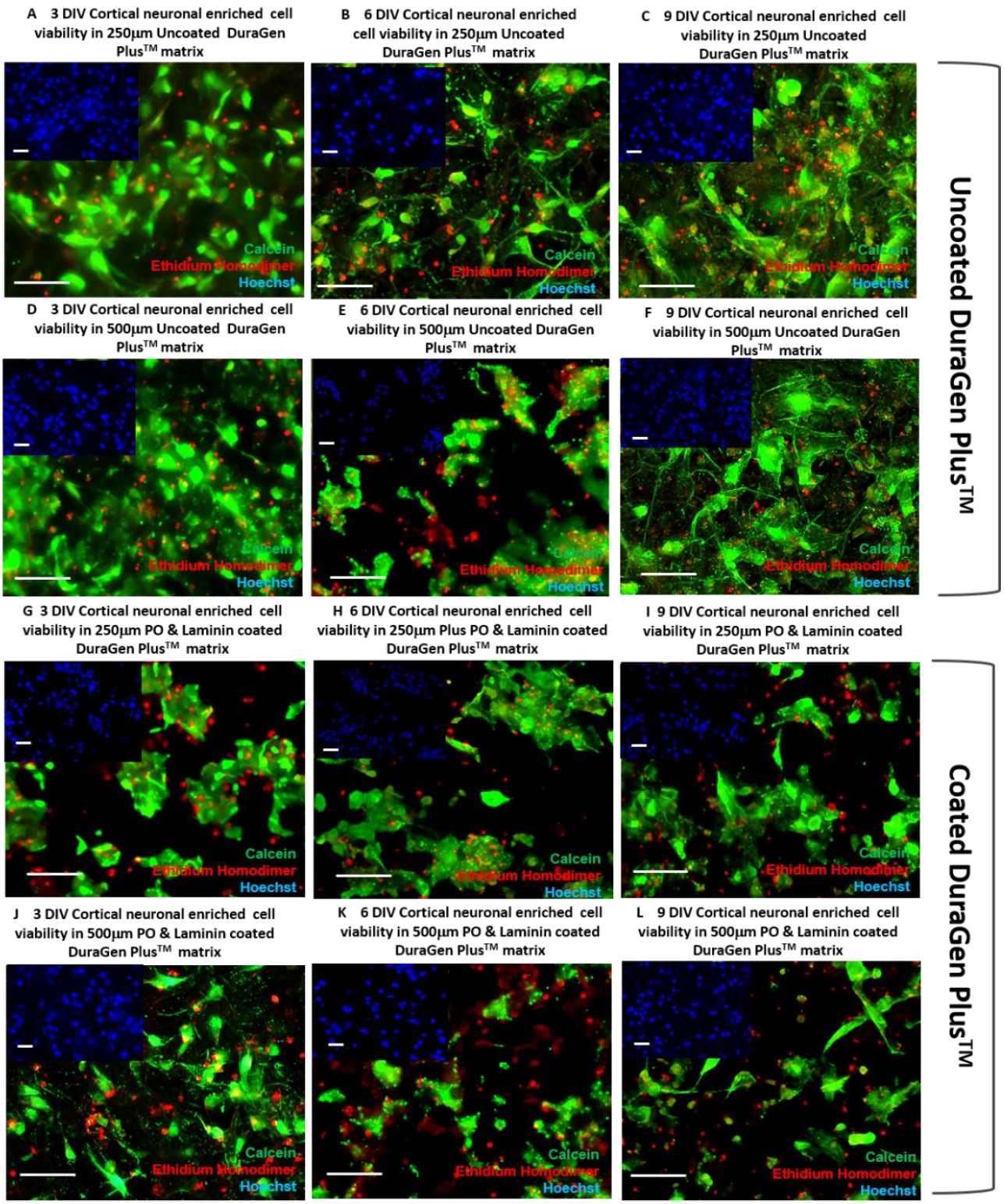

Figure 4.14 Pilot study: 3, 6 & 9 DIV cell viability of focally seeded, cortical neuronal enriched cells seeded onto 250µm and 500µm thickness slices of DuraGen Plus™ that was either uncoated, or coated with POR-N & laminin. Live cells are stained with calcein (green) with dead cells stained with ethidium homodimer (red). Images **Figure 4.14 continues below.**

Figure 4.14 continued. Images **A, B & C** represent viability on 250μm uncoated constructs at 3,6 & 9 DIV. **D,E & F** are of cortical neuronal enriched cells on 500μm uncoated constructs at 3,6 & 9 DIV. **G,H & I** represent viability of 250μm PO & laminin coated constructs and lastly **J,H & I** illustrate cells at 500μm PO & laminin coated constructs at 3,6 & 9 DIV respectively. n=1 All Z-stack CZI images were deconvolved with Huygens Professional version 19.04 (Scientific Volume Imaging, The Netherlands, http://svi.nl), using the CMLE algorithm, with signal to noise ratio (SNR):40 and maximum 50 iterations.

Table 4.4 Pilot study: Cell viability of cortical neuronal enriched cells focally seeded on DuraGen Plus™ Constructs: 250μm & 500μm Uncoated and POR-N & Laminin Coated (n=1)

Cell Viability (%)			
Seeding Density 4 x10^5 (cells/mL)	**Day 3**	**Day 6**	**Day 9**
250μm uncoated	71	65	70
500μm uncoated	67	65	66
250μm POR-N & Laminin	44	60	64
500μm POR-N & Laminin	54	56	56

Focal seeding of enzymatically dissociated, cortical neuronal cells onto 250 and 500μm, DuraGen Plus™ constructs, proved to be successful in reducing the percentage of cellular debris and improved cell viability when compared to mechanical dissociation. The cellular debris that remains within the constructs, is possibly due to the debris becoming embedded into the matrix and unable to be removed with multiple medium changes. It was also observed that coating the scaffold with POR-N and laminin did not improve viability when compared to the 250 and 500μm uncoated constructs. Therefore, the parameters taken forward were to use 250μm, uncoated DuraGen Plus™ constructs for optimal imaging and data analysis purposes, as observing morphological features of cells within the 500μm thickness constructs, was not as clearly distinguishable using microscopy in comparison to the 250mm scaffold.

4.3.4 Focal seeding of cortical neuronal enriched cells on 250mm uncoated DuraGen Plus™

The 3DIV viability of the neuronal enriched cells using focal seeding was approximately 60% (Figure 4.15 A & D) however, this decreased to 57% and 58% at 6 and 9DIV respectively Figure 4.15 B & C), suggesting that overall viability reduced to below 60% with an increase in time.

Histological staining at 12DIV confirmed the presence of TUJ-1 neurons, which were evidenced by the staining of multiple extended processes (neurites) projecting from the cell body. The neurons however did appear fragmented in some regions. Additionally, from the subpopulation of Tuj-1 neurons, there were 55% GABA positive

neurons which exhibited co-localisation of nuclei staining for GABA Figure 4.16 A & D). However, there was no evidence of VGLUT positive neurons within the construct.

The DuraGen Plus™ constructs were also co-stained with Tuj-1 and GFAP which demonstrated that 54% of the population were astrocytes, appearing morphologically fibrous with multiple processes extending from the cell body Figure 4.16 B & E). Lastly, the oligodendrocytes which were co-stained with MBP and TUJ-1, constituted to 2% of the overall population, appearing highly branched and occasionally situated on top of neurons (Figure 4.16 C & F).

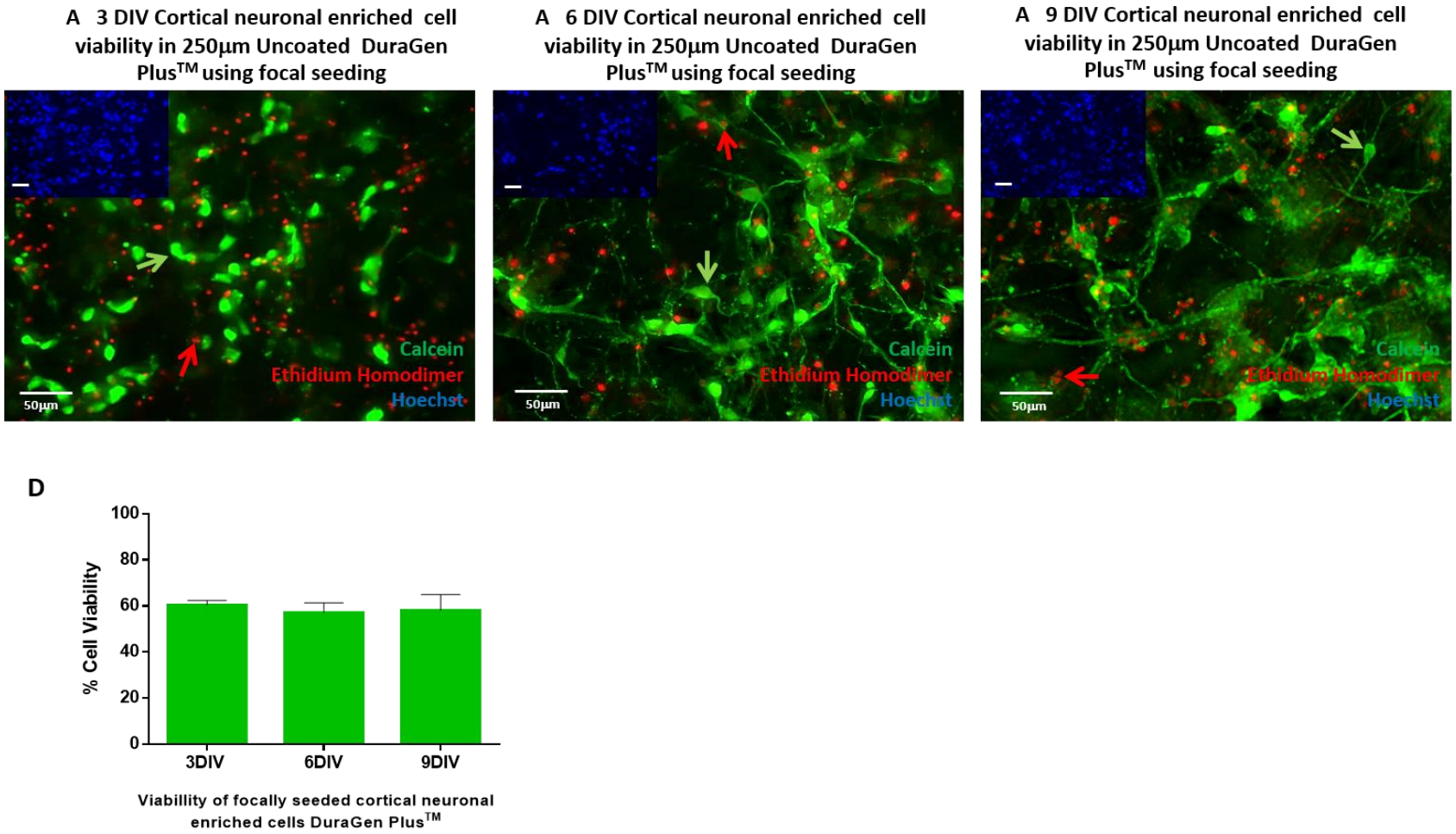

Figure 4.15 Viability of focally seeded, cortical neuronal enriched cells in DuraGen Plus™ matrix. A, **B** & **C** respectively demonstrating 3DIV, 6DIV and 9DIV cell viability in the DuraGen Plus™ constructs using enzymatic dissociation and the direct seeding technique. Green arrows indicate the presence of viable cells whereas the red arrows indicate dead cells. **Figure 4.15 continues below.**

Figure 4.15 continued. Graph **D** represents viability at 3DIV, 6DIV and 9DIV . Graph indicates that overall cell viability in the constructs is >50% across all time points. n=3. The total viable cells counted at 3 DIV was 1669 out of 2796. In comparison, at 6 DIV, a total of 2227 cells were counted where 1254 cells were viable. Lastly, a total of 1592 cells out of 2659 neuronal cells were viable on the matrix. Data was analysed by one-way ANOVA with Bonferroni's MCT and is expressed as mean ± SD. There was no significant difference in viability ($P > 0.05$) in the DuraGen^{TM} constructs when comparing 3DIV, 6DIV and 9DIV timepoints. All Z-stack CZI images were deconvolved with Huygens Professional version 19.04 (Scientific Volume Imaging, The Netherlands, http://svi.nl), using the CMLE algorithm, with signal to noise ratio (SNR):40 and maximum 50 iterations.

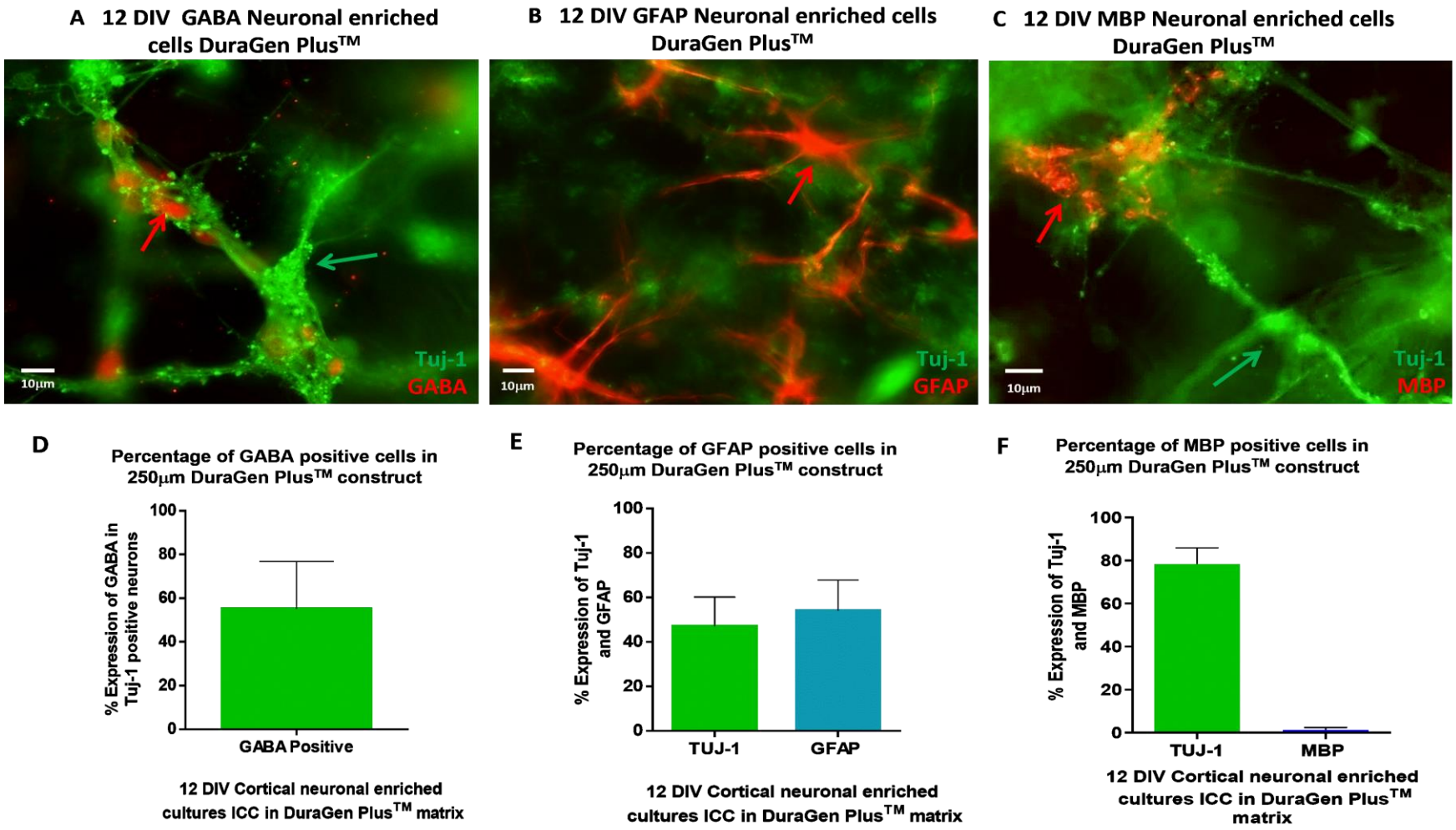

Figure 4.16 Neuronal enriched cells in DuraGen Plus™ matrix. A) Illustrates 12 DIV GABA neurons (red arrow) co-stained with TUJ-1 (green arrow). **B)** Astrocytes stained with GFAP (red arrow) and neurons with TUJ-1 (green). **Figure 4.16 continues below.**

Figure 4.16 continued. C) shows the presence of oligodendrocytes (MBP, red arrow) with neurons (TUJ-1, green arrow). **D, E** and **F** graphically illustrates 12 DIV percentage expression of cell specific markers. n=3. The total cells counted for graph D was 1417 cells, with 640 cells being GABA positive. For graph E, a total of 2344 cells were counted with 1355 cells stained positive for Tuj-1 and 989 cells GFAP positive. A total of 848 cells were counted for graph F with 703 cells being Tuj-1 positive and 18 cells being MBP positive with the remaining 129 cells being unstained nuclei.

4.4 Discussion

4.4.1 DuraGen Plus™ can support the survival and maturation of myelinogenic cells when co-seeded with astrocytes

To the best of my knowledge, the survival and maturation of oligodendrocyte lineage cells, when co-cultured with astrocytes as a supportive cell population, in the surgical grade matrix DuraGen Plus™ has been demonstrated for the first time.

It was evident from the data that viability for oligodendrocyte lineage cells when seeded as a pure population on DuraGen Plus™ decreased once the cells were differentiated from OPCs (3DIV) to mature oligodendrocytes(14DIV). Various approaches were trialled to improve viability which firstly included trialling the thicknesses 250μm and 500μm in addition to coating the DuraGen Plus™ matrix with POR-N & laminin. These approaches demonstrated that at 3DIV, viability of the cells may have been >65% in all the constructs (coated and uncoated); this however decreased to <40% by 14DIV. Coating DuraGen Plus™ constructs was therefore ineffective for improving overall cell health at 14DIV, as the data was similar to that of the uncoated constructs. Likewise, Russell and Lampe, (2017), showed that laminin incorporation into a 3D hydrogel, for the proliferation and maturation of OPCs had minimal effect on their viability.

Next, using a focal cell seeding approach with a purified population of oligodendrocyte lineage cells, and an increased seeding density to ensure that there were enough cells that adhered to the construct, also demonstrated 60% viable cells at 3DIV but this decreased to 30% by day 14. The protocol which was successful in

improving overall cell viability by 14 DIV involved co-culturing oligodendrocyte lineage cells with astrocytes. Viability at 3 and 7DIV was reported as being >77%, but this did decrease to 66% by 14DIV. However, when compared to 14DIV data, generated using the other protocols, there was an overall 27% increase in viability from using the co-culture protocol.

Transplanting a population of cells which has a viability of less than 50% within the scaffold, into already damaged regions of the CNS is unfavourable, as the dead cells which are adhered to the construct may trigger a further inflammatory immune response involving the infiltration of microglia which in turn, secrete factors such as pro inflammatory cytokines nitric oxide and ROS that make it a hostile environment for regeneration (Xu *et al.*, 2020).

4.4.2. How has co-culturing astrocytes aided in oligodendrocyte lineage viability and maturation?

Once astrocytes were incorporated into the oligodendrocyte lineage constructs, overall cell viability had increased to >77% across the 3DIV and 7 DIV timepoints and 66% at 14DIV. Furthermore, the incorporation of astrocytes contributed to a 37% increase in overall viability throughout the construct at 14DIV, which was calculated by comparing the viability of the focally seeded, isolated population of oligodendrocyte lineage cells at 14DIV, to the 14DIV data of the co-cultured constructs.

Histological staining also showed the presence of highly branched oligodendrocytes at 7DIV and 14DIV with approximately 40- 50% MBP positive cells at day 7 and 20-

35% at day 14, with the remaining percentages being GFAP positive astrocytes. The increase in the astrocyte population from 7DIV to 14DIV within the construct is because astrocytes are a proliferative cell population, whereas oligodendrocytes are post-mitotic (Miron, Kuhlmann and J, 2011; Clavreul *et al.*, 2019). Hence, oligodendrocytes lose their proliferative capacity when they mature from their precursor state and therefore, the population of oligodendrocytes does not increase.

Oligodendrocytes are sensitive to environmental changes and thus, in the CNS they are supported by cells such as astrocytes (Court and Alvarez, 2016). Astrocytes play a critical role in providing structural support and trophic factors for neurons and synergistically, promoting myelination (Court and Alvarez, 2016). Studies have shown that astrocytes are also associated with a variety of roles for oligodendrocyte lineage cells including regulating proliferation, survival and differentiation into myelinating cells (Nash *et al.*, 2011; Kıray *et al.*, 2016; Traiffort *et al.*, 2020). This is achieved by the astrocytes secreting chemokines and cytokines, both of which influence the regulation of myelination. Specifically, astrocytes secrete the cytokines LIF & CNTF, which promote the survival and maturation of oligodendrocytes, with CNTF specifically showing its capability of protecting oligodendrocytes from apoptosis and myelin destruction, both in vitro and in vivo (Kıray *et al.*, 2016).

Future studies could include, to investigate whether these protective mechanisms mentioned above are occurring within the co-constructs by measuring expression of LIF and CNTF in the co-cultured DuraGen Plus™ constructs. This could be assessed by conducting an enzyme-linked immunosorbent assay (ELISA) to detect the presence and concentration of these chemokines (Sun *et al.*, 2016; Yang *et al.*, 2020). Additionally, myelin formation of the mature oligodendrocytes present within the co-cultures could be quantified by measuring MBP via β-galactosidase activity,

using an ELISA assay. Moreover, the results could be compared against oligodendrocyte lineage cells seeded as isolated populations in the DuraGen Plus™ constructs (Stankoff and Zalc, 2002).

Another approach to encourage myelination and protect the cell population could include genetically engineering OPCs to express CNTF and seeding the cells onto the DuraGen Plus™ constructs. Cao *et al.*, (2010) demonstrated that OPCs infected with retroviruses to express CNTF, which were transplanted into an adult rat, contused thoracic spinal cord model ,9 days post injury, survived seven weeks after transplantation and integrated into the injured spinal cord. The study also stated that the survival of the CNTF-OPC grafts increased four-fold in comparison to the OPCs expressing green florescent protein. The disadvantage however of using retroviruses though include the risk of insertional mutagenesis and possibly tumour formation (Thomas et al., 2003; Anson, 2004).

4.4.3 Future plans and direction of research for oligodendrocyte lineage and astrocyte co-construct

Taking the oligodendrocyte lineage and astrocyte DuraGen Plus™ construct forward, future studies would need to determine the therapeutic benefits of the scaffold using *in vitro experimental SCI models and specifically, to determine whether the graft could integrate and promote remyelination* within the region. These could include SCI models of contusion, compression , ischemia, reperfusion injury and various types of lacerations including cuts and tears (Minakov *et al.*, 2018).Moving towards *in vivo* testing, the oligodendrocyte lineage and astrocyte co-construct could also be implanted into a murine spinal cord injury model for investigative studies involving

regaining locomotor recovery, testing the immunogenic nature of the graft in the host site and also the integration of the cells within the site (Fakhoury, 2015). Furthermore, for neurological applications this DuraGen Plus™ co-construct could be used to treat demyelinating regions within a SCI area, or for neurodegenerative conditions such as Multiple Sclerosis, which is a chronic inflammatory, immune mediated demyelinating attack of the myelin sheath. The co-construct would introduce an exogenous supply of OPCs to replace the damaged myelinating cells in the lesioned areas, thereby promoting remyelination (Miron *et al.*, 2011).

4.4.4 Cortical neuronal enriched cell encapsulation into DuraGen Plus™

To the best of my knowledge, the survival and maturation of post-natal, cortical neuronal enriched cells in the DuraGen Plus™ matrix has been demonstrated for the first time

The mechanical dissociation of the cortical cells generated a significant amount of cellular debris which affected cell viability, as only 20% of the cells were viable, and there were dead cells adhered onto the DuraGen Plus™ matrix. The amount of debris in the constructs may have been produced due to mechanically dissociating the cells by mincing the cortices with a scalpel, and with 21 and 23 gauge hypodermic needles, thereby creating a percentage of non-viable cells that could not be removed from the matrix. Additionally, the meninges in post-natal neuronal cultures are more adherent to tissue and thus, cultures may yield a lower percentage of viable cells (Weinert *et al.*, 2015). Therefore, a method of enzymatically dissociating the cortices was used, as the latter process mainly involves the proteolytic enzymes trypsin and DNAse to dissociate the cells (Miersch *et al.*, 2018).

The enzymatic dissociation protocol was shown to be successful in reducing the amount of debris within the constructs when observed microscopically in comparison to the mechanical dissociation method, with viability being reported as between 56% and 60% in the pilot studies which is an approximate 40% increase when compared with the previous method.

Immunocytochemistry for the pilot study showed that within the constructs, there were Tuj-1 and GFAP positive cells, therefore confirming that neurons and astrocytes were both present .It was also noted that the neuronal cell bodies were clustered into regions of the matrix, possibly within the pores, with minimal extension of their cellular processes extending outwards. It was anticipated that the cells would be distributed throughout the construct with evidence of interconnected neural networks which are seen in an *in vivo* neural circuit (Soletta *et al.*, 2017). However, the cells within the DuraGen Plus™ matrix appeared to be restricted as clusters in the matrix pores upon microscopic examination.

Possible reasons why an interconnected network may not have occurred could include the method used to seed the cells onto the matrix, i.e. cells were flooded into a 24-well and were allowed to adhere to the matrix. However, the desired density of cells may not have been achieved using this method, and the final density on the construct may have been reduced. Therefore, focal seeding as described by Adesida *et al.*, (2012) was trialled which involved seeding a concentrated population of cells ($4x10^5$) directly onto the construct.

Alongside the focal seeding approach, the thicknesses 250μm and 500μm DuraGen Plus™ matrix were trialled; they were either coated with POR-N and laminin or uncoated. It was found however that neither of the thicknesses, or coating of the

material increased cell viability, with viability again, being recorded as >60% (n=1) for the coated and uncoated constructs with the exception of viability being 56% in the 500μm POR-N and laminin matrix. Although PO & laminin has been mentioned in literature as being supportive for neuronal growth, it has not shown to being ineffective for coating DuraGen Plus™ for the purpose of this study (Ge *et al.*, 2015). A similar finding was reported for oligodendrocyte lineage cell constructs with use of POR-N & laminin.

With the refined parameters taken forward being 250μm uncoated focally seeded constructs, biological repeats demonstrated that viability was 60% at 3DIV and 58% at 9DIV for the post-natal, cortical neuronal enriched cells (n=3). Similar findings for viability were reported by Rabinowitz *et al.*, (2005) who also trialled DuraGen Plus™ but to determine its effect on the growth of embryonic cortical neurons harvested from E19 rats. The authors used a $1cm^2$ piece of DuraGen Plus™ matrix cut into 30μm slices that were then situated on top of a poly-L-lysine coverslip and seeded with a density of $2x10^4$ cells/mL cortical neurons. Neuronal viability at 3DIV was measured as 70% which decreased to 42% by 10DIV. Rabinowitz ***et al's*** (2013) also emphasised that although DuraGen Plus™ did not promote greater neuronal survival, it did not lose the ability to support neurons *in vitro*, likewise to our study.

Characterisation of the neuronal enriched cells encapsulated into the matrix using the focal seeding technique, showed that the Tuj-1 positive neurons within the construct appeared to be distributed throughout, with the extension of processes extending from the soma into different planes, and appeared to be following the random direction of the matrix. It was noted however that the neurons within the construct appeared to have punctate staining which could possibly be remnants of cellular debris that had adhered to the matrix when using enzymatic dissociation, or it may be

due to any remnants of trypsin that has remained from the dissociation process slowly degrading the collagen. Trypsin is reported to having collagenolytic activity towards type 1 collage (van Deemter *et al.*, 2013). A possible explanation for the degradation of the construct may be that as DuraGen Plus™ is composed of 95% type 1 collagen, the proteolytic enzyme could have potentially hindered the durability of the biomaterial matrix. The cells also generate collagenases and proteases which may also have an effect on the integrity of the matrix.

Finch *et al.*, (2020) as mentioned previously, encapsulated NSCs into the DuraGen Plus™ matrix which gave rise to neurons, astrocytes and oligodendrocytes. There was however no evidence of extensive cellular debris present within the construct. This may be because prior to seeding the NSCs onto the scaffold, the cells were initially seeded and maintained for a week in a culture grade flask, with frequent medium changes which cleared the cellular debris generated from the dissociation process. In comparison to our study, the neuronal enriched cells derived using enzymatic dissociation, were directly seeded onto the DuraGen Plus™ matrix and hence, cellular debris adhered to the matrix.

Future studies for a possible solution for resolving the issue of debris adhering to the DuraGen Plus™ fibres and the potential degrading of the biomaterial by using trypsin, could be to trial a 20% concentration of a percoll grade treatment for yielding the post-natal cortical neuronal enriched cells. This concentration would be high enough to separate out cellular debris and without affecting membrane integrity of the cells (Juan *et al.*, 2012). This would firstly involve treating the tissue with DNase to prevent the cells clumping. The tissue would then be put through a percoll gradient, in which a density gradient for the cells is produced in order to separate the myelin, cellular debris, and red blood cells from the viable cells (Juan *et al.*, 2012;

Miersch *et al.*, 2018; Matsuyoshi *et al.*, 2019).This protocol in turn, could further reduce the cellular debris within the biomaterial scaffold and potentially, resolve the issue of punctate staining.

4.4.5 Future plans and direction of research for neuronal DuraGen Plus™ constructs

Once the matter of cellular debris within the construct has been resolved, additional studies could be conducted to assess functionality of the cells within the DuraGen Plus™ construct. This would involve investigating the electrophysiological properties of the neurons by using the patch-clamp technique, in order to assess the electrical activity of the cells by measuring the opening and closing of voltage dependent sodium and potassium channels (Marchini *et al.*, 2019). The results could then be compared to determine whether the electrical activity of the cells within the construct correlates to what is seen *in vivo.*

The DuraGen Plus™ neuronal enriched construct could also be implanted into *in vitro* and *in vivo*, spinal cord injury models to determine whether the exogenous, pre-differentiated neural circuit can integrate within the lesion site by bridging the host-graft interface and promote regeneration. During *in vitro* and *in vivo* testing, it is also important to assess whether the scaffold protects the cells against an immune attack and limit the effect of surrounding scar formation which may prevent axonal outgrowth into the site of injury (Liu *et al.*, 2018).

4.4.6 Conclusion

In conclusion, it has been successfully demonstrated that by utilising the FDA approved, surgical grade biomaterial DuraGen Plus™, it was possible to generate

and sustain a myelinogenic cell population when co-cultured with astrocytes, and showed that with further research, it has potential for use as an implantable scaffold in injures and conditions which result in demyelination. Using DuraGen Plus™ for encapsulating neuronal enriched cells, however, must be further modified to improve the viability of the cell population within the construct and reduce debris. Once this has been optimised, there is scope to produce a pre-differentiated neural circuit in the matrix, that can be integrated into lesioned sites of injury in the CNS to promote regeneration.

Chapter 5

Investigating Cellevate scaffolds to induce alignment of oligodendrocyte lineage cells derived from the mouse mixed glial culture model

5.1 Introduction

5.1.1 The importance of having aligned structures within neural implants

Neural cells within the CNS are naturally aligned to enable synaptic transmission of electrical signals along extensive lengths of tissue (Kamudzandu *et al.*, 2015). Spinal cord injuries can irreversibly disrupt the native unidirectional, aligned architecture that directs and guides axons and glial cells toward their appropriate target within the spinal tracts, thereby leading to permanent functional impairment (Tian *et al,.* 2015).

Biodegradable scaffolds have been trialled extensively as a temporary structure to sustain the delivery of exogenous cells and biomolecules, in order to support neo tissue formation at the damaged sites (Nguyen *et al.*, 2017). Many biomaterials that have been referred to in the general introduction show potential for supporting transplant cell populations. Although often these scaffolds have an isotropic architecture, therefore may lack the ability to direct and guide axonal growth through the heavily damaged and disorganised regions in SCI, and this structure may also hinder neural cell integration and regeneration (Solanki *et al.*, 2013; Nguyen *et al.*, 2017). It would therefore be beneficial to utilise nanofiber scaffolds, to generate aligned structures that mimic *in vivo* neuro-cytoarchitecture, in order to guide cell orientation, migration ,differentiation and also the deposition of the extracellular matrix to promote neuroregeneration (Kamudzandu *et al.*, 2015).

Electrospun aligned nanofibers seeded with neural cells have been shown to aid in neurite extension and axonal guidance from as early as 2005 (Schaub *et al.*, 2016). Yang *et al.*, (2005) seeded NSCs derived from a C17.2 cell line onto aligned , biodegradable poly-L-lactic acid (PLLA) fibres which demonstrated that the fibres were capable of guiding neurite outgrowth from the NSCs, along the length of the fibres. It was also observed that the scaffold promoted NSC differentiation, therefore showing its potential to be used as cell carrier for neural transplantation in the CNS.

Although axonal regeneration is the end objective, oligodendrocytes are an essential population to target as they are required for saltatory signal conduction in axons and without myelin ensheathment, signal conduction in axons cannot occur efficiently, thus resulting in axonal degeneration and functional impairment (Sasaki *et al.*, 2007; Y. Lee *et al.*, 2013). It is therefore imperative to address replacing damaged oligodendrocytes to promote remyelination, at the sites of injury in order to allow the conduction of efficient nerve impulses (Milbreta *et al.*, 2019).

Researchers have trialled growing oligodendrocyte lineage cells on aligned nanofiber scaffolds previously. For example, Hyysalo *et al.*,(2017) demonstrated how hESC line-derived neurons, astrocytes and OPCs were cultured onto aligned poly(e-caprolactone) (PCL) nanofiber platforms to guide cell migration and orientation, in order to produce a functional cell graft that may be appropriate for repairing spinal cord injuries. The results demonstrated that neurons and astrocytes migrated out of their clusters along the laminin coated fibres and appeared to be highly aligned with the fibres of the scaffold. OPCs that were seeded onto the scaffold as aggregates, had appeared to attach to the nanofibers and migrate out of the aggregates to align with the fibres of the scaffold. The authors however described that there was evidence of OPCs that appeared to look both aligned and non-aligned within the

scaffold and that there was a greater degree of alignment observed in the neurons and astrocytes. Furthermore, Hyysalo *et al.*,(2017) described that there was a high percentage of viability seen in the neuronal and astrocyte seeded scaffolds, but no comments were made regarding the viability of the OPCs within it. Additionally, it is unknown whether the PCL scaffold can support a mature population of oligodendrocytes, and whether the cells can align within the scaffold. Furthermore, the data for this study was generated using cell lines, which do not mimic the behaviour of primary neural cells, therefore, it would be beneficial if the study was repeated with primary neural cells (Jenkins *et al.*, 2016). (Hyysalo *et al.*, (2017) also described encapsulating the nanofiber scaffold into a 3D collagen hydrogel, therefore suggesting that although the scaffold can align cells, use of the scaffold independently with cells would not mimic an *in vivo* 3D environment.

In another study, Bechler, (2019) collaborated with the company AMSBIO who produced Mimetix, an electrospun, medical grade polymer, consisting of poly-L-Lactide (PLLA) to produce an aligned microfiber scaffold. The fibres of the scaffold were 2μm thick and the overall depth of the scaffold being 50μm. Bechler, (2019)) utilised the scaffolds to create an assay to investigate the intrinsic mechanisms of oligodendrocyte lineage cells that regulate the formation of the myelin sheath. Primary rodent OPCs were used and seeded onto PDL coated Mimetix scaffolds at a density of 30,000 cells per scaffold, in a 12 well plate. The results showed that the assay allowed for the analysis of myelination at 3 and 7 DIV within the scaffold. In addition, at 14 DIV, an analysis of the number of sheaths per oligodendrocyte was also recorded. The results demonstrated that there was incomplete sheath formation at 7 DIV on the scaffold and complete sheath formation at 14 DIV. Additionally, it was also reported that 80% of the OPCs had matured into oligodendrocytes by 14DIV.

This study however did not report on the viability of the oligodendrocyte lineage cells within the scaffold and additionally, no analysis was conducted to determine the degree of alignment of the cells in comparison to the aligned fibres.

5.1.2 Investigating the utility of Electrospun Cellevate nano matrices for cellular alignment

Another nanofiber of interest is Cellevate 3D aligned nano matrices. Cellevate is a group of synthetic and biocompatible, minimally immunogenic, electrospun PCL nanofiber scaffolds that imitate the extracellular matrix (ECM) proteins, collagen and elastin (Zalis *et al.*, 2016). Collagen is a main structural ECM component which contributes to cell adhesion control, chemotaxis, cell migration and tensile strength (Frantz *et al.*, 2010). Elastin is an ECM protein that is present as fibres in healthy networks, providing durability and elasticity of tissues, due to its flexibility, and is primarily found in the skin, lungs and aorta (Aziz *et al.*, 2016).

Some distinguishing factors of Cellevate scaffolds which sets them apart from other nanofiber providers, is that these scaffolds are generated by their patented high-throughput, electrospinning technique, which significantly improves well-to-well and batch to batch consistency and thus, reduces experimental variation. In addition, these scaffolds are scalable and reproducible for widespread industrial use (Cellevate, 2020). Furthermore, the Cellevate scaffolds have been described as providing a true 3D microenvironment in comparison to other 3D nanofiber scaffolds that have been reported to resemble a rugged 2D surface. The aligned scaffolds arrive pre-sterilised prior to experimental use and importantly, the nanofibers provide the cells with a 3D environment similar, to collagen and elastin fibres found in the ECM that cells reside *in vivo*. The 3D environment has been described by Cellevate

to enable creating greater similarities between the cultured cells, and cells seen *in vivo*. Therefore using cells generated on the aligned scaffold would allow for the mimicking of *in* vivo conditions, thereby making them a relevant choice for use for research (Cellevate, 2020).

The Cellevate aligned 3D matrix has been used in different avenues of research including exploration of physical and chemical cues on retinal cell fate; promotion of accelerated wound closure; investigating hNPC behaviour on aligned scaffolds and the effects on cellular migration and phenotypic differentiation and for bridging *in vivo* peripheral nerve injuries (Zalis *et al.*, 2016; Ottosson, Jakobsson and Johansson, 2017; Frost *et al.*, 2018).

A non-aligned Cellevate scaffold has been trialled by Jakobsson *et al.*,(2017) to investigate the growth of a 3D human neuronal network consisting of neurons and astrocytes derived from a hNPC cell line which was seeded onto a highly porous, low density electrospun PCL Cellevate scaffold of unaligned fibres. The fibre diameter of the scaffolds was approximately 517 nm (0.517μm), with the mean pore area reported as 50μm^2, and the overall depth being 600μm. Jakobsson *et als'.*,(2017) results showed that the electrospun scaffolds promoted neuronal differentiation into highly integrated 3D networks, formed of astrocytes and inhibitory and excitatory synapses which showed extensive neurite growth, thereby resembling an *in vivo* intermingled neuronal and astrocyte network. The 3D neuronal model would be beneficial in investigating neural engineering approaches for structural support and for also investigating axonal guidance once implanted into the CNS.

Although the non-aligned PCL fibres have shown to be beneficial for establishing a 3D neuronal model, it would be advantageous to repeat this study using aligned PCL Cellevate scaffolds in order to mimic *in vivo* neuro-cytoarchitecture.

Aligned Cellevate scaffolds have been used in areas of research such as wound repair, to investigate the effect of the aligned matrix and to determine its effect on cell migration and ultimately wound closure. Accelerated wound repair was achieved by Ottosson *et al*,(2017) who created a fibroblast based, *in vitro* model to investigate artificial wound repair, and concluded that utilising aligned PCL scaffolds was beneficial for rapid wound closure.

Englund-Johansson *et al.*,(2017) investigated the growth of neurons and astrocytes derived from a hPNC cell line, which were seeded onto aligned electrospun PLLA Cellevate scaffolds, to observe the influence of the aligned scaffold on hNPC behaviour, in terms of cellular differentiation, migration and alignment. The results showed the aligned PLLA scaffold promoted cell migration out from their neutrospheres by 10DIV, to form an elongated distribution pattern across the scaffold. Analysis showed that the GFAP positive astrocytes migrated at longer distances from the seeding site in comparison to the DCX positive neurons. It was also observed that the neurons appeared elongated within the aligned scaffold, and that they migrated along the elongated, bipolar astrocytes in the direction of the aligned fibres. Quantification for the total number of DCX and GFAP positive cells within the aligned scaffold was approximately 57% in comparison to 41% in the non-aligned PLLA scaffold. Additionally, there were approximately 20% neurons and 39% astrocytes respectively within the aligned fibres, in comparison to 8% to 20% neurons and 32% astrocytes on the non-aligned fibres. Englund-Johansson *et al.*,(2017) demonstrated that the aligned PLLA Cellevate matrix could significantly

influence cellular migration, phenotypic characteristics, and directionality of the neural cells on the aligned fibres. It was also emphasised that there is scope for using the aligned scaffold alongside hNPCs, to investigate neurotoxicity and cellular replacement therapies in regenerative medicine. This study however did not report on the viability of the differentiated neural cells as the authors only reported cell counts on the number of viable spheres, 2 days post seeding which was between 86% and 90%. Therefore, further studies are required for calculating the percentage of viable differentiated cells within the scaffold.

Zalis *et al.*,(2016) used the aligned Cellevate scaffolds for ocular research in retinal neurodegeneration cell replacement therapies. As donor received photoreceptors have been reported to show poor cell survival and integration in the damaged region in patients, Zalis *et als's.*,(2016) rationale for utilizing Cellevate PCL scaffolds was to provide a 3D microenvironment that could potentially resolve the related issues. Thus, there was potential that the chemical and physical cues, provided by the scaffold, could improve cell adhesion and alignment, in addition to neurite outgrowth and allow the expression of phonotypical markers of post-natal murine retinal cells (RPNCs). The study involved using RPNCs that were seeded onto aligned Cellevate matrices which consisted of PCL fibres coated with/ without laminin. The fibre diameter of the PCL scaffolds was approximately 577 nm (0.577μm). Bechler, (2019) stated that a fibre diameter between 0.5μm and 4μm is an ideal fibre thickness for oligodendrocyte lineage growth. The results emphasised that aligned scaffolds, coated with laminin, showed alignment of cells and longer neurite outgrowth in comparison to Cellevate scaffolds that consisted of unaligned fibres. Furthermore, the cell viability of RPNCs on a flat surface (control, glass), laminin coated and uncoated aligned Cellevate scaffolds was also compared, and it was reported that

there was no significant difference in cell viability when compared to the control (Zalis *et al.*, 2016).

As described in the literature above thus far, Cellevate scaffolds have been shown to possess the properties to enable the aligning of cell populations in the orientation of the fibres, due to their physical and chemical cues. They have also demonstrated the facility to mimic native ECM tissue structure alignment and have been shown to have no negative effects *in vitro* on cell viability thus far.

Although neurospheres, neurons and astrocytes have successfully been grown within the aligned Cellevate scaffolds, this has not been demonstrated with oligodendrocyte lineage cells.

Trialling to grow a primary myelinogenic cell population within a 3D aligned scaffold would be beneficial for cell transplantation, as axonal regeneration is not possible without myelin ensheathment of the axons.

Aims

In summary, the aims of this chapter were to investigate:

1. Whether a population of oligodendrocyte lineage cells, derived from primary mice cortices could adhere and align to the Cellevate scaffold.

2. If the aligned scaffold promotes the maturation and differentiation of oligodendrocyte lineage cells.

3. Whether OPCs and myelinating oligodendrocytes retain their cell-specific markers at 3 and 7 DIV.

4. If oligodendrocyte lineage cells could survive at 3DIV in the OPC state and 7DIV in their differentiated and matured state in the scaffold.

5.2 Results

5.2.1 Oligodendrocyte lineage cell survival on non-aligned and aligned Cellevate scaffolds was greater than 55% at 3 and 7 Days

At 3 DIV, enriched populations of oligodendrocyte lineage cells were seeded at a density of 6 x 10^4 cells/mL on non-aligned fibres which served as a control and aligned fibres which were observed to have adhered onto the construct and there was evidence of viable cells on the scaffolds (Figure 5 A&B). After quantification it was found cell viability was greater than 75% at this time point (n=4) (Figure 5.0 E). Viability however decreased to approximately 58% and 55% respectively (n=4) on the non-aligned and aligned scaffold at 7DIV, after 7 days in differentiation medium (Figure C, D &F)

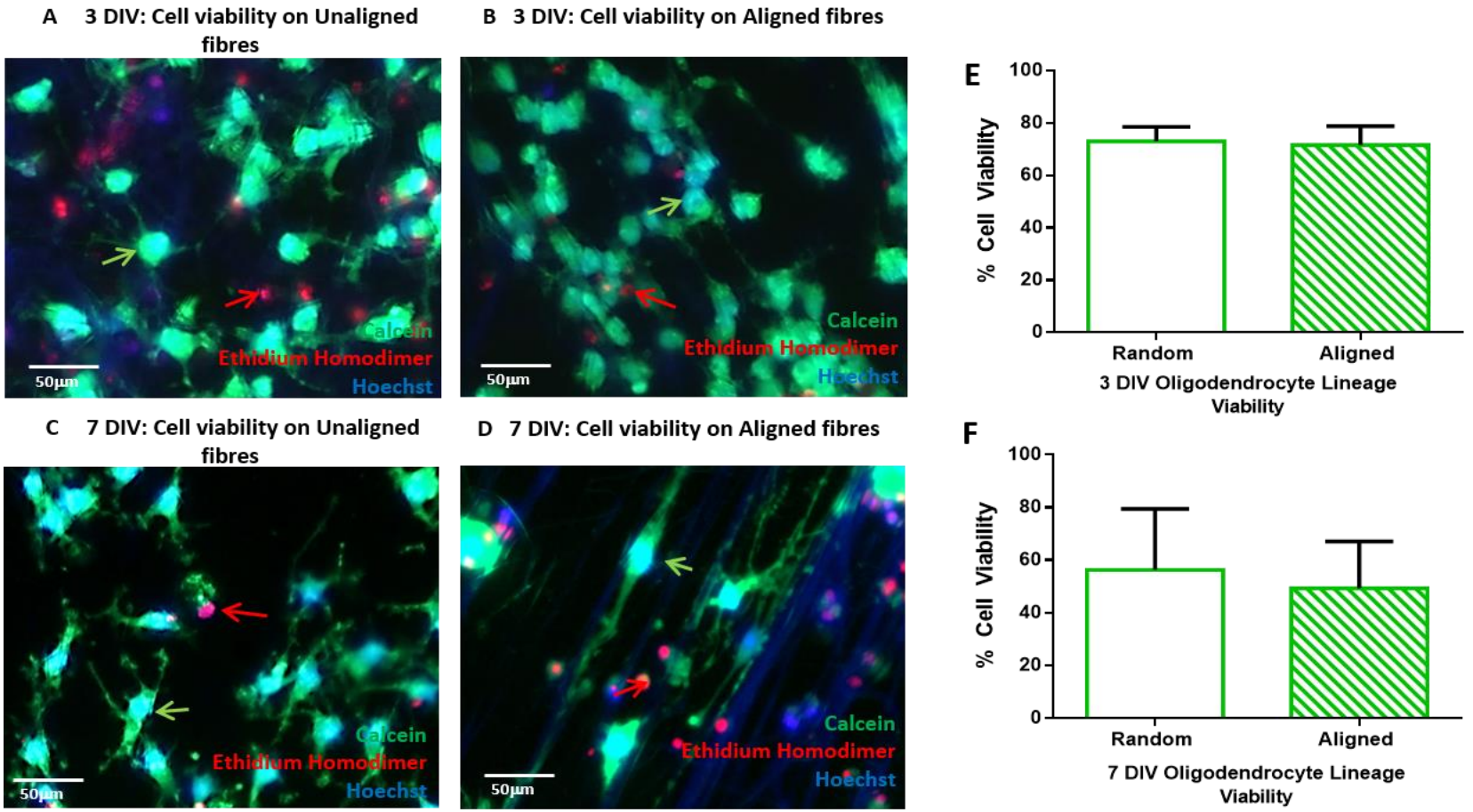

Figure 5.0. Viability of oligodendrocyte lineage cells at 3 and 7 DIV on unaligned and aligned Cellevate scaffolds was over 55%. Live cells were stained green with Calcein, dead cells in red with ethidium homodimer and cell nuclei were stained blue with hoechst. **A)** shows 3DIV oligodendrocyte lineage cells on an unaligned scaffold. **Figure 5.0 continues below.**

Figure 5.0 continued. B) 3DIV oligodendrocyte lineage cells on an aligned scaffold. **C) & D)** show 7DIV, matured oligodendrocyte lineage cells in the unaligned and aligned Cellevate scaffold respectively. **E) & F)** graphically illustrates the percentage viability of the oligodendrocyte lineage cells at 3 and 7DIV on the Cellevate scaffolds. For graph E, a total of 4429 cells were counted for the 3 DIV unaligned scaffold with 3349 cells stained positive for calcein. In comparison, a total of 3443 cells was counted for 3 DIV aligned scaffolds with 2567 cells recorded as being viable. For graph F, at 7 DIV a total of 1443 cells were counted for the unaligned scaffolds with 796 of the cells counted as viable whereas, a total of 1150 cells were counted for the 7 DIV aligned scaffolds with a viable cell population of 592. Data was analysed using an unpaired t-test with Welch's correlation which demonstrated there was no significant difference in cell viability between oligodendrocyte lineage cells grown on random and aligned fibres at 3DIV and 7DIV respectively ($P>0.05$), n=4 3DIV, n=4 7DIV.

5.2.2 Directionality analysis demonstrated Oligodendrocyte lineage cell alignment at 3 days

Histological staining confirmed the presence of NG2 positive cells, indicating the presence of OPCs in the 3 DIV oligodendrocyte lineage non-aligned (Figure 5.1) and aligned (Figure 5.2) scaffolds, with quantification confirming that >90% of the cells within the non-aligned and aligned scaffolds were OPCs (Figure 5.3). Furthermore, the cells within the non-aligned scaffold appeared to extend cellular processes in all directions in no particular pattern,

To measure the degree alignment of the oligodendrocyte lineage cells on the non-aligned and aligned scaffolds, the fluorescence immunocytochemistry images,

alongside their phase counterparts were processed in Image J to conduct a directionality analysis, in order to determine whether the cells follow the direction and orientation of the fibres.

Directionality analysis from three biological repeats for the 3DIV unaligned scaffolds, (Figure 5.1 B, D & E) confirmed that the cells were in fact randomly aligned on the scaffold ,with the blue line representing no fibre alignment and the pink line representing no cellular alignment.

The OPCs in the 3DIV aligned scaffold however, appeared to follow the fiber direction, with evidence of bipolar processes of the cells aligning with fibres (Figure 5.2 A, C & D). Directionality analysis from three biological repeats also demonstrated that the OPCs followed the direction of the fibres, with the blue line representing the fibres following a specific angle and the pink line indicating peaks which correlates with the angle of the fibres and thereby, representing cellular alignment (Figure 5.2 B, D & E).

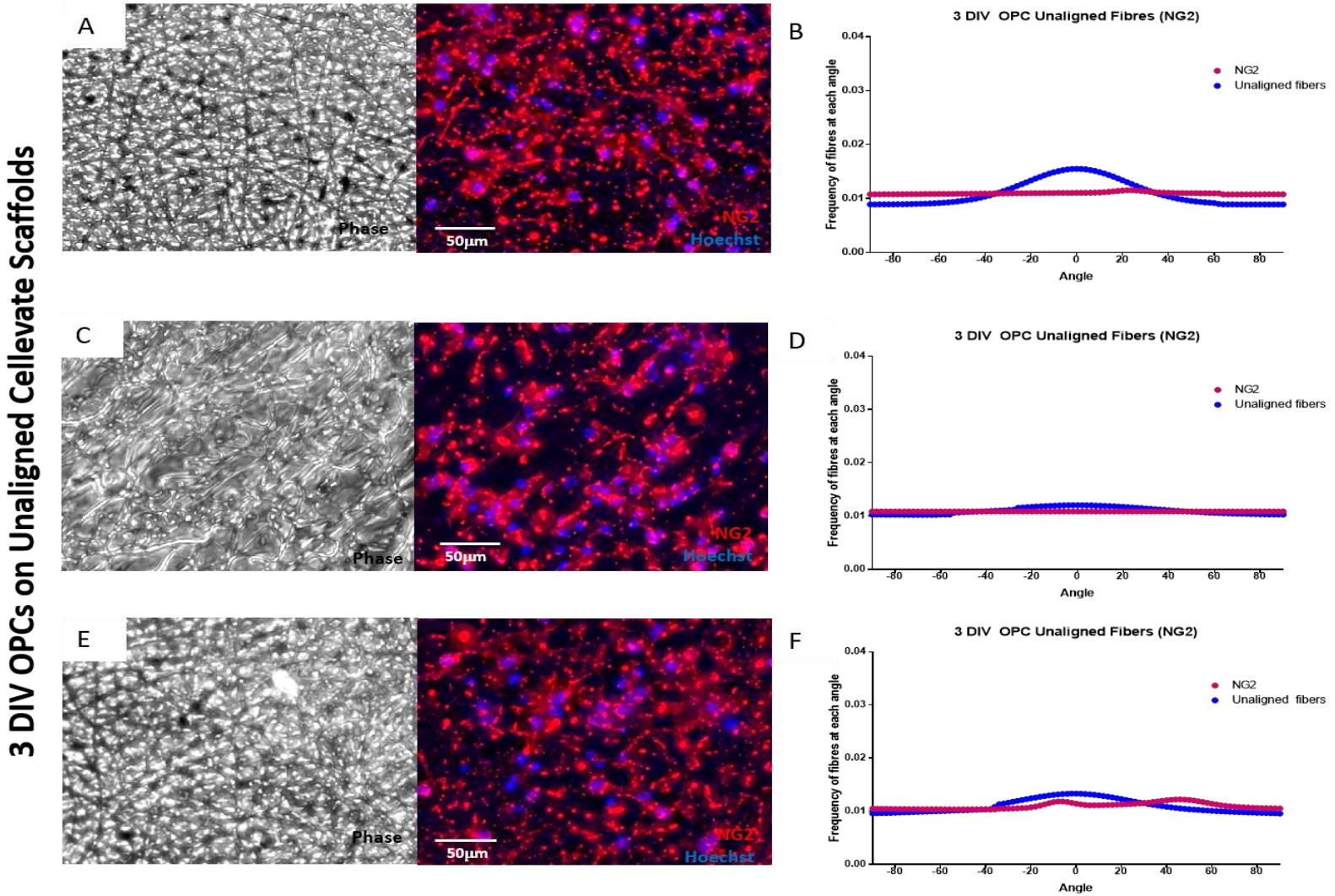

Figure 5.1. 3DIV NG2 expression in oligodendrocyte lineage cell populations grown on unaligned Cellevate scaffolds with their corresponding directionality graph. Representative images of oligodendrocyte lineage cells stained with NG2 (red), an OPC marker and hoechst on unaligned scaffolds n=4. **Figure 5.1 continues below.**

Figure 5.1 continued. Image **A** corresponds with graph **B,** image **C** corresponds with **D** and image **E** corresponds with **F**. All Z-stack CZI images were deconvolved with Huygens Professional version 19.04 (Scientific Volume Imaging, The Netherlands, http://svi.nl), using the CMLE algorithm, with signal to noise ratio (SNR):40 and maximum 50 iterations. The total cells counted for an n=4 was 3538 with 3323 of the cells being NG2 positive with 215 cells staining for a non-specific marker.

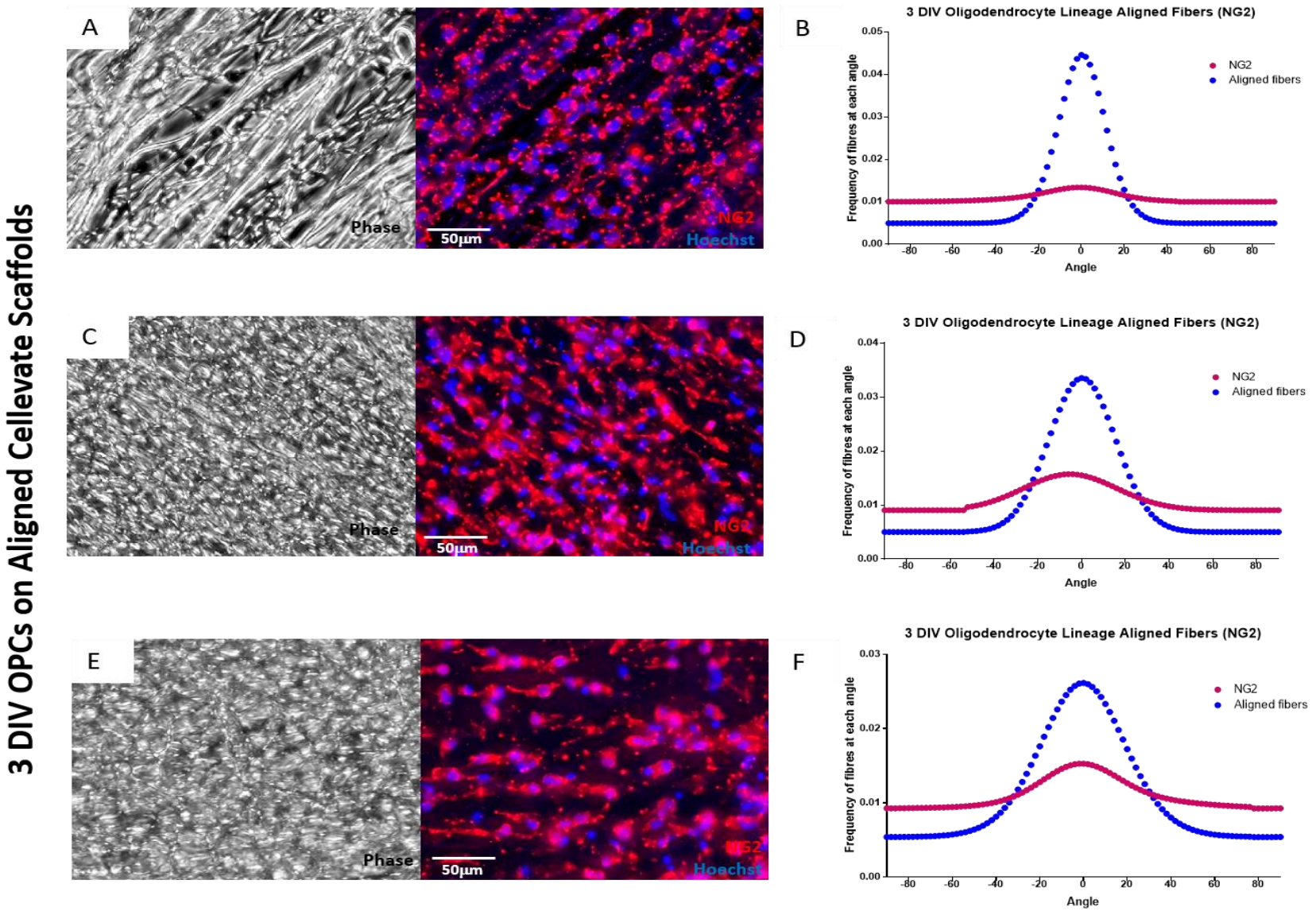

Figure 5.2. 3DIV NG2 expression in oligodendrocyte lineage cell populations grown on aligned Cellevate scaffolds.

Representative images of oligodendrocyte lineage cells were stained with NG2 (red), an OPC marker and hoechst on aligned scaffolds n=4. **Figure 5.2 continues below.**

Figure 5.2 continued. Image **A** corresponds with graph **B,** image **C** corresponds with **D** and image **E** corresponds with **F**. All Z-stack CZI images were deconvolved with Huygens Professional version 19.04 (Scientific Volume Imaging, The Netherlands, http://svi.nl), using the CMLE algorithm, with signal to noise ratio (SNR):40 and maximum 50 iterations. Total cells counted for an n=4 was 2895 with 2703 NG2 positive cells and 192 cells staining for a non-specific marker.

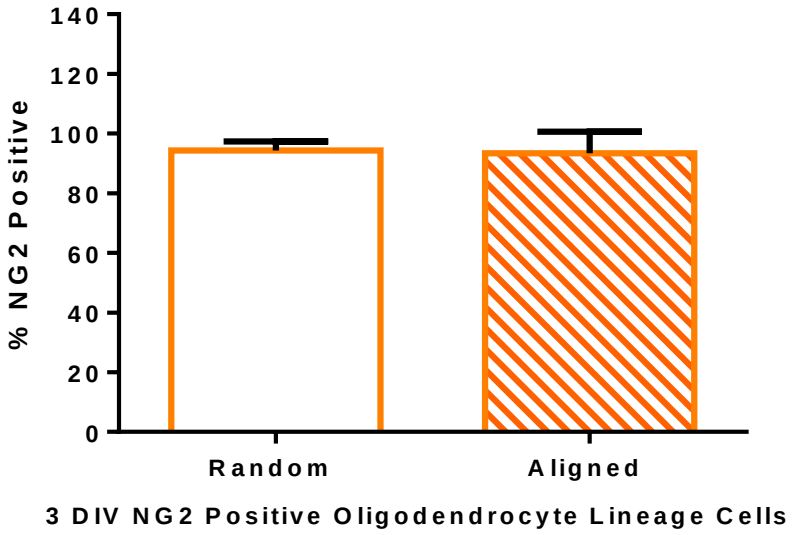

Figure 5.3. NG2 expression in oligodendrocyte lineage cell at 3DIV in unaligned and aligned scaffolds Data was analysed using an unpaired t-test with Welch's correlation which demonstrated there was no significant difference in cell viability between oligodendrocyte lineage cells grown on random and aligned fibres at 3DIV respectively (P>0.05), n=4.

5.2.2 Oligodendrocyte lineage cells did not appear to align on the Cellevate scaffold at day 7

At 7DIV, once the oligodendrocyte precursor cells were grown in medium which supported differentiation, MBP expression which is a marker for myelinating oligodendrocytes was measured in the non-aligned and aligned scaffolds. There was reported to being 30% and 50% of MBP positive oligodendrocytes in the non-aligned and aligned Cellevate scaffolds respectively (Figure 5.6), with possibly the remainder of the cell population being NG2 positive OPCs.

In terms of cell alignment, phenotypically the cells appeared to be randomly aligned and following no particular direction within the non-aligned scaffold (Figure 5.4 A, C & E) with directionally analysis also confirming this (Figure 5.4 B,D&E).

The oligodendrocytes in the 7 DIV aligned scaffolds however, displayed a mixture of both aligned and unaligned cells in the scaffolds (Figure 5.5 A,C&D), with cellular processes following the direction of the fibres (Figure5.5 A&E) and with other oligodendrocytes appearing highly branched but unaligned (Figure 5.5 C). Directionality analysis of the cells on the aligned scaffold also demonstrated that some regions showed evidence of cellular alignment which correlated with its complimentary image (Figure 5.5 A & graph B), whereas other regions although appeared to show aligned oligodendrocytes, the graph did not detect any alignment (Figure E & graph F). Regions of cells that evidently did not appear to show alignment, had similar directionality graphs to the cells on the unaligned scaffolds (Figure 5.5 C & graph D).

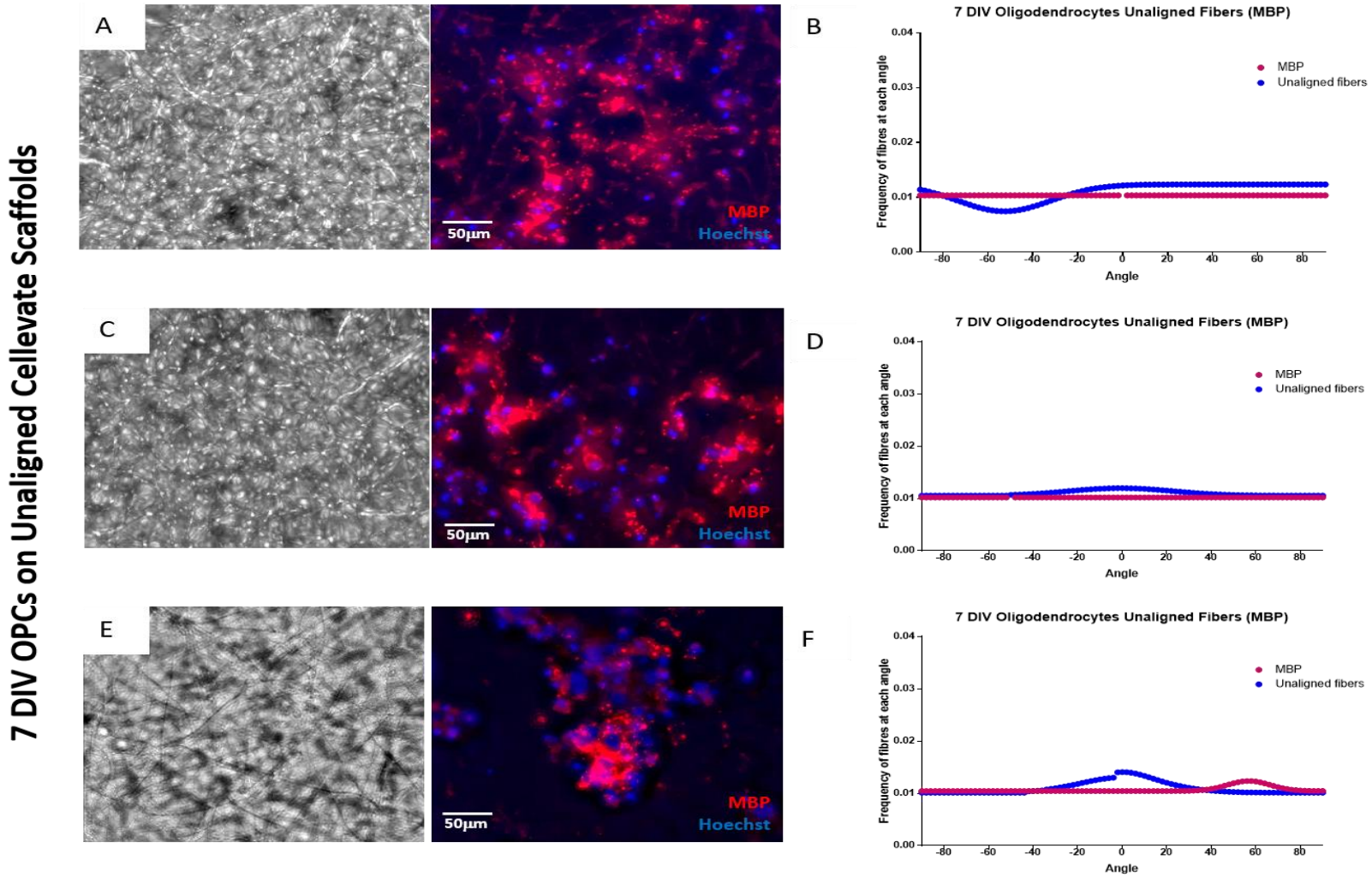

Figure 5.4. 7DIV MBP expression in oligodendrocyte lineage cell populations grown on unaligned Cellevate scaffolds.

Representative images of oligodendrocyte lineage cells were stained with MBP (red), an Oligodendrocyte marker and hoechst on aligned scaffolds n=3. **Figure 5.4 continues below.**

Figure 5.4 continued. Image **A** corresponds with graph **B,** image **C** corresponds with **D** and image **E** corresponds with **F**. All Z-stack CZI images were deconvolved with Huygens Professional version 19.04 (Scientific Volume Imaging, The Netherlands, http://svi.nl), using the CMLE algorithm, with signal to noise ratio (SNR):40 and maximum 50 iterations. Total cells counted for an n=3 was 540 of which 150 cells were MBP positive, with the remainder of 390 cells staining for hoeschst.

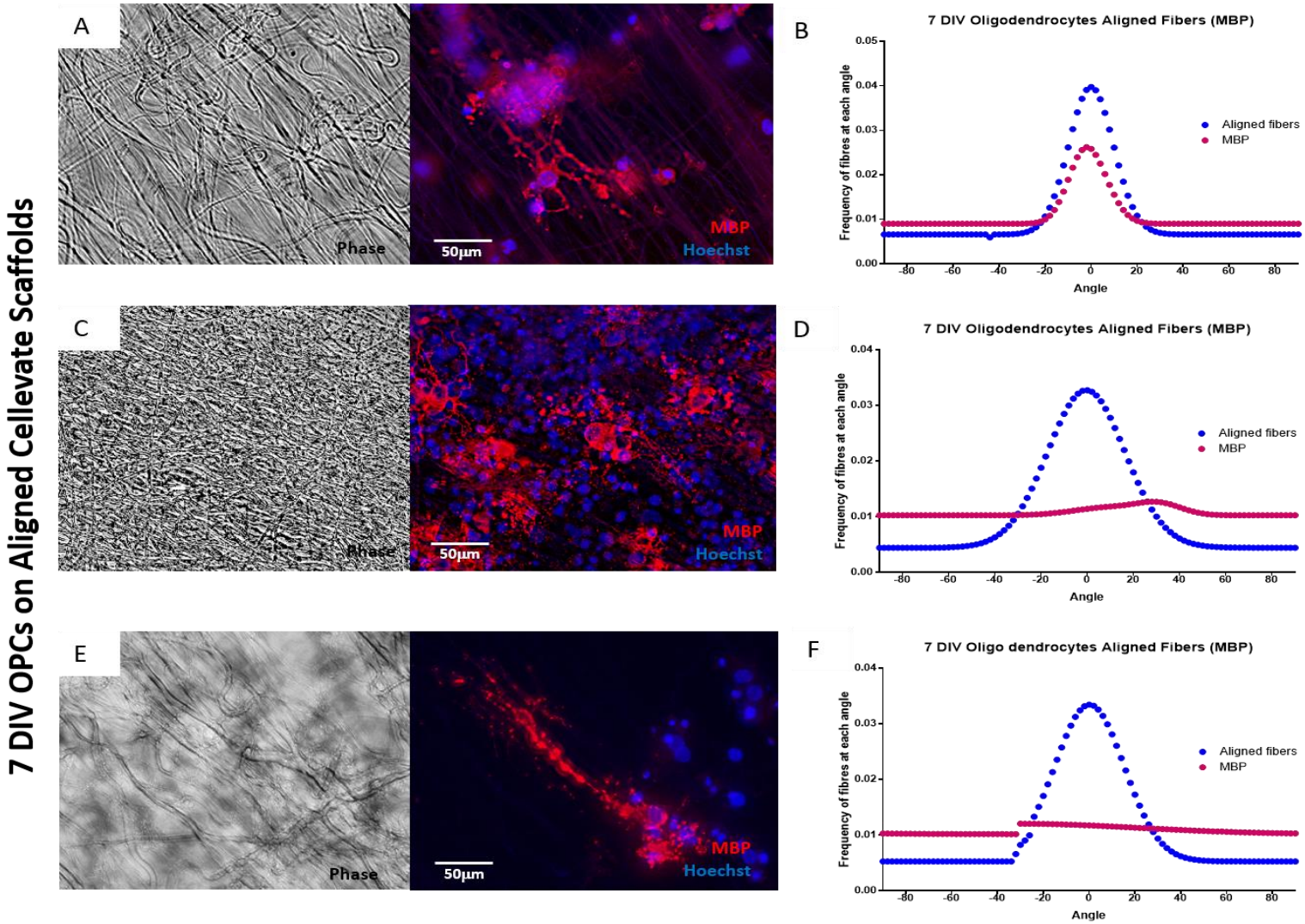

Figure 5.5. 7DIV MBP expression in oligodendrocyte lineage cell populations grown on aligned Cellevate scaffolds.

Representative images of oligodendrocyte lineage cells were stained with MBP (red), an Oligodendrocyte marker and hoechst on aligned scaffolds n=3. **Figure 5.5 continues below.**

Figure 5.5 continued. Image **A** corresponds with graph **B,** image **C** corresponds with **D** and image **E** corresponds with **F**. All Z-stack CZI images were deconvolved with Huygens Professional version 19.04 (Scientific Volume Imaging, The Netherlands, http://svi.nl), using the CMLE algorithm, with signal to noise ratio (SNR):40 and maximum 50 iterations. The total cells counted for an n=3 was 803 of which 352 of the cells were MBP positive, with the remainder of 451 cells staining for hoescht.

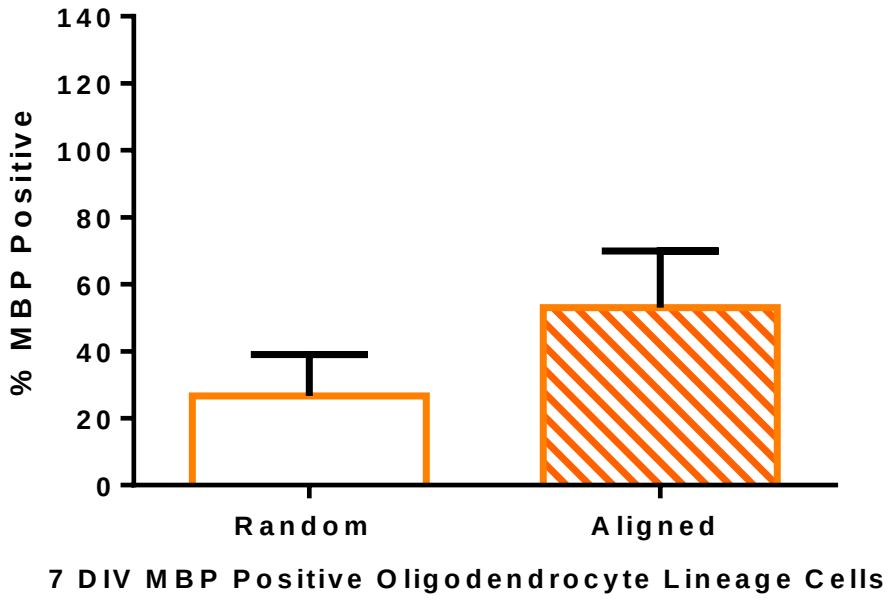

Figure 5.67. MBP expression in oligodendrocyte lineage cell at 7DIV in unaligned and aligned scaffolds. Data was analysed using an unpaired t-test with Welch's correlation which demonstrated there was no significant difference in MBP expression between oligodendrocyte lineage cells grown on random and aligned fibres at 7DIV respectively (P>0.05), n=4.

The 7DIV results therefore, showed that oligodendrocyte alignment on the aligned scaffold, was not as prominent in comparison to the 3DIV alignment data. This may be due to the act of cutting away the fibres from the scaffold and fixing prior to imaging which may have potentially affected the alignment of the highly branched oligodendrocytes at 7 DIV, on the aligned scaffold. Therefore, scaffolds that were utilised for cell viability assays and were not removed from the bracket, which kept the fibres in place, were consequently processed to measure oligodendrocyte lineage cell directionality.

5.2.3 Calcein stained oligodendrocyte lineage cells demonstrated slight cellular alignment at day 7

The directionality analysis of the calcein stained cells on non-aligned and aligned scaffolds at 3 and 7 DIV, demonstrated that there was alignment at 3DIV within the aligned scaffolds (Figure 5.7 A & E). Additionally, there was a small peak at 7DIV for oligodendrocyte lineage cells on the aligned scaffold (Figure 5.7 C & G) in comparison to no peak in directionality for cells in the unaligned scaffold (Figure 5.7 D & H). This therefore suggests that there was slight alignment of the cells at 7DIV, however the alignment was not as significant when compared to cells in the 3DIV aligned scaffolds.

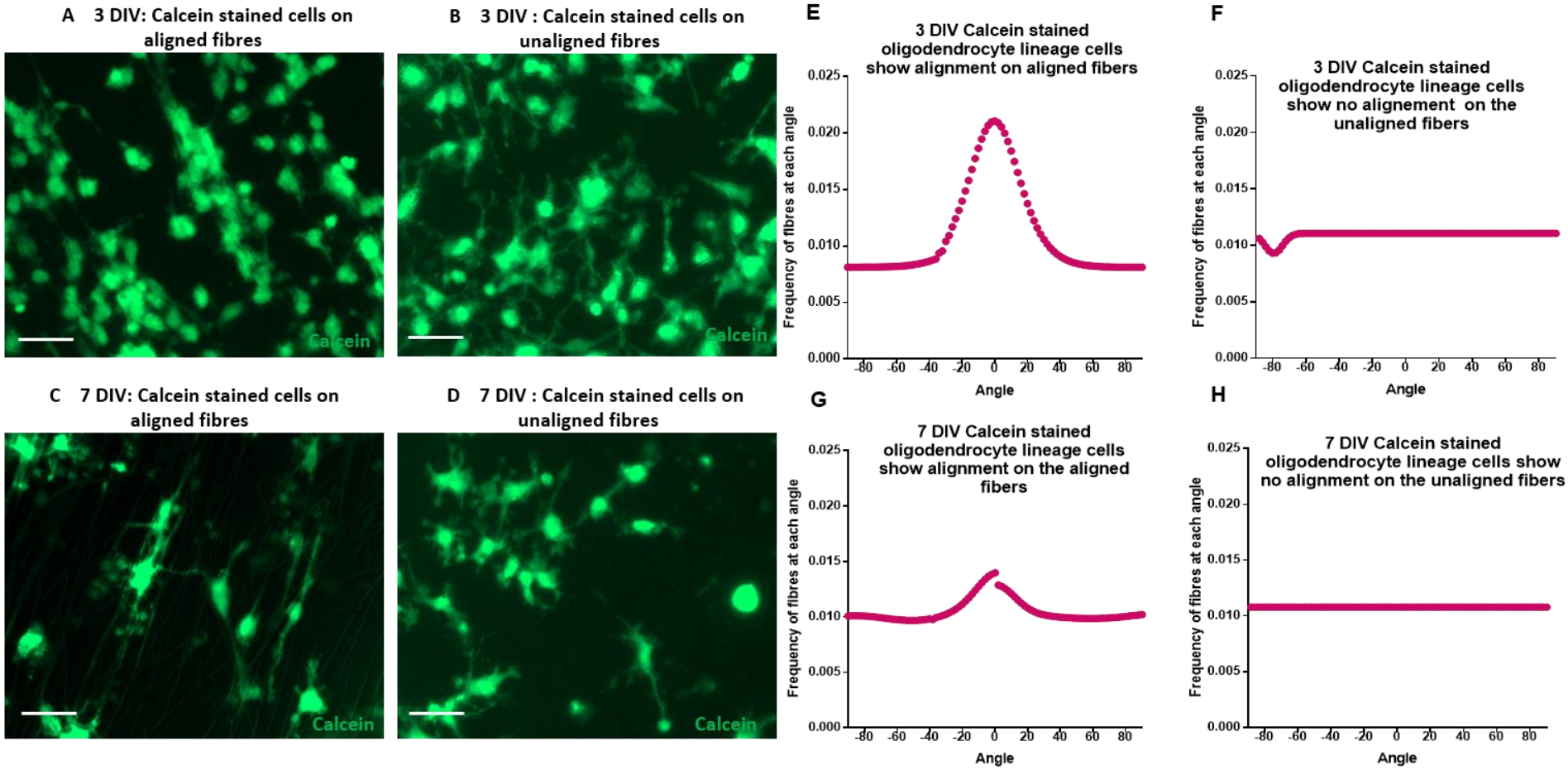

Figure 5.7. Measurement of oligodendrocyte lineage cell alignment on unaligned and aligned scaffolds using calcein stained cells. A & B shows the alignment of oligodendrocyte lineage cells at 3DIV on aligned and unaligned scaffolds respectively with **C & D** showing 7DIV cell aligned on both aligned and unaligned scaffolds. **Figure 5.7 continues below.**

Figure 5.7 continued. Graphs **E & F** illustrates alignment of oligodendrocyte lineage cells at 3DIV on aligned and unaligned scaffolds with **G & H** demonstrating alignment at 7DIV on aligned and unaligned scaffolds respectively n=3.Scale bar represents 50μm.

5.2.4 SEM images on oligodendrocyte lineage cells in the non-aligned and aligned Cellevate scaffolds

Scanning electron microscopy (SEM) was also conducted on the non-aligned and aligned Cellevate scaffolds, seeded with rat derived oligodendrocyte lineage cells to observe the interaction of the cells with the scaffolds. It appeared that at 3DIV, oligodendrocyte lineage cell bodies within the non-aligned constructs were situated on top of the scaffold, with some cellular processes wrapping round the non-aligned fibres (Figure 5.8 A&B). The oligodendrocyte lineage cells within the aligned scaffold also appear to be situated on top of the scaffold with some of the processes of the cells seem to be aligning with the fibres (Figure 5.8 C&D).

SEM images of oligodendrocyte lineage cells, in the non-aligned scaffold at 7DIV, demonstrated that the cells bodies were again, situated on top of the fibres however it was difficult to associate the cellular processes which were following all directions of the scaffold, to a specific cell body (Figure 5.9 A&B).

The cell bodies of oligodendrocyte lineage cells within the 7DIV aligned scaffold in comparison, appeared to be situated in between fibres, with evidence of multiple cellular process extension, which were following the direction of the aligned fibres (Figure 5.9 C&D).

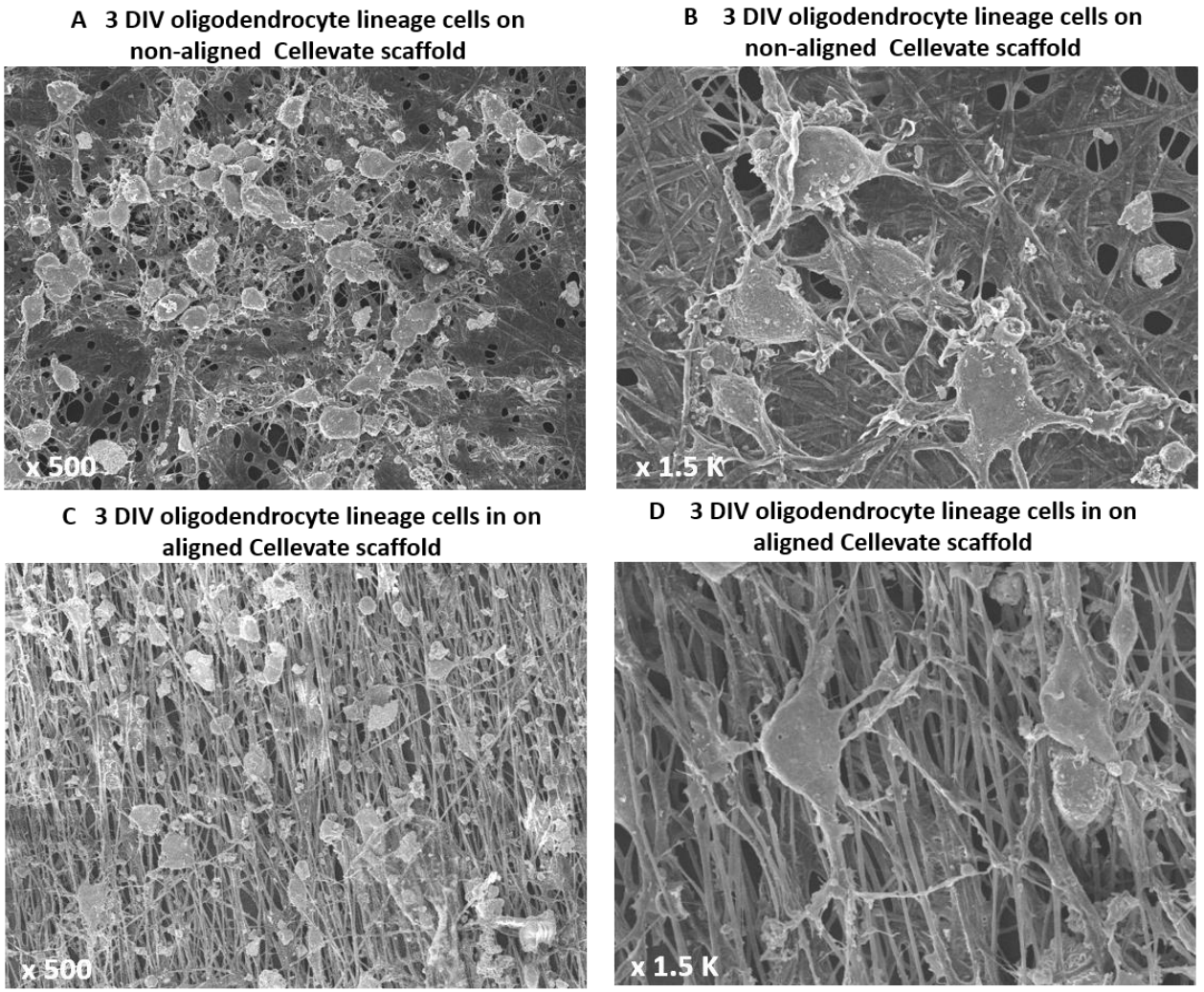

Figure 5.8. SEM images of rat oligodendrocyte lineage cells on non-aligned and aligned Cellevate scaffolds at 3 DIV. **A)** represents 3DIV oligodendrocytes cells on the non-aligned Cellevate scaffold at x 500 magnification. **B)** represents 3DIV oligodendrocytes cells on the non-aligned Cellevate scaffold at x1.5 K magnification. **C)** represents 3DIV oligodendrocytes cells on the aligned Cellevate scaffold at x 500 magnification. **D)** represents 3DIV oligodendrocytes cells on the aligned Cellevate scaffold at x1.5 K magnification.

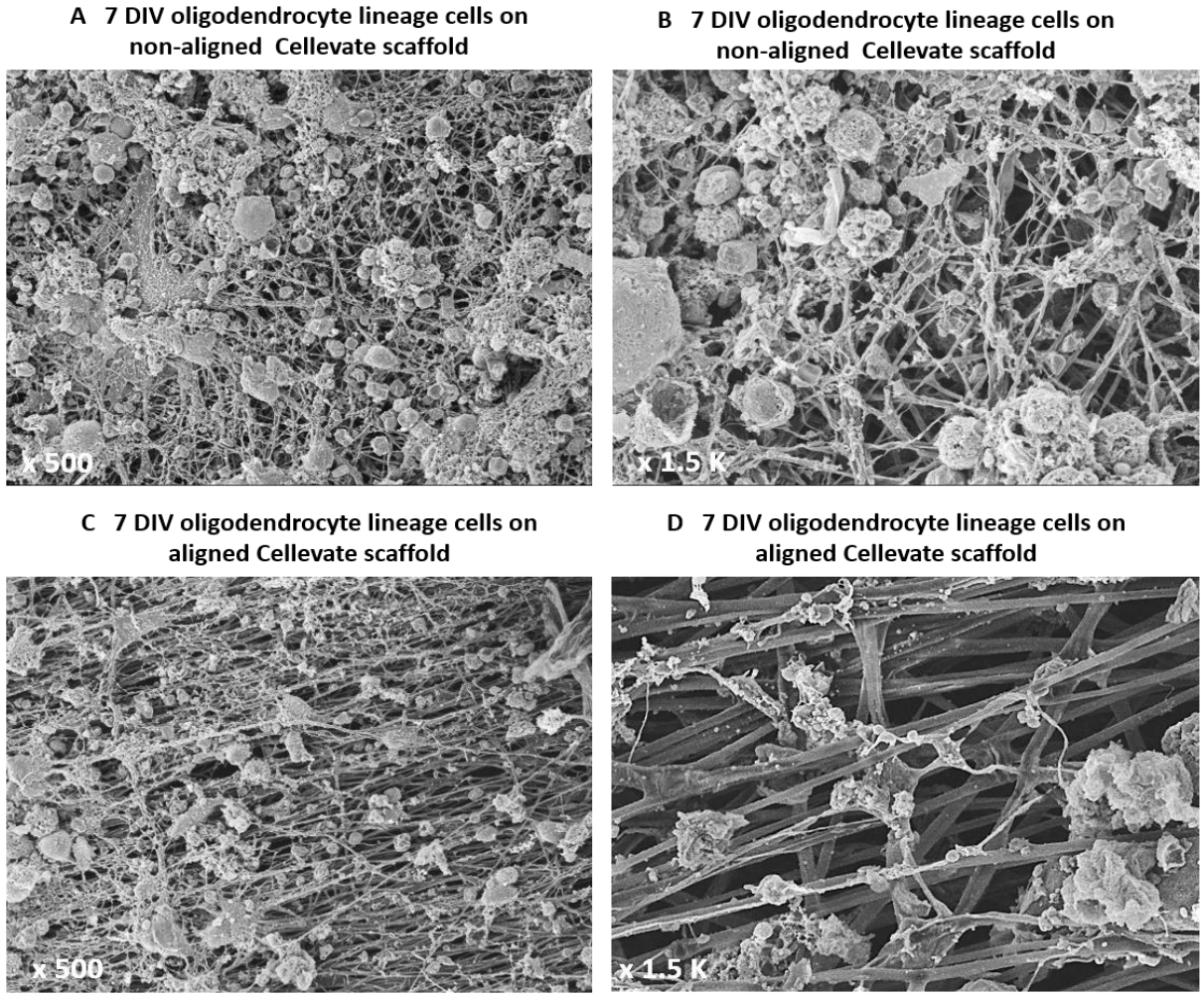

Figure 5.9. SEM images of rat oligodendrocyte lineage cells on non-aligned and aligned Cellevate scaffolds at 7 DIV. A) represents 7DIV oligodendrocytes cells on the non-aligned Cellevate scaffold at x 500 magnification. **B)** represents 7DIV oligodendrocytes cells on the non-aligned Cellevate scaffold at x1.5 K magnification. **Figure 5.9 continues below.**

Figure 5.9 continued. **C)** represents 7DIV oligodendrocytes cells on the aligned Cellevate scaffold at x 500 magnification. **D)** represents 7DIV oligodendrocytes cells on the aligned Cellevate scaffold at x1.5 K magnification.

5.3 Discussion

To the best of my knowledge, it has been demonstrated for the first time the survival and alignment of precursor oligodendrocyte lineage cells on electrospun, 3D aligned PCL Cellevate scaffolds.

The fibres within the scaffold allowed for the adherence of the oligodendrocyte lineage cells as seen in the SEM images. This was possibly due to the composition of the scaffold being collagen and elastin, and due to the coating of the fibres with POR-N and laminin, which all aided cellular attachment (Chelli *et al.*, 2014; Chaubaroux *et al*, 2015).

5.3.1 Aligned Cellevate PCL scaffolds support OPC populations however viability decreases in differentiated cultures by day 7

Viability at 3 DIV in the constructs was approximately 80% in both the non-aligned and aligned scaffolds, suggesting that the scaffold can support a healthy population of precursor cells. Additionally, viability was higher using the Cellevate PCL scaffold, in comparison to a study by Li *et al.*, (2015), who seeded OPCs onto coverslips with PCL nanofibers and reported viability being 48%. Cell viability however decreased to approximately 55% within the scaffold at 7DIV, when OPCs were differentiated into oligodendrocytes. When viability was compared to oligodendrocyte lineage cells grown on a 2D surface, our laboratory has previously shown that viability of rodent OPCs and oligodendrocytes cultured on glass coverslips has been reported to being >95% (Jenkins *et al.*, 2013).

A decrease in viability within the aligned scaffold would be a substantial issue for cell transplantation as this may trigger a further inflammatory response by microglia within the site of SCI, thereby making it a hostile environment for regeneration (Gadani *et al.*, 2016; Xu *et al.*, 2020). The decrease in viability may be due to there being a lack of supporting glial cells such as astrocytes. Astrocytes provide trophic factors for oligodendrocytes and promote myelination, via the secretion of cytokines such as LIT and CNTF as these molecules have a capacity to protect oligodendrocytes from apoptosis (Kıray *et al.*, 2016). Weightman*,et al*, (2014) demonstrated that pre-seeding astrocytes onto an aligned poly-L,D-lactic acid nanofiber scaffold, 2 days prior to seeding OPCs, significantly improved OPC survival and maturation in comparison to OPCs seeded alone. Furthermore, at 8DIV, the OPCs showed potential to differentiate into heavily process-bearing MBP positive oligodendrocytes, with large sheets of membrane that appeared to contact both the nanofibers and pre-aligned astrocytes. Therefore, it may be beneficial to trial co-culturing OPCs with astrocytes to improve 7DIV viability and myelination (Vecino and Kwok, 2016).

5.3.2 OPCs appeared aligned within the Cellevate PCL nanomatrix

Histological staining showed that there were different phenotypes of oligodendrocyte lineage cell morphologies on the aligned scaffold in comparison to the non-aligned matrix. At 3DIV, there was >90% NG2 positive OPCs within the aligned and non-aligned scaffolds. There was also evidence of alignment of OPCs evident when analysing immunostained and SEM images, with OPC bipolar processes extending in both directions of the scaffold in an aligned manner, in comparison to OPCs on the non-aligned scaffold appearing to extend cellular processes in no particular pattern.

This observation was further supported by the directionality analysis which emphasised that the OPCs on the aligned scaffold followed the direction of the fibre and this was seen in most regions of the construct.

The alignment of the OPCs was possibly due to the structure of the fibres, coating, and also because of haptotaxis which enables the interaction of extracellular molecules to synergise with receptors on the plasma membrane of the cells, producing concise, intracellular signal transduction channels. In turn, these pathways control the assembly and arrangement of the actin cytoskeleton. Situated at both the front and rear end of cells, these pathways are responsible, possibly for driving the direction of cellular alignment along the Cellevate scaffold (Berzat and Hall, 2010).

At 7DIV, 50% of the cell population within the aligned scaffolds were MBP positive oligodendrocytes in comparison to 30% in the non-aligned scaffold. The remainder of the cell population within the scaffolds were possibly NG2 positive precursors. Cell alignment however was not consistent throughout the aligned Cellevate matrix as seen in the immunohistochemistry and SEM images, in comparison to 3DIV data, as there were regions where the myelinogenic cells appeared to be unaligned, which was similar to the cells on the non-aligned fibres. Cellular alignment at 7DIV was also analysed using calcein stained cells, as the scaffold was not removed from the bracket, thus keeping the fibres in place. There was evidence of alignment of the myelinogenic cells in some regions on the aligned scaffold however again, this was not as significant in comparison to OPC alignment.

Enhancement and the frequency of myelinating oligodendrocyte alignment within the Cellevate scaffold, could possibly be improved by incorporating astrocytes as they have been described in literature for encouraging oligodendrocyte cell alignment

and promoting the adhesion of oligodendrocyte process to axons (Meyer-Franke *et al* 1999; Ishibashi *et al.*, 2006).

5.3.3 Conclusion

In conclusion it has been demonstrated that an enriched population of oligodendrocyte lineage cells seeded onto an aligned PCL Cellevate scaffold, can predominantly support the growth and alignment of 3DIV oligodendrocyte precursor cells and enable expression of its cell specific marker. Further optimisation however is required to improve 7DIV viability of the mature oligodendrocyte within the Cellevate scaffolds.

5.3.4 Future direction of research

To improve viability of mature oligodendrocytes within the aligned Cellevate scaffold, future studies could include coating the aligned Cellevate fibres with tenascin C (TN-C) to improve the viability of myelinating oligodendrocytes. TN-C is a glycoprotein that interacts with cell surface ligands and is implicated in OPC differentiation, myelination and survival (Vecino and Kwok, 2016). Further research is also required to understand the relationship between the oligodendrocyte lineage cells and the aligned Cellevate scaffold. Investigations include determining whether the scaffold allows OPC proliferation, which can be analysed using an EDU assay, as this is an essential characteristic that is required to rapidly respond to injury *in vivo* (Li and Leung, 2015). *In vitro* investigations should also consider implanting the oligodendrocyte lineage aligned constructs into an *in vitro* SCI model, to determine if axonal remyelination can be achieved, and to also investigate if the aligned scaffold

permits directed linear neurite outgrowth across the lesion site to re-establish lost neuronal connections (Günther *et al.*, 2015). Moving towards *in vivo* testing, the OPC seeded, aligned Cellevate construct could also be implanted into demyelinated lesion sites into rodent SCI models, to investigate the immunogenic response of the graft within the host, integration of the graft into the site and to also observe whether locomotor recovery can be achieved (Qin *et al.*, 2018).

Chapter 6

Concluding Comments

6.1 Summary of key research findings

The research presented in this thesis has demonstrated the applicability of *in vitro* primary murine neural models of mixed glial and neuronal enriched cells, for the testing of oligodendrocyte lineage and neuronal cells encapsulated in biomaterials, in order to assess the efficacy of the scaffolds to support transplant cell populations, for SCI repair. The key findings presented in this thesis have been summarised below.

Chapter 3 Development of new culture systems utilising post-natal murine brains to isolate major neural cell populations

This chapter demonstrated the development of robust and reproducible, *in vitro* primary neural models that can be utilised for biomaterial testing. The mixed glial model matured and stratified to give rise to microglia, OPCs and astrocytes by 10 DIV. Additionally, sequential shaking of microglia, OPCs and trypsinisation of astrocytes allowed for the production of isolated glial fractions with viability >90% and cell purity being reported as >93%, with <7% residual cross-cell-contamination. Enzymatic dissociation of postnatal murine cortices allowed for the generation of a neuronal enriched model, consisting of >80% viability across all time points. In addition, the culture supported the maturation of neuronal and glial cells with determined proportions of each cell type reported as 45-50% Tuj-1 positive neurons as well as approximately 50% GFAP positive astrocytes and less than 10% oligodendrocytes.

6.3 Chapter 4 Utilisation of DuraGen PlusTM as 3-Dimensional matrix for oligodendrocyte lineage cell and cortical neuronal cell encapsulation

The murine derived, neural cell models were utilised for the testing of a surgical grade biomaterial. Oligodendrocyte lineage cells derived from the mixed glial model, were co-seeded with astrocytes, which acted as a supportive cell population onto the FDA approved matrix DuraGen Plus™ and demonstrated that the OPCs could mature into myelinating oligodendrocyte lineage cells. Additionally, the neuronal enriched cells derived from post-natal murine cortices were also seeded onto DuraGen Plus™ and showed that the scaffold enables the maturation of neurons, although future work is required to investigate ways of improving the viability of the cells to >60% within the construct.

Chapter 5 Investigating Cellevate scaffolds to induce alignment of oligodendrocyte lineage cells derived from the mouse mixed glial culture model

Oligodendrocyte lineage cells, derived from the mixed glial model, were seeded onto a 3D aligned PCL Cellevate scaffold, which promoted the alignment of OPCs, and sustained a viable cell population. However, directionality analysis and SEM imaging of the mature oligodendrocytes within the construct demonstrated that the cells were not as prominently aligned in comparison to OPC and additionally viability had reduced to 55% by 7DIV.

The implications of these findings have been discussed in detail within each chapter, in addition, to the future direction for development of the biomaterial constructs and their applicability in SCI research for neural cell replacement therapies.

It is important to note here that there were limitations of some of the methods developed for the generation of the cell encapsulated scaffolds in both chapters 4 and 5. This included low cell viability for oligodendrocyte lineage and neuronal enriched cells (chapter 4A and B respectively) when using the flooding of cells seeding method. Viability however, was improved once a focal cell seeding approach was employed. The formation of a co-construct by adding astrocytes with oligodendrocyte lineage cells improved cellular viability and appeared to promote myelination into mature oligodendrocytes within the scaffold. The focal cell seeding method alone, however, did not improve viability for the neuronal enriched DuraGen Plus^{TM} constructs. Mechanical dissociation of cortical tissue was changed to enzymatic dissociation. This did result in an improvement in cell viability and reduced cellular debris. Though, there were limitations to this method as viability remained below 60% which is unfavourable, as a predominantly healthy population of cells should be transplanted into the spinal cord. Further improvements must be made to the method in order to improve the overall health of the transplant cell population which is discussed in chapter 4. For oligodendrocyte lineage cells seeded onto Cellevate (Chapter 5), there was a decrease in viability at 7DIV. Therefore, the method has to be improved in order to resolve this. A potential way of achieving this could be by coating the scaffold with glycoproteins and utilising astrocytes as a supportive cell.

In this thesis, I have demonstrated how the development of two distinct *in vitro* neural models has the potential to be used for many therapeutic avenues within the neural tissue engineering field to further spinal cord injury research. The postnatal murine models are capable of being used to understand the formation of neural networks and to also investigate how cellular encapsulation within biomaterials, can influence

neural cell fate. Additionally, investigations using the biomaterials DuraGen Plus™ for the development of oligodendrocyte lineage and neuronal cells constructs, as well as Cellevate, for oligodendrocyte lineage cellular alignment, two biomaterials consisting of distinct structural properties, has given insight into how these scaffolds can support neural cell differentiation, maturation and survival. This current research adds to the regenerative neurology community by showing that these biomaterials may have the potential to be used for cellular replacement for SCI. This could be determined by utilising *in vitro* models, to investigate whether the graft can integrate into the damaged spinal cord and therefore, promote neural cell growth.

References

1. Adams, C. F. *et al.* (2016) 'Nanoengineering neural stem cells on biomimetic substrates using magnetofection technology', *Nanoscale*, 8(41), pp. 17869–17880. doi: 10.1039/c6nr05244d.
2. Adesida, A. B. *et al.* (2012) 'Oxygen tension is a determinant of the matrix-forming Phenotype of cultured human meniscal Fibrochondrocytes', *PLoS ONE*, 7(6), pp. 1–8. doi: 10.1371/journal.pone.0039339.
3. Aebersold, M. J. *et al.* (2018) 'Simple and Inexpensive Paper-Based Astrocyte Co-culture to Improve Survival of Low-Density Neuronal Networks', *Frontiers in Neuroscience*, 12(February), pp. 1–14. doi: 10.3389/fnins.2018.00094.
4. Ahlemeyer, B. and Baumgart-vogt, E. (2005) 'Optimized protocols for the simultaneous preparation of primary neuronal cultures of the neocortex , hippocampus and cerebellum from individual newborn (P0 . 5) C57Bl / 6J mice', 149, pp. 110–120. doi: 10.1016/j.jneumeth.2005.05.022.
5. Akdemir, R. S., Huang, A. Y. and Deneen, B. (2020) 'Astrocytogenesis : where , when , and how', *F1000 Research*, 9.
6. Almad, A., Sahinkaya, F. R. and McTigue, D. M. (2011) 'Oligodendrocyte Fate after Spinal Cord Injury', *Neurotherapeutics*, 8(2), pp. 262–273. doi: 10.1007/s13311-011-0033-5.
7. Alnasser, Y. *et al.* (2018) 'Preferential and Increased Uptake of Hydroxyl-Terminated PAMAM Dendrimers by Activated Microglia in Rabbit Brain Mixed Glial Culture', *Molecules*, 23(5). doi: 10.3390/molecules23051025.
8. Amer, M. H., White, L. J. and Shakesheff, K. M. (2015) 'The effect of injection using narrow-bore needles on mammalian cells: Administration and formulation considerations for cell therapies', *Journal of Pharmacy and Pharmacology*, 67(5), pp. 640–650. doi: 10.1111/jphp.12362.
9. Anson, D. S. (2004) 'The use of retroviral vectors for gene therapy-what are the risks? A review of retroviral pathogenesis and its relevance to retroviral

vector-mediated gene delivery', *Genetic Vaccines and Therapy*, 2, pp. 1–13. doi: 10.1186/1479-0556-2-9.

10. Azari, H. and Reynolds, B. A. (2016) 'In vitro models for neurogenesis', *Cold Spring Harbor Perspectives in Biology*, 8(6), pp. 1–11. doi: 10.1101/cshperspect.a021279.

11. Aziz, J. *et al.* (2016) 'Molecular Mechanisms of Stress-Responsive Changes in Collagen and Elastin Networks in Skin', *Skin Pharmacology and Physiology*, 29(4), pp. 190–203. doi: 10.1159/000447017.

12. Balasubramanian, S. *et al.* (2016) 'Page 1 of 58 1', *Tissue Engineering Part A*, (22(11–12)), pp. 885–898. doi: 10.1089/ten.tea.2016.0103 PMCID: PMC4913501.

13. Baldassarro, V. . *et al.* (2016) 'In Vitro Testing of Biomaterials for Neural Repair : Focus on Cellular Systems and High-Content Analysis', *BioResearch*, 5, pp. 201–211. doi: 10.1089/biores.2016.0025.

14. Banker, G. A. and Cowan, W. M. (1977) 'Rat hippocampal neurons in dispersed cell culture', *Brain Research*, 126(3), pp. 397–425. doi: 10.1016/0006-8993(77)90594-7.

15. Barateiro, A. and Fernandes, A. (2014) 'Temporal oligodendrocyte lineage progression: In vitro models of proliferation, differentiation and myelination', *Biochimica et Biophysica Acta - Molecular Cell Research*. Elsevier B.V., 1843(9), pp. 1917–1929. doi: 10.1016/j.bbamcr.2014.04.018.

16. Beattie, M. . *et al.* (2002) 'ProNGF Induces p75-Mediated Death of Oligodendrocytes following Spinal Cord Injury', *Bone*, 23(1), pp. 1–7.

17. Beaudoin, G. M. J. *et al.* (2012) 'Culturing pyramidal neurons from the early postnatal mouse hippocampus and cortex', *Nature Protocols*. Nature Publishing Group, 7(9), pp. 1741–1754. doi: 10.1038/nprot.2012.099.

18. Bechler, M. E. (2019) 'A neuron-free microfiber assay to assess myelin sheath formation', *Methods in Molecular Biology*, 1936, pp. 97–110. doi: 10.1007/978-

1-4939-9072-6_6.

19. Bennett (2018) *Cerafix® Dura Repair*. Available at: http://www.bennetthealth.net/wp-content/uploads/2017/11/Cerafix-General-Brochure-.pdf.

20. Bergles, D. E. and Richardson, W. D. (2016) 'Oligodendrocyte development and plasticity', *Cold Spring Harbor Perspectives in Biology*, 8(2), pp. 1–28. doi: 10.1101/cshperspect.a020453.

21. Berzat, A. and Hall, A. (2010) 'Cellular responses to extracellular guidance cues', *EMBO Journal*. Nature Publishing Group, 29(16), pp. 2734–2745. doi: 10.1038/emboj.2010.170.

22. Bhartiya, D. *et al.* (2013) 'An Overview of Pluripotent Stem Cells', in *Intech*. doi: dx.doi.org/10.5772/55130.

23. Blakemore, W. F. and Irvine, K. A. (2008) 'Endogenous or exogenous oligodendrocytes for remyelination', *Journal of the Neurological Sciences*, 265(1–2), pp. 43–46. doi: 10.1016/j.jns.2007.08.004.

24. Boese, A. C. *et al.* (2018) 'Neural stem cell therapy for subacute and chronic ischemic stroke', *Stem Cell Research and Therapy*. Stem Cell Research & Therapy, 9(1), pp. 1–17. doi: 10.1186/s13287-018-0913-2.

25. Bracken, M. B. *et al.* (1997) 'Administration of methylprednisolone for 24 or 48 hours or tirilazad mesylate for 48 hours in the treatment of acute spinal cord injury: Results of the Third National Acute Spinal Cord Injury randomized controlled trial', *Journal of the American Medical Association*, 277(20), pp. 1597–1604. doi: 10.1001/jama.277.20.1597.

26. Caliari, S. and Burdick, J. A. (2016) 'A practical guide to hydrogels for cell culture', *Nature Methods*. Nature Publishing Group, 13(5), pp. 405–414. doi: 10.1038/nmeth.3839.

27. Cangellaris, O. IV. and Gillette, M. U. (2018) 'Biomaterials for enhancing neuronal repair', *Frontiers in Materials*, 5(April). doi: 10.3389/fmats.2018.00021.

28. Cao, Q. *et al.* (2010) ‘Transplantation of ciliary neurotrophic factor-expressing adult oligodendrocyte precursor cells promotes remyelination and functional recovery after spinal cord injury’, *Journal of Neuroscience*, 30(8), pp. 2989–3001. doi: 10.1523/JNEUROSCI.3174-09.2010.

29. Caputi, A. *et al.* (2013) ‘The long and short of GABAergic neurons’, *Current Opinion in Neurobiology*. Elsevier Ltd, 23(2), pp. 179–186. doi: 10.1016/j.conb.2013.01.021.

30. Caron, I. *et al.* (2016) ‘Biomaterials A new three dimensional biomimetic hydrogel to deliver factors secreted by human mesenchymal stem cells in spinal cord injury’, *Biomaterials*, 75, pp. 135–147. doi: 10.1016/j.biomaterials.2015.10.024.

31. Carter, M. and Shieh, J. (2015) ‘Chapter 14 - Cell Culture Techniques’, in *Guide to Research Techniques in Neuroscience*, pp. 295–310. doi: 10.1016/B978-0-12-800511-8.00014-9.

32. Cellevate (2020) *Cellevate FAQ*, *Cellevate*. Available at: www.cellevate.com/faq.

33. Chaubaroux, C., Perrin-schmitt, F. and Senger, B. (2015) ‘Cell Alignment Driven by Mechanically Induced Collagen Fiber Alignment in Collagen / Alginate Coatings’, 21(9), pp. 881–888. doi: 10.1089/ten.tec.2014.0479.

34. Chelli, B. *et al.* (2014) ‘Neural cell alignment by patterning gradients of the extracellular matrix protein laminin’.

35. Chen, Y. *et al.* (2007) ‘Isolation and culture of rat and mouse oligodendrocyte precursor cells’, *Nature Protocols*, 2(5), pp. 1044–1051. doi: 10.1038/nprot.2007.149.

36. Chung, W. ., Allen, N. J. and Eroglu, C. (2015) ‘Astrocytes Control Synapse Formation, Function, and Elimination’, *Cold Spring Harbor Laboratory Press*, 7(a020370), pp. 1–19.

37. Clavreul, S. *et al.* (2019) ‘Cortical astrocytes develop in a plastic manner at both clonal and cellular levels’, *Nature Communications*. Springer US, 10(1), pp. 1–14. doi: 10.1038/s41467-019-12791-5.

38. Cosgrove, R. . *et al.* (2007) ‘Safety and efficacy of a novel polyethylene glycol hydrogel sealant for watertight dural repair’, *Neurosurgery*, 106, pp. 52–58. doi: 10.3171/jns.2007.106.1.52.

39. Court, F. A. and Alvarez, J. (2016) ‘Glial Cells in Health and Disease of the CNS’, *Advances in experimental medicine and biology*, 949(949), pp. 183–201. doi: 10.1007/978-3-319-40764-7.

40. Cristante, A. *et al.* (2012) ‘Therapeutic approaches for spinal cord injury’, 67(10), pp. 1219–1224. doi: 10.6061/clinics/2012(10)16.

41. Czepiel, M. *et al.* (2011) ‘Differentiation of induced pluripotent stem cells into functional oligodendrocytes’, *Glia*, 59(6), pp. 882–892. doi: 10.1002/glia.21159.

42. Dasgupta, S. and Ray, S. . (2017) ‘Diverse Biological Functions of Sphingolipids in the CNS: Ceramide and Sphingosine Regulate Myelination in Developing Brain but Stimulate Demyelination during Pathogenesis of Multiple Sclerosis’, *Journal of Neurology and Psychology*, 5(1), pp. 01–07. doi: 10.13188/2332-3469.1000035.

43. Duncan, I. D. *et al.* (2017) ‘Thin myelin sheaths as the hallmark of remyelination persist over time and preserve axon function’, *Proceedings of the National Academy of Sciences of the United States of America*, 114(45), pp. E9685–E9691. doi: 10.1073/pnas.1714183114.

44. Egawa, N. *et al.* (2017) ‘A Novel Three-Dimensional Culture System for Oligodendrocyte Precursor Cells Naohiro’, *Stem cells and development*,

26(14), pp. 1078–1085. doi: 10.1089/scd.2016.0306.

45. Ellenbroek, B. and Youn, J. (2016) ‘Rodent models in neuroscience research : is it a rat race ?’, pp. 1079–1087. doi: 10.1242/dmm.026120.

46. Englund-Johansson, U., Netanyah, E. and Johansson, F. (2017) ‘Tailor-Made Electrospun Culture Scaffolds Control Human Neural Progenitor Cell Behavior—Studies on Cellular Migration and Phenotypic Differentiation’, *Journal of Biomaterials and Nanobiotechnology*, 08(01), pp. 1–21. doi: 10.4236/jbnb.2017.81001.

47. Fakhoury, M. (2015) ‘Spinal cord injury: Overview of experimental approaches used to restore locomotor activity’, *Reviews in the Neurosciences*, 26(4), pp. 397–405. doi: 10.1515/revneuro-2015-0001.

48. Farhy-Tselnicker, I. and Allen, N. J. (2018) ‘Astrocytes, neurons, synapses: A tripartite view on cortical circuit development’, *Neural Development*. Neural Development, 13(1), pp. 1–12. doi: 10.1186/s13064-018-0104-y.

49. Farrag, M. and Leipzig, N. (2018) ‘Subcutaneous Maturation of Neural Stem Cell-Loaded Hydrogels Forms Region-Specific Neuroepithelium’, *Cells*, 7(10), p. 173. doi: 10.3390/cells7100173.

50. Fehlings, M. G. *et al.* (2012) ‘Early versus Delayed Decompression for Traumatic Cervical Spinal Cord Injury : Results of the Surgical Timing in Acute Spinal Cord Injury Study (STASCIS)’, *PLoS ONE*, 7(2). doi: 10.1371/journal.pone.0032037.

51. Fernandes, A. R. and Chari, D. M. (2014) ‘A multicellular, neuro-mimetic model to study nanoparticle uptake in cells of the central nervous system’, *Integrative Biology (United Kingdom)*. Royal Society of Chemistry, 6(9), pp. 855–861. doi: 10.1039/c4ib00085d.

52. Fernandes, A. R. and Chari, D. M. (2016) ‘SC Cellular and Neural Engineering Group , Institute for Science and Technology in Medicine ’, *Journal of Controlled Release*. Elsevier B.V. doi: 10.1016/j.jconrel.2016.06.039.

53. Finch, L. *et al.* (2020) ‘Safe nanoengineering and incorporation of transplant populations in a neurosurgical grade biomaterial , DuraGen Plus TM , for protected cell therapy applications’, *Journal of Controlled Release*. Elsevier, 321(October 2019), pp. 553–563. doi: 10.1016/j.jconrel.2020.02.028.

54. Franklin, R. J. M. and Ffrench-Constant, C. (2008) ‘Remyelination in the CNS: From biology to therapy’, *Nature Reviews Neuroscience*, 9(11), pp. 839–855. doi: 10.1038/nrn2480.

55. Franklin, R. J. M. and Goldman, S. A. (2015) ‘Glia disease and repair—Remyelination’, *Cold Spring Harbor Perspectives in Biology*, 7(7), pp. 1–28. doi: 10.1101/cshperspect.a020594.

56. Frantz, C., Stewart, K. M. and Weaver, V. M. (2010) ‘The extracellular matrix at a glance’, *Journal of Cell Science*, 123(24), pp. 4195–4200. doi: 10.1242/jcs.023820.

57. Frost, H. K. *et al.* (2018) ‘Electrospun nerve guide conduits have the potential to bridge peripheral nerve injuries in vivo’, *Scientific Reports*, 8(1), pp. 1–13. doi: 10.1038/s41598-018-34699-8.

58. Gadani, S. *et al.* (2016) ‘Dealing with Danger in the CNS: The Response of the Immune System to Injury’, *Neuron*, 87(1), pp. 47–62. doi: 10.1016/j.neuron.2015.05.019.Dealing.

59. Ge, H. *et al.* (2015) ‘Poly-L-ornithine promotes preferred differentiation of neural stem/progenitor cells via ERK signalling pathway’, *Scientific Reports*. Nature Publishing Group, 5(September), pp. 1–10. doi: 10.1038/srep15535.

60. Ge, L. and Chen, S. (2020) ‘Recent advances in tissue adhesives for clinical medicine’, *Polymers*, 12(4). doi: 10.3390/POLYM12040939.

61. Geng, X. *et al.* (2017) ‘Biological membrane-packed mesenchymal stem cells treat acute kidney disease by ameliorating mitochondrial-related apoptosis’, *Scientific Reports*, 7(1), pp. 1–12. doi: 10.1038/srep41136.

62. Gersey, Z. C. *et al.* (2017) ‘First human experience with autologous Schwann

cells to supplement sciatic nerve repair: Report of 2 cases with long-term follow-up', *Neurosurgical Focus*, 42(3). doi: 10.3171/2016.12.FOCUS16474.

63. Ginhoux, F. *et al.* (2013) 'Origin and differentiation of microglia', *Frontiers in Cellular Neuroscience*, 7(MAR), pp. 1–14. doi: 10.3389/fncel.2013.00045.

64. Giorgi-Coll, S. *et al.* (2017) 'Succinate supplementation improves metabolic performance of mixed glial cell cultures with mitochondrial dysfunction', *Scientific Reports*. Springer US, 7(1), pp. 1–9. doi: 10.1038/s41598-017-01149-w.

65. Giraudo, M. . *et al.* (2020) 'Angiogenic Potential in Biological Hydrogels', *Biomedicines*, 8(436), pp. 1–15. doi: 10.3390/biomedicines8100436.

66. Goldman, S. A. and Kuypers, N. J. (2015) 'How to make an oligodendrocyte', pp. 3983–3995. doi: 10.1242/dev.126409.

67. Gordon, J., Amin, S. and White, M. K. (2013) 'General overview of neuronal cell culture', *Neuronal Cell Culture: Methods and Protocols*, 1078, pp. 35–44. doi: 10.1007/978-1-62703-640-5.

68. Gorecka, J. *et al.* (2019) 'The potential and limitations of induced pluripotent stem cells to achieve wound healing', *Stem Cell Research and Therapy*. Stem Cell Research & Therapy, 10(1), pp. 1–10. doi: 10.1186/s13287-019-1185-1.

69. Grant, I. *et al.* (2002) 'The co-application of sprayed cultured autologous keratinocytes and autologous fibrin sealant in a porcine wound model', *British Journal of Plastic Surgery*, 55(3), pp. 219–227. doi: 10.1054/bjps.2002.3810.

70. Grienberger, C. and Konnerth, A. (2012) 'Imaging Calcium in Neurons', *Neuron*. Elsevier Inc., 73(5), pp. 862–885. doi: 10.1016/j.neuron.2012.02.011.

71. Guest, J. *et al.* (2011) 'Technical aspects of spinal cord injections for cell transplantation. Clinical and translational considerations', *Brain Research Bulletin*. Elsevier Inc., 84(4–5), pp. 267–279. doi: 10.1016/j.brainresbull.2010.11.007.

72. Günther, M. I. *et al.* (2015) 'Cell-seeded alginate hydrogel scaffolds promote

directed linear axonal regeneration in the injured rat spinal cord', *Acta Biomaterialia*, 27, pp. 140–150. doi: 10.1016/j.actbio.2015.09.001.

73. Hall, E. D. (2011) 'Antioxidant Therapies for Acute Spinal Cord Injury', *Neurotherapeutics*, 8(2), pp. 152–167. doi: 10.1007/s13311-011-0026-4.

74. Han, H. . *et al.* (2020) 'Postoperative thecal sac compression induced by hydrogel dural sealant after spinal schwannoma removal', *Korean Journal of Neurotrauma*, 16(1), pp. 99–104. doi: 10.13004/KJNT.2020.16.E10.

75. Harlowa, D. and Macklin, W. (2014) 'Inhibitors of myelination: ECM changes, CSPGs and PTPs', *Experimental Neurology*, 23(1), pp. 1–7. doi: 10.1016/j.expneurol.2013.10.017.Inhibitors.

76. Hassan, N. F. *et al.* (1991) 'Isolation and characterization of newborn rabbit brain-derived microglia', *Clinical Immunology and Immunopathology*, 59(3), pp. 426–435. doi: 10.1016/0090-1229(91)90038-C.

77. Herzog, C. *et al.* (2019) 'Rapid clearance of cellular debris by microglia limits secondary neuronal cell death after brain injury in vivo', *Development (Cambridge)*, 146(9). doi: 10.1242/dev.174698.

78. Hill, C. E. *et al.* (2007) 'Early necrosis and apoptosis of Schwann cells transplanted into the injured rat spinal cord', *European Journal of Neuroscience*, 26(March), pp. 1433–1445. doi: 10.1111/j.1460-9568.2007.05771.x.

79. Hlavac, N., Kasper, M. and Schmidt, C. E. (2020) 'Progress toward fi nding the perfect match : hydrogels for treatment of central nervous system injury', *Materials Today Advances*. Elsevier Ltd, 6, p. 100039. doi: 10.1016/j.mtadv.2019.100039.

80. Hoffman-kim, D., Mitchel, J. A. and Bellamkonda, R. V (2010) 'Topography , Cell Response , and Nerve Regeneration', *Annual Reveiw of Biomedical Engineerins*, 12, pp. 203–231. doi: 10.1146/annurev-bioeng-070909-105351.

81. Hopfner, U. *et al.* (2018) 'Fibrin glue enhances adipose-derived stromal cell cytokine secretion and survival conferring accelerated diabetic wound healing',

Stem Cells International, 2018. doi: 10.1155/2018/1353085.

82. Hosseini, S. *et al.* (2016) 'Transplantation of neural stem cells cultured in alginate scaffold for spinal cord injury in rats', *Asian Spine Journal*, 10(4), pp. 611–618. doi: 10.4184/asj.2016.10.4.611.

83. Hughes, P. *et al.* (2007) 'The costs of using unauthenticated, over-passaged cell lines: How much more data do we need?', *BioTechniques*, 43(5), pp. 575–586. doi: 10.2144/000112598.

84. Huygens (2020) 'Huygens Deconvolution software Huygens Deconvolution, Scientific Volume Imaging', *Huygens Deconvolution, Scientific Volume Imaging*. Available at: https://svi.nl/Huygens-Deconvolution#References.

85. Hyysalo, A. *et al.* (2017) 'Aligned Poly(ε-caprolactone) Nanofibers Guide the Orientation and Migration of Human Pluripotent Stem Cell-Derived Neurons, Astrocytes, and Oligodendrocyte Precursor Cells In Vitro', *Macromolecular Bioscience*, 17(7), pp. 1–8. doi: 10.1002/mabi.201600517.

86. Integra (2010) *Ultra Pure Collagen ™ Dural repair*, *Integra life sciences*. Available at: http://www.cardion.cz/file/90/duragen-ultrapure-collagen.pdf.

87. Integra (2018) *DuraGen Plus matrix*, *Integra life sciences*. Available at: http://www.integralife.eu/products/neuro/duraplasty/duragen-plus-matrix-2/.

88. Integra Life (2014) *DuraSeal Dural Sealant System Tender Package*. Available at: http://www.neuromiss.gr/sites/default/files/DuraSeal_EN.pdf.

89. Integra Life (2018) 'DuraSeal Xact Spinal Sealant System', *Integra*, p. 2018. Available at: https://www.integralife.eu/products/neuro/duraplasty/duraseal-xact-sealant-system-adhesion-barrier-2/.

90. Ishibashi, T. *et al.* (2006) 'Astrocytes promote myelination in response to electrical impulses', *Neuron*, 49(6), pp. 823–832. doi: 10.1016/j.neuron.2006.02.006.

91. Jager, L. . *et al.* (2016) 'Effect of enzymatic and mechanical methods of dissociation on neural progenitor cells derived from induced pluripotent stem

cells', *Advanced Medicine*, (61(1)), pp. 78–84. doi: 10.1016/j.advms.2015.09.005.Effect.

92. Jakobsson, A. *et al.* (2017) 'Three-dimensional functional human neuronal networks in uncompressed low-density electrospun fiber scaffolds', *Nanomedicine: Nanotechnology, Biology, and Medicine*. The Authors, 13(4), pp. 1563–1573. doi: 10.1016/j.nano.2016.12.023.

93. Jeffery, A. F. *et al.* (2014) 'Hyaluronic acid-based 3D culture model for in vitro testing of electrode biocompatibility', *Biomacromolecules*, 15(6), pp. 2157–2165. doi: 10.1021/bm500318d.

94. Jenkins, S. ., Roach, P. and Chari, D. . (2015) 'Development of a nanomaterial bio-screening platform for neurological applications', *Nanomedicine: Nanotechnology, Biology, and Medicine*. Elsevier Inc., 11(1), pp. 77–87. doi: 10.1016/j.nano.2014.07.010.

95. Jenkins, S. I. *et al.* (2013) 'Differences in magnetic particle uptake by CNS neuroglial subclasses: Implications for neural tissue engineering', *Nanomedicine*, 8(6), pp. 951–968. doi: 10.2217/nnm.12.145.

96. Jenkins, S. I. *et al.* (2016) '"Stealth" nanoparticles evade neural immune cells but also evade major brain cell populations: Implications for PEG-based neurotherapeutics', *Journal of Controlled Release*. Elsevier B.V., 224, pp. 136–145. doi: 10.1016/j.jconrel.2016.01.013.

97. Juan, W. . *et al.* (2012) 'Optimal Percoll concentration facilitates flow cytometric analysis for annexin V/propidium iodine-stained ischemic brain tissues', *Cytometry Part A*, 81 A(5), pp. 400–408. doi: 10.1002/cyto.a.22021.

98. Kaar, A., Morley, S. J. and Rae, M. G. (2017) *An Efficient and Cost-effective Method of Generating Postnatal (P2 - 5) Mouse Primary Hippocampal Neuronal Cultures*, *Journal of Neuroscience Methods*. Elsevier B.V. doi: 10.1016/j.jneumeth.2017.05.020.

99. Kallai, I. *et al.* (2010) 'Quantitative, structural, and image-based mechanical

analysis of nonunion fracture repaired by genetically engineered mesenchymal stem cells', *Journal of Biomechanics*, 43(12), pp. 2315–2320. doi: 10.1016/j.jbiomech.2010.04.031.

100. Kalsi, P., Thom, M. and Choi, D. (2017) 'Histological effects of fibrin glue and synthetic tissue glues on the spinal cord: are they safe to use?', *British Journal of Neurosurgery*. Informa UK Limited, trading as Taylor & Francis Group, 31(6), pp. 695–700. doi: 10.1080/02688697.2017.1359491.

101. Kamber, D., Erez, H. and Spira, M. E. (2009) 'Local calcium-dependent mechanisms determine whether a cut axonal end assembles a retarded endbulb or competent growth cone', *Experimental Neurology*. Elsevier Inc., 219(1), pp. 112–125. doi: 10.1016/j.expneurol.2009.05.004.

102. Kamudzandu, M. *et al.* (2015) 'Nanofibrous scaffolds supporting optimal central nervous system regeneration: an evidence-based review', *Journal of Neurorestoratology*, p. 123. doi: 10.2147/jn.s70337.

103. Kaneko, A. and Sankai, Y. (2014) 'Long-Term Culture of Rat Hippocampal Neurons at Low Density in Serum-Free Medium : Combination of the Sandwich Culture Technique with the Three-Dimensional Nanofibrous Hydrogel PuraMatrix', 9(7). doi: 10.1371/journal.pone.0102703.

104. Katoh, H., Yokota, K. and Fehlings, M. G. (2019) 'Regeneration of spinal cord connectivity through stem cell transplantation and biomaterial scaffolds', *Frontiers in Cellular Neuroscience*, 13(June), pp. 1–22. doi: 10.3389/fncel.2019.00248.

105. Kaur, C., Rathnasamy, G. and Ling, E. A. (2017) 'Biology of microglia in the developing brain', *Journal of Neuropathology and Experimental Neurology*, 76(9), pp. 736–753. doi: 10.1093/jnen/nlx056.

106. Khaing, Z. Z. *et al.* (2015) 'Injectable Hydrogels for Spinal Cord Repair : A Focus on Swelling and Intraspinal Pressure', *Cells Tissues Organs*, 16, pp. 67–84. doi: 10.1159/000446697.

107. Khan, N. *et al.* (2013) 'Prevalence of corticosteroids use and disease

course after initial steroid exposure in ulcerative colitis', *Digestive Diseases and Sciences*, 58(10), pp. 2963–2969. doi: 10.1007/s10620-013-2748-0.

108. Kıray, H. *et al.* (2016) 'The multifaceted role of astrocytes in regulating myelination', *Experimental Neurology*, 283, pp. 541–549. doi: 10.1016/j.expneurol.2016.03.009.

109. De Kleijn, K. M. A. *et al.* (2019) 'Reappraisal of Human HOG and MO3.13 Cell Lines as a Model to Study Oligodendrocyte Functioning', *Cells*, 8(9). doi: 10.3390/cells8091096.

110. Knight, V. . and Serrano, E. . (2017) 'Hydrogel scaffolds promote neural gene expression and structural reorganization in human astrocyte cultures', *PeerJ*, 2017(1). doi: 10.7717/peerj.2829.

111. Koss, K. M. *et al.* (2017) 'Improved 3D hydrogel cultures of primary glial cells for in vitro modelling of neuroinflammation', *Journal of Visualized Experiments*, 2017(130), pp. 1–11. doi: 10.3791/56615.

112. Krenick, R. *et al.* (2011) 'Specification of Transplantable Astroglial Subtypes from Human Pluripotent Stem Cells', *Nat Biotechnology*, 29(6), pp. 528–534. doi: 10.1038/nbt.1877. Specification.

113. Kubinová, Š. and Sikova, E. (2012) 'Biomaterials combined with cell therapy for treatment of spinal cord injury', *Future medicine*, 7, pp. 207–224. doi: 10.2217/rme.11.121.

114. Kuijlaars, J. *et al.* (2016) 'Sustained synchronized neuronal network activity in a human astrocyte co-culture system', *Scientific Reports*. Nature Publishing Group, 6(October 2016), pp. 1–14. doi: 10.1038/srep36529.

115. Kumamaru, H. *et al.* (2013) 'Therapeutic activities of engrafted neural stem/precursor cells are not dormant in the chronically injured spinal cord', *Stem Cells*, 31(8), pp. 1535–1547. doi: 10.1002/stem.1404.

116. Lautenschläger, J. *et al.* (2018) 'An Easy-to-Implement Protocol for Preparing Postnatal Ventral Mesencephalic Cultures', 12(March), pp. 1–10.

doi: 10.3389/fncel.2018.00044.

117. Lee, J. and Thumbikat, P. (2015) ‘Pathophysiology, presentation and management of spinal cord injury’, *Orthapedics*. Elsevier Ltd, 33(6), pp. 238–247. doi: 10.1016/j.mpsur.2015.04.003.

118. Lee, S. . *et al.* (2013) ‘Postoperative Cervical Cord Compression Induced by Hydrogel Dural Sealant (DuraSeal®)’, *Korean Journal of Spine*, 10(1), p. 44. doi: 10.14245/kjs.2013.10.1.44.

119. Lee, Y. *et al.* (2013) ‘Oligodendroglia metabolically support axons and contribute to neurodegeneration’, *Nature*, 487(7408), pp. 443–448. doi: 10.1038/nature11314.Oligodendroglia.

120. Lehmann, K., Steinecke, A. and Bolz, J. (2012) ‘GABA through the ages: Regulation of cortical function and plasticity by inhibitory interneurons’, *Neural Plasticity*, 2012. doi: 10.1155/2012/892784.

121. Lenz, K. M. and Nelson, L. H. (2018) ‘Microglia and beyond: Innate immune cells as regulators of brain development and behavioral function’, *Frontiers in Immunology*, 9(APR). doi: 10.3389/fimmu.2018.00698.

122. Li, L. *et al.* (2016) ‘Recent advances of biomaterials in biotherapy’, *Regenerstive Biomaterials*, pp. 1–7. doi: 10.1093/rb/rbw007.

123. Li, N. and Leung, G. K. K. (2015) ‘Oligodendrocyte Precursor Cells in Spinal Cord Injury: A Review and Update’, *BioMed Research International*. Hindawi Publishing Corporation, 2015. doi: 10.1155/2015/235195.

124. Li, S. *et al.* (2019) ‘Rapid and Efficient Differentiation of Rodent Neural Stem Cells into Oligodendrocyte Progenitor Cells’, *Developmental Neuroscience*, 41(1–2), pp. 79–93. doi: 10.1159/000499364.

125. Li, X. *et al.* (2013) ‘Engineering an in situ crosslinkable hydrogel for enhanced remyelination’, *FASEB Journal*, 27(3), pp. 1127–1136. doi: 10.1096/fj.12-211151.

126. Li, Y. *et al.* (2015) 'Function as a Neuron-Free Model for Myelination Study', *Biomacromolecules*, 15(1), pp. 319–326. doi: 10.1021/bm401558c.Nanofibers.

127. Liu, S. *et al.* (2018) 'Biomaterial-supported cell transplantation treatments for spinal cord injury: Challenges and perspectives', *Frontiers in Cellular Neuroscience*, 11(January). doi: 10.3389/fncel.2017.00430.

128. Liu, Z., Yang, Y., He, L., Pang, M., Luo, C., Liu, B. and Rong, L., 2019. High-dose methylprednisolone for acute traumatic spinal cord injury. *Neurology*, 93(9), pp.e841-e850.

129. Liggett, S. B. (2004) 'Genetically modified mouse models for pharmacogenomic research.', *Nature Reviews Genetics 5(9), 657–663. doi:10.1038/nrg1429*, 3(September), pp. 3–9.

130. Lin, K. . *et al.* (2010) 'DuraSeal as a Ligature in the Anastomosis of Rat Sciatic Nerve Gap Injury', *Journal of Surgical Research*. Elsevier Ltd, 161(1), pp. 101–110. doi: 10.1016/j.jss.2008.10.020.

131. Lin, L. *et al.* (2017) 'Characteristics of primary rat microglia isolated from mixed cultures using two different methods', *Journal of Neuroinflammation*. Journal of Neuroinflammation, 14(1), pp. 1–10. doi: 10.1186/s12974-017-0877-7.

132. Lucas, S. M., Rothwell, N. J. and Gibson, R. M. (2006) 'The role of inflammation in CNS injury and disease', *British Journal of Pharmacology*, 147(SUPPL. 1), pp. 232–240. doi: 10.1038/sj.bjp.0706400.

133. Macewan, M. R. *et al.* (2018) 'Comparative analysis of a fully-synthetic nanofabricated dura substitute and bovine collagen dura substitute in a large animal model of dural repair', *Interdisciplinary Neurosurgery*. Elsevier, 13(May), pp. 145–150. doi: 10.1016/j.inat.2018.05.001.

134. MacEwan, M. R., Kovacs, T. and Ray, W. Z. (2018) 'Novel

nanofabricated dura substitute effectively repairs dural defects independent of defect size in a canine duraplasty model', *Interdisciplinary Neurosurgery: Advanced Techniques and Case Management*. Elsevier, 14(June), pp. 150–155. doi: 10.1016/j.inat.2018.08.006.

135. Maier, I. C. *et al.* (2009) 'Differential effects of anti-Nogo-A antibody treatment and treadmill training in rats with incomplete spinal cord injury', *Brain*, 132(6), pp. 1426–1440. doi: 10.1093/brain/awp085.

136. Maitz, M. F. (2015) 'Applications of synthetic polymers in clinical medicine', *Biosurface and Biotribology*. Elsevier, 1(3), pp. 161–176. doi: 10.1016/j.bsbt.2015.08.002.

137. Mamelak, M. (2018) 'Parkinson ' s Disease , the Dopaminergic Neuron and Gammahydroxybutyrate', *Neurology and Therapy*. Springer Healthcare, 7(1), pp. 5–11. doi: 10.1007/s40120-018-0091-2.

138. Marchini, A. *et al.* (2019) 'Multifunctionalized hydrogels foster hNSC maturation in 3D cultures and neural regeneration in spinal cord injuries', *Proceedings of the National Academy of Sciences of the United States of America*, 116(15), pp. 7483–7492. doi: 10.1073/pnas.1818392116.

139. Marquardt, L. and Heilshorn, S. (2016) 'Design of Injectable Materials to Improve Stem Cell Transplantation', *Current Stem Cell Reports*. Current Stem Cell Reports, 2(3), pp. 207–220. doi: 10.1007/s40778-016-0058-0.

140. Matsuyoshi, Y. *et al.* (2019) 'Isolation and purification of satellite cells from young rats by percoll density gradient centrifugation', *Methods in Molecular Biology*, 1889, pp. 81–93. doi: 10.1007/978-1-4939-8897-6_6.

141. Mccarthy, Ken D., DeVellis, J. (1980) 'PREPARATION OF SEPARATE ASTROGLIAL AND OLIGODENDROGLIAL CELL CULTURES FROM RAT CEREBRAL TISSUE Downloaded from jcb . rupress . org on July 27 , 2012 A novel method has been developed for the preparation of nearly pure separate cultures of astrocytes and o', 85(June).

142. McCarthy, K. . and De Vellis, J. (1980) ‘PREPARATION OF SEPARATE ASTROGLIAL AND OLIGODENDROGLI AL CELL CULTURES FROM RAT CEREBRAL TISSUE’, 86(June), pp. 890–902. doi: 10.1083/jcb.85.3.890.

143. McDonald, J. W. (1999) ‘Repairing the damaged spinal cord.’, *Scientific American*, 281(3), pp. 64–73. doi: 10.1038/scientificamerican0999-64.

144. Mecha, M. *et al.* (2011) ‘An easy and fast way to obtain a high number of glial cells from rat cerebral tissue : A beginners approach .’, *Protocol Exchange*, pp. 1–15. doi: 10.1038/protex.2011.218.

145. Mederos, S., González-Arias, C. and Perea, G. (2018) ‘Astrocyte–Neuron Networks: A Multilane Highway of Signaling for Homeostatic Brain Function’, *Frontiers in Synaptic Neuroscience*, 10(November), pp. 1–12. doi: 10.3389/fnsyn.2018.00045.

146. Meeker, R. and Williams, K. (2015) ‘Dynamic nature of the p75 neurotrophin receptor in response to injury and disease’, *Journal of Neuroimmune Pharmacol*, 9(5), pp. 615–628. doi: 10.1007/s11481-014-9566-9.Dynamic.

147. Mekhail, M., Almazan, G. and Tabrizian, M. (2014) ‘Biomaterials Science’, *Biomaterials Science*. Royal Society of Chemistry, (1). doi: 10.1039/c4bm00215f.

148. Meyer-Franke, A., Shen, S. and Barres, B, A. (1999) ‘Astrocytes induce oligodendrocyte processes to align with and adhere to axons’, *Molecular and Cellular Neurosciences*, 14(4–5), pp. 385–397. doi: 10.1006/mcne.1999.0788.

149. Miersch, C., Stange, K. and Röntgen, M. (2018) ‘Effects of trypsinization and of a combined trypsin, collagenase, and DNase digestion on liberation and in vitro function of satellite cells isolated from juvenile porcine muscles’, *In Vitro Cellular and Developmental Biology - Animal*. In Vitro Cellular & Developmental Biology - Animal, 54(6), pp. 406–412. doi: 10.1007/s11626-018-0263-5.

150. Milbreta, U. *et al.* (2019) ‘Scaffold-Mediated Sustained, Non-viral Delivery of miR-219/miR-338 Promotes CNS Remyelination’, *Molecular Therapy*. Elsevier Ltd., 27(2), pp. 411–423. doi: 10.1016/j.ymthe.2018.11.016.

151. Minakov, A. N. *et al.* (2018) ‘Experimental Models of Spinal Cord Injury in Laboratory Rats’, 10(38), pp. 4–10.

152. Miron, V. E., Kuhlmann, T. and Antel (2011) ‘Cells of the oligodendroglial lineage, myelination, and remyelination’, *Biochimica et Biophysica Acta - Molecular Basis of Disease*. Elsevier B.V., 1812(2), pp. 184–193. doi: 10.1016/j.bbadis.2010.09.010.

153. Montoro, S., Medeiros, S. and Alves, G. M. (2014) *Nanostructured Hydrogels*, *Nanostructured Polymer Blends*. Elsevier Inc. doi: 10.1016/B978-1-4557-3159-6.00010-9.

154. Moshayedi, P. *et al.* (2014) ‘The relationship between glial cell mechanosensitivity and foreign body reactions in the central nervous system’, *Biomaterials*. Elsevier Ltd, 35(13), pp. 3919–3925. doi: 10.1016/j.biomaterials.2014.01.038.

155. Moutin, E. *et al.* (2020) ‘Procedures for Culturing and Genetically Manipulating Murine Hippocampal Postnatal Neurons’, 12(April), pp. 1–16. doi: 10.3389/fnsyn.2020.00019.

156. MS (2020) *National Multiple Sclerosis Society; Types of MS*, *Multiple Sclerosis Society*. Available at: http://www.nationalmssociety.org/What-is-MS/Types-of-MS.

157. Murray, S. *et al.* (2010) ‘Mouse gestation length is genetically determined’, *PLoS ONE*, 5(8). doi: 10.1371/journal.pone.0012418.

158. Nam, H. *et al.* (2015) ‘Adult human neural stem cell therapeutics: Current developmental status and prospect’, *World Journal of Stem Cells*, 7(1), p. 126. doi: 10.4252/wjsc.v7.i1.126.

159. Nash, B., Ioannidou, K. and Barnett, S. C. (2011) ‘Astrocyte phenotypes and their relationship to myelination’, *Journal of Anatomy*, 219(1), pp. 44–52. doi: 10.1111/j.1469-7580.2010.01330.x.

160. Nash, R. *et al.* (2017) ‘High-dose immunosuppressive therapy and autologous HCT for relapsing-remitting MS’, *Neurology*, 88(9), pp. 842–852. doi: 10.1212/WNL.0000000000003660.

161. Nazari, B. *et al.* (2019) ‘Fibrin hydrogel as a scaffold for differentiation of induced pluripotent stem cells into oligodendrocytes’, *Journal of Biomedical Materials Research - Part B Applied Biomaterials*, 108(1), pp. 192–200. doi: 10.1002/jbm.b.34378.

162. Nguyen, L. H. *et al.* (2017) ‘Three-dimensional aligned nanofibers-hydrogel scaffold for controlled non-viral drug/gene delivery to direct axon regeneration in spinal cord injury treatment’, *Scientific Reports*. Nature Publishing Group, 7(February), pp. 1–12. doi: 10.1038/srep42212.

163. NHS England (2013) ‘NHS Standard Contract for Spinal Cord Injuries’, *for Complex Disability Equipment- Prosthetics (All Ages)*, 1(1), pp. 1–31. Available at: http://www.england.nhs.uk/wp-content/uploads/2013/06/d01-com-dis-equ-prosth.pdf.

164. NICE (2016) ‘Spinal injury: assessment and initial management Spinal injury assessment: assessment and imaging for spinal injury NICE Guideline NG41 Methods, evidence and recommendations Spinal injury assessment Contents’, (February).

165. NSCISC (2017) *Spinal Cord Injury Facts and Figures at a Glance*, *National Spinal Cord Injury Statistics Centre (NSCISC)*.

166. NSCISC (2020) *Facts and Figures at a Glance*, *National Spinal Cord Injury Statistics Centre (NSCISC)*. Available at: https://www.nscisc.uab.edu/Public/Facts and Figures 2020.pdf.

167. Nutma, E. *et al.* (2020) ‘Astrocyte and Oligodendrocyte Cross-Talk in

the Central Nervous System', *Cells*, 9(3), p. 600. doi: 10.3390/cells9030600.

168. Obuchowicz, E. *et al.* (2006) 'Amitriptyline and nortriptyline inhibit interleukin-1β and tumour necrosis factor-α release by rat mixed glial and microglial cell cultures', *International Journal of Neuropsychopharmacology*, 9(1), pp. 27–35. doi: 10.1017/S146114570500547X.

169. Ottosson, M., Jakobsson, A. and Johansson, F. (2017) 'Accelerated wound closure - Differently organized nanofibers affect cell migration and hence the closure of artificial wounds in a cell based in vitro model', *PLoS ONE*, 12(1), pp. 1–15. doi: 10.1371/journal.pone.0169419.

170. Oyinbo, C. A. (2011) 'Secondary injury mechanisms in traumatic spinal cord injury a nugget', *Acta Neurobiologiae Experimentalis*, 71(2), pp. 281–299.

171. Pacifici, M. and Peruzzi, F. (2012) 'Isolation and Culture of Rat Embryonic Neural Cells : A Quick Protocol', (May), pp. 1–5. doi: 10.3791/3965.

172. Pantoja, I. *et al.* (2020) 'IPSCs from people with MS can differentiate into oligodendrocytes in a homeostatic but not an inflammatory milieu', *PLoS ONE*, 15(6), pp. 1–19. doi: 10.1371/journal.pone.0233980.

173. Pease, D. . *et al.* (2007) 'Transplantation of Schwann Cells and/or Olfactory Ensheathing Glia into the Contused Spinal Cord: Survival, Migration, Axon Association, and Functional Recovery', *Glia*, 55:976–100. doi: 10.1002/glia.

174. Pellett, S. *et al.* (2015) 'Human Induced Pluripotent Stem Cell Derived Neuronal Cells Cultured on Chemically- Defined Hydrogels for Sensitive In Vitro Detection of Botulinum Neurotoxin', *Nature Publishing Group*. Nature Publishing Group, (September), pp. 1–12. doi: 10.1038/srep14566.

175. Pereira, I. M. *et al.* (2019) 'Filling the gap: Neural stem cells as a promising therapy for spinal cord injury', *Pharmaceuticals*, 12(2), pp. 1–32. doi: 10.3390/ph12020070.

176. Pereira, T. *et al.* (2014) 'Effects of human mesenchymal stem cells

isolated from Wharton's jelly of the umbilical cord and conditioned media on skeletal muscle regeneration using a myectomy model', *Stem Cells International*, 2014. doi: 10.1155/2014/376918.

177. Piao, J. ., Wang, Y. and Duncan, I. . (2013) 'CD44 Is Required for the Migration of Transplanted Oligodendrocyte Progenitor Cells to Focal Inflammatory Demyelinating Lesions in the Spinal Cord', *Glia*, 61(May 2012), pp. 361–367. doi: 10.1002/glia.22438.

178. Pickard, M. R. and Chari, D. M. (2010) 'Robust uptake of magnetic nanoparticles (MNPs) by central nervous system (CNS) microglia: Implications for particle uptake in mixed neural cell populations', *International Journal of Molecular Sciences*, 11(3), pp. 967–981. doi: 10.3390/ijms11030967.

179. Pinkernelle, J. *et al.* (2012) 'Magnetic nanoparticles in primary neural cell cultures are mainly taken up by microglia', *BMC Neuroscience*. BioMed Central Ltd, 13(1), p. 32. doi: 10.1186/1471-2202-13-32.

180. Pressler, R. and Auvin, S. (2013) 'Comparison of brain maturation among species: An example in translational research suggesting the possible use of bumetanide in newborn', *Frontiers in Neurology*, 4 APR(April), p. 1. doi: 10.3389/fneur.2013.00036.

181. Qin, C. *et al.* (2018) 'Induced pluripotent stem cell transplantation improves locomotor recovery in rat models of spinal cord injury: A systematic review and meta-analysis of randomized controlled trials', *Cellular Physiology and Biochemistry*, 47(5), pp. 1835–1852. doi: 10.1159/000491064.

182. Rabinowitz, L. *et al.* (2005) 'Growth of rat cortical neurons on DuraGen, a collagen-based dural graft matrix.', *Neurological research*, 27(8), pp. 887–894. doi: 10.1179/016164105X49364.

183. Rauvala, H. *et al.* (2017) 'Inhibition and enhancement of neural regeneration by chondroitin sulfate proteoglycans', *Neural Regeneration Research*, 12(5), pp. 687–691. doi: 10.4103/1673-5374.206630.

184. Ray, J. *et al.* (1993) ‘Proliferation, differentiation, and long-term culture of primary hippocampal neurons’, *Proceedings of the National Academy of Sciences of the United States of America*, 90(8), pp. 3602–3606. doi: 10.1073/pnas.90.8.3602.

185. Reemst, K. *et al.* (2016) ‘The indispensable roles of microglia and astrocytes during brain development’, *Frontiers in Human Neuroscience*, 10(NOV2016), pp. 1–28. doi: 10.3389/fnhum.2016.00566.

186. Roppongi, R. T., Champagne-jorgensen, K. P. and Siddiqui, T. J. (2017) ‘Low-Density Primary Hippocampal Neuron Culture’, (April), pp. 1–7. doi: 10.3791/55000.

187. Russell, L. N. and Lampe, K. J. (2017) ‘Oligodendrocyte Precursor Cell Viability, Proliferation, and Morphology is Dependent on Mesh Size and Storage Modulus in 3D Poly(ethylene glycol)-Based Hydrogels’, *ACS Biomaterials Science and Engineering*, 3(12), pp. 3459–3468. doi: 10.1021/acsbiomaterials.7b00374.

188. Sahu, M. . *et al.* (2019) ‘Culturing primary neurons from rat hippocampus and cortex’, *Neuronal Signalling*, 0(April), pp. 1–10. doi: 10.1101/491118.

189. Sasaki, M. *et al.* (2007) ‘Remyelination of the injured spinal cord’, *Progress in Brain Research*, 161, pp. 419–433. doi: 10.1016/S0079-6123(06)61030-3.

190. Schaub, N. J. *et al.* (2016) ‘Electrospun Fibers for Spinal Cord Injury Research and Regeneration’, *Journal of Neurotrauma*, 33(15), pp. 1405–1415. doi: 10.1089/neu.2015.4165.

191. Schmalz, P. *et al.* (2018) ‘Use of an Absorbable Synthetic Polymer Dural Substitute for Repair of Dural Defects: A Technical Note’, *Cureus*, 10(1), pp. 1–5. doi: 10.7759/cureus.2127.

192. Schoenfeld, R. *et al.* (2010) ‘Oligodendroglial differentiation induces

mitochondrial genes and inhibition of mitochondrial function represses oligodendroglial differentiation', *Mitochondrion*. Mitochondria Research Society, 10(2), pp. 143–150. doi: 10.1016/j.mito.2009.12.141.

193. Sciarretta, C. and Minichiell, L. (2010) 'The Preparation of Primary Cortical Neuron Cultures and a Practical Application Using Immunofluorescent Cytochemistry', *Methods in Molecular Biology*, 633(1), pp. 29–56. doi: 0.1007/978-1-59745-019-5_16.

194. Sengupta, P. (2013) 'The laboratory rat: Relating its age with human's', *International Journal of Preventive Medicine*, 4(6), pp. 624–630.

195. Serrano-aroca, Á. (2018) 'Enhancement of Hydrogels ' Properties for Biomedical Applications : Latest Achievements Enhancement of Hydrogels ' Properties for Biomedical Applications : Latest Achievements', in Sajjad Haider and Adnan Haider (ed.) *Intechopen*, pp. 91–120. doi: 10.5772/intechopen.71671.

196. Shin, S. S. *et al.* (2015) 'Neuroprotective effects of collagen matrix in rats after traumatic brain injury', *Restorative Neurology and Neuroscience*, 33(2), pp. 95–104. doi: 10.3233/RNN-140430.

197. Shoichet, M. ., Tate, C. . and Bauman, M. (2008) 'Indwelling Neural Implants: Strategies for Contending with the In Vivo Environment.', in *Indwelling Neural Implants: Strategies for Contending with the In Vivo Environment.* CRC Press/Taylor & Francis, p. 3941. Available at: https://www.ncbi.nlm.nih.gov/books/NBK3941/.

198. Siddiqi, F. and Wolfe, J. H. (2016) 'Stem Cell Therapy for the Central Nervous System in Lysosomal Storage Diseases', *Human Gene Therapy*, 27(10), pp. 749–757. doi: 10.1089/hum.2016.088.

199. Siebert, J. R., Eade, A. M. and Osterhout, D. J. (2015) 'Biomaterial Approaches to Enhancing Neurorestoration after Spinal Cord Injury: Strategies for Overcoming Inherent Biological Obstacles', *BioMed Research International*, 2015. doi: 10.1155/2015/752572.

200. Silvestro, S. *et al.* (2020) ‘Stem cells therapy for spinal cord injury: An overview of clinical trials’, *International Journal of Molecular Sciences*, 21(2), pp. 1–26. doi: 10.3390/ijms21020659.

201. Sloka, J. S. and Stefanelli, M. (2005) ‘Multiple Sclerosis’, *Multiple Sclerosis*. doi: 10.1191/1352458505ms1190oa.

202. Sofroniew, M. V. and Vinters, H. V. (2010) ‘Astrocytes: Biology and pathology’, *Acta Neuropathologica*, 119(1), pp. 7–35. doi: 10.1007/s00401-009-0619-8.

203. Solanki, A. *et al.* (2013) ‘Axonal Alignment and Enhanced Neuronal Differentiation of Neural Stem Cells on Graphene-Nanoparticle Hybrid Structures Aniruddh’, *Advance Material*, 25(38)(11), pp. 5477–5482. doi: 10.1002/adma.201302219.

204. Soletta, J. H. *et al.* (2017) ‘Identification of Functionally Interconnected Neurons Using Factor Analysis’, *Computational Intelligence and Neuroscience*, 2017. doi: 10.1155/2017/8056141.

205. Spinalcord (2020) *Spinal Cord Spinal cord injury statistics*, *Spinal Cord*. Available at: https://www.spinalcord.com/blog/2017-spinal-cord-injury-statistics-you-ought-to-know.

206. Spitzer, S. . *et al.* (2018) ‘Oligodendrocyte Progenitor Cells Become Regionally Diverse and Heterogeneous with Age’, *Neuron*, 101(3), pp. 459-471.e5. doi: 10.1016/j.neuron.2018.12.020.

207. Stankoff, B. and Zalc, B. (2002) ‘Ciliary Neurotrophic Factor (CNTF) Enhances Myelin Formation: A Novel Role for CNTF and CNTF-Related Molecules’, *Journal of Neuroscience*, 22(21), pp. 9221–9227

208. Stolp, H. *et al.* (2012) ‘The Long and the Short of it: Gene and Environment Interactions During Early Cortical Development and Consequences for Long-Term Neurological Disease’, *Frontiers in Psychiatry*, 3(June), pp. 8–15. doi: 10.3389/fpsyt.2012.00050.

209. Stuijver, D. J. F. *et al.* (2013) 'Use of oral glucocorticoids and the risk of pulmonary embolism: A population-based case-control study', *Chest*, 143(5), pp. 1337–1342. doi: 10.1378/chest.12-1446.

210. Sun, M. *et al.* (2016) 'Ciliary neurotrophic factor-treated astrocyte-conditionedmedium increases the intracellular free calcium concentration in rat cortical neurons', *Biomedical Reports*, 4(4), pp. 417–420. doi: 10.3892/br.2016.602.

211. Sünwoldt, J. *et al.* (2017) 'Neuronal culture microenvironments determine preferences in bioenergetic pathway use', *Frontiers in Molecular Neuroscience*, 10(September), pp. 1–11. doi: 10.3389/fnmol.2017.00305.

212. Takahashi, K. and Yamanaka, S. (2006) 'Induction of Pluripotent Stem Cells from Mouse Embryonic and Adult Fibroblast Cultures by Defined Factors', *Cell*, 126(4), pp. 663–676. doi: 10.1016/j.cell.2006.07.024.

213. Takahashi, Y. *et al.* (2011) 'Comparative study of methods for administering neural stem/progenitor cells to treat spinal cord injury in mice', *Cell Transplantation*, 20(5), pp. 727–739. doi: 10.3727/096368910X536554.

214. Talovic., M. *et al.* (2017) 'Laminin Enriched Scaffolds for Tissue Engineering Applications', *Advances in Tissue Engineering & Regenerative Medicine: Open Access*, 2(3), pp. 194–200. doi: 10.15406/atroa.2017.02.00033.

215. Tam, R. Y. *et al.* (2014) 'Regenerative therapies for central nervous system diseases: A biomaterials approach', *Neuropsychopharmacology*. Nature Publishing Group, 39(1), pp. 169–188. doi: 10.1038/npp.2013.237.

216. Tay, T. L. *et al.* (2017) 'Microglia across the lifespan: from origin to function in brain development, plasticity and cognition', *Journal of Physiology*, 595(6), pp. 1929–1945. doi: 10.1113/JP272134.

217. Thomas, C. E., Ehrhardt, A. and Kay, M. A. (2003) 'Progress and

problems with the use of viral vectors for gene therapy', *Nature Reviews Genetics*, 4(5), pp. 346–358. doi: 10.1038/nrg1066.

218. Themistocleous, M. S. *et al.* (2017) 'The Insertion of Electrodes in the Brain for Electrophysiological Recording or Chronic Stimulation Is Not Associated With Any Biochemically Detectable Neuronal Injury', *Neuromodulation*, 20(5), pp. 424–428. doi: 10.1111/ner.12598.

219. Tian, L., Prabhakaran, M. P. and Ramakrishna, S. (2015) 'Strategies for regeneration of components of nervous system: Scaffolds, cells and biomolecules', *Regenerative Biomaterials*, 2(1), pp. 31–45. doi: 10.1093/rb/rbu017.

220. Tickle, J. A. *et al.* (2016) 'Endocytotic potential governs magnetic particle loading in dividing neural cells: Studying modes of particle inheritance', *Nanomedicine*, 11(4), pp. 345–358. doi: 10.2217/nnm.15.202.

221. Tickle, J. A. and Chari, D. M. (2019) 'Less is more: Investigating the influence of cellular nanoparticle load on transfection outcomes in neural cells', *Journal of Tissue Engineering and Regenerative Medicine*, 13(9), pp. 1732–1737. doi: 10.1002/term.2909.

222. Tognatta, R. *et al.* (2020) 'Astrocytes Are Required for Oligodendrocyte Survival and Maintenance of Myelin Compaction and Integrity', *Frontiers in Cellular Neuroscience*, 14(April), pp. 1–17. doi: 10.3389/fncel.2020.00074.

223. Traiffort, E. *et al.* (2020) 'Astrocytes and Microglia as Major Players of Myelin Production in Normal and Pathological Conditions', *Frontiers in Cellular Neuroscience*, 14(April), pp. 1–21. doi: 10.3389/fncel.2020.00079.

224. Trounson, A. (2011) 'New perspectives in human stem cell therapeutic research', *BMC Medicine*, 7. doi: 10.1186/1741-7015-7-29.

225. Trounson, A. and McDonald, C. (2015) 'Stem Cell Therapies in Clinical Trials: Progress and Challenges', *Cell Stem Cell*. Elsevier Inc., 17(1), pp. 11–

22. doi: 10.1016/j.stem.2015.06.007.

226. Tsui, C. T. *et al.* (2020) ‘Applying a novel 3D hydrogel cell culture to investigate activation of microglia due to rotational kinematics associated with mild traumatic brain injury’, *Journal of the Mechanical Behavior of Biomedical Materials*. Elsevier Ltd, 114, p. 104176. doi: 10.1016/j.jmbbm.2020.104176.

227. UBC (2018) *UBC ANIMAL CARE COMMITTEE Guidelines for Management and Maintenance of Rodent Breeding Colonies*, *UBC ANIMAL CARE COMMITTEE Guidelines*. Available at: https://animalcare.ubc.ca/sites/default/files/documents/Guidelines on the Management and Maintenance of Rodent Breeding Colonies 2018.pdf.

228. Udomruk, S. *et al.* (2018) ‘Sesamin suppresses LPS-induced microglial activation via regulation of TLR4 expression’, *Journal of Functional Foods*. Elsevier, 49(July), pp. 32–43. doi: 10.1016/j.jff.2018.08.020.

229. van Deemter, M. *et al.* (2013) ‘Trypsin-mediated enzymatic degradation of type II collagen in the human vitreous’, *Molecular Vision*, 19(May 2012), pp. 1591–1599.

230. Van, N. and Gail, A (2016) ‘Drugs, Devices, and the FDA: Part 1: An Overview of Approval Processes for Drugs’, *JACC: Basic to Translational Science*. Elsevier, 1(3), pp. 170–179. doi: 10.1016/j.jacbts.2016.03.002.

231. Van, N. and Gail, A. (2016) ‘Drugs, Devices, and the FDA: Part 2: An Overview of Approval Processes: FDA Approval of Medical Devices’, *JACC: Basic to Translational Science*. Elsevier, 1(4), pp. 277–287. doi: 10.1016/j.jacbts.2016.03.009.

232. Vasile, C., Stoleru, E. and Baican, M. (2020) ‘New developments in medical applications of hybrid hydrogels containing natural polymers’, *Molecules*, 25(7). doi: 10.3390/molecules25071539.

233. Vecino, E. and Kwok, J. C. F. (2016) ‘The Extracellular Matrix in the Nervous System: The Good and the Bad Aspects’, in *Intech Open access*.

Available at: https://www.intechopen.com/books/advanced-biometric-technologies/liveness-detection-in-biometrics.

234. Vellis, J. De and Cole, R. (2011) 'Chapter 4 Preparation of Mixed Glial Cultures from Postnatal Rat Brain', 814, pp. 49–59. doi: 10.1007/978-1-61779-452-0.

235. De Vries, G. and Boullerne, A. I. (2010) 'Glial cell lines: An overview', *Neurochemical Research*, 35(12), pp. 1978–2000. doi: 10.1007/s11064-010-0318-9.

236. Wang, A. S., Armstrong, E. and Armstrong, A. W. (2013) 'Corticosteroids and wound healing: Clinical considerations in the perioperative period', *American Journal of Surgery*. Elsevier Inc, 206(3), pp. 410–417. doi: 10.1016/j.amjsurg.2012.11.018.

237. Wang, S. *et al.* (2014) 'Human iPSC-derived oligodendrocyte progenitors can myelinate and rescue a mouse model of congenital hypomyelination', *Bone*, 12(2), pp. 252–264. doi: 10.1016/j.stem.2012.12.002.Human.

238. Watson, P. M. D. *et al.* (2017) 'Bioengineered 3D Glial Cell Culture Systems and Applications for Neurodegeneration and Neuroinflammation', *SLAS Discovery*, 22(5), pp. 583–601. doi: 10.1177/2472555217691450.

239. Weightman, A., Jenkins, S. and Pickard, M. (2014) 'Alignment of multiple glial cell populations in 3D nanofiber scaffolds : Toward the development of multicellular implantable scaffolds for repair of neural injury', *Nanomedicine: Nanotechnology, Biology, and Medicine*. Elsevier Inc., 10(2), pp. 291–295. doi: 10.1016/j.nano.2013.09.001.

240. Weihe, E. *et al.* (2006) 'Three Types of Tyrosine Hydroxylase-Positive CNS Neurons Distinguished by Dopa Decarboxylase and VMAT2 Co-Expression', 26(0), pp. 659–678. doi: 10.1007/s10571-006-9053-9.Three.

241. Weinert, M. *et al.* (2015) 'Isolation, culture and long-term maintenance of primary mesencephalic dopaminergic neurons from embryonic rodent

brains', *Journal of Visualized Experiments*, (96), pp. 1–5. doi: 10.3791/52475.

242. Westergaard, N. *et al.* (1992) 'Synthesis and release of GABA in cerebral cortical neurons co-cultured with astrocytes from cerebral cortex or cerebellum', *Neurochemistry International*, 20(4), pp. 567–575. doi: 10.1016/0197-0186(92)90036-Q.

243. WHO (2013) *World Health Organization Spinal cord injury fact sheet*, *World Health Organisation*. Available at: https://www.who.int/en/news-room/fact-sheets/detail/spinal-cord-injury.

244. WHO (2017) 'Neurological Disorders: Public Health Challenges', in *World Health Organisation*. doi: 10.1001/archneurol.2007.19.

245. Wiatrak, B. *et al.* (2020) 'PC12 Cell Line: Cell Types, Coating of Culture Vessels, Differentiation and Other Culture Conditions Benita', *Cells*, (9(4): 958). doi: 10.3390/cells9040958.

246. Wilems, T. S. *et al.* (2015) 'Combination therapy of stem cell derived neural progenitors and drug delivery of anti-inhibitory molecules for spinal cord injury', *Acta Biomaterialia*. Acta Materialia Inc., 28, pp. 23–32. doi: 10.1016/j.actbio.2015.09.018.

247. Xu, G. . *et al.* (2004) 'Concentrations of glutamate released following spinal cord injury kill oligodendrocytes in the spinal cord', *Experimental Neurology*, 187(2), pp. 329–336. doi: 10.1016/j.expneurol.2004.01.029.

248. Xu, J. *et al.* (2020) 'Injectable Gelatin Hydrogel Suppresses Inflammation and Enhances Functional Recovery in a Mouse Model of Intracerebral Hemorrhage', *Frontiers in Bioengineering and Biotechnology*, 8(July), pp. 1–15. doi: 10.3389/fbioe.2020.00785.

249. Yang, F. *et al.* (2005) 'Electrospinning of nano/micro scale poly(l-lactic acid) aligned fibers and their potential in neural tissue engineering', *Biomaterials*, 26(15), pp. 2603–2610. doi: 10.1016/j.biomaterials.2004.06.051.

250. Yang, S. *et al.* (2020) 'Self-assembling peptide hydrogels functionalized

with LN- And BDNF- mimicking epitopes synergistically enhance peripheral nerve regeneration', *Theranostics*, 10(18), pp. 8227–8249. doi: 10.7150/thno.44276.

251. Yawo, H. and Kuno, M. (1985) 'Calcium dependence of membrane sealing at the cut end of the cockroach giant axon', *Journal of Neuroscience*, 5(6), pp. 1626–1632. doi: 10.1523/jneurosci.05-06-01626.1985.

252. Ye, Z. and Sontheimer, H. (1998) 'Astrocytes Protect Neurons From Neurotoxic Injury by Serum Glutamate', 248(August 1997), pp. 237–248.

253. Zalis, M. . *et al.* (2016) 'Exploration of physical and chemical cues on retinal cell fate', *Molecular and Cellular Neuroscience*. The Authors, 75, pp. 122–132. doi: 10.1016/j.mcn.2016.07.006.

254. Zheng, W. *et al.* (2018) 'Differentiation of glial cells from hiPSCs: Potential applications in neurological diseases and cell replacement therapy', *Frontiers in Cellular Neuroscience*, 12(August). doi: 10.3389/fncel.2018.00239.